Genetic characterisation of the *Drosophila* Mitochondrial Calcium Uniporter in physiological and neurodegenerative contexts

This dissertation is submitted for the degree of Doctor of Philosophy

by

Thomas Patrick Gleeson

Darwin College

September 2019

Thesis Declaration

This thesis is the result of my own work and includes nothing which is the outcome of work done in collaboration except as declared in the Preface and specified in the text. It is not substantially the same as any that I have submitted, or, is being concurrently submitted for a degree or diploma or other qualification at the University of Cambridge or any other University or similar institution except as declared in the Preface and specified in the text. I further state that no substantial part of my dissertation has already been submitted, or, is being concurrently submitted for any such degree, diploma or other qualification at the University of Cambridge or any other University or similar institution except as declared in the Preface and specified in the text. It does not exceed the prescribed word limit for the relevant Degree Committee.

Preface

This project was a collaborative effort with other members of the Whitworth lab, namely R. Tufi, A. Terriente-Felix, and V. L. Hewitt, and our collaborators from the University of Padua, S. von Stockum and E. Ziviani. I am grateful for their contributions, and they are credited accordingly in the text.

Thesis summary

Thomas Patrick Gleeson

Genetic characterisation of the Drosophila Mitochondrial Calcium Uniporter in physiological and neurodegenerative contexts

Neurodegenerative conditions such as Alzheimer's disease (AD) and Parkinson's disease (PD) are a growing medical and social burden for which no disease-modifying therapies exist, necessitating greater understanding of their underlying pathobiology. Mitochondrial health and calcium signalling have come to the fore in the study of both conditions, and mitochondrial calcium dynamics, which play a crucial role in basal metabolism and cell death, have potential to be a key player in the disease process. Though mitochondrial calcium influx had long been observed through electrophysiology and other work, the genetic basis for this process has only recently been described. The uniporter is comprised of MCU, the pore-forming component; EMRE, which coordinates the complex architecture and is required for *in vivo* calcium uptake; and MICU1-3, which regulate the flow of ions. Animal models have emerged for some uniporter genes, but variable effects have left their physiological role uncertain. The genetic tractability of the *Drosophila melanogaster* model system makes it well situated to address this, and its short lifespan facilitates investigation of diseases of aging, but it has been little utilised in the study of the uniporter.

Here, I complete a full suite of genetic tools for interrogating mitochondrial calcium uniporter components conserved in *Drosophila melanogaster*, through molecular cloning, P-element transposition, and CRISPR-mediated targeted mutagenesis. Knockouts of *MCU* and *EMRE*, both essential for *in vivo* uniporter activity, are largely tolerated in the fly, though lifespan is reduced, especially for *MCU*. Metabolic features of these mutants also diverge. The loss of the regulatory *MICU1* results in developmental lethality, preceded by organismal dysfunction. Crucially, this was not rescued by *MCU* or *EMRE* knockout, indicating the presence of a uniporter-independent role of *MICU1*. Knockouts of *MICU3*

were viable but displayed defects associated with tissues in which the gene is more expressed.

In addition to characterisation of the physiological role of these genes, I crossed them to *Drosophila* models of neurodegenerative disease, primarily *Pink1* loss. Reduction of *MCU* strikingly rescued *Pink1*-associated deficits, with more variable rescue against *parkin*, demonstrating some specificity for mitophagy-independent *Pink1* functions. *MCU* loss also markedly improved a mutant amyloid expressing model of Alzheimer's disease. As well as shedding light on the physiological requirements of mitochondrial calcium uniporter components, my work therefore argues for a subset of neurodegenerative conditions being amenable to modification of mitochondrial calcium influx. Further work should build on this potential target to attempt to ameliorate these otherwise intractable diseases.

Acknowledgements

I am indebted to the MRC Doctoral Training Programme for ensuring that completing this PhD did not result in my being financially indebted. The departmental travel fund of the Mitochondrial Biology Unit also allowed me to participate in several conferences and training programmes; all were fruitful both for the project and for my professional growth.

Without Dr. Alexander Whitworth, this PhD would not have been academically, financially, or indeed emotionally viable. Thank you for tailoring your style of supervision to my needs, and for knowing them better than I often did. I have learned a lot by your example: the logic that shapes the questions to be asked, the research methods to answer them, and the management to see that they do get answered in the end. I am confident that these lessons and skills will benefit me in years to come.

My advisor, Professor Massimo Zeviani, warmly welcomed me into the Unit, and I thank him for his encouragement and constructive discussions of the project. I have benefitted from his leadership of the MBU, and I wish him every success in his new role.

The people of the Whitworth lab have made my second home a place worth being. Roby, the project is all the better for your involvement. Your biochemical expertise was a perfect match for my greenhorn status, and you have taught me much. Álvaro, you seemed to have endless patience and I picked up many things with a lot less stress than I might have done as a result. Thanks for putting up with me in California – I hope you had as much fun as I did! Simo, you were a great person to start alongside, and I have always looked up to the way you think about science. Victoria, I am grateful for you always finding time for me, and I hope I have learned to cut through to the key point half as well as you can. Leonor, your formidable work ethic ensured there was always a friendly face in the lab, and our chats inspired new directions for the project on a surprisingly regular basis. Sarah, Clare, and now Ana, the lab (let alone my project) could not function without you. Juliette and Wing Hei, I apologise for being so bad at peeling oranges, but I hope I have helped you with the trials of your own studies; you have with mine. Aitor and Natalie, you have been incredibly approachable in and out of the lab, and I am grateful for all the chances we've had to talk. Ivana, Jasper, Federica, and Sofia, you may not have been here long, but you made a true scientific and personal impact, on my work and myself.

I am incredibly grateful to the somewhat freeform thesis formatting guidelines of the University of Cambridge, allowing my Acknowledgements to spill over into a second page without major academic rebuke. I imagine this will result in some archaic ceremonial slight at the appropriate time.

To Mum, Dad, Martha, my family who are too numerous to include by name, and my friends, of which I also have a few. I am not entirely sure what you all made of this potentially foolhardy endeavour, but I cannot remember a single instance of anything but unconditional love and support, much as it has been for any other aspect of my life. I know that such acceptance is a rarity, and it straightens my back every day.

Specific thanks are due to my Mum, who painstakingly proofread about two hundred pages of (to her, hopefully not the examiners) mainly gibberish to find the tautologies, typos, and terribly contrived alliterative devices. Points will have to be deducted for not teaching me how to peel an orange though.

Finally, to David, for everything.

Table of Contents

List of Figures

List of Tables

List of Abbreviations

$\Delta\psi_m$:	Mitochondrial membrane potential
ΔpH:	pH difference across mitochondrial membrane
$[Ca^{2+}]_c$:	Cytoplasmic calcium concentration
$[Ca^{2+}]_m$:	Mitochondrial calcium concentration
$[Na^{+}]_m$:	Mitochondrial sodium concentration
AD:	Alzheimer's disease
APP:	Amyloid precursor protein
CaM:	Calmodulin (calcium-modulated protein)
CCCP:	Carbonyl cyanide *m*-chlorophenylhydrazone
CsA:	Cyclosporin A
CRISPR:	Clustered regularly interspersed palindromic repeats
DISC:	Death-inducing signalling complex
ER:	Endoplasmic Reticulum
ERMES:	Endoplasmic reticulum-mitochondria encounter structure
$FADH_2$:	Flavin adenine dinucleotide (reduced)
FCCP:	Carbonyl cyanide-p-trifluoromethoxyphenylhydrazone
HDR:	Homology directed repair
IMM:	Inner mitochondrial membrane
IMS:	Intermembrane space
IP3:	Inositol-1,4,5-triphosphate
IP3R:	Inositol-1,4,5-triphosphate receptor
LINE:	Long interspersed nuclear elements
LTR:	Long terminal repeat
MOMP:	Mitochondrial outer membrane permeabilization
MPPP:	1-methyl-4-phenyl-4-propionoxypiperidine
mPTP:	Mitochondrial permeability transition pore
MPTP:	1-methyl-4-phenyl-1,2,5,6-tetrahydropyridine
NADH:	Nicotinamide adenine dinucleotide (reduced)
NHEJ:	Non-homologous end joining
Nnt:	Nicotinamide nucleotide transhydrogenase
OMM:	Outer mitochondrial membrane
PAM:	Protospacer adjacent motif
PD:	Parkinson's disease
qRT-PCR:	Quantitative Reverse Transcription PCR
RaM:	Rapid mode (of calcium uptake)
RFLP:	Restriction fragment length polymorphism
ROS:	Reactive oxygen species
RuR:	Ruthenium red
RyR:	Ryanodine receptor
SOCE:	Store-operated calcium entry
SINE:	Short interspersed nuclear elements
SNCA:	α-synuclein
SNpc:	Substantia nigra *pars compacta*
TCA cycle:	Tricarboxylic acid cycle (Krebs cycle)
TE:	Transposable element
UAS:	Upstream activating sequence
UPS:	Ubiquitin-proteasome system

1. Introduction

First identified in the late 19th Century from advances in optical microscopy and tissue staining, the mitochondrion (or initially 'bioblast') was first described as intracellular 'elementary organisms', mediating essential processes (Altmann, 1890; Ernster and Schatz, 1981). Though largely unsupported by experimental evidence at the time, these predictions would prove remarkably prescient. During the following century, the mitochondrion has increasingly been found to play a crucial role in essential biological pathways and is now widely regarded to have arisen from an endosymbiotic event between the ancestral eukaryote and a prokaryote most closely related to contemporaneous α-proteobacteria (reviewed in Gray, 1999).

Though mitochondria act generally as a hub of metabolic signalling, they are perhaps best known specifically for their role in cellular respiration. Shortly after their discovery, key respiratory enzymes were isolated from mitochondrial fractions, beginning with Complex II and IV (Hogeboom, Claude and Hotch-Kiss, 1946), and within five years, other oxidative phosphorylation complexes, enzymes of the TCA cycle, and β-oxidation pathway (Kennedy and Lehninger, 1949; Lehninger, 1949). Mechanisms for oxidative phosphorylation originally revolved around the so-called 'high-energy intermediate' of respiration (Slater, 1953), but this would prove elusive. Instead, ADP phosphorylation is now understood to be the product of the electrochemical gradient established through the proton pumping action of the respiratory chain (Mitchell, 1961).

The presence of non-nuclear DNA within mitochondria provided compelling evidence to support their bacterial origin (Nass and Nass, 1963). Mitochondrial DNA encodes core proteins of the respiratory chain, and its mutations are notable both for their unique inheritance pattern, and wide-ranging and variable phenotypic consequence, due to tissue-specific heteroplasmy. Furthermore, mitochondrial dysfunction is being demonstrated to contribute to an ever-growing list of genetic disorders linked to nuclear DNA (reviewed in Vafai and Mootha, 2012). In addition to underlining the importance of this organelle, such evidence provides an opportunity to revisit our understanding of the aetiology and pathobiology of these conditions, and to construct novel therapeutic strategies.

1.1. Mitochondrial calcium dynamics

The divalent cation calcium is ubiquitous in biology. As well as an enzyme cofactor, it acts as a secondary messenger for a wide array of signal transduction pathways. Additionally, cellular and organellar membrane potentials are influenced by the flux of calcium, particularly in the case of neurons, where voltage-gated channels provide the mechanistic basis for action potential generation.

Initial observations of heart tissue homogenates demonstrated the majority of calcium was concentrated in the mitochondrial fraction (Slater and Cleland, 1953). However, mitochondrial biochemistry was preoccupied with the search for the high-energy intermediate, and interest in the field did not build until the observation that calcium could reversibly uncouple respiration (reviewed in Carafoli, 2003). This led to two seminal papers describing the accumulation of calcium inside mitochondria, to a level far beyond previous expectations (DeLuca and Engstrom, 1961; Vasington and Murphy, 1962). With the field at this burgeoning stage, it was still possible to determine from inhibitor studies that mitochondrial calcium accumulation competed with ATP synthesis for respiratory chain-derived energy. Additionally, the discovery of matrix calcium-phosphate salts laid the foundation for mitochondria as buffers of cytosolic calcium (Rossi and Lehninger, 1963). The basic properties of mitochondrial calcium transport were established over the following decade, but during this time mitochondrial calcium dynamics was considered in terms of its effects on cytosolic calcium fluxes.

1.1.1. Buffering of cytosolic calcium transients

The uptake of calcium necessarily reduces the local extramitochondrial concentration. Therefore, spatial control of mitochondria, as well as their uptake machinery, can be exploited to shape extramitochondrial calcium transients. For example, calcium release from the endoplasmic reticulum (ER) occurs primarily via the inositol-1,4,5-triphosphate receptor (IP3R). IP3R-mediated calcium release is activated or inhibited by the local calcium concentration to a maximal activation at 0.2 µM (Bezprozvanny, Watras and Ehrlich, 1991). Further pharmacological studies in *Xenopus* oocytes confirmed that inhibition of mitochondrial calcium uptake modulated IP3R activity (Jouaville *et al.*, 1995), demonstrating that mitochondria could shape ER calcium transients.

In polarised cells, mitochondrial positioning is even more tightly controlled to provide calcium buffering capacity. Pancreatic acinar cells require a high local calcium concentration for exocytosis of secretory granules. Mitochondria surround these apical pole regions, forming a 'firewall' that confines the local rises in calcium concentration to protect the nucleus-containing basolateral cell region (Tinel *et al.*, 1999). Application of carbonyl cyanide *m*-chlorophenylhydrazone (CCCP), which depolarises the mitochondrial membrane potential ($\Delta\Psi_m$) thereby removing the driving force for mitochondrial calcium influx, blocked mitochondrial calcium buffering and caused the local rises in cytoplasmic calcium to spread throughout the cell.

Neurons, some of the most morphologically elaborate cells, also use mitochondrial positioning to shape calcium currents. In the synapse, mitochondrial calcium uptake maintains a low cytoplasmic concentration at rest, but also potentiates evoked synaptic transmission by avoiding inhibition of presynaptic calcium channels (Medler and Gleason, 2002). Similarly, mitochondrial calcium uptake avoids depletion of synaptic vesicles during tonic stimulation of motor neurons, which sustains phasic neurotransmitter release (David and Barrett, 2003). In neurons, synaptic activity induces alterations in cytoplasmic calcium that propagate to the nucleus, inducing the transcription factor Npas4 via calmodulin (CaM) kinase to repress genes associated with mitochondrial uptake (Qiu *et al.*, 2013). This allows for reciprocal control of cytoplasmic and mitochondrial calcium dynamics.

1.1.2. Tricarboxylic acid (TCA) cycle regulation

One of the most fundamental metabolic pathways, exploited by all aerobic organisms, is the tricarboxylic acid (TCA), or Krebs cycle. Here, acetate is oxidised to yield carbon dioxide, while the reducing equivalents NADH and $FADH_2$ fuel the respiratory chain. This is coupled with pyruvate oxidation, or the link reaction, which connects the TCA cycle to glycolysis. In the rate-limiting steps of the TCA cycle, the isocitrate dehydrogenase enzyme catalyses the oxidation and subsequent decarboxylation of isocitrate to α-ketoglutarate via an oxalosuccinate intermediate, generating NADH in the process. Next, α-ketoglutarate dehydrogenase catalyses a similar reaction, combining α-ketoglutarate and thiolated Coenzyme A by oxidative decarboxylation to form succinyl-CoA, also generating NADH.

Initial studies of mitochondrial calcium transport were concerned with the effects of mitochondrial dynamics on the wider cellular context, but direct effects on mitochondria themselves soon emerged, beginning with the TCA cycle. The activity of isocitrate and α-ketoglutarate dehydrogenases were found to directly bind calcium via EF-hand domains, which stimulated enzymatic activity (Denton, Richards and Chin, 1978; McCormack and Denton, 1979). Similarly, pyruvate dehydrogenase, the enzyme responsible for pyruvate oxidation, is also regulated by calcium though by a more indirect route. An inhibitory phosphate group is removed via the PDP1 enzyme, which is activated through calcium binding to its EF-hands. The regulation of these enzymes provides a key control point for supplying oxidative phosphorylation, which allows for metabolic supply and demand to be coupled. In the pancreatic acinar cells outlined in Section 1.1.1, rises in apical pole Ca^{2+} are buffered by mitochondria, which stimulates ATP production, in turn facilitating exocytosis.

TCA cycle regulation by calcium is not fully conserved. Invertebrates such as the locust and blowfly have been demonstrated to possess isocitrate and α-ketoglutarate dehydrogenases that are insensitive to calcium (McCormack and Denton, 1981). It is unclear whether related genera such as *Drosophila* are similarly insensitive, and if the TCA cycle might still be under the control of mitochondrial calcium simply via a different enzyme, but nevertheless warrants caution.

1.1.3. Calcium and cell death

Apoptosis, the process of controlled cellular degradation, is essential for developmental and physiological function. Multiple apoptotic pathways exist, with distinct stimuli, yet they converge on initiator caspases, that in turn activate executioner caspases, which begin degradation. For example, the mammalian extrinsic apoptotic pathway begins with the recognition of the presence or absence of extracellular ligands by specific plasma membrane receptors. This promotes the formation of the death-inducing signalling complex (DISC) and subsequent activation of the initiator caspase 8 (Kischkel *et al.*, 1995), and corresponding activation of the executioner caspases 3 (Stennicke *et al.*, 1998) and 7 (reviewed in Lamkanfi and Kanneganti, 2010).

Mammalian intrinsic apoptosis centres on the BCL2 family, which includes pro- and anti-apoptotic proteins. Apoptotic stimuli perturb this balance, causing BAX and BAK to assemble in the outer mitochondrial membrane in large pores, leading to mitochondrial outer membrane permeabilization (MOMP) (reviewed in Tait and Green, 2010). This causes release of pro-apoptotic species such as cytochrome c into the cytosol, where it interacts with APAF1 and pro-caspase 9, and the resulting apoptosome activates caspase 9 (Li *et al.*, 1997), with downstream maturation of executioner caspases 3 and 7 (reviewed in Slee *et al.*, 1999). So, although induced by different stimuli through separate mechanisms, both intrinsic and extrinsic pathways converge on the caspase cascade, leading to similar morphological features that group them together as apoptosis.

A separate mitochondrial cell death pathway centres around the mitochondrial permeability transition, triggered by a sustained high mitochondrial calcium concentration. The mitochondrial permeability transition pore (mPTP) allows for solute passage up to ~1.5 kDa (Haworth and Hunter, 1979), and this dramatic increase in mitochondrial permeability causes osmotic swelling of the organelle (Hunter, Haworth and Southard, 1976). The resulting loss of membrane potential ablates ATP production, triggering necrotic processes.

Other forms of cell death exist, but the three outlined above are perhaps the most well studied. Calcium dynamics impinge on both extrinsic and intrinsic apoptotic pathways. Caspase 8 activity is regulated in a calcium-dependent manner (Jo *et al.*, 2004). Cytoplasmic calcium inhibits apoptosome formation, thereby blocking pro-caspase 9 maturation (Bao *et al.*, 2007). More directly, high mitochondrial calcium is the prototypical trigger for mPTP opening (Hunter and Haworth, 1979). Though MOMP and mPTP opening are independent events, some degree of interconnectivity is suggested by the observation that BCL2 family proteins modulate calcium leak from the ER via the IP3R (reviewed in Gross and Katz, 2017). Thus, in addition to vital roles in mitochondrial function and the regulation of cellular calcium signalling, mitochondrial calcium fluxes are key in cell death processes. It is therefore vital to fully understand how mitochondria transport calcium, but as will be discussed, the molecular entities responsible for mitochondrial calcium uptake have only recently begun to be characterised.

1.2. The mitochondrial calcium uniporter

1.2.1. Pre-molecular history of mitochondrial calcium uptake

Studies of calcium uptake in isolated mitochondria began in the 1960s (DeLuca and Engstrom, 1961; Vasington and Murphy, 1962), and a wealth of evidence began to accumulate on the nature of mitochondrial calcium transport mechanisms. However, the field fell into obscurity for several decades as *in vivo* evidence began to suggest only nanomolar scale calcium could be liberated from mitochondria (Somlyo, Bond and Somlyo, 1985), and that this organelle displayed an order of magnitude lower affinity than the ER, which became the focus of calcium signalling research. However, radiolabelled Ca^{2+} was preferentially incorporated into mitochondria rather than ER fractions, and was disrupted by chemical uncouplers, demonstrating that energised mitochondria could uptake large amounts of calcium *in vivo* (Carafoli, 1967). The discrepancy between these data was eventually reconciled following the development of a live mitochondrial calcium concentration ($[Ca^{2+}]_m$) sensor: mitochondrially-targeted aequorin (Rizzuto *et al.*, 1992). This revealed calcium released from the ER was taken up by mitochondria with dynamics that did not correspond to the rise in the mean cytoplasmic calcium concentration ($[Ca^{2+}]_c$), and direct perfusion of cells with a physiological concentration of calcium failed to evoke mitochondrial uptake (Rizzuto *et al.*, 1993). This evidence formed the 'microdomain' theory, in which high local $[Ca^{2+}]_c$ hotspots stimulate the low affinity mitochondrial uptake.

1.2.2. Inter-organelle calcium signalling

Many proteins are calcium-responsive, but to different ion concentrations, and must be activated in different contexts. To allow for this fine spatiotemporal control, calcium is compartmentalised across impermeable membranes, so that its flux can be controlled by the activity of specific channel complexes. The concentration gradient can be profound, for example at the plasma membrane, where the concentration of calcium in the bulk cytosol (~100 nM) is maintained 10,000-fold lower than in the extracellular space (~1 mM) (Phillips and Voeltz, 2016), which allows for fast and efficient signalling. Similarly, as the classical intracellular calcium store, the endoplasmic reticulum maintains a steep concentration gradient with the surrounding cytoplasm. Multiple channel families mediate ER calcium influx/efflux to provide homeostatic control of lumenal levels and signal integration.

To maintain intracellular calcium stores, extracellular calcium is taken into the cell via store-operated calcium entry (SOCE). This was observed in electrophysiological studies for many years before the identification of the STIM and ORAI proteins, now known to be the classical mechanism for SOCE (Liou *et al.*, 2005; Roos *et al.*, 2005; Feske *et al.*, 2006; Vig *et al.*, 2006; Zhang *et al.*, 2006). Here, STIM senses ER calcium depletion through EF-hand domains and translocates to ER-plasma membrane junctions, where ORAI channels are recruited and induce cytosolic calcium uptake. Endoplasmic reticulum stores are then replenished via SERCA pumps, a family of P-type ATPases that utilise the energy from ATP hydrolysis to transport calcium against its concentration gradient into the reticulum lumen in a 1:2 ATP/Ca^{2+} ratio. Vertebrates have three paralogs, SERCA1-3, that are differentially expressed across cell types, as are the corresponding splice variants, adding complexity to ER calcium uptake (reviewed in Vandecaetsbeek *et al.*, 2011).

The endoplasmic reticulum features two primary active mechanisms of calcium extrusion: the ryanodine receptor (RyR) and inositol-1,4,5-triphosphate receptor (IP3R) families. Both feature three mammalian isoform (with a single of each conserved in *Drosophila melanogaster*). Ryanodine receptors are a class of large (over 2 MDa) homotetrameric ion channel. The interaction between calcium and specific RyR high- and low-affinity binding sites allows for channel activation at micromolar cytosolic calcium concentrations and inhibition in the millimolar range (reviewed in Lanner *et al.*, 2010). RyR-mediated calcium release therefore auto-amplifies up to a limit, establishing a cytosolic calcium wave crucial for excitation-contraction coupling in skeletal and cardiac muscle. Such waves can be propagated from an IP3R-mediated calcium spike, and the cleavage of membrane-bound phosphatidylinositol 4,5-bisphosphate into diacyl glycerol and the free cytosolic IP3R ligand inositol-1,4,5-triphosphate (IP3) bridges intracellular signalling with ER calcium release. Similar to ryanodine receptors, IP3R features both high affinity activating calcium binding sites and low affinity inhibitory sites, and the effect of IP3 is to allosterically remove this inhibition, making calcium the true IP3R agonist (Mak, McBride and Foskett, 1998).

In addition to active processes, passive leak of ER lumenal calcium has been observed. The mediator of this current remains elusive, with several proposed candidates (reviewed in Camello *et al.*, 2002). More contemporary proposals include proteins of the TMBIM family (Chang *et al.*, 2014) and the translocon-ribosome complex (Lomax *et al.*, 2002; Van Coppenolle *et al.*, 2004). Regardless, passive ER calcium leak serves to balance the actions of SERCA under resting physiological conditions, as evidenced from classical experiments pharmacologically inhibiting SERCA with thapsigargin, which depletes ER calcium stores via leak currents and serves as a model for ER stress and unfolded protein response induction (reviewed in Oslowski and Urano, 2011).

Following the discovery of cellular calcium microdomains, it was observed that the ER and mitochondrial networks are in apposition at sites of mitochondrial calcium uptake (Rizzuto *et al.*, 1998). Their functional relevance was confirmed by the artificial manipulation of ER-mitochondrial distance, which influenced the uptake rate (Csordás *et al.*, 2010). Presently, contact sites have been characterised between myriad organelles, allowing for lipid exchange, ion transfer, and organelle biogenesis (reviewed in Helle *et al.*, 2013). ER calcium release is categorised according to its magnitude and dispersal, from small localised 'blips' from individual channels, to 'puffs' arising from local clusters, to 'waves' that cover inter-cluster distances (Smith *et al.*, 2009). Receptor clustering increases the probability of calcium puff formation (Dickinson, Swaminathan and Parker, 2012), and IP3R clusters are enriched at organelle contact sites (Rizzuto *et al.*, 2009; Atakpa *et al.*, 2018), allowing for specific control of ER calcium transfer.

Membrane contact sites are facilitated by tethering complexes, which bring the two organelles into proximity. Between the ER and mitochondria, a complete tethering complex termed ERMES has been characterised in yeast (Kornmann *et al.*, 2009). Several mammalian tethers have been proposed, but are still putative (reviewed in Phillips and Voeltz, 2016). For example, mitofusin 2 was shown to mediate ER-mitochondrial calcium transfer, though this was not without controversy (de Brito and Scorrano, 2008; Filadi *et al.*, 2015; Naon *et al.*, 2016). Additionally, ER-resident VAPB and mitochondrial PTPIP51 have been reported to form contact sites with relevance for calcium signalling (Stoica *et al.*, 2014). GRP75 has also been suggested to mediate ER-mitochondrial contacts to facilitate calcium transfer by binding VDAC1 and IP3R (Schwarzer *et al.*, 2002; Szabadkai *et al.*, 2006). Recently, PDZD8 was identified as a paralog (Wideman *et al.*, 2018) of the ER-bound component of the ERMES complex, Mmm1 (Hirabayashi *et al.*, 2017). Pending replication, this would provide the basis to discover additional components of the metazoan complex, as well as facilitating *in vivo* manipulation of ER-mitochondrial contact sites.

1.2.3. Features of the mitochondrial calcium uniporter

The mitochondrial calcium uniporter, a unidirectional transport complex, had long been proposed based on radiolabelling experiments and the use of pharmacological inhibitors such as the ruthenium red dye (Vasington *et al.*, 1972). Ruthenium red, being a mixture of compounds, is quite non-selective, and the isolation of the Ru360 constituent enabled more potent and selective inhibition of the uniporter (Ying *et al.*, 1991). However, despite these studies it remained unclear if the biochemical species responsible for the process was a true carrier protein, or an ion channel. Electrophysiological studies, patch-clamping the inner mitochondrial membrane, demonstrated the presence of an inwardly rectifying, highly selective mitochondrial calcium current (Kirichok, Krapivinsky and Clapham, 2004). The high current density confirmed that the mitochondrial calcium uniporter is mediated by an ion channel, driven by the electrochemical gradient. An extremely high affinity for Ca^{2+} was reported, seemingly in contrast with the insensitivity of mitochondria to low calcium concentrations.

Mitochondrial calcium entry dissipates the membrane potential, but also stimulates matrix dehydrogenases to generate reducing equivalents to feed the respiratory chain. Complexes I, III, and IV activity increases the proton gradient, thereby increasing ATP production. To rebalance ΔpH and $\Delta\Psi_m$, some of the gradient is diverted to export calcium from mitochondria, through the sequential actions of the mitochondrial Na^+/H^+ and Na^+/Ca^{2+} exchangers. An outline of this mitochondrial ion transfer circuit is given in Figure 1.

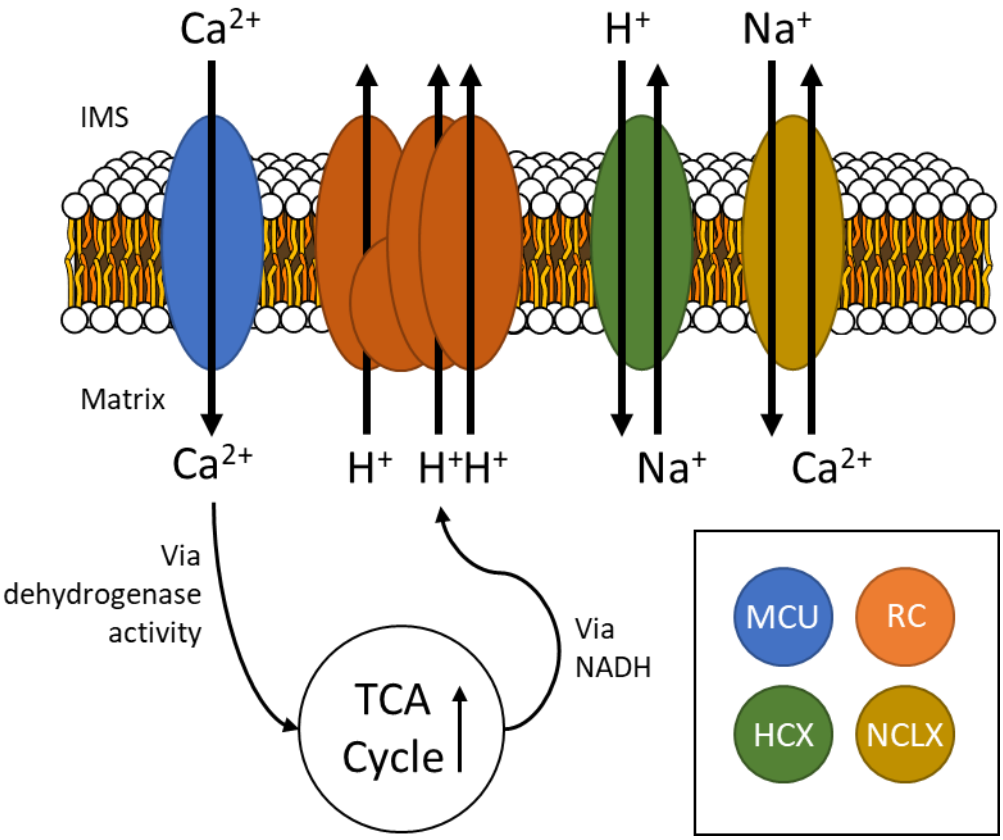

Figure 1. Schematic of mitochondrial calcium cycling. MCU: mitochondrial calcium uniporter, RC: respiratory chain (ion transfer by Complex I, III, and IV), HCX: mitochondrial H^+/Ca^{2+} exchanger, NCLX: mitochondrial Na^+/Ca^{2+} exchanger. Figure adapted based on (Boyman *et al.*, 2013).

1.2.4. Discovery of MCU complex components

The first molecularly characterised component of the uniporter complex was the regulator MICU1, in 2010 (Perocchi *et al.*, 2010). This served as a platform for the identification of the pore itself, MCU, a year later (Baughman *et al.*, 2011; De Stefani *et al.*, 2011). This was quickly followed by the other gatekeepers MICU2 and MICU3 (Plovanich *et al.*, 2013), a dominant-negative subunit MCUb (Raffaello *et al.*, 2013), and EMRE (Sancak *et al.*, 2013), which is essential for *in vivo* channel activity. The pace of these discoveries, by contrast to the pre-molecular era, underscores the importance of the initial discovery of MICU1, and the power of comparative genomics and other bioinformatic approaches in attacking otherwise intractable problems.

Additional reported uniporter components remain controversial or exist in isolated clades. MCUR1 was first identified in 2012 (Mallilankaraman, Cárdenas, *et al.*, 2012) as an additional regulatory uniporter subunit, based on its knockdown ablating mitochondrial calcium uptake. Subsequent work attributed this instead to defective cytochrome *c* oxidase assembly (Paupe *et al.*, 2015). Complicating matters, MCUR1 has been reported to bind MCU and EMRE as a molecular scaffold (Tomar *et al.*, 2016), as well as regulating the mPTP threshold when exogenously expressed in *D. melanogaster* cells (Chaudhuri *et al.*, 2016). Trypanosomes, where MCUb does not act in a dominant-negative fashion, have two additional MCU paralogs, termed MCUc and MCUd, which do shape mitochondrial calcium currents (Huang and Docampo, 2018).

1.2.5. MCU

The pore-forming component of the uniporter is an approximately 40 kDa two-pass inner mitochondrial membrane protein (Baughman *et al.*, 2011; De Stefani *et al.*, 2011), with both termini facing the matrix side (Baughman *et al.*, 2011). The loop between the two transmembrane domains in the intermembrane space features a DIME motif, which mutagenesis studies showed was essential for channel activity, as well as inhibition by ruthenium-based compounds (Baughman *et al.*, 2011).

The structure of MCU has been under intense investigation in recent years, as it would facilitate the design of new, more specific and potent uniporter (ant)agonists, as well as yielding insights into global uniporter stoichiometry and organisation. An initial NMR/EM-based model proposed a pentameric organisation, running contrary to the previous literature (Oxenoid *et al.*, 2016). However, a harsh detergent was used prior to crosslinking when determining this pentamer formation (as noted by Baradaran *et al.*, 2018), which was then used to constrain the EM data, rather than this arising as a feature of the model directly. Furthermore, the protein used lacked the N-terminal domain, which may fold and assemble differently. Four back-to-back papers were recently published using full-length MCU and agree on a tetrameric organisation (Baradaran *et al.*, 2018; Fan *et al.*, 2018; Nguyen *et al.*, 2018; Yoo *et al.*, 2018), with a representative example given in Figure 2. Interestingly, these structures do not resemble mitochondrial carriers or typical Ca^{2+} channels, instead bearing some resemblance to ionotropic glutamate receptors (Yoo *et al.*, 2018). The structure of full-length *H. sapiens* MCU-EMRE has also emerged, and confirms the tetrameric organisation, as well as suggesting that uniporter complexes form dimers that may influence their sub-organellar localisation (Wang *et al.*, 2019).

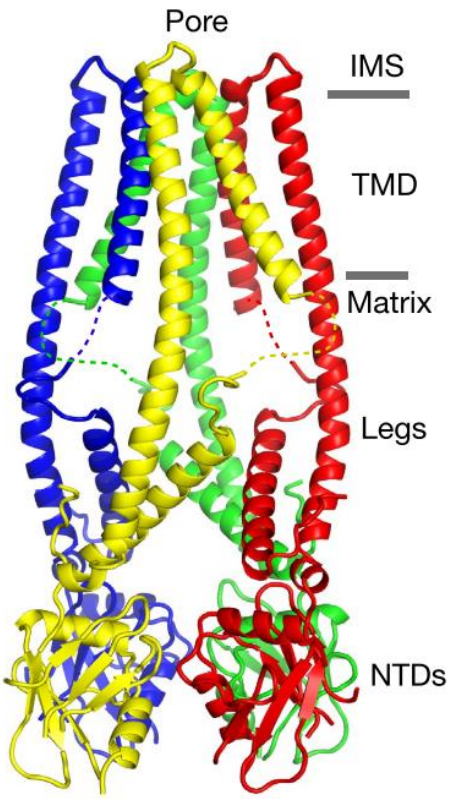

Figure 2. Representative MCU Cryo-EM structure, in this case *Cyphellophora europaea*, reproduced from Baradaran *et al.*, 2018. IMS: intermembrane space, TMD: transmembrane domain, NTDs: N-terminal domains.

Ruthenium based inhibitors of the uniporter have been used prior to the discovery of MCU but suffer from poor selectivity. The molecular identification of uniporter components enabled a wide-scale screen of clinically approved small molecules in a reconstituted yeast system, yielding mitoxantrone, which acts as a reversible, selective inhibitor of uniporter current (Arduino *et al.*, 2017). Similarly, high-throughput screening of small molecules uncovered a cell-permeable inhibitor termed DS16570511 that inhibits uniporter activity in isolated mitochondria and HEK293A cell lines (Kon *et al.*, 2017). A refinement of the ruthenium-based inhibitors has been recently announced (Woods *et al.*, 2019), with higher potency, but would still suffer from specificity issues.

1.2.6. MCUb

Sequence analysis of *MCU* highlighted a vertebrate-restricted related gene with roughly 50% similarity, *CCDC109B*, later termed *MCU*b (Raffaello *et al.*, 2013). Due to substitutions in the pore-forming region, MCUb does not form calcium-conductive channels in the inner mitochondrial membrane, and channels with higher MCUb:MCU stoichiometry accordingly have lower calcium transport capacity, in a dominant negative process (Raffaello *et al.*, 2013). This provides an explanation for the tissue-specific variance in uniporter activity, notably lower in the mammalian heart (Fieni *et al.*, 2012), where MCUb shows ~3-fold higher expression compared to skeletal muscle (Raffaello *et al.*, 2013).

In vivo studies of MCUb have recently begun with the generation of a knockout cell line and a mouse model expressing MCUb in a cardiomyocyte-restricted tamoxifen-inducible fashion (Lambert *et al.*, 2019). As expected, MCUb knockout cells displayed increased mitochondrial buffering of agonist-evoked cytosolic calcium transients, but interestingly also lead to increased expression of MCU and EMRE at the protein level, suggesting a synergistic action on MCU activity. Cardiomyocyte-restricted expression of MCUb reduced infarct size following left coronary artery ligation, and reduced mitochondrial swelling, which is indicative of mPTP opening, but also transiently impaired spare respiratory capacity and cardiac contractile reserves. These models will be valuable for further investigation of the *in vivo* contribution of this vertebrate uniporter component in other biological processes and pathological models.

1.2.7. EMRE

EMRE is a small single-pass membrane protein of approximately 11 kDa in humans. In addition to its transmembrane helix it features a highly acidic C-terminal region. The exact function of this domain is debated and depends on the overall orientation of the protein. The C-terminal domain has been proposed to reside on the matrix side of the IMM, where it would reportedly serve as a Ca^{2+} sensor (Vais *et al.*, 2016). More studies support the C-terminus on the side of the intermembrane space (IMS), however (Tsai, M-F *et al.*, 2016; Tsai, C-W *et al*., 2017; Yamamoto *et al.*, 2016), and arguably have stronger evidence for this claim in the form of protease degradation assays. Here the function of the C-terminus appears to be in coordinating MCU-MICU1 binding, as deletion of this region leads to increased calcium uptake at low $[Ca^{2+}]_c$ without an altered response to high $[Ca^{2+}]_c$, consistent with MICU1 loss (Tsai *et al.*, 2016).

Though human MCU protein can conduct calcium currents in planar lipid bilayers, reconstitution experiments demonstrated that *in vivo* EMRE is required for metazoan channel activity (Kovács-Bogdán *et al.*, 2014). Reconstitution experiments demonstrated that the CC1 and CC2 coiled-coil domains of MCU are essential for uniporter activity regardless of the presence of EMRE (Yamamoto *et al.*, 2019), and recent structures of human MCU-EMRE complexes showed that the CC2 helices incorporate a juxtamembrane loop that acts as an exit gate for the channel (Wang *et al.*, 2019). Also, this recent study suggests a mechanistic basis for the MCU-EMRE interaction: EMRE binds TM1 and TM2 of MCU, and an N-terminal β-hairpin pulls the CC2 helices of MCU away from the pore exit, with their accompanying juxtamembrane loop. This EMRE-induced conformational change allows ions to freely pass into the vestibule. A graphical overview of this model is given in Figure 3.

Additionally, a study based on chimeric MCU from *Dictyostelium discoideum* (which is EMRE-independent) and *H. sapiens* has confirmed that EMRE directly binds TM1 and TM2 of MCU, and identified a ten amino acid stretch that confers EMRE dependence (MacEwen *et al.*, 2019, preprint). Rather than the binding site of the β-hairpin, this motif appears to map to the juxtamembrane loop itself, providing strong agreement for this being the key region for EMRE regulation of the uniporter.

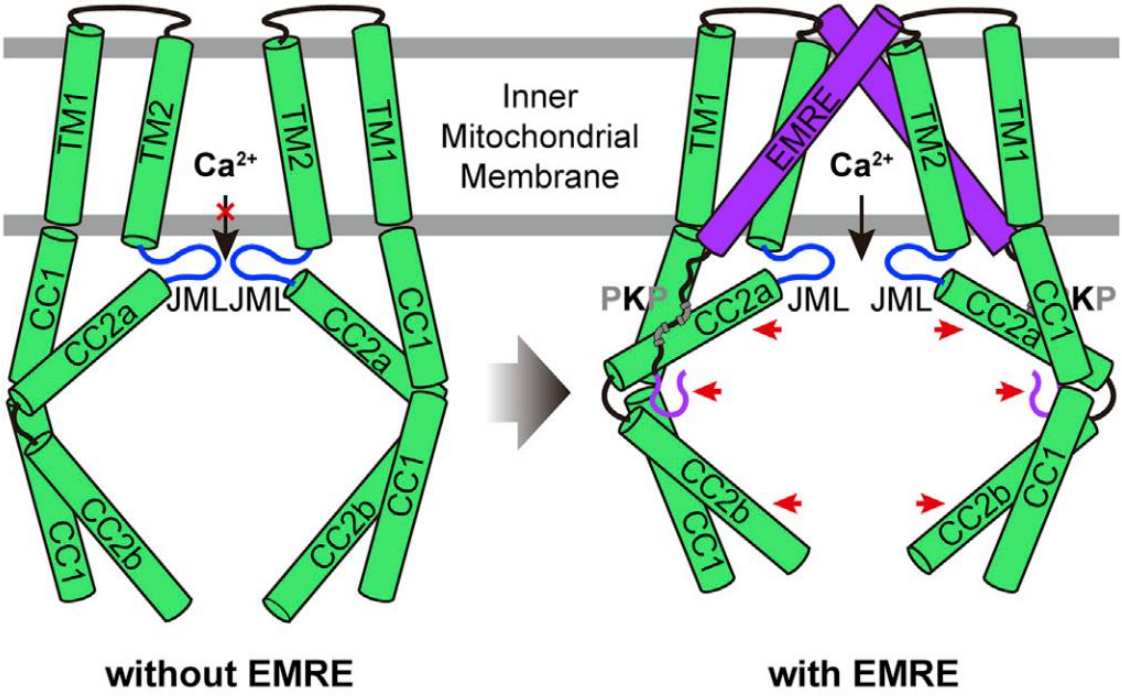

Figure 3. Structural model for EMRE-CC2-JML based regulation of MCU activity, reproduced from Wang *et al.*, 2019. JML: juxtamembrane loop,

The role of EMRE in bridging MCU and MICU1 been shown to lead to an important consequence in the form of the Hook or prozone effect (König *et al.*, 2016; Tsai *et al.*, 2017). An excess of EMRE will lead to MCU-EMRE and MICU1-EMRE dimers that cannot bind each other. The resulting excess of MCU-EMRE forms dysregulated channels and leads to excessive mitochondrial calcium uptake and overload. Thus, the level of EMRE is a key control point for the appropriate expression of the entire uniporter. The m-AAA protease AFG3L2 degrades EMRE to counteract the prozone effect and has been linked to spinocerebellar ataxia type 28 and hereditary spastic paraplegia type 7, suggesting an association between the uniporter and neurological and neurodegenerative disorders.

1.2.8. MICU1

The apparent insensitivity of mitochondria to cytosolic calcium seems at odds with the high affinity of MCU, but the identification of MICU1, the first member of the uniporter to be discovered (Perocchi *et al.*, 2010), addressed this question. A 54 kDa peripheral inner membrane protein, MICU1 contains several EF-hand domains, which coordinate calcium, allowing it to sense the level of the ion. These domains were initially reported facing the matrix side of the membrane (Mallilankaraman, Doonan, *et al.*, 2012), but subsequent work demonstrates the opposite orientation, with the EF-hands acting as calcium sensors in the intermembrane space (Csordás *et al.*, 2013).

MICU1 serves as a 'gatekeeper' for the uniporter, keeping the channel closed when the level of extramitochondrial calcium is low, and opening the pore when the EF-hands are occupied (see Figure 4). This biphasic regulation is crucial for the high affinity uniporter to respond specifically to large calcium transients, allowing it to rapidly integrate signals at mitochondrial contact sites whilst reducing the potential for matrix Ca^{2+} overload and resulting permeability transition. Mammalian MICU1 forms heterodimers with MICU2 via a Mia40-induced disulphide bond (Petrungaro *et al.*, 2015), that regulates the activation properties of the uniporter (see Section 1.2.9).

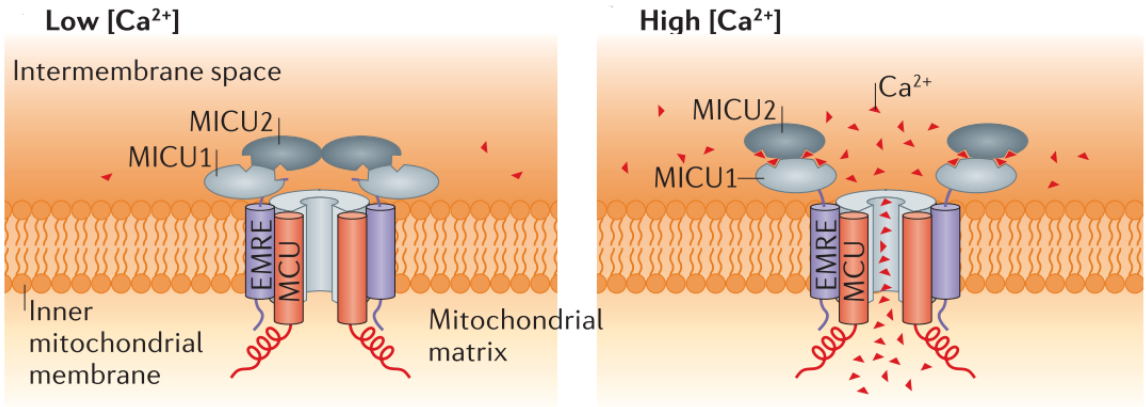

Figure 4. Ca^{2+}/MICU1-dependent uniporter regulation, reproduced from Kamer and Mootha, 2015.

The physical nature of the MICU1-MCU interaction remained elusive until recently, when two studies demonstrated that MICU1 directly binds the aspartate ring formed from the DIME motif of MCU (Paillard *et al.*, 2018; Phillips, Tsai and Tsai, 2019). These works differ in their assignment of the binding site on MICU1, either a DIME-interacting domain comprising K438, R440, and R443 (Paillard *et al.*, 2018), or the R119 and R154 arginine residues (Phillips, Tsai and Tsai, 2019). In both models, the obstruction of the aspartate ring of MCU mimics the action of ruthenium-based inhibitors (Cao *et al.*, 2017).

The human MICU1 splice variant MICU1.1 binds calcium much more efficiently than its counterpart, and when incorporated into the uniporter increases sensitivity to low cytoplasmic calcium concentrations (Vecellio Reane *et al.*, 2016). MICU1.1 is specifically expressed in skeletal muscle, so allows mitochondrial calcium uptake to be enhanced to match the high ATP demands of this tissue.

MICU1 has also been demonstrated to bestow the uniporter with selectivity for Ca^{2+} over Mn^{2+} (Kamer *et al.*, 2018; Wettmarshausen *et al.*, 2018). In human cells and *C. elegans*, ablation of MCU increased Mn^{2+} tolerance, whilst MICU1 knockout cells were more sensitive (Kamer *et al.*, 2018). In the uniporter-lacking *S. cerevisiae*, introduction of MCU and EMRE sensitised to Mn^{2+}, and was rescued by additional expression of MICU1 (Wettmarshausen *et al.*, 2018). These results elaborate a link between uniporter regulation and manganese toxicity, which is implicated in several neurodegenerative diseases.

A recent study has demonstrated that MICU1 localises to inner boundary membranes rather than within cristae, where it stabilises cristae junctions to prevent cytochrome c release (Gottschalk *et al.*, 2019). In low cytoplasmic Ca^{2+} other uniporter components are quite evenly distributed within mitochondria. However, ER calcium release caused recruitment of MCU and EMRE to the inner boundary membrane. This model posits MICU1 hexamers as promoting cristae stability until activation, at which point they break into dimers and acts as a diffusion trap to sequentially recruit MCU and EMRE at inner boundary membranes. This allows for cristae dynamics and energy production to be coordinated through the mitochondrial influx of calcium.

1.2.9. MICU2

First bioinformatically identified as a paralog of MICU1 (Plovanich *et al.*, 2013), MICU2 stabilises MICU1 and *vice versa* in cultured cells, and its knockdown was reported in this initial work to resemble that of MICU1, with slower uptake and reduced mitochondrial calcium carrying capacity. However, a later study showed the opposite effect, with decreased $[Ca^{2+}]_m$ in MICU2 knockdown cells, and overexpression leading to increased concentration (Patron *et al.*, 2014). Electrophysiological work additionally showed decreased P_o in lipid bilayers expressing MCU and MICU2, albeit resulting from sodium transport in the near absence of free calcium. The authors posit MICU1 as a positive regulator of the complex, and MICU2 as a specifically negative regulator. In contrast, the two proteins have been proposed to work cooperatively to provide channel gatekeeping (Kamer and Mootha, 2014; Kamer, Grabarek and Mootha, 2017). Potentially reconciling these two models, MICU2 was shown to increase the threshold of MICU1 gatekeeping, acting both as a cooperative gatekeeper and a negative regulator (Payne *et al.*, 2017).

Crystal structures of MICU2 have been recently reported in mouse (Kamer *et al.*, 2019) and human (Wu *et al.*, 2019; Xing *et al.*, 2019). In the mouse structure, MICU2 largely resembles MICU1, with key differences at the C-terminal helix which is essential for activity *in vivo*. One of the human structures lacked this C-helix, so could not be directly compared. Both human structures were reported as a homodimer, and as a heterodimer with MICU1. Given that MICU2 cannot bind MCU directly, it is unclear if such MICU2 homodimers exist or have functional relevance *in vivo*.

1.2.10. MICU3

MICU3 was first identified in the same study as for MICU2 (Plovanich *et al.*, 2013), but was not characterised beyond reporting its tissue-specific murine expression to central nervous tissues. Crystal structures have been reported for truncated MICU3 in Ca^{2+}-free and Ca^{2+}-bound states (Xing *et al.*, 2019), and suggest that it operates similarly to MICU2 when extramitochondrial calcium levels are low. Expression of MICU3 in HeLa cells ablated mitochondrial calcium uptake of a small bolus in MICU1 or MICU2 knockdown conditions, indicating that it may be able to compensate for some of the function of these other MICU proteins.

Another study positions MICU3 as an enhancer of mitochondrial calcium uptake (Patron *et al.*, 2018). Expression of MICU3 in HeLa cells potentiated the increase in $[Ca^{2+}]_m$ following histamine stimulation. Buffering extramitochondrial calcium to 400 nM, MICU3 expression allowed for matrix Ca^{2+} accumulation, contrary to the work outlined previously. The discrepancy between these results, obtained in a straight overexpression paradigm using cultured cells, may be resolved by *in vivo* characterisation of this gene product. However, at the outset of this work, no *in vivo* models existed for MICU3. Similarly, though Patron *et al*. demonstrate that MICU3 forms dimers with MICU1 and not MICU2, the presence of MICU3 homodimers cannot be excluded from their work, and *in vivo* expression of MICU3 in a MICU1 knockout background would illuminate any compensatory potential between these two uniporter regulators.

1.2.11. Uniporter conservation

The identification of MICU1 enabled not only the discovery of MCU, but also phylogenetic analysis to uncover the degree of uniporter conservation. MCU is widely conserved across plants and metazoans, with loss events in some protists and fungi, and its presence almost always co-occurs with MICU1, except in the case of fungi where MICU1 is almost always absent (Bick, Calvo and Mootha, 2012). Interestingly, the *MCU* and *MICU1* genes are adjacent specifically in vertebrate genomes suggesting some co-transcriptional regulation has evolved in this branch.

The uniporter components conserved in *Drosophila melanogaster* are *MCU*, *MICU1*, *MICU3*, and *EMRE*. The remainder of this thesis will focus on these components, the predicted molecular weights and amino acid conservation of which are given in Table 1. Sequence alignments are similarly given in Figure 6-Figure 9, with key regions highlighted. Overall, a high degree of sequence similarity/identity can be observed. However, the stoichiometry and organisation of the full human or fly uniplex remains unclear and cannot therefore be compared. The assumed uniporter architecture is given in Figure 5. Based on recent structural work, the tetrameric MCU pore is likely to be in 1:1 stoichiometry with EMRE (Wang *et al.*, 2019), and this will likely be conserved in flies. MCU-EMRE: MICU stoichiometry is less clear but is also assumed to be 1:1. MICU3 will be present in specific tissues, but in its absence, MICU1 homodimers may be dominant.

Table 1. Conservation (% similarity and identity) between human and fruit fly components of the mitochondrial calcium uniporter, along with respective molecular weights, based on sequence information deposited in Uniprot.

Gene	Organism	Molecular Weight	Similarity	Identity
MCU	*H. sapiens*	39.9 kDa	66%	45%
	D. melanogaster	42.5 kDa		
EMRE	*H. sapiens*	11.4 kDa	68%	58%
	D. melanogaster	10.8 kDa		
MICU1	*H. sapiens*	54.4 kDa	64%	48%
	D. melanogaster	60.3 kDa		
MICU3	*H. sapiens*	60.7 kDa	62%	47%
	D. melanogaster	57.4 kDa		

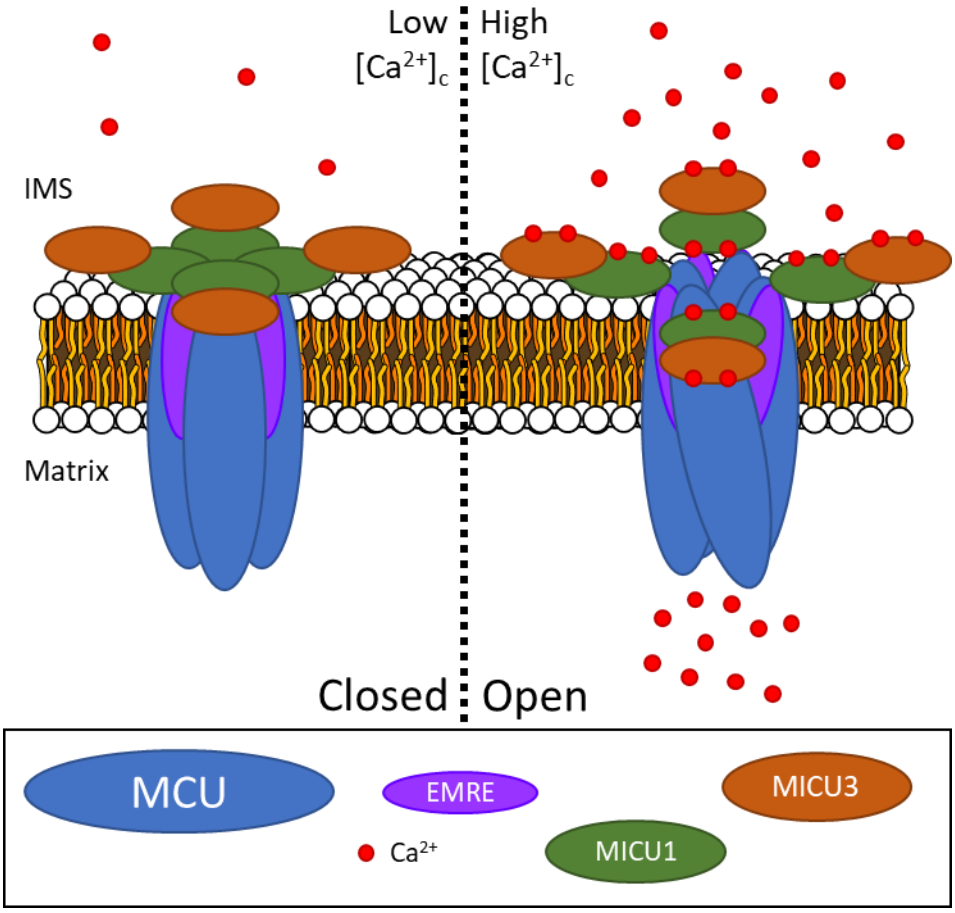

Figure 5. Proposed architecture of the *Drosophila* mitochondrial calcium uniporter, in closed conformation due to low $[Ca^{2+}]_c$, and in an open conformation when $[Ca^{2+}]_c$ rises, due to local ER release, for example.

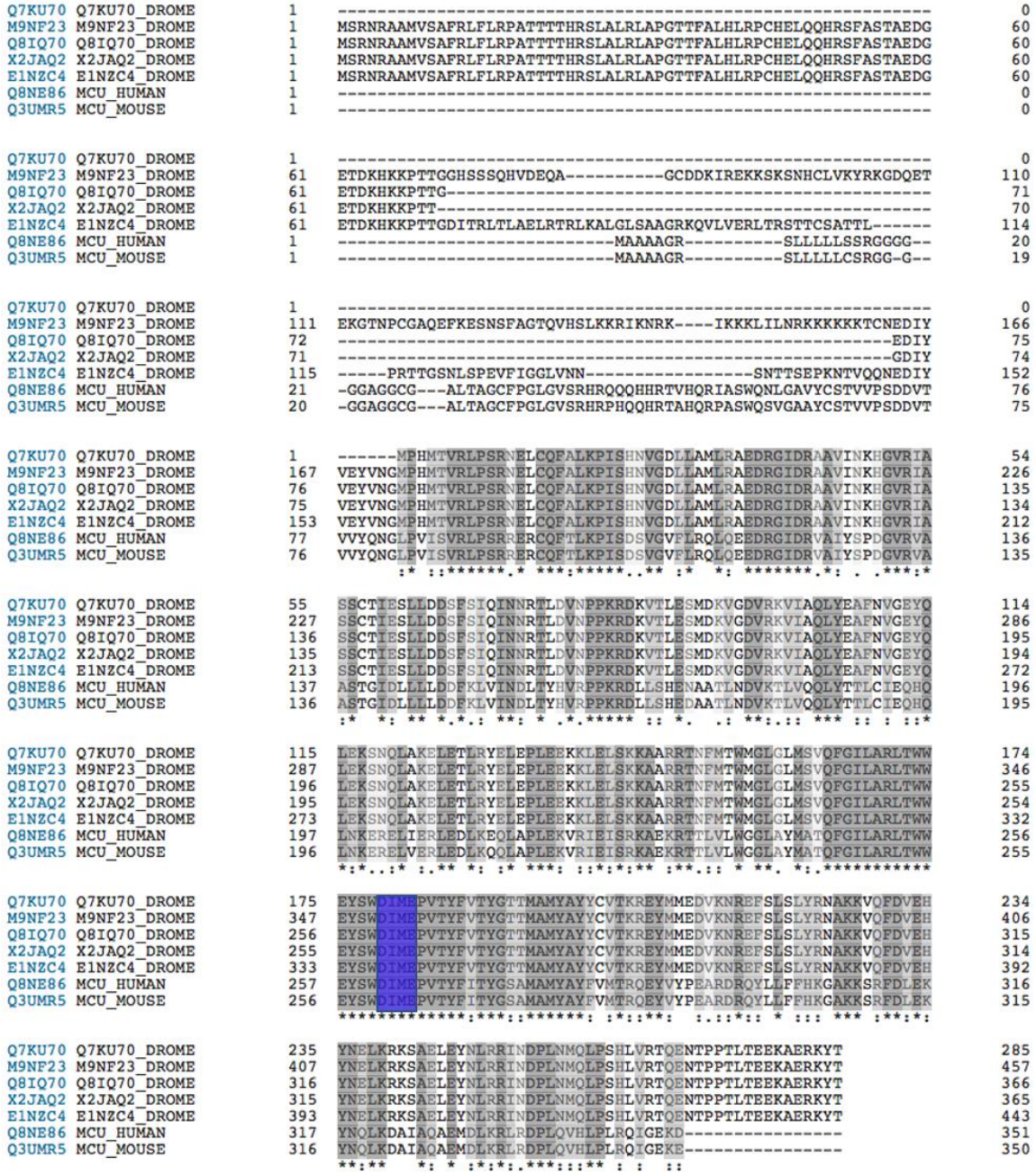

Figure 6. Protein sequence alignment between *H. sapiens*, *M. musculus*, and *D. melanogaster* (all isoforms) MCU. Blue alphanumeric codes on the left side of the figure represent Uniprot accession IDs. Darker shading in the alignment represents increased similarity. Blue highlighted residues indicate the critical DIME motif.

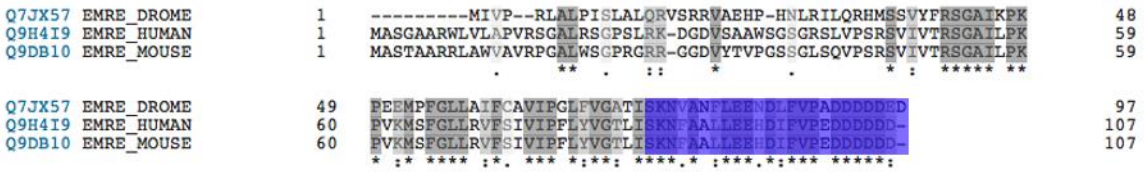

Figure 7. As Figure 6, for EMRE. Blue shaded region represents C-terminal acidic domain.

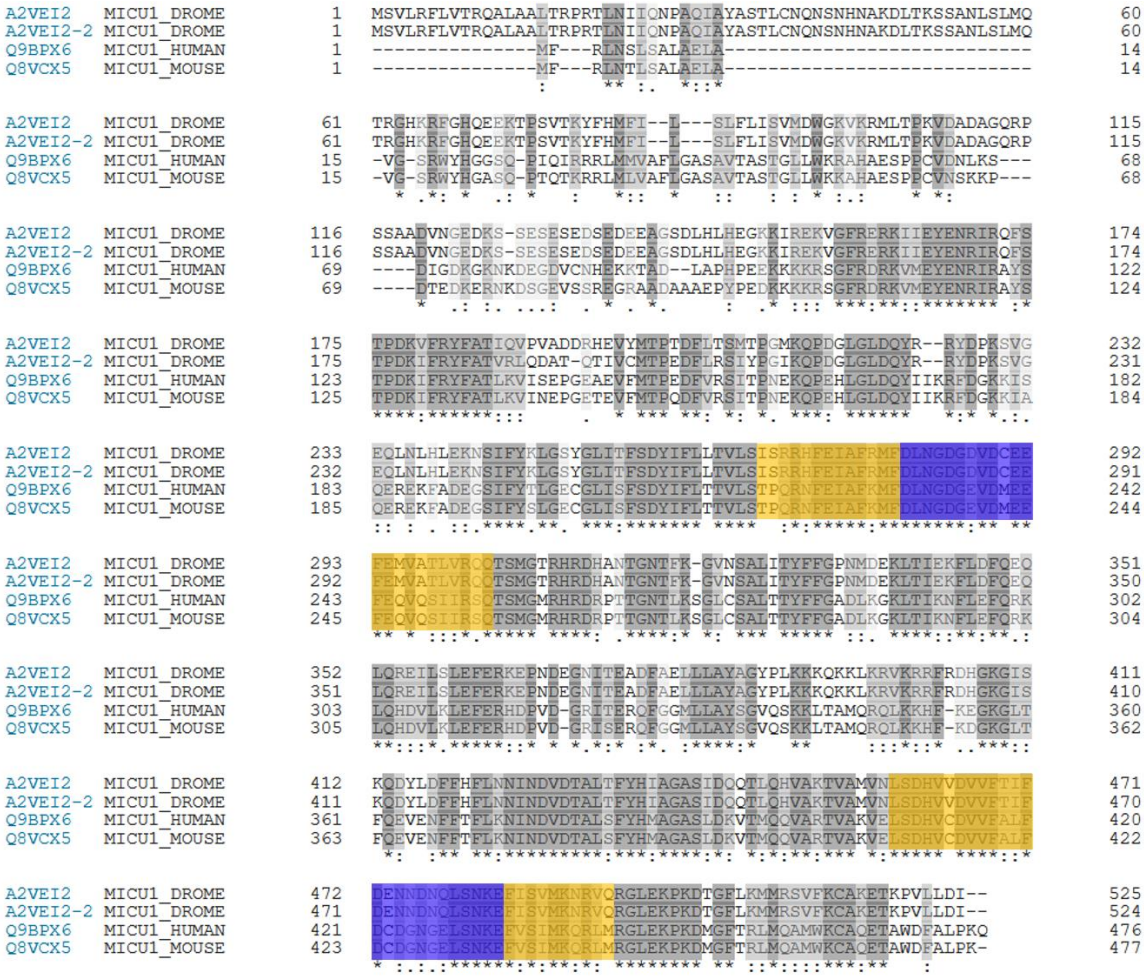

Figure 8. As Figure 6, for MICU1. Blue shaded region represents Ca^{2+} binding region of the larger EF-hand domain, in turn shaded yellow.

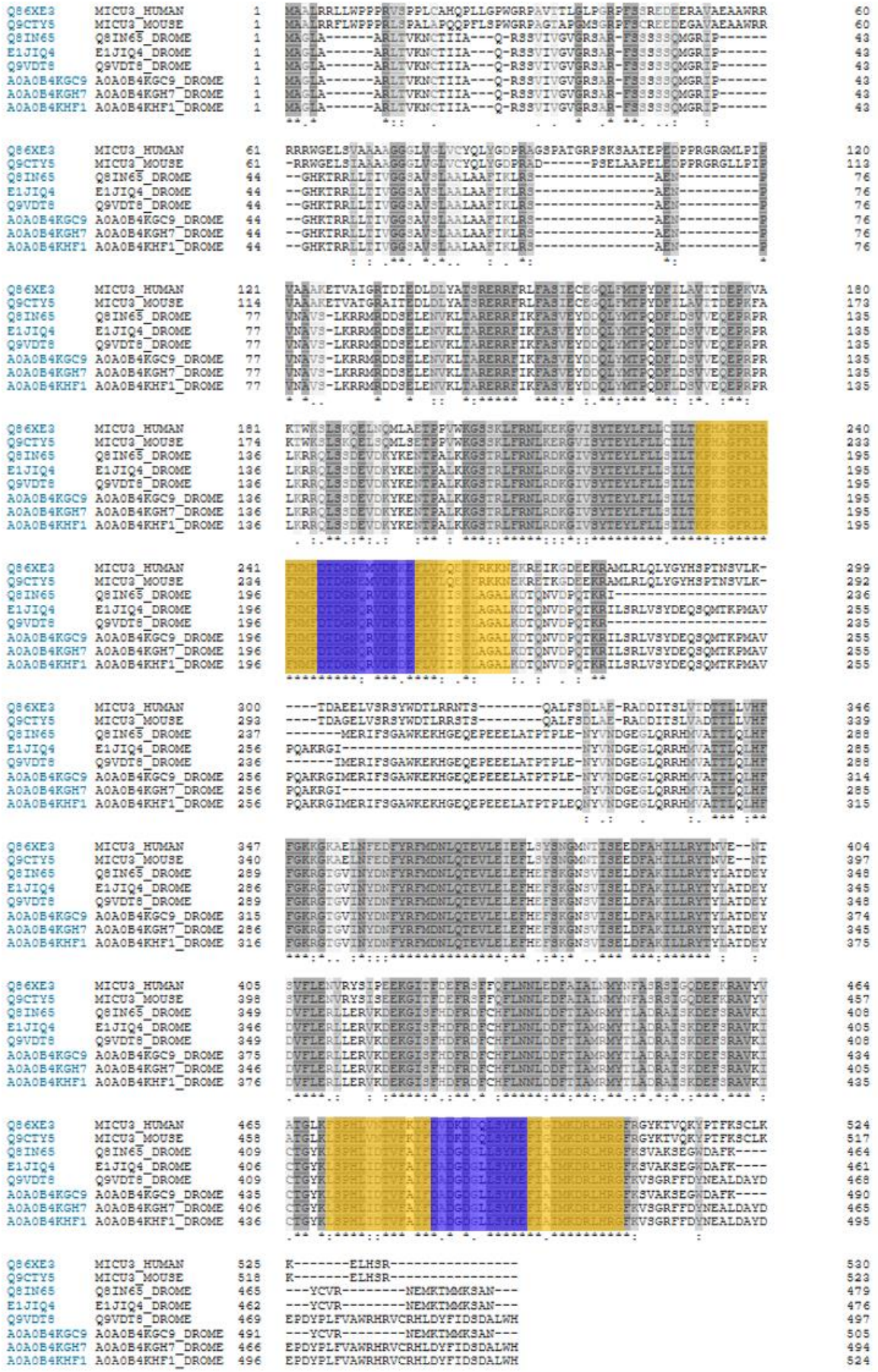

Figure 9. As Figure 8, for MICU3.

1.2.12. Proposed alternative uptake pathways

Electrophysiological studies have challenged the existence of a single mode of mitochondrial calcium entry, via the uniporter. Application of calcium pulses to isolated liver mitochondria yielded rapid sequestration of the ion that was quickly inhibited (Sparagna *et al.*, 1995). It is unclear if this so-called rapid mode (RaM) is mediated by an alternative uniporter conformation or a separate molecular entity. Both are sensitive to ruthenium-based inhibitors, but these are rather non-specific. In any case, RaM calcium uptake is hypothesised to allow for Ca^{2+} pulse sequences to maintain metabolic activity (Sparagna *et al.*, 1995). Other calcium currents have been reported that may or may not overlap with the RaM. Two distinct calcium currents were identified in human cardiac mitoplasts, which differed in their gating properties and sensitivity to Ru360 inhibition (Michels *et al.*, 2009). In HeLa mitoplasts, three currents were isolated (i-MCC, b-MCC, xl-MCC), again differing in their sensitivity to ruthenium compounds, in this case ruthenium red (Bondarenko *et al.*, 2013). MCU knockdown HeLa cells show a compensatory increase in xl-MCC (Bondarenko *et al.*, 2014). Recently, mitochondria from *Mcu* knockout mouse brain were shown to have residual mitochondrial calcium uptake, which maintained respiratory capacity (Hamilton *et al.*, 2018). In all cases, the molecular entities responsible remain unclear; several candidate alternative calcium uptake pathways have been proposed, but all remain controversial.

Mitochondrial uncoupling proteins depolarise the inner membrane to generate free energy in the form of heat. UCP2 and UCP3 were suggested to regulate mitochondrial calcium influx on the basis of overexpression, knockdown, and mutagenesis experiments in cultured cells and isolated mitochondria from murine models (Trenker *et al.*, 2007), but this was strongly refuted (Brookes *et al.*, 2008). One possible explanation is that UCP2/3 instead modulate the canonical uniporter current (Bondarenko *et al.*, 2015), integrating signals like ATP availability (Motloch *et al.*, 2016) and posttranslational modifications, such as PRMT1-mediated methylation of MICU1 (Madreiter-Sokolowski *et al.*, 2016). On the weight of this evidence, it seems unlikely that UCP2/3 are responsible for an alternative mitochondrial calcium influx pathway, whilst still playing a key role in the regulation of this process. Interestingly, MICU1 methylation by PRMT1 was recently shown to block its recruitment of MCU and EMRE to boundary membranes, but this was rescued by the action of UCP2 (Gottschalk *et al.*, 2019).

LETM1 was first described in associated with the Wolf-Hirschhorn syndrome locus (Endele *et al.*, 1999), and was later characterised as a K^+/H^+ antiporter (Nowikovsky *et al.*, 2004). Challenging this model, a siRNA screen in *Drosophila* identified *CG4589*, the homolog of human *LETM1*, as significantly affecting the mitochondrial transport of Ca^{2+} and H^+ (Jiang, Zhao and Clapham, 2009). Additionally, purified LETM1 protein was able to reconstitute Ca^{2+} transport in liposomes. Further reconstitution experiments suggested a preference for Ca^{2+} transport over K^+ (Tsai *et al.*, 2014). However, several objections have been raised (reviewed by Nowikovsky and Bernardi, 2014), and later work suggested that Ca^{2+} fluxes were secondary to disrupted monovalent cation transport (Austin *et al.*, 2017). One possible reconciliation between these two competing models is regulatory switching of LETM1 cation selectivity by protein factors not present in the reconstituted system (Nowikovsky and Bernardi, 2014), but this has yet to be addressed experimentally.

Mitochondrial calcium efflux had long been ascribed in part to a Na^{2+}/Ca^{2+} antiporter, and this was eventually molecularly identified as NCLX (Palty *et al.*, 2010). The stoichiometry of NCLX is still debated, with electrogenic 3:1 exchange of Na^{+} and Ca^{2+} and electroneutral 2:1 exchange proposed. Thermodynamic modelling of NCLX activity suggested that the exchanger could reverse direction in conditions of extramitochondrial high Ca^{2+}/low Na^{+} (Boyman *et al.*, 2013). This reversibility has been further suggested to generate functionally relevant mitochondria Ca^{2+} oscillations (Samanta, Mirams and Parekh, 2018). However, others have suggested that an electrogenic NCLX could only mediate mitochondrial calcium influx in depolarised mitochondria, owing to the highly negative membrane potential (Finkel *et al.*, 2015). It remains unclear if NCLX reversal may be achievable in local microdomains of high mitochondrial calcium.

1.3. Physiological roles of the uniporter

The molecular identification of mitochondrial calcium uniporter genes has enabled cell and animal-based studies to address the contribution of mitochondrial calcium uptake in physiology and pathobiology. For example, targeting zebrafish *mcu* by morpholino disrupted cell migration through decreased actin polymerisation, with corresponding effects on gastrulation (Prudent *et al.*, 2013). Similar cell migration deficits were observed with pharmacological inhibition or knockdown of *MCU* in a human breast cancer cell line (Tang *et al.*, 2015), and was confirmed in another breast cancer line and in HeLa cells (Prudent *et al.*, 2016). Cell migration is an integral part of wound healing (reviewed in Shaw and Martin, 2009). In a *C. elegans* model, wounding caused rapid mitochondrial calcium uptake that generated mitochondrial superoxide to signal actin-based wound closure, and this was blocked by *mcu-1* knockout (Xu and Chisholm, 2014). In addition to $[Ca^{2+}]_m$-mediated effects, mitochondrial buffering of cytoplasmic calcium is anticipated to also be relevant, as mechanical wounding of endothelial cells generated $[Ca^{2+}]_c$ waves that trigger the transcription of immediate early genes like *c-fos* and *c-jun* (Tran *et al.*, 1999).

Recently, the uniporter has been linked to the control of mitotic progression through a mitochondrial calcium transient at the spindle checkpoint (Zhao *et al.*, 2019). Such transients appear to counteract the drop in ATP that occurs in early mitosis, and the nutrient sensor AMPK phosphorylates MCU at Ser75 to increase calcium transfer, linking nutrient availability to bioenergetic capacity.

The effect of mitochondrial calcium buffering on intracellular calcium homeostasis is explored in Section 1.1.1, but specific effects of the mitochondrial calcium uniporter have also been reported. In cultured mast cells, MCU knockdown accelerated the decay of cytoplasmic Ca^{2+} oscillations arising from leukotriene receptor stimulation via LTC_4, due to decreased mitochondrial buffering increasing the local cytoplasmic Ca^{2+} concentration at the mitochondria-ER contact site, inhibiting IP3R-mediated calcium release from the ER (Samanta, Douglas and Parekh, 2014)

Bulk recycling of cellular components is classically achieved through autophagy, where unnecessary or dysfunctional components are trafficked to lysosomes. Of the three forms of autophagy (macroautophagy, microautophagy, and chaperone-mediated autophagy), macroautophagy has been shown to be Ca^{2+}-regulated. Briefly, induction of macroautophagy causes double membrane phagophores elongate to engulf the target material, and following a maturation process, these autophagosomes are trafficked to and fuse with lysosomes. Macroautophagy can be subdivided into mTOR-dependent and -independent pathways, both of which are regulated by intracellular calcium levels through CaMKKβ-mediated activation of the mTORC regulator AMPK (Høyer-Hansen *et al.*, 2007) or through the actions of the inositol-1,4,5-triphosphate receptor (Sarkar *et al.*, 2005; Criollo *et al.*, 2007) respectively. These can be indirectly modulated through mitochondrial calcium buffering. Additionally, mitochondrial calcium uptake can be more directly linked to AMPK-associated autophagy, through its effects on the TCA cycle. MCU inhibition suppresses oxidative phosphorylation thereby reducing ATP levels, which activates AMPK leading to increased autophagy (Cárdenas *et al.*, 2010; Tang and Wu, 2019a). This system has been recently examined as a cardioprotective strategy in heart failure (Yu *et al.*, 2018; Tang and Wu, 2019b).

Mitochondrial positioning is tightly controlled, especially in highly elaborated cells such as neurons, which may measure metres in length, depending on the organism. Mitochondria are trafficked from the soma down the axon in an anterograde fashion to energetically support synaptic signalling, and retrograde movement is also observed, which may represent damaged mitochondria being returned to the cell body for repair and/or recycling. Mitochondrial motility is achieved through tethering to motor proteins by the actions of Miro and Milton family proteins (Stowers *et al.*, 2002; Guo *et al.*, 2005; Glater *et al.*, 2006). Though Milton is not calcium regulated, Miro protein contain EF-hands that arrest mitochondrial movement when Ca^{2+}-bound (Saotome *et al.*, 2008; Macaskill *et al.*, 2009; Wang and Schwarz, 2009), whereby Miro directly binds the kinesin motor domain, preventing microtubule interactions (Wang and Schwarz, 2009). Additionally, the calcium-binding state of Miro affected mitochondrial morphology through Drp1 (Saotome *et al.*, 2008). As for the IP3R inhibition outlined above, the activity of the mitochondrial calcium uniporter would necessarily affect Miro Ca^{2+} binding through local buffering.

Mitochondria are dynamic organelles, balancing fission and fusion processes to maintain a responsive network. Fission begins with ER-mediated mitochondrial constriction, and sequential division of the IMM and OMM. Recent work has demonstrated that elevated $[Ca^{2+}]_m$ leads to IMM constriction, priming mitochondria for division (Cho *et al.*, 2017), and that this process is promoted by actin polymerisation by ER-bound INF2, which increases ER-mitochondrial contact (Chakrabarti *et al.*, 2017). The dynamin-related GTPase Drp1, which enacts the final membrane scission event of mitochondrial fission, is phosphorylated at Ser616 to promote mitochondrial fragmentation (Taguchi *et al.*, 2007). Loss of MCU induced Drp1 hyperphosphorylation via CaMKII through reduced $[Ca^{2+}]_c$ clearance, with corresponding fragmentation and cell cycle arrest (Koval *et al.*, 2019). Similarly, high $[Ca^{2+}]_c$ promoted mitochondrial fragmentation in the presence of Miro proteins (Saotome *et al.*, 2008).

General mitochondrial aspects of cell death pathways are discussed in Section 1.1.3, but the mitochondrial calcium uniporter remains a key target both to probe the process experimentally and for therapeutic modulation. Drp1 SUMOylation during cell death has been shown to stabilise ER-mitochondrial contacts, leading to increased Ca^{2+} transfer, and in turn cristae remodelling and cytochrome c release (Prudent *et al.*, 2015). Prior to the first *in vivo* uniporter models, *MCU* knockdown was shown to inhibit the rise in $[Ca^{2+}]_m$ seen following NMDA receptor activation, and was neuroprotective in an excitotoxic cell model (Qiu *et al.*, 2013). Interestingly, synaptic activity represses *MCU* expression through nuclear Ca^{2+} signalling, further indicating the importance of mitochondrial calcium uptake in neuronal homeostasis. Similarly, pharmacological inhibition of mitochondrial calcium uptake was neuroprotective in a similar model (Angelova *et al.*, 2018), though it remains unclear if the compound used targeted the uniporter specifically, as it inhibited only low extramitochondrial calcium-associated uptake. Moving to a global context, mPTP opening was not observed in *Mcu* knockout mice, though curiously, did not protect against cell death and blocked the benefit of the classical pharmacological mPTP inhibitor cyclosporin A (Pan *et al.*, 2013). This hints at complexity beyond the excess calcium-mPTP opening model; further supported by recent work in which murine MCU knockout brains retain some degree of calcium uptake, with incomplete mPTP inhibition (Hamilton *et al.*, 2018).

The activity of the mitochondrial calcium uniporter has also been linked to skeletal muscle trophism in a murine model system (Mammucari *et al.*, 2015). Through PGC-1α4 and IGF1-Akt/PKB signalling, MCU overexpression led to skeletal muscle hypertrophy, and shRNA-mediated MCU knockdown to atrophy. This extended to a muscle-restricted MCU knockout mouse, which displayed a metabolic switch to β-oxidation compensating for reduced TCA intermediate supply (Gherardi *et al.*, 2018), which was confirmed in a coincident study (Kwong *et al.*, 2018). Mitochondrial dynamics and muscle trophism have also been linked by mitochondrial calcium dynamics; loss of pro-fission *Drp1* causes skeletal muscle atrophy via increased uptake that was successfully blocked by MCU knockdown (Favaro *et al.*, 2019). These studies demonstrate the rate of mitochondrial calcium uptake is carefully balanced to ensure appropriate muscle mass. In addition to examining the physiological role of the uniporter, animal models have begun to emerge allowing for the *in vivo* requirement of mitochondrial calcium to be examined.

1.3.1. Animal models

The description of the first mouse loss-of-function Mcu mutant by Pan et al. came as a challenge to the consideration of mitochondrial calcium dynamics as essential for life (Pan *et al.*, 2013). Assessed on a mixed C57BL/6 and CD1 genetic background, homozygous mutants were viable. No mitochondrial calcium uptake was detected, either directly loading isolated cells with calcium, or through ligand-induced release from intracellular stores. However, a shift in birth ratio suggested partial lethality, and the mutant on an inbred C57BL/6 background was embryonic recessive lethal (penetrance not reported, presumed complete) (Murphy *et al.*, 2014). Several explanations have been put forward for the difference in viability seen between the two genetic backgrounds of the $Mcu^{-/-}$ mice. From personal communications, the more supported concept is a genetic factor in the CD1 strain that rescues the lethality. However, the presence of synthetic lethality in the C57BL/6 strain seems just as likely, and the preference for one scenario over the other may indicate a presumption about the dispensability of MCU. For example, the C57BL/6J substrain harbours a mutation in the mitochondrial proton pump Nnt (Nicotinamide nucleotide transhydrogenase), with corresponding consequences for the NADPH/NADP+ ratio (Toye *et al.*, 2005; Ronchi *et al.*, 2013). The presence of other mutations affecting mitochondrial function could underlie this genetic background effect and cannot be discounted at present.

A collection of recent studies has examined the contribution of uniporter-mediated calcium uptake to cardiac function (Holmström *et al.*, 2015; Kwong *et al.*, 2015; Luongo *et al.*, 2015; Rasmussen *et al.*, 2015; Wu *et al.*, 2015). This was evaluated in either a global knockout (Holmström *et al.*, 2015), cardiomyocyte-restricted knockout (Kwong *et al.*, 2015; Luongo *et al.*, 2015), or cardiomyocyte-restricted expression of a dominant-negative mutant (Rasmussen *et al.*, 2015; Wu *et al.*, 2015). In a global Mcu knockout, cardiac function was not affected in basal or stress conditions (Holmström *et al.*, 2015). However, though well tolerated under basal conditions, cardiomyocyte-specific Mcu loss inhibited ATP production and mPTP opening with an acute calcium challenge (Kwong *et al.*, 2015), as well as showing reduced left ventricle contractility coupling to β-adrenergic stimulation via isoproterenol (Luongo *et al.*, 2015). Compensation in the global knockout likely underlies the differing responses to stress conditions. A germline restricted Cre-recombinase was also used to generate global heterozygous mutants, which failed to produce viable homozygous offspring when interbred (Luongo *et al.*, 2015). However, this was done in a C57BL/6 inbred background, as in Pan *et al*, so carries the same caveats.

An initial mouse *Micu1* knockout was found to be fully perinatally lethal (Antony *et al.*, 2016), but a subsequent study reported the presence of escapers (Liu *et al.*, 2016). Survivors displayed several behavioural/biochemical phenotypes that spontaneously ameliorated with age. The authors associated this surprising finding with a reduction in EMRE protein, and accordingly established a cross with an *Emre* knockout line to yield *Micu1*$^{-/-}$ *Emre*$^{+/-}$ mice. This would presumably counteract dysregulated uniporter gatekeeping through an overall reduction of mitochondrial calcium uptake. Indeed, *Micu1*$^{-/-}$ *Emre*$^{+/-}$ mice were born in a Mendelian ratio. However, though *Emre*$^{-/-}$ mice were viable, no double homozygous mice were observed, which goes against the hypothesis that *Micu1*-associated lethality is entirely due to the dysregulation of the uniporter.

An Emre knockout mouse was published in the context of the study examining Micu1 (Liu *et al.*, 2016). In the same mixed genetic background as for $Mcu^{-/-}$, homozygous Emre mutants were viable with a Mendelian birth ratio and lacked detectable mitochondrial calcium uptake. This provides further evidence for the dispensability of canonical uniporter function, though this supporting evidence comes from the same group as the initial $Mcu^{-/-}$ and is therefore not independent. The viability of $Emre^{-/-}$ in the inbred C57BL/6 background (leading to non-viable $Mcu^{-/-}$) has not yet been reported. A more complete characterisation of murine Emre loss can be expected, and already a dependence of in vivo uptake on the C-terminal domain of Emre has been reported at a conference (Syder *et al.*, 2018).

The *in vivo* function of the mitochondrial calcium uniporter has begun to be explored in *D. melanogaster*. *MCU* was identified in a siRNA screen for genes affecting olfactory memory (Walkinshaw *et al.*, 2015), and a follow-up study showed that mushroom body-specific knockdown impaired olfactory memory without compromising learning (Drago and Davis, 2016). Interestingly, this effect was only observed with knockdown during the pupal phase, suggesting that developmental aberrations underlie this deficit. Indeed, structural abnormalities were observed in mushroom body neurons. Choi and colleagues expanded this through the creation of a *MCU* knockout through P-element imprecise excision methodology as outlined in Section 3.1. (Choi *et al.*, 2017). These mutants were homozygous viable, with normal weight, food intake, circulating triglycerides, and starvation-induced autophagy. *MCU* KO flies showed resistance to H_2O_2-associated apoptosis, which aligns with observations from cell lines (Liao *et al.*, 2015).

1.4. Mitochondrial aspects of neurodegenerative disease

As the world ages, neurodegenerative diseases represent a rapidly growing disease burden. In more economically developed countries, where this demographic transition is further advanced, neurodegeneration places a significant challenge on the resources of medical and care systems. In Europe, the Cost of Illness of dementia for 2008 was estimated at €177 billion (Wimo *et al.*, 2010). Demographic trends will exacerbate this problem in the coming decades. In the case of Alzheimer's disease (AD), the most common form of dementia, the number of patients is projected to quadruple from 2006 to 2050 (Brookmeyer *et al.*, 2007). Despite this enormous strain, current therapeutic interventions provide only symptomatic relief.

Given this unanswered need, any disease-modifying treatments that could reverse or even slow the course of the disease would be of immense benefit. For example, a 2007 study projected that a two-year delay in AD onset would result in 22.7 million fewer global cases of the disease in 2050 (Brookmeyer *et al.*, 2007). However, neurodegenerative disease candidate therapies are notorious for poor results in the clinic. For AD, no disease-modifying drugs have been approved, and even symptomatic treatments have an approval rate of only 0.4% (Calcoen, Elias and Yu, 2015). This indicates the need to further understand the underlying pathobiology of neurodegeneration.

1.4.1. Parkinson's disease

First described as the 'shaking palsy' by James Parkinson over 200 years ago (Parkinson, 2002, historical review), Parkinson's disease (PD) has always been primarily clinically described by its motor features. As well as the key diagnostic finding of bradykinesia, PD is typically associated with muscle rigidity, rest tremor, or postural instability (Gibb and Lees, 1988). Though typically present in less than one percent of the general population, the prevalence of PD can rise as high as 4% in older groups (de Lau and Breteler, 2006).

The neuropathologist F. H. Lewy noted the presence of proteinaceous inclusions in the brains of PD patients, and these were eponymised as Lewy bodies after Lafora noticed their presence in the substantia nigra of PD brains (Engelhardt, 2017). This region, named for its pigmentation, is a basal ganglia midbrain structure which plays important roles in reward circuits and the control of movement. Dopaminergic neurons are lost primarily in the *pars compacta* subregion (SNpc), more specifically the ventrolateral part of the SNpc (Fearnley and Lees, 1991). This mainly innervates the striatum, which again underpins motor planning and reward functions, providing a histopathological correlate of behavioural PD symptoms. The specific loss of dopaminergic neurons led to the hypothesis that supplementing dopamine levels in the brain might benefit Parkinson's patients.

Dopamine replacement therapy was a revolution in the pharmaceutical management of PD, providing dramatic improvements in patient symptoms. However, it does not address the underlying mechanisms of the disease, and benefit declines with long-term use (Marsden and Parkes, 1977), necessitating higher doses of dopamine precursors, which can induce dyskinesia (Thanvi, Lo and Robinson, 2007). Deep brain stimulation mitigates these side-effects, allowing for drug dose to be lowered, but again does not target the disease process, eventually being overcome by its progression. This roadblock highlights the need for further understanding of the cellular basis of PD.

The first clues of the pathogenic mechanism of PD came from an unlikely source. Recreational users of the synthetic meperidine analog 1-methyl-4-phenyl-4-propionoxypiperidine (MPPP) had in fact been exposed to the contaminant 1-methyl-4-phenyl-1,2,5,6-tetrahydropyridine (MPTP). Initially reported in a single case (Davis *et al.*, 1979) and expanded to four others (Langston *et al.*, 1983), these individuals developed symptoms of parkinsonism, including responsiveness to levodopa. Investigating the mechanism of toxicity for this pharmacological Parkinson's disease mimic would therefore generate hypotheses of PD aetiology. MPTP accumulates up to 40-fold in mitochondria (Ramsay, Salach and Singer, 1986), where it inhibits the activity of Complex I of the respiratory chain (Ramsay *et al.*, 1987), with the resulting increase in reactive oxygen species triggering cell death. However, Complex I has been suggested to be dispensable for MPTP toxicity (Choi *et al.*, 2008). Nevertheless, mitochondrial effects of MPTP are numerous, and implicate the biology of this organelle in Parkinson-like contexts.

Initially, PD was thought to be a sporadic condition, but the identification of mutations in α-synuclein (SNCA) were linked to a familial form of the disease (Polymeropoulos *et al.*, 1997). This rapidly led to the identification of α-synuclein as the major constituent of Lewy bodies (Spillantini *et al.*, 1997), where it aggregates to form insoluble fibrils. SNCA has been observed to localise to mitochondria and pathological mutations are associated with multiple dysfunctions of this organelle, again linking mitochondria and PD. Since the discovery of SNCA (reviewed in Mullin and Schapira, 2013), several mutations have been linked to familial PD, which can be used to infer the nature of the sporadic form. Many of these disease genes are associated with mitochondria, but perhaps the two most well characterised are PARK2 (Matsumine *et al.*, 1997) and PARK6 (Valente *et al.*, 2001), otherwise known as *Parkin* (Kitada *et al.*, 1998) and *PINK1* (Valente *et al.*, 2004).

PINK1 encodes a mitochondrially localised serine/threonine kinase. PINK1 is successfully translocated through the outer (OMM) and inner mitochondrial membrane (IMM) when the membrane potential is high, where it is degraded through sequential proteolytic cleavage by the matrix protease MPP (Greene *et al.*, 2012) and the IMM protease PARL (Deas *et al.*, 2011). This reveals an N-degron that results in retrotranslocation to the cytosol and proteasomal degradation. A drop in mitochondrial membrane potential, indicative of organellar/cellular stress, causes the stalled mitochondrial import of PINK1, stabilising it on the outer mitochondrial membrane. Here, it phosphorylates both the Parkin enzyme in its ubiquitin-like domain (Kondapalli *et al.*, 2012), as well as the substrate ubiquitin itself (Kane *et al.*, 2014; Koyano *et al.*, 2014), in both cases at Serine 65.

The ubiquitin proteasome system (UPS) selectively targets proteins for degradation, through the coordination of three enzymatic steps. After ubiquitin is activated through an E1-catalysed reaction, the E3 ubiquitin ligase Parkin acts in the third step, catalysing the transfer of the degradation tag ubiquitin from an adapter E2 protein to the target protein (reviewed in Hochstrasser, 1996). Parkin-mediated ubiquitination promotes proteasomal degradation and/or mitophagy. The selective autophagic degradation of mitochondria, or mitophagy, is vital to prevent the accumulation of dysfunctional mitochondria, which would compromise respiration.

Polyubiquitin chains are a molecular signal for proteasomal degradation, and are linked together through isopeptide bonding between an internal lysine of the target protein and the C-terminal glycine of ubiquitin (Kirisako *et al.*, 2006). Monomeric ubiquitin itself features several ubiquitination sites, and a variety of branched or unbranched ubiquitin chains can therefore be built up, which differ in their signalling role. For example, classical Lys48 chains target proteins for proteasomal degradation, whereas Lys63 chains have been proposed to recruit autophagic cargo receptors (reviewed in Grumati and Dikic, 2018). However, the role of *parkin* in K63-mediated autophagy has come into question (Shiba-Fukushima *et al.*, 2014), and K6 chains have been proposed to mediate this function instead (Durcan *et al.*, 2014).

Rodent models of Parkinson's disease are a promising strategy for preclinical research, but have suffered from poor concordance between patient and model phenotypes; familial PD mutations that cause severe early-onset PD such *PINK1* or *PRKN* loss-of-function have little to no detrimental effect in mutant animals (Perez and Palmiter, 2005; Kitada *et al.*, 2007). By contrast, the powerful genetic model *Drosophila melanogaster* has played a key role in illuminating the physiological requirements of these and related genes. As well as establishing a mitochondrial role for Parkin (Greene *et al.*, 2003), genetic complementation studies in the fly demonstrated that Parkin acts downstream of PINK1 in a common pathway (Clark *et al.*, 2006; Park *et al.*, 2006). *Pink1*/*parkin*-deficient *Drosophila* display reduced lifespan and motor ability, muscle and dopaminergic degeneration, and mitochondrial swelling, in alignment with PD patients (importantly, Lewy body-like aggregates are not seen, as flies lack a *SNCA* homolog). Fly models have also been developed against other familial PD mutations, such as *DJ-1* loss-of-function (Meulener *et al.*, 2005) or mutant *LRRK2* (Liu *et al.*, 2008), but *Pink1* and *parkin* models remain the most developed. Due to the less ambiguous phenotypic consequence of *Pink1*/*parkin* loss, *Drosophila* have been widely used to study the *in vivo* function of these genes, and have shown roles in mitochondrial morphology (Poole *et al.*, 2008) and mitophagy (Vincow *et al.*, 2013; J. J. Lee *et al.*, 2018).

Direct evidence linking Parkinson's disease to mitochondrial calcium dynamics came from Gandhi and colleagues, using a cell model of PINK1 deficiency (Gandhi *et al.*, 2009). Sensitisation of $\Delta\psi_m$ to calcium stimuli, reduced mitochondrial calcium carrying capacity, and increased mitochondrial/cytosolic ROS production were observed in PINK1-deficient neurons. Pharmacological inhibition of the NCLX phenocopied the PINK1 loss, and addition of Na^+ induced a smaller rise in $[Na^+]_m$ in Pink1-deficient neurons than control, leading the authors to suggest that the loss of PINK1 inhibits the extrusion of Ca^{2+} from mitochondria via the mitochondrial sodium-calcium exchanger (NCLX). The resulting increase in matrix Ca^{2+} allows physiological ion transients to open the mPTP, resulting in cell death. A concomitant reduction in respiration reduces the mitochondrial membrane potential and causes accumulation of mitochondrial ROS, which both also bring mitochondria closer to the threshold for mPTP opening. It is worth noting that evidence for NCLX modulation by PINK1 arises largely from similarity between PINK1 KD neurons

and those with pharmacologically inhibited NCLX, and this phenocopying does not provide robust evidence for a direct interaction. However, the authors build on this in a later work (Kostic *et al.*, 2015), rescuing calcium phenotypes of PINK1 through PKA activation or phosphomimetic NCLX. Promoting mitochondrial calcium efflux and inhibition of influx would be predicted to give similar outcomes, so these studies also implicate the targeting of the mitochondrial calcium uniporter in PD.

Recent studies have associated the mitochondrial calcium uniporter with PINK1 models of disease. In zebrafish, the nonsense mutation *pink1*^{Y431*} creates a functional null allele, which causes dopaminergic neuron loss and impaired Complex I activity in the larval stage (Soman *et al.*, 2017). Morpholinos directed at *mcu* or *micu1* rescued the dopaminergic neuron loss, but *vdac* reduction did not. The authors do not address this, and despite the presumably tight association between the inner and outer mitochondrial membranes at the point of calcium entry the discrepancy between these interactions is worth additional investigation. In incremental advance was recently published, showing similar rescue with a CRISPR-generated *mcu* mutant, and benefit in a MPTP model of PD (Soman *et al.*, 2019).

Recently, a *Drosophila* study has interrogated ER-mitochondrial calcium transfer in the context of Pink1 (K.-S. Lee *et al.*, 2018). As in the cell-based study outlined above, matrix Ca^{2+} was elevated with loss of *Pink1*, with corresponding dopaminergic neuron mitochondrial swelling/aggregation and cell loss. These phenotypes were rescued with knockdown of *IP3R* or *MCU*, as well as VDAC knockdown, in contrast to the zebrafish study. This supports a mitochondrial calcium overload hypothesis for PD aetiology and implicates the wider ER-mitochondrial calcium axis as a potential target for therapeutic intervention.

1.4.2. Alzheimer's disease

Alzheimer's disease (AD) is the most common neurodegenerative condition, first reported by Alois Alzheimer in 1907 (Alzheimer *et al.*, 1995, historical review). Primarily characterised by initially mild cognitive impairment, key functions decline leading to aphasia, apraxia, or agnosia (McKhann *et al.*, 1984), but a definitive diagnosis cannot be made without histopathological observation of atrophic tissue containing the extracellular amyloid plaques and intracellular neurofibrillary tangles that characterise the condition. Such deposits can also be seen in the otherwise healthy elderly, but their abundance and distribution is altered in AD (Tiraboschi *et al.*, 2004).

In Alzheimer's disease, cholinergic signalling in the cortex and basal forebrain declines as the disease progresses. Using a similar justification as the successful dopamine replacement therapy for Parkinson's disease, acetylcholinesterase inhibitors were employed, which compensate for acetylcholine reduction by blocking its hydrolysis. However, such treatments are of limited benefit, providing only a modest degree of symptomatic relief (Birks, 2006; Birks, Chong and Grimley Evans, 2015; Birks and Harvey, 2018), and neuron loss continues unabated. A greater understanding of AD aetiology is needed to create disease-modifying strategies.

Evidence for the genetic basis of Alzheimer's disease came from an unexpected direction. A protein had been isolated from the beta-sheet rich amyloid plaques of AD brains (George G Glenner and Wong, 1984), but did not show homology to any known protein at the time. Down Syndrome, which arises from Chromosome 21 trisomy, invariably leads to AD, at an earlier age than seen in other cases (Olson and Shaw, 1969). The key amyloid deposits on post-mortem brain examination were also seen, and contained the previously discovered beta protein (G G Glenner and Wong, 1984). This raised the prospect that an AD-causative gene could be mapped to Chromosome 21, and a large research effort eventually determined this to be what is now called the amyloid precursor protein (APP) (Goldgaber *et al.*, 1987; Kang *et al.*, 1987; Robakis *et al.*, 1987; Tanzi *et al.*, 1987).

APP encodes a pro-peptide that is cleaved sequentially by the actions of β- and γ-secretases to yield the amyloid beta (Aβ) peptide. Instead, α-secretase may cleave within the Aβ domain, and further processing by γ-secretase generates the neuroprotective APPsα (Mattson *et al.*, 1993), which ameliorates Aβ-induced increases in intracellular calcium (Goodman and Mattson, 1994). Mutations in APP itself make up only a minority of familial AD cases, but mutations in two components of γ-secretase, PSEN1 and PSEN2, explain much of the remaining disease risk (Mullan *et al.*, 1992; Levy-Lahad, Wasco, *et al.*, 1995; Levy-Lahad, Wijsman, *et al.*, 1995). These mutations enhance the production of Aβ over that of APPsα. This genetic evidence formed the basis of the amyloid cascade hypothesis, which positions Aβ as the key driver of AD, though contention remains over the precise toxic species in terms of aggregate size, and the protective or deleterious contribution of amyloid plaques.

AD therapies to date have largely exploited the amyloid theory through efforts to reduce the level of Aβ, or the resulting plaques. These have included β- and γ-secretase inhibitors to limit production, or antibodies targeted at plaques. However, these have led to high-profile failures in the clinic (Egan *et al.*, 2018; Honig *et al.*, 2018; Biogen/Eisai, 2019; Roche, 2019), which cast a shadow over the underlying hypothesis. Proponents argue that the patient group needs further stratification, or that interventions will have to be targeted earlier for any benefit.

The human MAPT gene encodes a family of six proteins generated by alternative splicing that are collectively referred to as tau proteins (Goedert *et al.*, 1989). These have key roles in microtubule assembly and stability (Weingarten *et al.*, 1975), with obvious implications for axonal transport. Crucially, tau was identified as the key component of the intracellular neurofibrillary tangles from AD brain (Goedert *et al.*, 1988). Tau can be phosphorylated at multiple sites, and initial phosphorylation events prime other sites for modification, allowing for additional control of the process. Glycogen synthase kinase 3β (GSK3β) bypasses this checkpoint, phosphorylating tau at primed and unprimed sites (Cho and Johnson, 2003), leading to a hyperphosphorylated species that resembles that found in neurofibrillary tangles (Hanger *et al.*, 1992).

Excessive amounts of excitatory amino acids such as glutamate cause overactivation of ionotropic glutamate receptors, such as NMDAR and AMPAR. Particularly in the case of the NMDA receptor, this leads to a prolonged calcium influx into neurons that can cause pathological activation of calpains, phospholipases etc. NMDAR antagonists such as memantine have been developed for AD, but similar to cholinesterase inhibitors provide only modest symptomatic relief (McShane *et al.*, 2019).

The powerful invertebrate model organism, *Drosophila melanogaster*, has been used to address several aspects of AD pathobiology. Independent groups have created transgenic flies for the human $A\beta_{42}$ peptide or its precursor APP, under the control of the Gal4/UAS system, allowing for precise spatiotemporal control of gene expression (Finelli *et al.*, 2004; Greeve *et al.*, 2004; Crowther *et al.*, 2005a; Iijima *et al.*, 2008). Similarly, transgenic *Drosophila* expressing human tau protein of varying repeat lengths have been generated (Williams, Tyrer and Shepherd, 2000; Wittmann *et al.*, 2001; Jackson *et al.*, 2002), but are outside the scope of this review. Neuronal expression of human $A\beta_{42}$ results in reduced lifespan, protein accumulation, and neurodegeneration, recapitulating key features of the human disease. These models have already been used to provide insight into developing AD features, such as glial biology (Ray, Speese and Logan, 2017) and intestinal microbiome disruption (Wu *et al.*, 2017). Links between mitochondrial biology and AD have also been established in *D. melanogaster*. For example, neuronal Aβ expression lead to reduced axonal transport of mitochondria with corresponding synaptic depletion (Zhao *et al.*, 2010). Additionally, the short lifespan and generation time of *Drosophila* allows rapid pre-clinical validation of therapeutic approaches before moving to higher organisms (Niccoli *et al.*, 2016).

The failure of therapies directly targeting amyloid plaques has provoked efforts to discover alternative strategies, and mitochondria have emerged as major players in this arena. AD patients displayed reduced Complex IV (Parker, Filley and Parks, 1990), α-ketoglutarate dehydrogenase (Gibson *et al.*, 1988), and pyruvate dehydrogenase (Sorbi, Bird and Blass, 1983) activity, which was also induced directly by the addition of Aβ (Casley *et al.*, 2002; Crouch *et al.*, 2005). Additionally, γ-secretase components can localise to mitochondria (Hansson *et al.*, 2004), as can Aβ peptides themselves (Hansson Petersen *et al.*, 2008). APP was also found to enter mitochondria through the translocases of the outer and inner mitochondrial membranes (TOM/TIM complexes), and its accumulation stalls the import of other mitochondrial proteins like nuclear-encoded Complex IV components, leading to mitochondrial dysfunction (Anandatheerthavarada *et al.*, 2003; Devi *et al.*, 2006).

Mitochondrial calcium has been implicated Alzheimer's disease. Treatment of neuronal cultures with oligomeric amyloid beta resulted in mitochondrial calcium overload, induction of the mPTP, and resulting apoptotic cell death (Sanz-Blasco *et al.*, 2008). Specific to the uniporter, pharmacological inhibition of MCU rescued amyloid beta-induced microglial apoptosis, whereas activation enhanced cell death (Xie *et al.*, 2017). Oligomeric amyloid beta was even associated with direct upregulation of MCU expression (Calvo-Rodriguez *et al.*, 2019). Recently, impaired mitochondrial calcium efflux was implicated in the pathogenesis of a mouse AD model (Jadiya *et al.*, 2019). Neuron-specific NCLX knockout exacerbated the classical 3xTg-AD model, and in the same system, transgenic expression of NCLX in adulthood slowed cognitive decline, and reduced amyloid load and tau phosphorylation. AD post-mortem brains and aged 3xTg-AD mice showed reduced expression of NCLX, and interestingly, MICU1 (and MCUb), suggesting that uniporter remodelling may also contribute to the mitochondrial calcium overload seen in AD. Genetic inhibition of the mitochondrial calcium uniporter therefore represents a useful avenue to investigate its role in *in vivo* models of amyloid toxicity.

1.5. The use of *Drosophila* as a genetic model system

The common fruit fly, or vinegar fly *Drosophila melanogaster* has been established as a key model organism in the study of genetics, since the pioneering work of Thomas Hunt Morgan at the turn of the 20th Century. The fruit fly has many characteristics that give it a niche among other systems. The poikilothermic fly metabolism varies according to the external temperature. At 25 °C, progression from embryo to adult is approximately nine days and occurs externally, allowing for simple observation of developmental aberrations. The short generation time makes *D. melanogaster* ideal for rapid execution of complex crossing schemes, and a lifespan of approximately two months is useful for studies of longevity and the diseases of aging. Perhaps the most important advantage of the fruit fly model system is its genetic tractability, with many extant libraries for gene manipulation. These are discussed in more detail in Section 3.1.

Increased genetic distance between flies and humans, relative to murine/human, lead some to question the applicability of findings in *Drosophila* models to clinically relevant environments. However, a substantial proportion of known human disease genes are conserved in *Drosophila* (Yamamoto *et al.*, 2014). The small size of the fruit fly can be a challenge when substantial amounts of biological material are required, but a short generation time and large brood size allows for rapid expansion of populations, to tens of thousands of individuals. These large populations alleviate statistical power concerns, especially as regulatory restrictions over cohort size do not apply (from the perspective of United Kingdom regulations).

By contrast, *Drosophila* are not able to compete with the speed of generating cultured models such as yeast and cell lines but offer key advantages in terms of applicability to human (patho)physiology. Flies display complex multicellular organisation up to the point of a brain that can support behaviours as advanced as locomotion, learning and memory, circadian rhythms, and social behaviours such as courtship. In summation, *Drosophila melanogaster* represents a powerful genetic model organism that provides a valuable niche, balancing the power to perform in-depth experiments with the applicability of their results to human biology. All *in vivo* experiments in this thesis have utilised *D. melanogaster*, and it has formed the basis for most *in vitro* biochemistry contained herein.

1.6. Thesis Aims

As summarised above, mitochondrial calcium dynamics represent a key control point for both physiological metabolism and cell death pathways, and its dysregulation is associated with many pathological conditions, including several neurodegenerative examples. Therefore, this project aimed to provide a comprehensive *in vivo* characterisation of the mitochondrial calcium uniporter in *Drosophila melanogaster*, as well as investigate its impact on neurodegenerative disease models.

Chapter 3 describes the generation of a complete genetic toolkit for knockdown, knockout, and transgenic expression of all uniporter components conserved in *D. melanogaster*. Building on established *Drosophila* stock libraries and previous work in the lab, I created tagged expression constructs and gene knockouts for *EMRE*, *MICU1*, and *MICU3*. *EMRE* and *MICU3* knockouts were generated through NHEJ following CRISPR-Cas9 induced DNA cleavage, whereas I employed the more classical P-element mobilisation for the *MICU1* mutant. Accordingly, this chapter provides some comparison between the two methods, and offers guidance for other *Drosophila* labs in the optimisation of such mutagenesis.

Using this genetic toolkit, Chapter 4 examines the *in vivo* consequences of manipulating uniporter component levels. The behavioural consequences of *MCU* and *EMRE* loss are compared, and the first *in vivo* characterisation of *MICU3* knockout is reported. Additional experiments examine mitochondrial morphology and regulation of pyruvate metabolism. These results inform the ongoing debate surrounding the dispensability of the uniporter for life, and lay the foundation for future work, such as probing the mechanistic basis of metabolic phenotypes.

The loss of *MICU1* provided especially dramatic phenotypes and have therefore been separately partitioned in Chapter 5. These are compared with the contemporary mouse knockout. The severe consequences of *MICU1* loss formed the basis for several genetic interaction studies, the results of which challenge the current view of its function.

Finally, the effects of uniporter manipulation on neurodegenerative models are described in Chapter 6. Based on the evidence associating their aetiology with altered mitochondrial calcium dynamics, models of *Pink1* loss and Aβ toxicity were selected. Uncovering a strong interaction between the uniporter and both models suggests that mitochondrial calcium uptake should be considered for therapeutic targeting in the treatment of these neurodegenerative diseases, and potentially others.

2. Materials and Methods

2.1. Drosophila husbandry

Flies were maintained on a 12:12 hour light/dark cycle in Sanyo incubators (MIR-254), on food containing cornmeal, agar, molasses, yeast, and propionic acid. Long-term fly storage was at 18°C, whereas expanded short-term stocks and genetic crosses, along with experimental crosses were kept at 25°C to shorten generation time. Unless otherwise specified, flies were immobilised via CO_2-induced anaesthesia. Anaesthesia was minimised as much as possible, and behavioural assays were performed the next day at the earliest.

A list of fly lines used in this study is given in Table 2, with their source and identifier code.

Table 2. Fly lines used, with source and ID. BDSC = Bloomington Drosophila Stock Center (RRID:SCR_006457). FlyORF = Zurich ORFeome Project (Bischof *et al.*, 2013).

Genotype	Source	ID
w^{1118}	BDSC	RRID: BDSC_6326
y^1 w^{67c23}; P{w^{+mC} y$^{+mDint2}$ = EPgy2}*MCU*^{EY01803}	BDSC	RRID: BDSC_16357
y^1 w^{67c23}; P{y$^{+mDint2}$ $w^{BR.E.BR}$ = SUPor-P}*MICU1*^{KG04119}	BDSC	RRID: BDSC_13588
y^1 M{w^{+mC} = nos-Cas9.P}ZH-2A w^*	BDSC	RRID: BDSC_54591
w^*; Kr^{If-1}/CyO; P{$w^{+mW.hs}$ = GAL4-*da*.G32}UH1	BDSC	RRID: BDSC_55850
w^*; P{$w^{+mW.hs}$ = GAL4-*arm*.S}11	BDSC	RRID: BDSC_1561
w^{1118}; M{w^{+mC}=*nSyb*-GAL4.P}ZH-86Fb/TM6B	BDSC	RRID: BDSC_68222
y^1 w^*; P{w^{+mC}=GAL4-*Mef2*.R}3	BDSC	RRID: BDSC_27390
w*; P{$w^{+mW.hs}$ = GawB}*tey*^{5053A}/TM6B, Tb^+	BDSC	RRID: BDSC_2702
w^{1118}; P{GD446}v9501/TM3	VDRC	v9501
P{KK109347}VIE-260B	VDRC	v110781
w^{1118}; P{GD3797}v45211	VDRC	v45211

w^{1118}; P{GD3076}v6786	VDRC	v6786
P{KK105775}VIE-260B	VDRC	v105566
P{NIG.4462R-4} II	NIG-FLY	N/A
P{NIG.4462R-3} III	NIG-FLY	N/A
w^{1118} P{GD4927}v49349	VDRC	v49349
y^1 sc^* v^1 sev^{21}; P{$y^{+t7.7}$ $v^{+t1.8}$ =TRiP.HMS02302}attP2	BDSC	RRID: BDSC_41909
M{UAS-MICU1.ORF.3xHA}ZH-86Fb	FlyORF	F000962
w^{1118}; P{w^{+mC} = UAS-mito-HA-GFP.AP}2/CyO	BDSC	RRID: BDSC_8442
w^{1118}; P{w^{+mC} = UAS-mito-HA-GFP.AP}3, e^1	BDSC	RRID: BDSC_8443
P{UAS-MCU}attP40	(Tufi *et al.*, 2019)	FlyBase: FBtp0137260
P{UAS-MCU}attP2	(Tufi *et al.*, 2019)	N/A
P{UAS-MICU1-B-HA}attP40	This study	N/A
P{UAS-MICU1-B-HA}attP2	This study	FlyBase: FBtp0137257
P{UAS-EMRE}attP40	This study	N/A
P{UAS-EMRE-myc}attP40	This study	N/A
P{UAS-EMRE}attP2	This study	N/A
P{UAS-EMRE-myc}attP2	This study	FlyBase: FBtp0137261
P{UAS-MICU3-A-V5}attP40	This study	FlyBase: FBtp0137258
P{UAS-MICU3-A-V5}attP2	This study	N/A
P{UAS-MICU3-C-V5}attP40	This study	FlyBase: FBtp0137259
P{UAS-MICU3-C-V5}attP2	This study	N/A
MCU^1	(Tufi *et al.*, 2019)	FlyBase: FBal0351717
MICU1^{32}	This study	FlyBase: FBal0351712

EMRE^{1}	This study	FlyBase: FBal0351719
EMRE^{2}	This study	FlyBase: FBal0351720
EMRE^{3}	This study	FlyBase: FBal0351721
MICU3^{27}	This study	FlyBase: FBal0351714
*w**; P{UAS-p35.H}BH2	BDSC	RRID: BDSC_5073
*w**; P{UAS-DIAP1.H}3	BDSC	RRID: BDSC_6657
Df(3L)H99, *kni*$^{ri\text{-}1}$ *p*^{p}/TM3, *Sb*^{1}	BDSC	RRID: BDSC_1576
w Pink1^{B9}/FM7.GFP	(Park *et al.*, 2006)	FlyBase: FBal0193144
w;*park*^{25}/TM6B.GFP	(Greene *et al.*, 2003)	FlyBase: FBal0146938
w[*]; P{w[+mC]=*ple*-GAL4.F}3	BDSC	RRID: BDSC_8848
P{UAS-Aβ.Arctic}	(Crowther *et al.*, 2005b)	FlyBase: FBtp0056417

2.2. Cloning

To mutagenise *EMRE* and *MICU3*, gRNAs targeting the genes were cloned into the pCDF4 vector (Port *et al.*, 2014). Briefly, forward and reverse primers were ordered containing the selected gRNA sequences. These were used in a PCR with pCFD4 as a template, to generate a construct for insertion. Separately, PCFD4 was linearised by restriction digestion with BbsI FD (Thermo Fisher Scientific). The construct and linearised vector were gel purified using a QIAquick Gel Extraction Kit (Qiagen) and assembled with a Gibson Assembly® Master Mix (New England Biolabs). After transforming into 10-β competent *E. coli*, cultures were plated in LBA with ampicillin. Colonies were sequenced using the primer outlined by Port and colleagues (GACACAGCGCGTACGTCCTTCG). Selected cultures were processed via Midiprep kit (Qiagen) and inserted into the *Drosophila* genome by ϕC31-mediated site-specific integration (BestGene Inc.). The attP40 (chromosome II) and attP2 (chromosome III) sites were used, avoiding the chromosome containing the target gene.

In this work, the following transgenic lines were cloned: UAS-*EMRE*-myc, UAS-*MICU1*-B-HA, UAS-*MICU3*-A-V5, UAS-*MICU3*-C-V5. *EMRE* was amplified directly from whole Oregon-R adult *D. melanogaster* by PCR, and for the other transgenes, cDNA clones were used as a template (UAS-*MICU1*-B-HA: IP17639, UAS-*MICU3*-A-V5: LD23951, UAS-*MICU3*-C-V5: RH09265). The relevant epitope tag was inserted via the reverse primer. Inserts were digested (*EMRE*: EcoRI/XhoI, *MICU1*/*MICU3*: NotI/XbaI), as was the pUASTattB vector (BestGene Inc.). These were then combined in the presence of T4 ligase and incubated overnight at 4°C. The following afternoon, the resulting constructs were incubated with 10-β competent *E. coli* for 45 minutes. After heat shock, these were added to SOC media for one hour at 37 °C before plating in LBA and being incubated overnight. Colony PCR using the standard UAS vector insert primers for the Whitworth lab (Fw: GCAACTACTGAAATCTGCCAAG, Rv: CACACCACAGAAGTAAGGTTCC) confirmed the presence of the construct. Positive colonies were moved to flasks containing 100ml LB and incubated overnight at 37 °C. Resulting cultures were processed via Midiprep kit (Qiagen) and sent for sequencing between UAS primers (GENEWIZ). Full coverage of the gene was obtained, confirming entire cloned gene aligned to the *Drosophila* reference

genome with 100% identity. Additionally, the orientation and sequence of other elements such as the epitope tag were verified. Selected constructs were sent for ϕC31-mediated site-specific integration into attP40 and attP2 sites (UAS-*EMRE*-myc: Department of Genetics, University of Cambridge, others: BestGene Inc.).

2.3. Mutagenesis

MICU1 mutants were generated through P-element mobilisation, which has a low frequency of imprecise excision events. P{SUPor-P}MICU1^{KG04119} was selected to create the *MICU1*^{32} allele. To achieve this, Δ2-3 transposase expressing flies were crossed to the relevant P-element stock. Virgin female progeny, containing a different mutagenesis event in each egg, were individually crossed to balancer males, and the progeny stabilised as balanced stocks. These were finally evaluated for deletions through a PCR primer pair spanning the P-element insertion site. Failure to yield a PCR product indicated a deletion event, and additional primers were designed to map breakpoints.

For *EMRE* and *MICU3*, virgin females of the *nos*-Cas9 line, which expresses the enzyme under the control of the germline restricted *nanos* promoter, were crossed to gRNA lines described in Section 2.2. Virgin female progeny, expressing both gRNA and Cas9 in their ova, were crossed to balancer males. Each offspring from this cross represents a unique mutant event, and single males were isolated and crossed to balancer virgin females to create stable lines. PCR primers spanning the predicted gRNA recognition site were used to generate products, which were gel-purified via a QIAquick Gel Extraction Kit (Qiagen) and sent for Sanger sequencing (GENEWIZ). Later, a RFLP strategy was devised to easily screen for the mutants isolated, namely *EMRE*^{1} and *MICU3*^{27}, using BcnI FD and MboII FD respectively (Thermo Fisher Scientific).

2.4. Behavioural Assays

2.4.1. Larval Crawling

Third instar larvae were collected from the food surface, and gently washed with distilled water and dried with a Kimwipe. Excessive washing was minimised at all stages. Individual larvae were placed on a fresh 1% agar plate, were they acclimatised for 30 seconds. After, the number of peristaltic waves was counted for 60 seconds. To minimise confounds from pheromones or other secreted factors, larvae of different genotypes were placed on different plates, and no more than six larvae were used with any one plate.

2.4.2. Eclosion Ratio

Genetic crosses were established using only balanced parents. Balancer chromosomes carry homozygous lethal mutations, so an expected third of total progeny would be homozygous. Flies were scored for balancer chromosome markers until the crosses were exhausted, to avoid confounds from delayed eclosion. The proportion of observed balanced/homozygous mutants was compared to the expected Mendelian ratio.

2.4.3. Climbing Assay

Unless otherwise specified, adult males 1-3 days post-eclosion were collected up to the day preceding the test, up to a maximum of 25 flies per group. On the day of the experiment, flies were moved to the ~23°C climbing room to acclimatise for 30 minutes, then placed in test tubes without food for 60 minutes. Flies were then placed in a counter-current apparatus as previously described (Greene *et al.*, 2003). After tapping to the bottom of the tube, flies had ten seconds to reach the upper portion of the apparatus, where they advanced to the next tube. After five successive trials, the average score was expressed as a climbing index.

2.4.4. Flight Assay

Up to a maximum of 25 adult males, 1-3 days post-eclosion, were placed into vials the day before the experiment. On the day of the experiment, vials were moved to the testing room at ~22°C, where they acclimatised for 30 minutes. Vials were then tapped into the top of a one litre graduated cylinder containing a vacuum grease-coated acetate sheet, via a funnel. The sheet was removed from the cylinder, and the immobilised flies in each of four equally divided sections were counted. Flies that did not adhere to the sheet were given a score of zero, and any that escaped the cylinder were not scored.

2.4.5. Sterility Assay

Single males or virgin females were isolated in individual vials with 2-3 partners of the opposite sex. Yeast was added to encourage fecundity. The fraction of crosses containing larvae (at any instar stage) was scored using a stereomicroscope up to approximately seven days.

2.4.6. Lifespan Assay

Crosses were established with equal numbers of parents to control for any overcrowding. Male progeny were collected under minimal CO_2 anaesthesia and placed in vials up to a maximum of 25 flies. These were maintained in standard (25°C, 12:12 hour light/dark) conditions, and moved onto fresh food thrice weekly. The number of dead flies was recorded on each flip, and any escapers were censored.

For starvation studies, the assay was set up as for the lifespan, but in empty vials containing Whatman filter papers. For full starvation, distilled water was added to the papers, and dead flies were counted every 12 hours. For sucrose only starvation, 5% sucrose solution was applied, with dead flies counted daily. In both cases, 100 µl of solution was added each day, except after paper replacement every ~ 3 days, when 200 µl was added.

To measure manganese tolerance, the assay was set up as for the lifespan, but on food containing manganese chloride tetrahydrate (Sigma, M3634) at the specified concentration (in general 0-100 mM). Dead flies were counted thrice weekly.

2.5. Mitochondrial imaging

2.5.1. Tissue Preparation

For flight muscle, adult males were dissected at the specified age in 4% paraformaldehyde. Using micro-scissors and fine forceps, the head and wings were removed. Then, the legs were cut, opening the cuticle around the level of the katepisternum. Using this opening, the thorax was divided along the midline into two halves. Thorax halves were fixed in 4% paraformaldehyde (Agar scientific; R1926) for 20 minutes at room temperature, before two PBS washes. Hemithoraces were mounted in Prolong Diamond Antifade Mountant (Thermo Fisher Scientific; P36961).

For adult brains, males at the specified age were dissected in PBS. After decapitation, the head cuticle was opened using fine forceps to expose the brain. Trachea and any remaining optic tissue were removed. Brains were fixed in 4% paraformaldehyde (Agar scientific; R1926) for 20 minutes at room temperature, washed with PBS thrice for 20 minutes each at room temperature, and mounted in mounted in Prolong Diamond Antifade Mountant (Thermo Fisher Scientific; P36961). In the case of the PPL1 clusters counted by R. Tufi, brains were stained with 1:200 mouse anti-TH (Immunostar #22941 RRID:AB_572268) for 72 hours at room temperature, followed by 1:200 anti-mouse-AF488 for 4 hours at room temperature, adapting a generalised protocol accordingly (Wu and Luo, 2006).

For larval motoneurons, larvae were pinned dorsal side up to a Sylgard (Sigma 761028) slide, stretched, and cut along the midline with micro-dissection scissors. Open larvae were bathed in dissection solution (128 mM NaCl, 1 mM EGTA, 4 mM $MgCl_2$, 2 mM KCl, 5 mM HEPES and 36 mM sucrose, adjusted to pH 7 using NaOH), the epidermis pinned back, and the guts and other internal organs removed, leaving the ventral nerve cord and motoneurons intact. These were taken immediately for live imaging, though motoneuron mitochondria remain motile for over an hour post-dissection when prepared in this way (V. L. Hewitt, personal communication).

2.5.2. Microscopy

Larval images were obtained through a Leica Microsystems DFC490 charge-coupled device attached to a Leica Microsystems MZ6 stereomicroscope at maximum zoom.

For both muscle and adult brain, fluorescence imaging was conducted with a Zeiss LSM 880 confocal microscope/Nikon Plan-Apochromat 63x/1.4 NA oil immersion objective. A single fluorophore (mitoGFP) was utilised, avoiding potential bleed-through, and an excitation laser of 488 nm was used. Gain and offset were adjusted to provide maximum dynamic range without signal saturation whilst minimising laser power. No photobleaching was observed, as expected given the high expression of this stable fluorophore.

Larval mitochondrial axonal transport was evaluated as previously described (Baldwin *et al.*, 2016). Movies were acquired using a Nikon E800 microscope with a 60x water immersion lens (NA 1.0 Nikon Fluor WD 2.0) and an LED light source driven by µManager 1.4.22 Freeware (Open Imaging) (Edelstein *et al.*, 2015). A CMOS camera (01-OPTIMOS-F-M-16-C) was used to record 100 frames at a rate of 1 frame per 2.5 seconds. Movies were converted into kymographs using Fiji (Schindelin *et al.*, 2012) and individual mitochondrial kymograph traces were manually classified into stationary, retrograde, or anterograde. Additionally, to quantify the mitochondrial length, single frames were thresholded and the maximum Feret diameter for each particle was calculated by the 'Analyze Particles' function of Fiji.

2.6. Molecular Biology

2.6.1. DNA Extraction

DNA was extracted from single flies using the squish prep approach. Single flies were immobilised in 1.5 ml microcentrifuge tubes at -20 °C for 2 minutes. With a P200 tip, flies were mashed for 10-20 seconds, then 50 µl squishing buffer (10 mM Tris-HCl pH 8.2, 1 mM EDTA, 25 mM NaCl, with freshly added Proteinase K to 200 $\mu g.ml^{-1}$) was expelled from the tip. Homogenates were incubated at 37 °C for 30-60 minutes, and proteinase K was inactivated at 95 °C for 2 minutes.

2.6.2. Polymerase Chain Reaction

In general, PCR reactions were conducted using a Taq master mix (New England Biolabs), containing dNTPs, $MgCl_2$, KCl, tracking dyes and stabilisers along with the enzyme. The master mix was combined with the relevant template DNA and primers, briefly vortexed, and placed in a thermocycler. The general program was as follows: 95 °C 30" | (30 x) 95°C 15", 60 °C 30", 68 °C 1' | 68 °C 5' | 12 °C hold. The annealing temperature, extension time, and number of cycles was adjusted as necessary. Primers used in this study (all ordered from Sigma) are shown in Table 3. After thermocycling, PCR products were typically loaded into a 1% agarose gel with 1X SYBR Safe (Thermo Fisher Scientific) and ran at 110 V for 45 minutes. Small products were run on a 2% agarose gel.

Table 3. Overview of primers used, with primary application, T_m, and extension time.

Name	Sequence	Application	T_m used	Extension time used
EMRE-myc Fw	GCGCGAATTCAAAATGATTGTCCCACGCCTGG	Cloning	Touchdown	30"
EMRE-myc Rv	GCGCCTCGAGTTACAGATCCTCTTCTGAGATGAGTTTTTGTTCATCCTCGTCGTCGTCGTC	Cloning	Touchdown	30"

MICU1-B-HA Fw	ATATATATATGCGGCCGCAAAATGTCTGTGCTGCGATTCC	Cloning	Touchdown	2’
MICU1-B-HA-Rv	GCGCTCTAGATTAAGCGTAATCTGGAACATCGTATGGGTAGATGTCCAGCAGCACA	Cloning	Touchdown	2’
MICU3-V5 Fw	ATATATATATGCGGCCGCAAAATGGCGGGTTTAGCGGC	Cloning	Touchdown	2’
MICU3-A-V5 Rv	GCGCTCTAGATCAGGTGCTATCCAGGCCCAGCAGGGGGTTGGGGATGGGCTTGCCGTGCCAAAGCGCAT	Cloning	Touchdown	2’
MICU3-C-V5 Rv	GCGCTCTAGATTAGGTGCTATCCAGGCCCAGCAGGGGGTTGGGGATGGGCTTGCCGTTTGCCGACTTCATCA	Cloning	Touchdown	2’
pCFD4 Seq	GACACAGCGCGTACGTCCTTCG	Sequencing	N/A	N/A
EMRE[1] Fw	GCGCTTTTCAACACTACTAC	PCR	60 °C	30”
EMRE[1] Rv	GGTATGACGGCACAGAAGATG	PCR	60 °C	30”
MICU3[27] Fw	CTCGATCTCTGATCCCGCA	PCR	60 °C	30”
MICU3[27] Rv	TCGTGCAGAAAACAACTACATTT	PCR	60 °C	30”
MICU1[32] Fw1	GCACAGTCACGTTATTGTTTACAT	PCR	60 °C	3’
MICU1[32] Rv1	CCCATTCAAGTCAAACATGCG	PCR	60 °C	3’

MICU1[32] Fw2	GACTTGAATGGGGATGGTG	PCR	60 °C	30”
MICU1[32] Rv2	CAAAGCCGAGTTCACACCC	PCR	60 °C	30”
MICU1[32] Fw16	TTTGACATCCACATTCCGACAGG	PCR	60 °C	6’ 30”
UAS Fw	GCAACTACTGAAATCTGCCAAG	PCR	60 °C	Variable
UAS Rv	CACACCACAGAAGTAAGGTTCC	PCR	60 °C	Variable
EMRE Fw	ACATGTCCAGCGTGTACTTTC	qRT-PCR	60 °C	30”
EMRE Rv	GGTATGACGGCACAGAAGATG	qRT-PCR	60 °C	30”
MICU3 Fw	GATCCACAAACCAAGCGAAT	qRT-PCR	60 °C	30”
MICU3 Rv	CCTCTTCCGGCTCTTGCT	qRT-PCR	60 °C	30”
MICU1 Fw	GTGGCCATGGTCAATCTTTC	qRT-PCR	60 °C	30”
MICU1 Rv	TTGTTGCTGAGTTGGTTGTCA	qRT-PCR	60 °C	30”
Rpl32 Fw	GCCGCTTCAAGGGACAGTATCTG	qRT-PCR	60 °C	30”
Rpl32 Rv	AAACGCGGTTCTGCATGAG	qRT-PCR	60 °C	30”

2.6.3. RNA extraction, cDNA synthesis, and qRT-PCR

qRT-PCR experiments were performed by R. Tufi. as part of our recent work (Tufi *et al.*, 2019). With permission, the relevant method description is quoted below.

"Isolation of total RNA was performed using the RNeasy RNA purification kit (QIAGEN); cDNA was synthesised from total RNA using ProtoScript® II first strand cDNA Synthesis Kit (New England BioLabs, E6560S) according to manufacturer's instructions. Total RNA concentration was ascertained spectrophotometrically, and equivalent amounts of total RNA underwent reverse transcription for each sample. Quantitative real-time PCR (qRT-PCR) was performed on a CFX96 Touch™ Real-Time PCR Detection System. Gene-specific primers were designed to have oligos spanning an intron whenever possible. Primer sequences were as follows: *EMRE* forward 5'-ACATGTCCAGCGTGTACTTTC-3' and reverse 5'-GGTATGACGGCACAGAAGATG-3'; *MICU1* forward 5'-GTGGCCATGGTCAATCTTTC-3' and reverse 5'-TTGTTGCTGAGTTGGTTGTCA-3'; *MICU3* forward 5-GATCCACAAACCAAGCGAAT-3' and reverse 5'-CCTCTTCCGGCTCTTGCT-3'; *sulfateless* forward 5'-AAGCTGTCGATTTGAGTAGCAA-3' and reverse 5'-GACTGTCCACTCGCAATCAG-3'; *javelin* forward 5'-GCGGATTTTTCCGTGAATC-3' and reverse 5'-TCTGGCTCTGGGTGTCATC-3'; and *RpL32* forward 5'-GCCGCTTCAAGGGACAGTATCTG-3' and reverse 5'-AAACGCGGTTCTGCATGAG-3'. Carryover DNA was removed with Turbo DNase free (Ambion, Cat. No. AM1907) according to the manufacturer's protocol. The relative transcript levels of each target gene were normalized against *RpL32* RNA levels; quantification was performed using the comparative C_T method (Schmittgen and Livak, 2008). "

2.6.4. Immunoblotting

MCU and EMRE expression was analysed from fly homogenates enriched for mitochondria. Approximately 100 flies per genotype were placed on ice for 5 minutes and homogenized in a glass tissue grinder with 2 mL of mitochondrial isotonic buffer (225 mM mannitol, 75 mM sucrose, 5 mM HEPES, 0.5 mM EGTA, 2 mM taurine, pH 7.25) at 4 °C for 30-60 seconds until uniform. Homogenates were centrifuged at 500 *g*, 4 °C for 5 min. Supernatants were passed through a 100 µm nylon sieve (Cell Strainer REF 352360, BD Falcon, USA) to remove wings and other debris. After additional centrifugation at 11000 *g*, 4 °C for 10 min, pellets were stored at -80 °C until use. On the day of the experiment, mitochondrial pellets were lysed in 50 µl RIPA buffer (50 mM Tris-HCl pH 8.0, 150 mM NaCl, 1 mM EDTA, 0.5% SDS, 1% (v/v) Triton X-100) supplemented with cOmplete mini EDTA-free protease inhibitors (Roche) for 10 min on ice. After three freeze-thaw cycles between dry ice and a 37 °C water bath, lysates were centrifuged at 20000 *g* for 5 min at room temperature, and the supernatants used for protein quantification and electrophoresis, where 4X Laemmli buffer (Bio-Rad) containing 1:10 β-mercaptoethanol (Sigma) was added.

For MICU1 and MICU3, flies were homogenized in a PBS-based lysis buffer with lithium dodecyl sulphate containing β-mercaptoethanol and supplemented with cOmplete mini EDTA-free protease inhibitors (Roche).

Equal amounts of proteins were loaded into 10% TGX Precast Gels (Bio-Rad), according to the manufacturer's instructions. A variable current at 200 V was passed through the gel for 40 minutes, or until well resolved. Gels were transferred to nitrocellulose membranes using the semi-dry TransBlot system (Bio-Rad), using the Mixed M_w TGX program. Transfer was evaluated with Ponceau S staining. Membranes were blocked for two hours at room temperature in 5% (w/v) dried skimmed milk powder in TBST (0.15 M NaCl, 10 mM Tris-HCl pH 7.5, 0.1% Tween 20). Blocked membranes were probed with the indicated primary and secondary antibodies. HRP-labelled secondaries were incubated in ECL-Prime (Amersham) for 5 minutes at room temperature and visualised with a ChemiDoc XRS+ molecular imager (Bio-Rad). Fluorescent secondaries were instead directly imaged in an Odyssey CLx system (Li-Cor).

The following commercial primary antibodies were used: mouse anti-ATP5A (Abcam ab14748; RRID:AB_301447; 1:20000), mouse anti-TH (Immunostar 22941; RRID:AB_572268; 1:200), rabbit anti-HA (Abcam ab9110; RRID:AB_307019; 1:1000), rabbit anti-Porin (Millipore PC548; RRID:AB_2257155; 1:5000), mouse anti-V5 (Thermo Fisher Scientific R960-25; RRID:AB_2556564; 1:2000), mouse anti-Myc (Cell Signalling, clone 9B11; RRID:AB_331783; 1:800). In addition, anti-MCU was generated in rabbits through inoculation with a KLH-conjugated peptide, RTQENTPPTLTEEKAERKY, targeting the C-terminal of the protein (Pepceuticals, 1:1000).

The following commercial secondary antibodies were used: goat anti-mouse-HRP (Abcam ab6789-1; RRID:AB_955439; 1:5000-1:40000), goat anti-rabbit-HRP (Invitrogen G21234; RRID:AB_2536530; 1:3000 to 1:5000), anti-mouse-AF488 (Invitrogen A11001; RRID:AB_2534069), anti-mouse-AF680 (Thermo Fisher Scientific A21057; 1:5000), anti-mouse-AF790 (Thermo Fisher Scientific A11374; 1:5000).

2.7. Membrane potential/Ca^{2+} flux

Assays were performed by collaborators in Padua (S. von Stockum, supervised by E. Ziviani). Approximately 50 whole adult flies were ground in a Dounce homogeniser with loose-fitting pestle, in a mannitol-sucrose buffer (225 mM mannitol, 75 mM sucrose, 5 mM HEPES, 0.1 mM EGTA, pH 7.4, 2% BSA). Debris was removed via centrifugation for 6 min at 1500 *g,* 4°C, filtering the supernatant. This was pelleted at 7000 *g*, 4°C, for 6 min, and resuspended in the mannitol-sucrose buffer without BSA, pelleted again in the same conditions, and resuspended ~50 µl of mannitol-sucrose buffer without BSA. The Biuret test quantified the resulting protein concentration.

Isolated mitochondria were used to measure mitochondrial Ca^{2+} flux and membrane potential in a plate reader format, using a Fluoroskan Ascent FL (Thermo Fisher Scientific). Experiments were performed at 25°C with the following settings: excitation: 485 nm, emission: 538 nm, bandpass filter: 10 nm. 2 µM Ruthenium Red was added to wells containing the incubation media (250 mM sucrose, 10 mM MOPS-Tris, 5 mM glutamate-Tris, 2.5 mM malate-Tris, 5 mM Pi-Tris, 10 µM EGTA, pH 7.4). Additionally, the media contained 0.5 µM Calcium Green 5N (Invitrogen C3737) for Ca^{2+} flux, or 0.4 µM Rhodamine123 (Rh123; Molecular Probes) for membrane potential readings. Mitochondria were then diluted to a concentration of 1 mg/ml in the media. 45 µM calcium chloride or 1 µM Carbonyl cyanide-p-trifluoromethoxyphenylhydrazone (FCCP) were added during the experiments as described in the figures.

2.8. Respirometry

Respiratory measurements were taken using an Oxygraph-2k high-resolution respirometer (OROBOROS Instruments). The Oroboros system is based on a polarographic oxygen sensor, where dissolved oxygen in a sealed chamber diffuses across a selectively permeable membrane, where a reduction in the sensor generates an electrical current from which the concentration can be computed. A cannula allows for the addition of substrates, uncouplers, and inhibitors, to assess respiratory activity in different modes. Chamber temperature was set to 30 ^{o}C, recording interval 2 seconds, stirrer at 750 rpm, with a chamber volume of 2 ml. Calibration with air-saturated medium was performed daily. For *MCU*[1] and *EMRE*[1], five flies per replicate for each genotype were homogenised in respiration buffer (120 mM sucrose, 50 mM KCl, 20 mM Tris-HCl, 4 mM KH_2PO_4, 2 mM $MgCl_2$, 1 mM EGTA, 1 g/l fatty acid-free BSA, pH 7.2). For *MICU3*[27], 5 heads per replicate were used, and for *MICU1*[32], five wandering L3 larvae. Data acquisition and analysis were carried out using Datlab software (OROBOROS Instruments). For coupled (state 3) assays, Complex I-linked respiration was measured at saturating concentrations of malate (chamber concentration 2 mM), glutamate (10 mM) and ADP, (2.5 mM). After, 0.15 µM rotenone, 10 mM succinate was added to evaluate Complex II-linked respiration. For *MICU1*[32] larvae, 10 mM proline was included for Complex I-linked respiration.

2.9. ATP measurement

Luciferase, which consumes ATP to catalyse the oxidation of luciferin to oxyluciferin, efficiently generates light at a wavelength depending on the species of origin. Recombinant luciferase has been modified to enhance its sensitivity as an ATP sensor. The CellTiter-Glo® Luminescent Cell Viability Assay (Promega) uses a recombinant luciferase premixed with the luciferin substrate and an optimised buffer to yield sensitivity at 1.5 x 10^{-15} moles ATP, with a dynamic range covering four orders of magnitude (https://promega.media/-/media/files/products-and-services/instruments/detection/tbs-technical-support-docs/997-9305.pdf?la=en, accessed 2019/08/03). The Whitworth lab has adapted this technique to measure ATP in *Drosophila* homogenates (Pogson *et al.*, 2014). Briefly, five male flies/genotype (approx. 3 days post-eclosion) were homogenized in 100 μL 6 M guanidine-Tris/EDTA, and immediately frozen in LN_2. Diluted homogenates (1:100 in homogenisation buffer) were mixed with the luciferase solution. Luminescence counts were measured using a SpectraMax Gemini XPS luminometer (Molecular Devices). The average luminescent signal from technical triplicates was normalised to protein levels via a BCA assay (Pierce BCA Protein Assay Kit). For *MICU3*[27], 10 fly heads were used per sample, and for *MICU1*[32], 10 larvae.

2.10. Statistical analysis

Data are reported as mean ± SD, SEM or 95% confidence interval (CI) as indicated in figure legends. Unless otherwise noted, n refers to biological replicates or number of animals tested.

For climbing and flight analysis, Kruskal-Wallis non-parametric test with Dunn's post-hoc correction for multiple comparisons was used. For lifespan experiments, significance levels were determined by log-rank tests and reported in the figure legends. Mitochondrial transport, and larval crawling, ATP, and Oroboros measurements analysed by two-tailed unpaired *t*-test. Categorial comparisons were made using the χ^2-test.

Where no built-in test for multiple comparisons was available, they were accounted for by controlling the false discovery rate through the two-stage linear step-up procedure of Benjamini, Krieger and Yekutieli (Benjamini, Krieger and Yekutieli, 2006). Significance testing using p values controls the false positive rate, as in the fraction of results where the null hypothesis is false that would be correctly rejected. However, this ground truth is impossible to know *a priori*, and the more relevant metric is the fraction of rejected null hypotheses that are indeed false – the false discovery rate. This rate (denoted Q) was set to 5%, or 0.05, to mimic the $p<0.05$ threshold for significance common in medical science. The advantage of computing the false discovery rate with the cited method is that the whole distribution of reported p values is considered to estimate the prior probability of a given result being true. For example, in a discovery-based approach where most comparisons will not be relevant, the p value distribution is largely uniform. In a hypothesis-based study, where a greater fraction of comparisons is likely to be significant, the p value distribution will become strongly right-skewed. This allows for increased power without sacrificing accuracy. Only biologically relevant comparisons were made, and all non-significant values were reported.

No data points were excluded from the analyses. Analyses were performed using GraphPad Prism software (RRID:SCR_002798), versions 7 and 8.

3. A genetic toolkit for mitochondrial calcium uniporter manipulation

3.1. Background and aims

The model organism *Drosophila melanogaster* provides an ideal system for genetic dissection of the biochemical underpinnings of health and disease. The short generation time of the fly allows for rapid genetic crossing schemes, and its short lifespan is particularly useful for the study of age-associated diseases. The *Drosophila* mitochondrial calcium uniporter conserves the major components from the human complex, namely: the pore forming *MCU* (initially termed *CG18769*), the small regulatory subunit *EMRE* (*CG17680*), and the channel gatekeepers *MICU1* (*CG4495*) and *MICU3* (*CG4662*). Key structural features of these proteins are also conserved, specifically any transmembrane domains, the DIME loop and coiled-coil domains of *MCU*, the C-terminal acidic domain of *EMRE*, and the EF-hands of *MICU1* and *MICU3*, as shown in Figure 10.

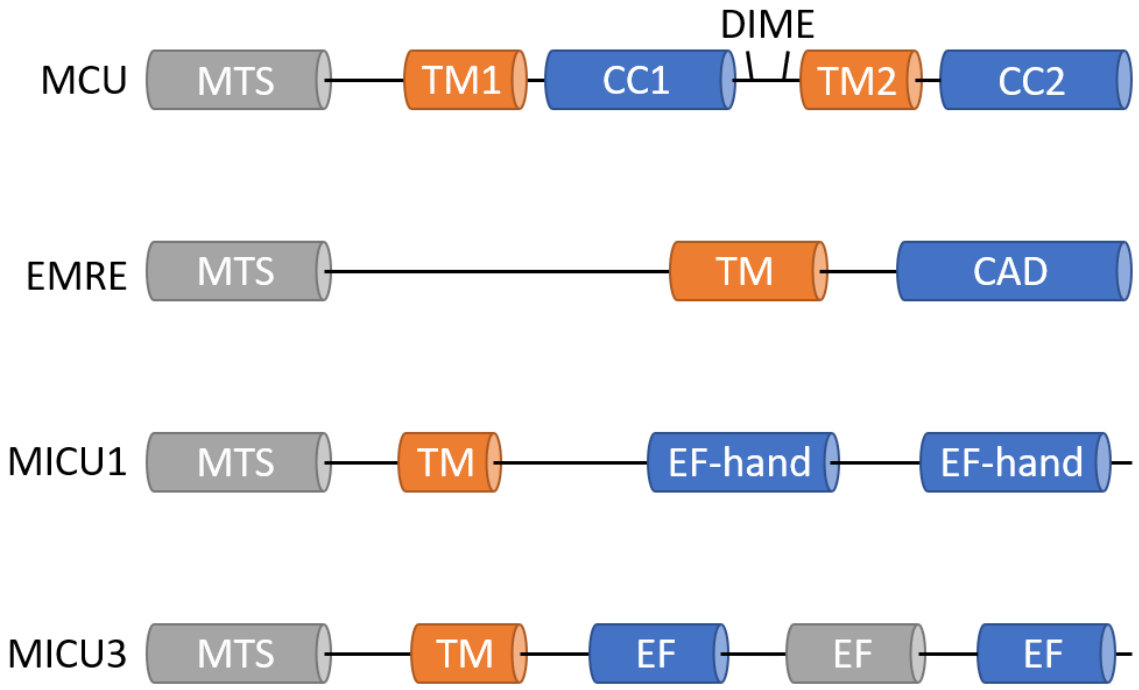

Figure 10. Domain organisation of *Drosophil*a uniporter proteins (not to scale). TM: transmembrane domain, CC: coiled-coil domain, CAD: C-terminal acidic domain, EF: EF-hand domain. The EF-hand domain indicated in MICU3 is predicted but does not bind calcium.

Perhaps the greatest strength of the fruit fly as an animal model is its long history of genetic manipulation, resulting in myriad available tools and expertise, making it one of the most genetically tractable model organisms. A variety of tools for genetic manipulation are used in this chapter, and so their methodological principles and applications are briefly outlined in the following sections.

3.1.1. CRISPR-Cas9

An unusual series of palindromic spaced repeats were first identified in archaea, and bioinformatic approaches found structurally related elements in a variety of bacterial species. Termed clustered regularly interspersed palindromic repeats (CRISPRs), bioinformatic comparison also detected conserved so-called CRISPR-associated (cas) genes near these loci. The spacer sequences between the repeats were found to align to DNA from phages to which these bacteria were resistant, suggesting that these elements may underlie an adaptive immune response (Mojica *et al.*, 2005). Forward genetic screening showed that bacteriophage resistance correlated with spacers matching phage sequences, and polymorphisms in this region were associated with loss of resistance (Barrangou *et al.*, 2007). This provided direct evidence for the role of CRISPRs in this immune response.

The bacterial CRISPR mechanism consists of three phases (Horvath and Barrangou, 2010). In the first, acquisition – phage DNA is captured and incorporated into CRISPR spacers. In the second phase, crRNA biogenesis – CRISPR arrays are transcribed into pre-crRNA, which is cleaved by Cas proteins or RNase III to yield mature crRNAs that are incorporated into the Cas complex. In the final phase, interference – CRISPR-Cas9 complexes recognise viral DNA matching the “programmed” crRNA, where the HNH and RuvC nuclease domains of Cas9 cleave both strands adjacent to a protospacer adjacent motif (PAM, sequence NGG) to create a double stranded break, disabling the viral agent.

Following double-stranded DNA cleavage, repair pathways are activated to attempt to repair the damage. Of the most relevance for mutagenesis are non-homologous end joining (NHEJ) and homology-directed repair (HDR). NHEJ directly re-ligates cleaved DNA using microhomology as a guide (Mahaney, Meek and Lees-Miller, 2009). This can lead to repair errors, causing small indels. By contrast, HDR relies on homologous recombination with another DNA strand used as a template for the repair (Jasin and Rothstein, 2013). An artificial repair construct can be provided to manipulate the resulting sequence, allowing for precise control of the nature of the final mutant.

Many varieties of CRISPR systems have been discovered (Makarova and Koonin, 2015), which can be divided into Class 1 – using multiunit effector complexes, and Class 2 – with a single protein effector. Most applications of CRISPR use the Cas9 system, which belongs to the single protein effector Class 2 system. A key innovation in the development of CRISPR-Cas9 was to combine the tracrRNA and crRNA into a single so-called 'guide'-RNA (gRNA). This simplified the cloning requirements for this system to work *in vivo.* An alternative to Cas9 is Cpf1, which requires a crRNA only. The two enzymes cut in distinct positions relative to their PAMs, which have different sequences, allowing for complementary approaches to target a wider range of sequences.

Initially adapted to human cell lines, this powerful technique has been leveraged for mutagenesis in *Drosophila*. The generation of transgenic *Cas9* expressing lines and standardised gRNA vectors has allowed for simple, high-efficiency genome editing (Port *et al.*, 2014). The transmission rates vary from 25-100% depending on the delivery method for the Cas protein and gRNA, whether by direct microinjection into embryos or transgenic expression. This work demonstrates that *Drosophila* are well suited to the CRISPR-Cas9 system for rapid generation of novel mutant lines.

3.1.2. P-element excision

Mobile DNA elements were first discovered by McClintock in maize (McClintock, 1950), and have since been expanded to a wide variety of transposable elements (TEs) that can be broadly divided into two classes. Class I TEs, or retrotransposons, propagate through the genome via an RNA intermediate that is reverse transcribed into a new location, resembling retroviral replication. Class I TEs include long terminal repeats (LTRs), long interspersed nuclear elements (LINEs), and short interspersed nuclear elements (SINEs). Both LTRs and LINEs encode the reverse transcriptase necessary for their propagation, whereas SINEs co-opt the replication machinery of LINEs, as they lack their own. Class II TEs, or DNA transposons, bypass the RNA intermediate through a cut-and-paste mechanism catalysed by encoded transposases (though some are instead replicative). These may jump non-specifically throughout the host genome, or target specific sequences, and can replicate when transposition occurs during genome replication.

In crosses between *Drosophila* strains, a peculiar syndrome known as hybrid dysgenesis was observed. As well as sterility, this would result in high mutational frequency, including chromosomal aberrations. This was eventually attributed to a group of Class II TEs termed P-elements (Rubin, Kidwell and Bingham, 1982). Interestingly, P-elements seem to have arisen within the last century, becoming widespread in wild-type isolates and remaining absent in older laboratory-maintained lines. These approximately 3 kb regions encode a transposase that targets inverted repeats within the transposon to catalyse excision and re-insertion. This transposition was found to be amenable to hijacking to deliver extrachromosomal genetic information to the fly germline (Spradling and Rubin, 1982). Thus, a long tradition using these TEs in *Drosophila* research began. Perhaps the most famous example of their use is the popular UAS-Gal4 system (Brand and Perrimon, 1993). Here, P-elements carrying the transcriptional activator *Gal4* from *S. cerevisiae* were randomly integrated into the fly genome, bringing the protein under the control of myriad *Drosophila* promoters. This enhancer-trap library can be combined with constructs containing the UAS (upstream activating sequence) motif to precisely control the spatiotemporal expression of the transgene. Today, P-elements have been inserted into a substantial fraction of known protein coding genes, in an attempt to disrupt their function through insertional mutagenesis (Bellen *et al.*, 2011). Such insertions can be

compensated for by splicing out the affected exon but can still provide a useful platform for further gene disruption efforts through imprecise excision of the transposon. When P-elements excise themselves, they often do so precisely, leaving behind a defined mutation. However, in a small proportion of events, DNA degrades from the site of double strand breakage before DNA repair occurs, leading to a potentially kilobase-scale deletion. Thus, P-element insertions provide a key resource for generating deletion events in or around target genes.

3.1.3. ϕC31-mediated site-specific integration

The *Streptomyces* temperate phage ϕC31 integrates into the host genome via site-specific recombination between two attachment sites: the host *attP* and phage *attB*. Importantly, this creates two new sites: *attL* and *attR*, which are unable to recombine in a similar fashion (Thorpe and Smith, 1998). This unidirectionality, along with its site-specificity, made the system an ideal candidate for insertion of transgenic elements in a model organism, and was accordingly adapted for use in *Drosophila* (Groth *et al.*, 2004). Throughout the genome, *attP* sites have been inserted via P-element transposition. This has allowed for simple precise transgenic insertions using plasmids containing an *att*B site, in the presence of the ϕC31 integrase. Constructs incorporated in this fashion allow for a consistent local genomic context, controlling for potential *cis*-regulatory elements, for example. As such, expression from *attP* sites is typically stable and consistent between lines, and can be dictated by the Gal4/UAS system with minimum variability.

3.1.4. Hypothesis and aims

A null allele for the uniporter pore, MCU^1, had already been created in the Whitworth lab. R. Tufi mobilised the P{EPgy2}EY08610 transposable element that sits just 5' of the transcript, creating an imprecise excision event deleting a ~1.5 kb region including the 3' UTR and canonical start codon common to all but one annotated isoform (schematic given in Figure 11). The remaining predicted transcript, MCU-E, was not detected by RT-qPCR (performed by R. Tufi). In any case, I was unable to predict mitochondrial localisation for this putative protein based on a potential MTS sequence (Table 4), so if this isoform exists at all, its functional role is unclear. The MCU^1 mutant was confirmed as a functional null through calcium uptake experiments performed by collaborators S. von Stockum. and E.

Ziviani. Transgenic expression constructs for MCU were cloned by R. Tufi and inserted in sites on chromosomes II and III, allowing for easy combination with other manipulations. Additionally, a transgenic MICU1-HA expression line was acquired from the FlyORF collection, and RNAi lines for all conserved uniporter components from various stock centres (detailed in Section 2.1). A summary of lines available at the start of my project is given in Table 5. The first project milestone was to expand this to a complete set of tools for each uniporter constituent, providing a foundation for a comprehensive study of this crucial protein complex.

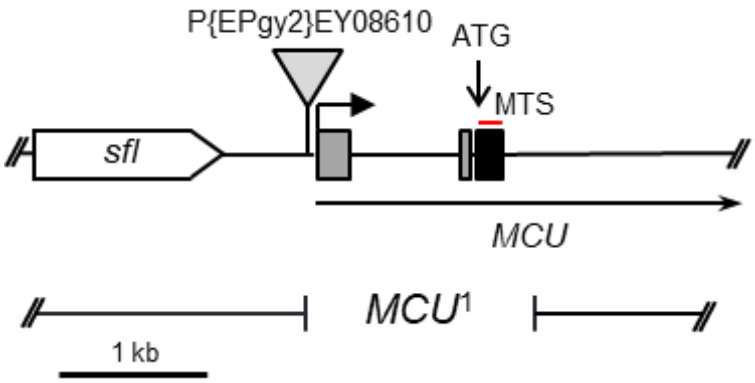

Figure 11. Reproduced from (Tufi *et al.*, 2019) - schematic of *MCU*[1] deletion mutant. The neighbouring gene *sfl* (*sulfateless*) is included. The P{EPgy2}EY08610 transposable element used to generate *MCU*[1] is displayed, along with the location of the *MCU*[1] breakpoints.

Table 4. Probability of mitochondrial import for MCU-E isoform as predicted by three programs. Notes represent additional information given by the program. From the Predotar documentation: 'If you are dealing with proteins that you already suspect to be targeted, look at the probabilities carefully; even a probability of 0.2 is well above "background" and may indicate a targeting sequence.'

Program	Predicted probability of mitochondrial import	Notes
MitoProt II	0.3649	Cleavage site: not predictable
Target P 1.1	0.325	Lowest reliability class (5)
Predotar	0.37	"possibly mitochondrial"

Table 5. Knockdown, mutant, and transgenic expression lines for conserved uniporter genes, either from stock centres or previous lab endeavours.

Gene	RNAi	Mutant	Transgenic
MCU (*CG18769)*	P{GD446}v9501	*MCU*[1]	P{UAS-MCU}attP40 P{UAS-MCU}attP2
MICU1 (*CG4495*)	P{GD4927}v49349 P{TRiP.HMS02302}attP2	None	P{UAS-MICU1-A-3xHA}ZH-86Fb
EMRE (*CG17680*)	P{KK109347}VIE-260B P{GD3797}v45211	None	None
MICU3 (*CG4662*)	P{GD3076}v6786 P{KK105775} P{NIG.4462R} II P{NIG.4462R} III	None	None

3.2. Cloning UAS-EMRE, -MICU1, -MICU3 transgenic lines

3.2.1. Transgenesis

Publicly available constructs or cDNAs were lacking for the single exon *EMRE*, so the gene was directly amplified from genomic DNA. For other transgenes, the following cDNA clones were used as templates: *MICU1*-B; IP17639, *MICU3*-A; LD23951, *MICU3*-C; RH09265. Primers were used as outlined in Table 6, with the reverse primer altered to create products for tagged and untagged constructs. Gel-extracted bands were combined with the pUAST-attB vector (BestGene Inc.) through restriction digest followed by T4 ligation. For *EMRE*, a double digest with EcoRI FD and XhoI FD was performed and for *MICU1* and *MICU3*, NotI FD and XbaI FD (Thermo Fisher Scientific). Constructs were transformed into 10-β competent *E. coli* and plated in LBA with ampicillin. Colony PCR was used to confirm the presence of the construct (example for EMRE in Figure 12). Positive colonies expanded in 100ml LB and processed via Midiprep (Qiagen). Sequencing between UAS primers (GENEWIZ) confirmed the features of the construct, and flies were sent for ϕC31 integrase-mediated site-specific recombination by commercial providers. All constructs were integrated into both attP40 and attP2 sites, which are situated on chromosomes II and III respectively. This allows for easy combination with other genetic manipulations. The pUASTattB vector is marked with the w^{+mC} minigene, which partially rescues the loss of eye pigmentation in *white* mutant flies and can be used as a selection marker to rapidly screen for transformants.

Table 6. Primers used for cloning UAS-EMRE and UAS-EMRE-myc. Sequence features highlighted in purple: EcoRI restriction site, orange: XhoI restriction site, pink: NotI restriction site, yellow: XbaI restriction site, green: start codon, red: stop codon, blue: epitope tag.

Primer	Sequence
EMRE-myc-F	GCGCGAATTCAAAATGATTGTCCCACGCCTGG
EMRE-myc-R	GCGCCTCGAGTTACAGATCCTCTTCTGAGATGAGTTTTTGTTCATCCTCGTCGTCGTCGTC
MICU1-B-HA-F	ATATATATATGCGGCCGCAAAATGTCTGTGCTGCGATTCC
MICU1-B-HA-R	GCGCTCTAGATTAAGCGTAATCTGGAACATCGTATGGGTAGATGTCCAGCAGCACA
MICU3-V5-F	ATATATATATGCGGCCGCAAAATGGCGGGTTTAGCGGC
MICU3-A-V5-R	GCGCTCTAGATCAGGTGCTATCCAGGCCCAGCAGGGGGTTGGGGATGGGCTTGCCGTGCCAAAGCGCAT
MICU3-C-V5-R	GCGCTCTAGATTAGGTGCTATCCAGGCCCAGCAGGGGGTTGGGGATGGGCTTGCCGTTTGCCGACTTCATCA

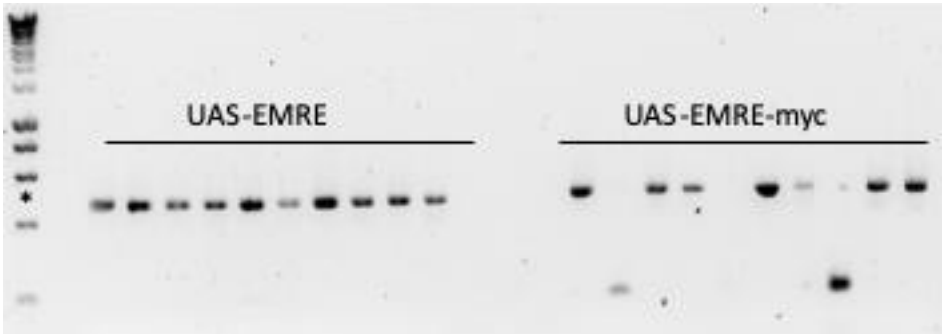

Figure 12. Colony PCR of UAS-EMRE and UAS-EMRE-myc constructs. Ten colonies for each construct were tested. * indicates approximate amplicon size for the construct. UAS-EMRE: 100% observed transformation efficiency, UAS-EMRE-myc: 70% (low weight bands indicate empty vector). Ladder: Hyperladder 1kb (Bioline)

3.2.2. Validation

The ϕC31 integrase uses defined recombination between specific sites, but there is still the possibility for inappropriate integration of the construct. Additionally, spontaneous mutations may occur in the transgene region. Although this rare event is unlikely to cause problems in the maintenance of an established stock, a deactivating mutation in a founding transformant would compromise the entire derived line. To rule this out, PCR was performed on transformant lines and the resulting products were sequenced. No mutations were detected in any transformant line.

UAS overexpression lines were crossed to ubiquitous Gal4 drivers. Transcript upregulation was confirmed by Western blot with primary antibodies directed against the relevant epitope tag (Figure 13). No antibody signal was detected in the Gal4 only control, as expected, with significant signal in driver/UAS combinations across all lines tested. As well as the cloned overexpression stocks, the publicly available UAS-MICU1-A-3xHA from FlyORF was tested, yielding detectable tagged protein. Size differences between UAS-MICU1 and UAS-MICU3 lines likely represent epitope tag sizes for MICU1, and differences in protein isoform size for MICU3. Interestingly, the apparent abundance of MICU3-C seemed much more than for MICU3-A. As these lines were integrated into the same site, they can be expected to express at a similar level, so the observed difference may instead reflect divergent protein stability. As functional consequences for protein overexpression are challenging to predict *a priori*, these Western blots remain the best foundational evidence for valid overexpression of the protein. Later work demonstrates rescue of mutant phenotypes by these transgenic lines, demonstrating that functional protein is produced (for *MICU1*: Section 5.3, *MICU3*: Section 4.4).

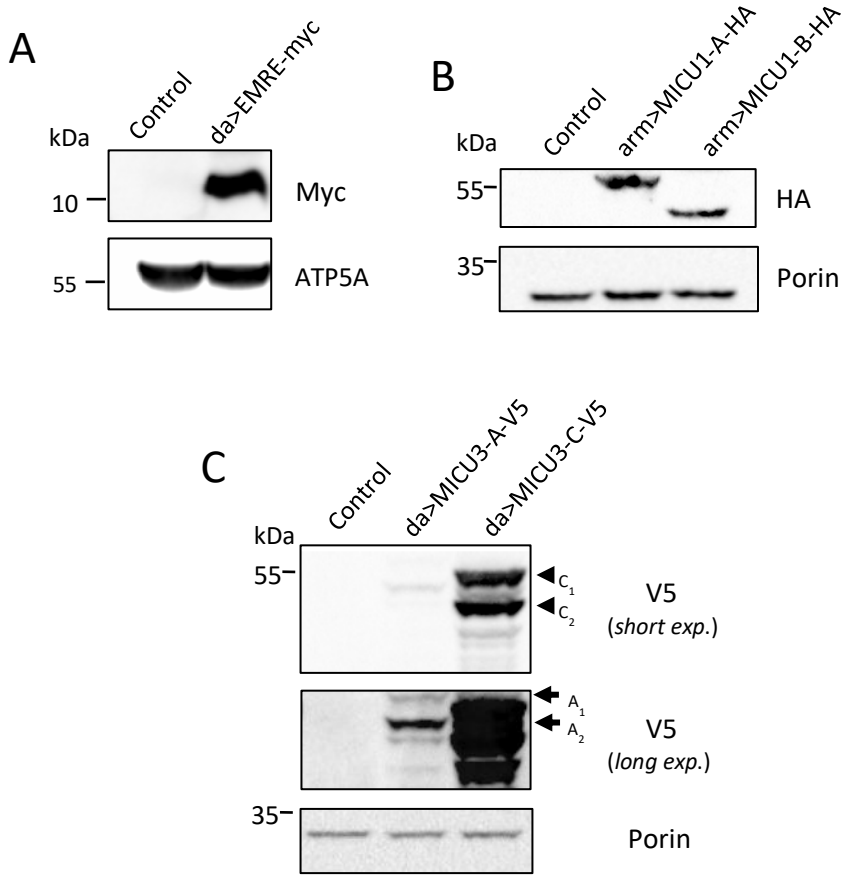

Figure 13. Western blots verifying transgenic overexpression of uniporter components. Control in each panel represents the relevant Gal4/+. Primary antibodies used in **A**: anti-myc (expected size: 12 kDa), with anti-ATP5A loading control (expected size: 59 kDa); **B**: anti-HA (expt. size: 64 kDa (A isoform)/62 kDa (B isoform)), with anti-Porin loading control (expected. size: 31 kDa); **C**: anti-V5 (expt. size: 58 kDa (A isoform)/56 kDa (C isoform)), with anti-Porin loading control. For panel C, bands corresponding to C_1 and C_2 represent MICU3-C with and without MTS, and similarly with A_1 and A_2 for MICU3-A. Panels **A** and **B** from data provided by R. Tufi.

3.3. Generating the null allele *MICU1*^{32} via P-element imprecise excision

3.3.1. Strategy

An overview of the *Drosophila MICU1* gene region is given in Figure 14. The transposable element P{SUPor-P}MICU1^{KG04119} was selected as a mutagenesis target. This P-element is located within the 6th exon common to both annotated isoforms of *MICU1*, yet surprisingly, was viable in homozygosity. This is possibly due to the entire exon being spliced out, which would not affect either the transmembrane helix or EF-hands of the resulting protein, but this was not determined experimentally.

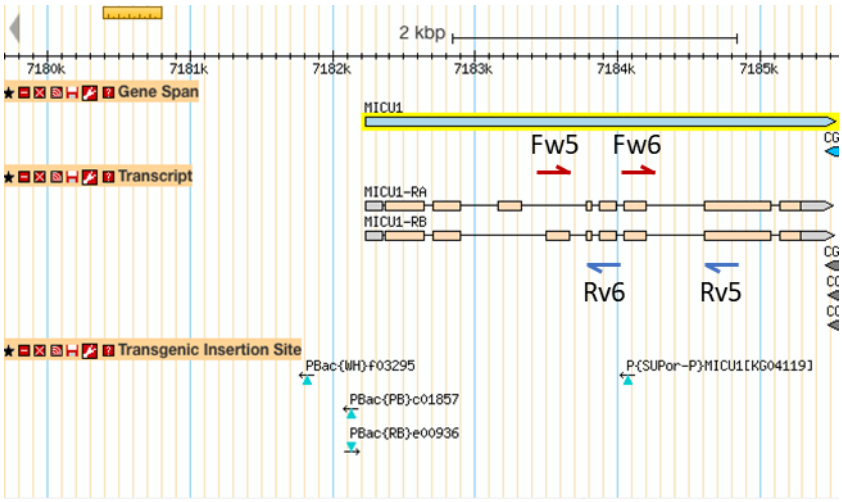

Figure 14. MICU1 Gene Region, including Transgenic Insertion Sites. The approximate locations of *MICU1* primer pairs Fw5/Rv6 and Fw6/Rv5 are given. Adapted from screen capture of Flybase GBrowse viewer (http://flybase.org/cgi-bin/gbrowse2/dmel/?Search=1;name=FBgn0031893, accessed 14/01/2019)

To achieve P-element excision, virgins of P{SUPor-P}MICU1^{KG04119} were crossed to a stock of Δ2-3 transposase. Single males of this genotype were separated and crossed to a chromosome II balancer to establish a total of 139 stable candidate lines. Initially the balancer chosen was CyO, but this was changed partway through the process to CyO P{w[+mC]=ActGFP}JMR1 in order to screen homozygosity pre-eclosion (by lack of GFP fluorescence) and more easily in the adults (by eye colour).

3.3.2. Mutagenesis

A single line, *MICU1*^{32}, was lethal both in homozygosity, and in *trans* to a deficiency covering the gene, Df(2L)Exel8019. DNA was amplified by PCR between Fw6/Rv5 primers, but not Fw5/Rv6 (Figure 14), indicating a deletion extending in the 5' direction from the P-element insertion. A. Terriente-Felix designed a series of Fw primers to test in combination with Rv5, eventually achieving a ~3.5 kb product using Fw16, which normally sits 11.8 kb distant. Sequencing this product showed a fragment of the original P-element remains in *MICU1*^{32}, but more importantly allowed for the deletion to be mapped to the following genomic coordinates; 2L:7173086-7184065. An overview of *MICU1*^{32} is given in Figure 15. This extends several kb upstream of *MICU1*, but the region is gene-sparse, so the deletion does not impinge on any other protein-coding genes. However, three long non-coding RNAs (CR44610-RA, CR46210-RA, and CR44613-RA) are deleted. The function of these specific lncRNAs is unknown, though more generally they are associated with transcriptional regulation. If their biological function is regulation of *MICU1* expression, then they would be irrelevant for evaluating a *MICU1* knockout line. If their effects are on other targets, there may be some unintended consequences from this mutation, though these are likely to be subtle. In any case, standard controls such as mutants in *trans* to deficiency lines and transgenic re-expression will provide evidence for the specificity of any observed phenotypes.

To easily screen for the presence/absence of *MICU1*^{32}, a PCR strategy was devised. The deleted region was too large for an amplicon to be easily generated to distinguish these mutants by size difference. Instead, two PCR primer pairs were developed. The first (Fw1: GCACAGTCACGTTATTGTTTACAT, Rv1: CCCATTCAAGTCAAACATGCG), amplifies a ~400 bp product in *MICU1*^{32}, but the primers are too far apart in the wild-type genome to amplify in standard conditions, though a long-range PCR can succeed. The second pair amplifies only in the wild-type (Fw2: GACTTGAATGGGGATGGTG, Rv2: CAAAGCCGAGTTCACACCC). Together, the zygosity of the mutant allele can be determined (Figure 16).

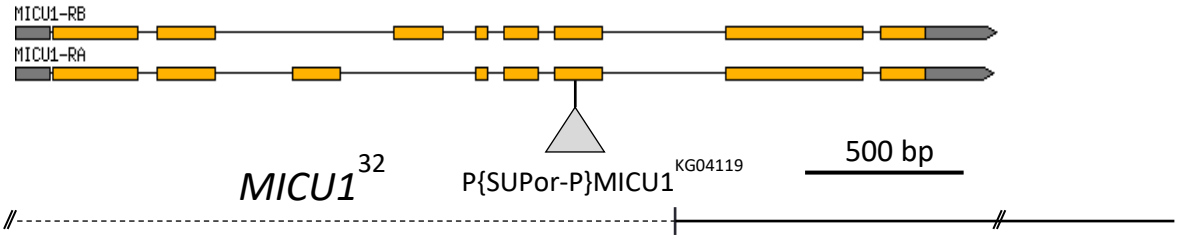

Figure 15. Schematic of MICU1[32] deletion mutant. The *MICU1* gene structure is given (adapted from Flybase GBrowse, see Figure 14), as is the insertion site of the P{SUPor-P}MICU1[KG04119] element used for mutagenesis. The resulting deletion, *MICU1*[32] is displayed (continues beyond left edge of figure).

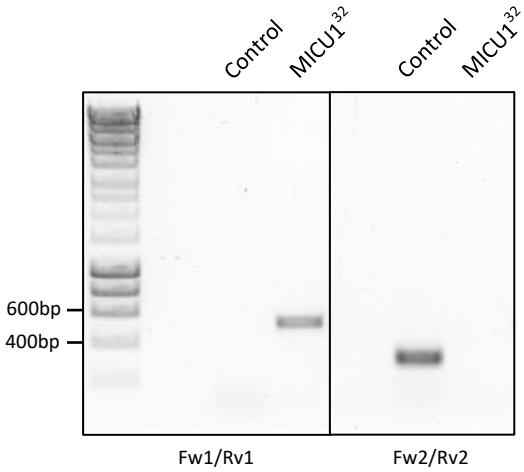

Figure 16. PCR strategy for detecting *MICU1*[32]. Left panel: PCR using Fw1/Rv1 gives a ~500 bp product in *MICU1*[32] and fails to amplify in the control (long range PCR can amplify this however). Right panel: PCR using Fw2/Rv2 gives a ~300 bp product in wild-type genomes but does not amplify in *MICU1*[32]. DNA ladder: Hyperladder 1kb (Bioline).

3.3.3. Validating *MICU1*^{32}

To determine the degree of transcript reduction in *MICU1*^{32}, qRT-PCR was employed (Figure 17). No appreciable transcript was detected in the mutant – this amount is likely to correspond to complete transcript loss, as expected from the sequence breakpoints. This confirms *MICU1*^{32} as an RNA null mutant. An attempt was made to measure the protein level of MICU1, but the commercially available antibody tested (HPA037480, Atlas Antibodies) did not recognise the *Drosophila* protein (data not shown). However, as the transcript was effectively absent, it logically follows that the allele is a genetic null, but this is independently confirmed in Section 5.3, where homozygous phenotypes are shared with a heterozygous mutant over a genetic deficiency. This is rescued by transgenic re-expression of MICU1, confirming the specificity of the mutant phenotype. Thus, the first *D. melanogaster* knockout for *MICU1* was generated, enhancing the suite of genetic tools available to study the mitochondrial calcium uniporter in this key organism.

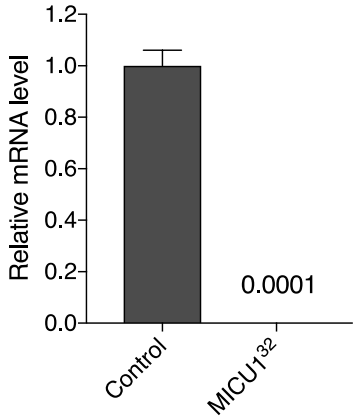

Figure 17. Relative transcript level of control (w^{1118}) and *MICU1*^{32} larvae. Error bars: SD. Transcripts were normalised against *RpL32*, and quantification was performed using the comparative C_T method (Schmittgen and Livak, 2008). Data generated by R. Tufi.

3.4. Generating *EMRE* and *MICU3* knockouts via CRISPR-Cas9 genome editing

3.4.1. Strategy

Both *EMRE* and *MICU3* gene loci did not contain any transposable elements suitable for knockout line generation. Instead, a CRISPR-based strategy was devised. The gene regions were scanned for optimal gRNA sequences using the CRISPR Optimal Target Finder (http://targetfinder.flycrispr.neuro.brown.edu) (Gratz *et al.*, 2014). Guides were selected to be as proximal to the canonical start codon as possible while excluding those with predicted off-target hits.

For the single exon *EMRE*, three guide RNAs were selected in total, all without predicted off-target sites. For *MICU3*, no suitable guides were detected in the first exon, but two were found in exon 2, termed Tg5 and Tg17. Both had predicted off-targets, but as none were in Chromosome III, where *MICU3* is located, any off-target mutations would be easy to breed out. The selected gRNAs are mapped in Figure 18; a summary is given in Table 7.

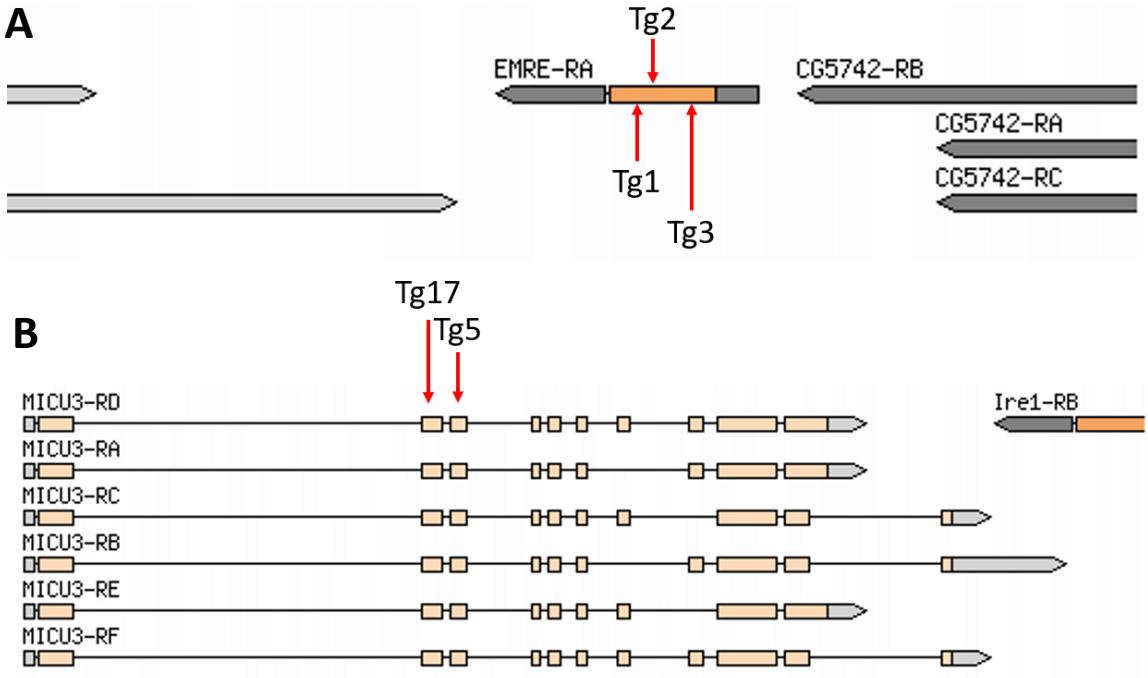

Figure 18. Genomic regions, adapted from FlyBase GBrowse output, of **A**: EMRE and **B**: MICU3, with locations of gRNA recognition sites marked by red arrows.

Table 7. Guide sequences used to mutagenize *EMRE and MICU3*. Green: protospacer adjacent motif (PAM), red pipe: predicted cut site. Genomic coordinates of any off-target sites are given, alongside their genetic context.

Guide Name	Guide Sequence	Off-target coordinates	Off-target location
EMRE-Tg1	GCAGGATC|CTTAGGTTATGGGGG	None	-
EMRE-Tg2	GCAGCGCG|TGTCGCGCCGGGTGG	None	-
EMRE-Tg3	GAACGATC|TGTTCGTGCCCGCGG	None	-
MICU3-Tg5	GAACACGC|CTGCTTTGAAGAAGG	4:234884..234906	*CG1674*
MICU3-Tg17	GAACGTAA|AACTGACGGCCCGGG	2R:21015708..21015730 2R:20932457..20932479	*CG3295* *Rx*

Selected guides were cloned into the pCFD4 vector, which allows for expression of two gRNAs simultaneously under the control of U6 promoters, following the protocol outlined by Port and colleagues (Port *et al.*, 2014). These constructs were inserted into the *Drosophila* genome via PhiC31-mediated recombination, on a different chromosome to the target locus. This was attP2 for *EMRE* (chromosome III), and attP40 for *MICU3* (chromosome II).

Mutagenesis was achieved by crossing these ubiquitously expressed gRNA stocks to a germline-restricted *nos*-cas9. Virgin females of this combination, expressing both gRNA and Cas9 in their oocytes, were crossed to balancer males. Male progeny were then individually crossed to balancer virgins to create lines for distinct mutagenesis events. An example schematic of this crossing scheme for *MICU3* is given in Figure 19. No lethality was observed for any target, so mutation events were detected by direct sequencing of the target region. PCR products were obtained using primers spanning the gRNA recognition sites, gel extracted, and sent for Sanger sequencing. To reduce turnaround time, lines were first evaluated as balanced heterozygotes, leading to mixed sequence traces in the case of a mutagenesis event. It was possible to extract indel breakpoints from these traces by excluding the reference sequence from double peaks, but this was not without difficulty, and to obtain a more robust list of breakpoints, candidate lines were later sequenced as homozygotes.

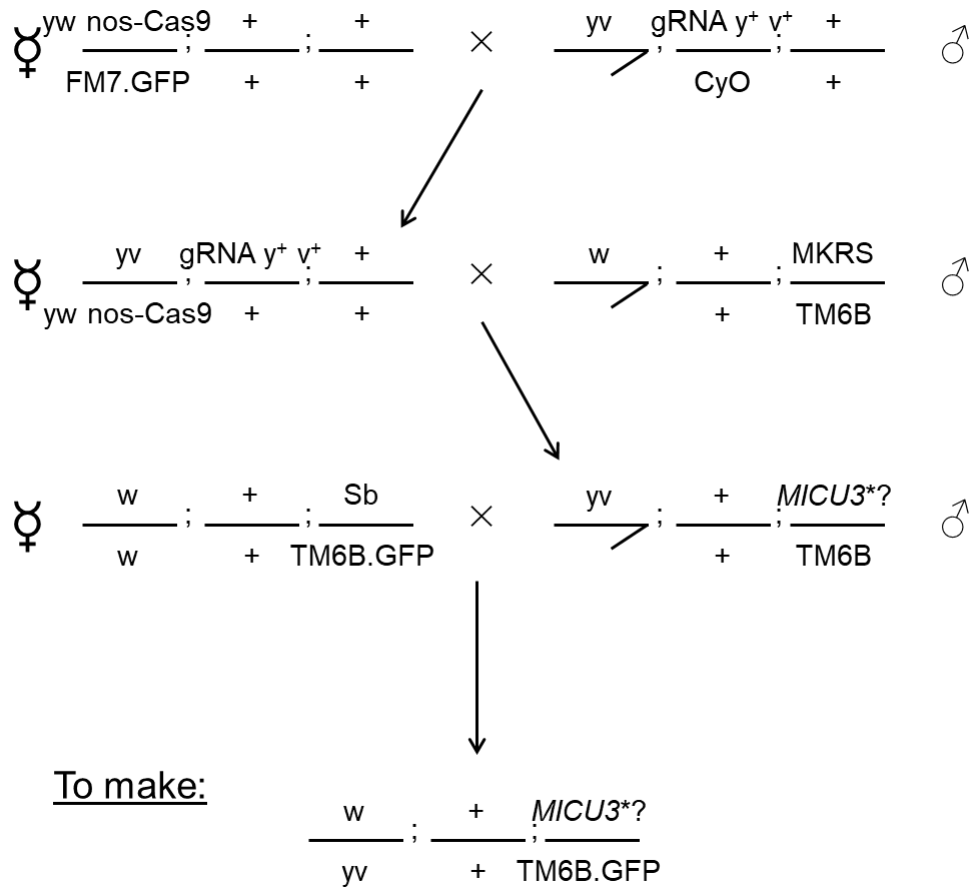

Figure 19. Example crossing scheme for generation of *MICU3* mutants by CRISPR-cas9 DNA cleavage.

3.4.2. Mutagenesis

For *EMRE*, 24 lines were sequenced, of which 22 (92%) showed some form of mutation. Several of these lead to a frameshift leading to a nonsense mutation. Three mutants were selected based on diversity in their effects on the predicted protein sequence: *EMRE*^{1}, *EMRE*^{2}, and *EMRE*^{3}. *EMRE*^{1} features the shortest resulting predicted protein overall, barely extending past the predicted mitochondrial targeting sequence. By contrast, *EMRE*^{2} has a large frameshifted amino acid sequence beyond the frameshift before truncation occurs. *EMRE*^{3} features an intermediate length protein, with the shortest 'missense' region of the three. For *MICU3*, 20 lines in total were sequenced, of which 3 (15%) showed some form of mutation. However, only one of these created a frameshift leading to a nonsense mutation (one of the others being an in-frame deletion, and one a frameshift deletion with a new exon beginning before any stop codon). This mutation, termed *MICU3*^{27}, comprises a single base deletion in exon 2. The location of each deletion is shown in Figure 20, and a summary is given in Table 8.

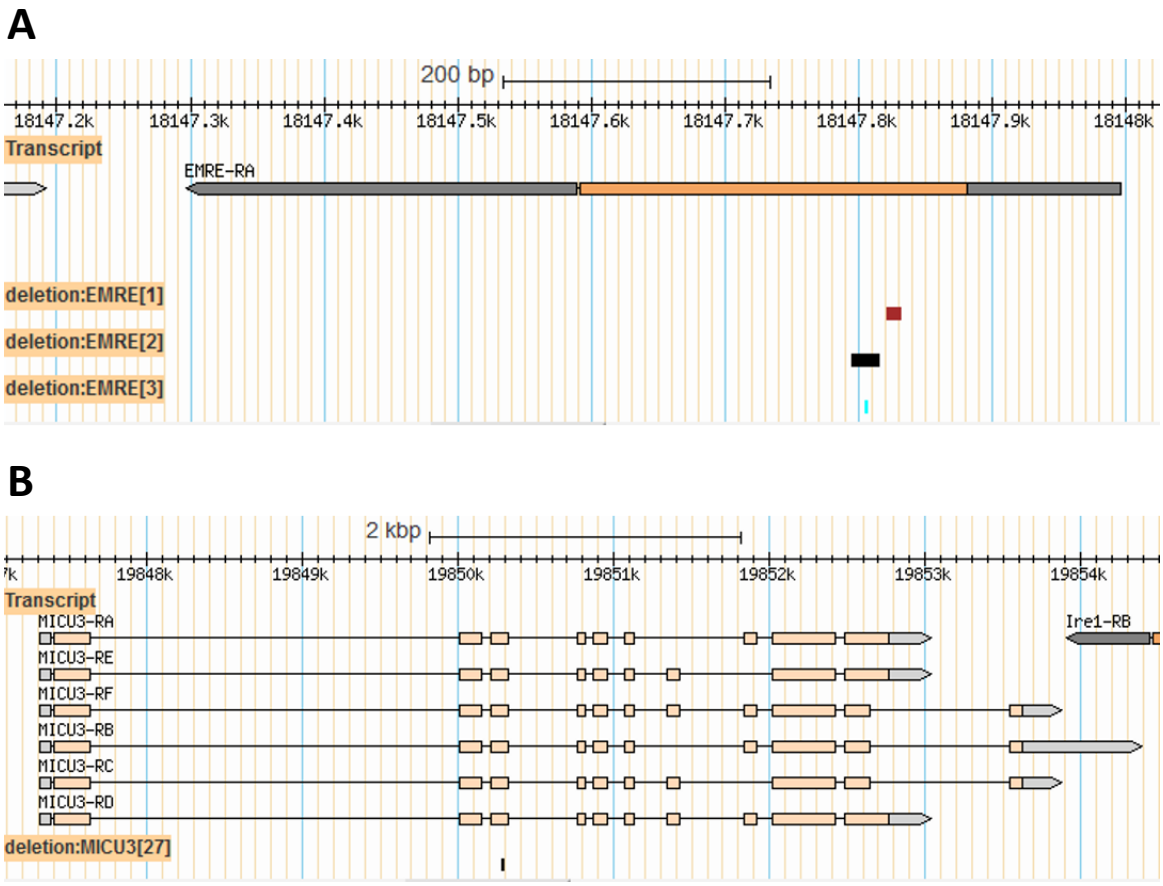

Figure 20. Genomic regions, from FlyBase GBrowse output, of **A**: *EMRE*, **B**: *MICU3*, with deleted regions for each mutant mapped and indicated by coloured bars.

Table 8. Genomic breakpoints for *EMRE* and *MICU3* mutants, with predicted effects on resulting protein sequence. Green text represents altered (missense) residues. All genomic coordinates correct as of FlyBase/BDGP Release 6 (Hoskins *et al.*, 2015).

Allele	Breakpoints	Predicted Protein Sequence
EMRE-WT	N/A	MIVPRLALPISLALQRVSRRVAEHPHNLRILQRH MSSVYFRSGAIKPKPEEMPFGLLAIFCAVIPGLFV GATISKNVANFLEENDLFVPADDDDDED*
EMRE[1]	2R:18147830-18147821	MIVPRLALPISLALQRV**WRNT***
EMRE[2]	2R:18147814-18147795	MIVPRLALPISLALQRVSRRVA**DPAAPHVQRVL SQWSHQTQARGDAIRPAGHLLCRHTGTLRGR HHQQERGQLSGGERSVRARG***
EMRE[3]	2R:18147805-18147805	MIVPRLALPISLALQRVSRRVAEHP**QT***
MICU3-WT	N/A	MAGLAARLTVKNCTIIAQRSSVIVGVGRSARFSS SSSQMGRIPGHKTRRLLTIVGGSAVSLAALAAFI KLRSAENPVNASLKRRMRDDSELENVKLTARER RFIKFASVEYDDQLYMTPQDFLDSVVEQEPRPR LKRRQLSSDEVDKYKENTPALKKGSTRLFRNLRD KGIVSYTEYLFLLSILTKPKSGFRIAFNMFTDGNQ RVDKDEFLVIISILAGALKDTQNVDPQTKRIMERI FSGAWKEKHGEQEPEEELATPTPLENYVNDGE GLQRRHMVATTLQLHFFGKRGTGVINYDNFYR FMDNLQTEVLELEFHEFSKGNSVISELDFAKILLR YTYLATDEYDVFLERLLERVKDEKGISFHDFRDFC HFLNNLDDFTIAMRMYTLADRAISKDEFSRAVKI CTGYKLSPHLIDTVFAIFDADGDGLLSYKEFIAIM KDRLHRGFKVSGRFFDYNEALDAYDEPDYPLFV AWRHRVCRHLDYFIDSDALWH*
MICU3[27]	3R:19850278-19850278	MAGLAARLTVKNCTIIAQRSSVIVGVGRSARFSS SSSQMGRIPGHKTRRLLTIVGGSAVSLAALAAFI KLRSAENPVNAVSLKRRMRDDSELENVKLTARE RRFIKFASVEYDDQLYMTPQDFLDSVVEQEPRP RLKRRQLSSDEVDKYKENTPAL**RRVPLVCFAT***

The CRISPR-induced deletions are too small to be distinguishable by simple PCR amplicon size difference. Instead, restriction fragment length polymorphism (RFLP) analysis was used. Primers were designed to create an amplicon with a unique restriction site, overlapping the deleted region. For *EMRE*[1] this was BcnI, and MboII for *MICU3*[27]. No suitable restriction site was present in *EMRE*[2] or *EMRE*[3]. RFLP examples for mutant DNA are given in Figure 21.

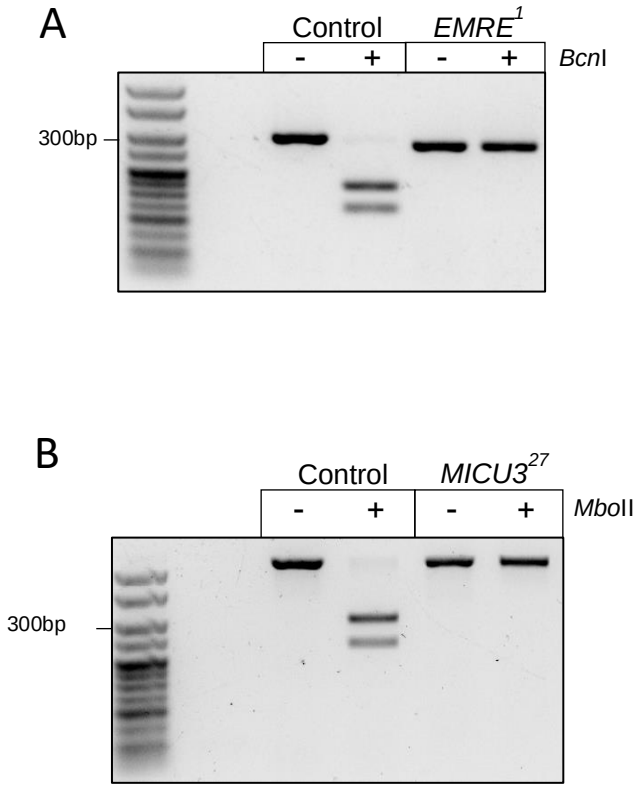

Figure 21. Example RFLP result distinguishing controls from **A**: *EMRE*[1] (using BcnI digest) or **B**: MICU3[27] (using MboII digest). DNA ladder: Hyperladder 25 bp (Bioline).

3.4.3. Validating *EMRE* knockouts

The *EMRE* knockout lines were attempted to be verified as protein nulls, but the commercially available antibody used in other organisms (sc-86337, Santa Cruz Biotechnology) did not recognise the *Drosophila* protein (data not shown), precluding this approach. Instead, stocks were sent to our collaborators in Padua for functional validation (experiments performed by S. von Stockum and E. Ziviani). Under extramitochondrial calcium loading at levels favourable to uniporter function, direct calcium measurements from isolated mitochondrial preparations confirmed a lack of uptake in the three homozygous mutants (Figure 22A), which mimicked the effect of pharmacological inhibition of the uniporter by ruthenium red (RuR).

As mitochondrial calcium uptake is electrophoretic, and so dependent on $\Delta\psi_m$, reduced membrane potential would inhibit the rate of calcium influx, confounding these results. Mitochondrial depolarisation by FCCP caused control mitochondria to expel Ca^{2+}, causing a rise in Calcium Green-5N fluorescence. However, no change in uptake rate was seen in *EMRE* mutants. The membrane potential was also directly measured through the quenching of rhodamine 123 fluorescence after being electrophoretically incorporated into mitochondria (Emaus, Grunwald and Lemasters, 1986). The rate of quenching is proportional to $\Delta\psi_m$ and occurs only in energised mitochondria. No difference in membrane potential was seen between control and *EMRE* mutants (Figure 22B), demonstrating that their mitochondria are in principle capable of mitochondrial calcium uptake. In summary, the three *EMRE* mutants can be confirmed as functional null mutants.

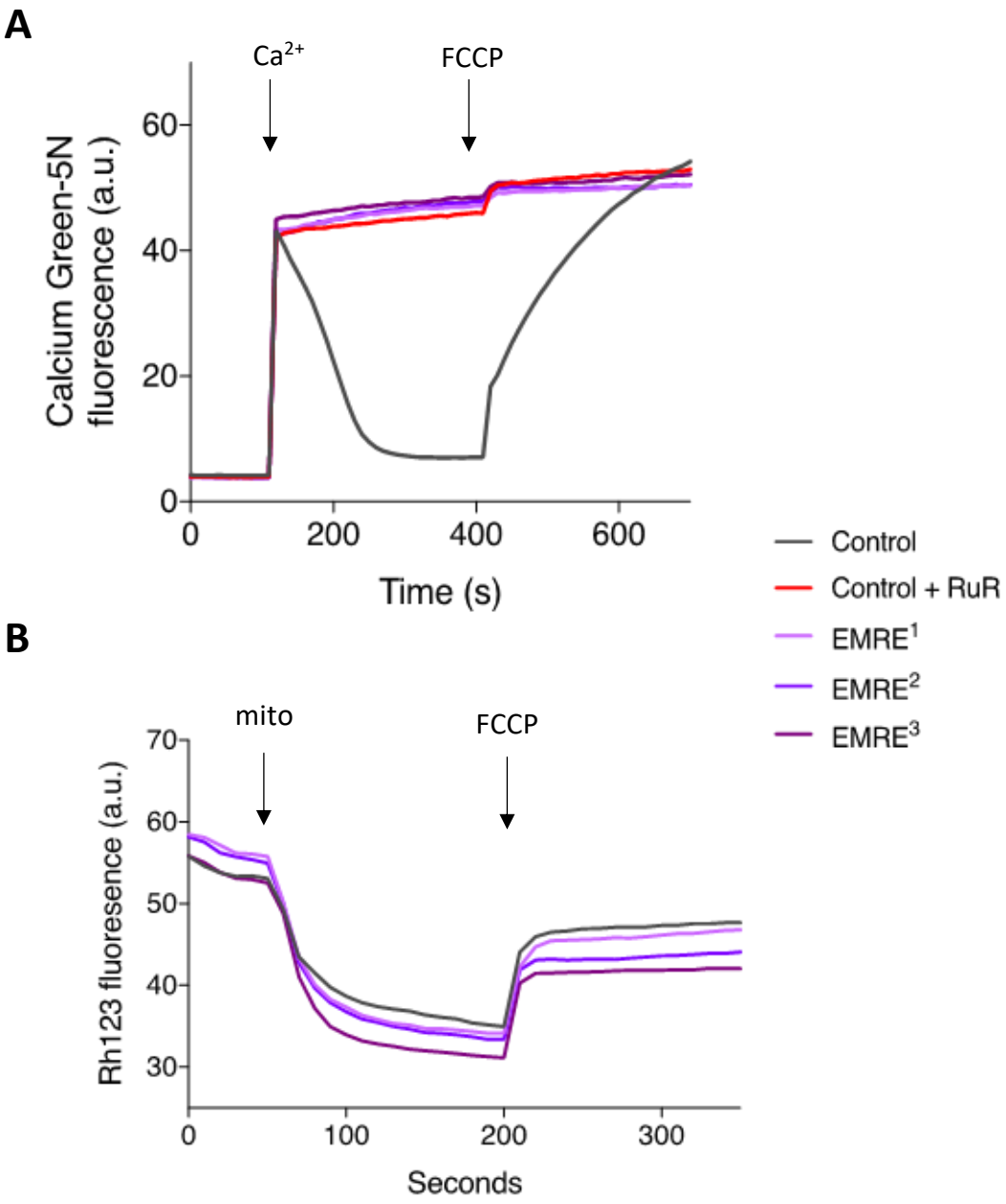

Figure 22. **A**: Representative Ca^{2+} uptake traces or **B**: representative traces of Rhodamine 123 (Rh123) fluorescence for isolated mitochondria from adult wild-type control flies (w^{1118}) and *EMRE*^{1}, *EMRE*^{2}, and *EMRE*^{3} mutants. At the indicated timepoints, the following additions were made: Ca^{2+}; 45 µM $CaCl_2$, FCCP; 1 µM FCCP, mito: isolated mitochondria. For **A**, mitochondria were added before the experiment start time. An additional group represents control flies pre-treated with 2 µM ruthenium red (RuR), which inhibits the uniporter. a.u.: arbitrary units. Data generated by S. von Stockum under the supervision of E. Ziviani

3.4.4. Validating *MICU3*^{27}

qRT-PCR was used to determine relative transcript levels in *MICU3*^{27} (Figure 23). *MICU3* expression is reported to be largely restricted to the CNS (Brown *et al.*, 2014; Aradska *et al.*, 2015), so RNA was extracted from adult fly heads. A significant decrease was observed, as might be expected from nonsense-mediated decay of a missense mutant transcript. This indicates the mutant is hypomorphic at the RNA level. The remaining mRNA would encode a highly truncated protein lacking functional elements including all predicted EF-hands. Though not directly proven, it is therefore highly likely that this mutation represents a complete functional null allele. Two commercial antibodies, HPA024771 and HPA024779 (Atlas Antibodies), were tested but failed to recognise *Drosophila* MICU3 (data not shown). Additional evidence that *MICU3*^{27} compromises gene function is given in Section 4.4, where a mutant phenotype is rescued though transgenic re-expression of MICU3. This links the phenotype to MICU3 specifically, and to loss-of-function mutation rather than a toxic gain-of-function. *MICU3*^{27} therefore represents the first *in vivo* knockout line for this gene and will be of use to researchers looking to probe the effects of mitochondrial calcium tuning in (patho)physiological conditions.

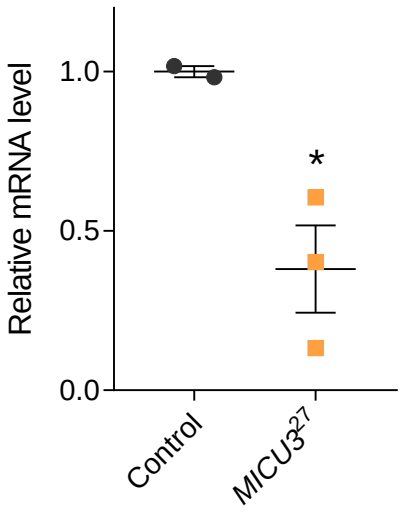

Figure 23. Relative transcript level of control (w^{1118}) and *MICU3*^{27} adult heads. Error bars: SEM. Transcripts were normalised against *RpL32*, and quantification was performed using the comparative C_T method (Schmittgen and Livak, 2008). *p<0.05 by unpaired two-tailed t test. Data generated by R. Tufi.

3.5. Discussion

The generation of *EMRE*[1] and *MICU3*[27] knockouts utilised the CRISPR-Cas9 system, which is still an evolving technique, especially in *Drosophila*. Some insight into its practicality can therefore be gleaned. Mutagenesis efficiency varied strongly between the two targets, with almost all *EMRE* events being confirmed as mutants, but a small fraction for *MICU3*. This may be due to differing on-target gRNA efficiency (Doench *et al.*, 2014), and accordingly, the *in vitro* efficiency of the three *EMRE* gRNAs was tested (data not shown). No gRNA showed complete *in vitro* cleavage, however, and correlation with *in vivo* performance was poor. Alternatively, these differences may arise from varying chromatin structure, which has been shown to alter the effects of NHEJ (Janssen *et al.*, 2019).

Both *EMRE*[1] and *MICU3*[27] have been confirmed as loss-of-function alleles, but this was more challenging to demonstrate than for *MICU1*[32], where the transcript is simply absent. This is especially important given the lack of suitable commercially available antibodies against *Drosophila* proteins. However, the mutation frequency for the CRISPR method was much improved versus imprecise P-element excision, as could be expected. Thus, an optimal method for gene knockout would use the efficiency of CRISPR to generate a deletion covering the canonical transcriptional start site, and ideally precisely the whole gene locus. This could be achieved by supplying a repair construct in addition to the gRNA and Cas9, allowing for HDR to induce the desired mutation, using the targeted DSBs of CRISPR-Cas9 to greatly improve its efficiency. Future mutagenesis projects in the lab will likely use this strategy to rapidly generate knockout alleles that are simple to verify.

The objective of this work was to expand the available genetic tools in *Drosophila* to include RNAi, knockout mutant, and transgenic overexpression lines for all conserved components of the mitochondrial calcium uniporter. Table 9 summarises the completion of this task, and includes the *MCU*[52] knockout line externally generated during the project (Choi *et al.*, 2017). As well as facilitating the rest of this thesis, the lines generated here will provide a useful resource to *Drosophila* researchers also wishing to interrogate *in vivo* function of mitochondrial calcium flux in health and disease.

Table 9. Knockdown, mutant, and transgenic expression lines for conserved uniporter genes, after the present work.

Gene	RNAi	Mutant	Transgenic
MCU (*CG18769)*	P{GD446}v9501	*MCU*^{1} *MCU*^{52}	P{UAS-MCU}attP40 P{UAS-MCU}attP2
MICU1 (*CG4495*)	P{GD4927}v49349 P{TRiP.HMS02302}attP2	*MICU1*^{32}	P{UAS-MICU1-A-3xHA}ZH-86Fb P{UAS-MICU1-B-HA}attP40 P{UAS-MICU1-B-HA}attP2
EMRE (*CG17680*)	P{KK109347}VIE-260B P{GD3797}v45211	*EMRE*^{1}	P{UAS-EMRE}attP40 P{UAS-EMRE-myc}attP40 P{UAS-EMRE}attP2 P{UAS-EMRE-myc}attP2
MICU3 (*CG4662*)	P{GD3076}v6786 P{KK105775} P{NIG.4462R} II P{NIG.4462R} III	*MICU3*^{27}	P{UAS-MICU3-A-V5}attP40 P{UAS-MICU3-A-V5}attP2 P{UAS-MICU3-C-V5}attP40 P{UAS-MICU3-C-V5}attP2

4. Characterisation of the *Drosophila* mitochondrial calcium uniporter

4.1. Background and Aims

Mitochondrial calcium uptake has been positioned as a fundamental biological process, coordinating energy supply with cellular demand, and underlying several cell death programs. However, genes previously thought to be essential for life have yielded viable knockout strains, such as myoglobin (Garry *et al.*, 1998) or creatine kinase (van Deursen *et al.*, 1993). This underlies an oft-unexpected potential for genetic compensation, which necessitates *in vivo* modelling of gene function to address true physiological requirements. Furthermore, pathways altered in a compensatory mechanism may themselves be a useful point of study, shedding light on genetic or functional interactions. Given the importance of the uniporter in health and disease, genetic manipulation of its constituents will potentially unveil new insights into key biological and pathological processes, which may provide avenues for therapeutic exploration.

Building on from initial studies of uniporter function outlined in Section 1.3.1, I sought to characterise the extant *MCU*^{1} mutant, as well as other mutants and overexpression lines described in Section 3. The *MCU*^{52} line generated by Choi and colleagues was published after our own *MCU*^{1} line was created, so has not been assessed, but comparisons are discussed where appropriate. Manipulating *MICU1* yielded several dramatic phenotypes which formed the basis for genetic interaction studies and is therefore characterised separately in Section 5. Here, I demonstrate global abolition of mitochondrial calcium uptake, through knockdown or knockout of *MCU* or *EMRE*, is tolerated in *D. melanogaster* development. Despite not affecting initial vitality, lifespan is shortened. The two mutants diverge in terms of metabolic phenotypes, suggesting an additional impact of the uniporter pore independent of calcium influx. Additionally, I report the first *in vivo* characterisation of MICU3, which results in strong deficits in specific tissues where the protein is physiologically enriched, but nevertheless is compensated for when considering readouts of global organismal health. These data weigh in on the debate surrounding the importance of mitochondrial calcium uptake for life, providing a basis for further investigation of the consequences of altered mitochondrial calcium dynamics in metabolism and aging.

4.2. RNAi/Overexpression Line Characterisation

Though genetic knockout can be considered the 'gold-standard' for investigating *in vivo* gene function, RNAi-driven knockdown is useful as an orthogonal approach. Coupling dsRNA expression to the GAL4-UAS enhancer-trap system allows for tissue-specific knockdown at defined relative strengths, and the viability of RNAi lines using these different drivers indicates essential tissue requirements for each gene. Overexpression constructs can also be brought under the control of the UAS promoter to examine phenotypes arising from simple overexpression in a range of tissues. Here, *MCU, EMRE*, and *MICU3* are explored using these tools, with the results summarised in Table 10.

First, the general physiological requirements of *MCU* were evaluated. Using the strong ubiquitous *da*-Gal4 (*daughterless* driver), *MCU* knockdown (via P{GD446}v9501) yielded viable adults (Figure 25A), as did overexpression of UAS-MCU (Figure 25B). No climbing phenotype was observed, indicating that manipulation of *MCU* is also compatible with vitality. We hypothesised that targeting *EMRE* would lead to similar organismal outcomes as *MCU*, as both would result in a lack of mitochondrial calcium uptake. Indeed, EMRE overexpression was viable, as was the P{GD3797}v45211 RNAi line, and did not cause a climbing deficit (Figure 25C). By contrast, the P{KK109347}VIE-260B line was lethal with all drivers used. As mentioned, RNAi lines come with several caveats, not least the potential for off-target sites, of which P{KK109347}VIE-260B is predicted to have three (Figure 24). Given the results for *MCU* manipulation, the more likely interpretation is that *EMRE* up- or downregulation is well tolerated in terms of viability.

Similarly, strong knockdown or overexpression of *MCU* or *EMRE* in neuronal tissue via nSyb-Gal4 (*neuronal Synaptobrevin*), or muscle via Mef2-Gal4 (*Myocyte enhancer factor 2*) resulted in viable adults. No climbing phenotype was observed for any manipulation (Figure 26A-B, Figure 27A-B), except *Mef2*-driven overexpression of a single MCU line, which had a marginally significant reduction of small effect size. As the same construct inserted in a different site gave no such phenotype, this small difference is likely erroneous.

	VDRC ID	Library	Construct ID	CG Number (r6.01)	Nearest Genes	Synonyms	ON Targets	OFF Targets
☐	104493	KK	109347	CG17680		BcDNA:RE55001 ...	1	3

Figure 24. VDRC stock details for P{KK109347}VIE-260B RNAi line targeting EMRE (CG17680). URL: https://stockcenter.vdrc.at/control/checkAdvancedSearch?VIEW_SIZE=100&product_id=104493. Accessed 2019/07/05.

Similarly, the 4 RNAi lines targeting MICU3, and the 2 corresponding transgenic constructs cloned, were tested using *da*-Gal4 (Figure 25D) and *Mef2*-Gal4 (Figure 27C). All combinations were viable to adulthood. Slight reductions in climbing ability were observed with MICU3 overexpression using the strong ubiquitous *da*-Gal4 driver. Additionally, a single RNAi line showed a modest impairment in locomotion. These varied results were more pronounced using *Mef2*-Gal4 mediated knockdown, with two lines showing no phenotype and two displaying a very pronounced reduction in climbing index. Muscle-specific MICU3 overexpression had no discernible effect. The strong impairment seen with *Mef2*-driven knockdown is perhaps surprising given the lack of phenotype with *da*-Gal4. Although *da*-driven expression can be easily observed in muscle, for example with a mitochondrially-targeted GFP (as shown later in Figure 30), *Mef2*-Gal4 may be more expressed in this specific tissue, leading to stronger knockdown.

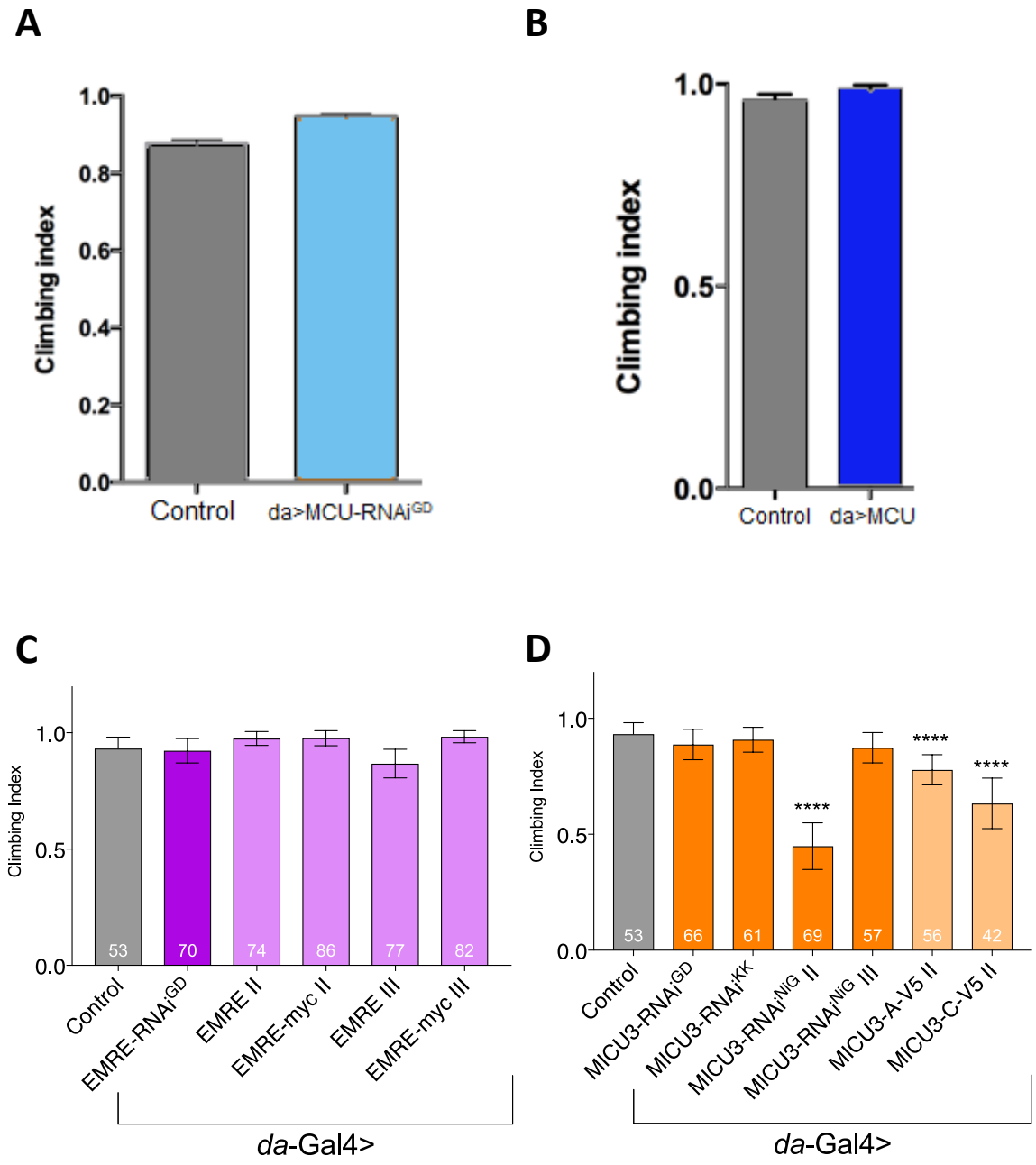

Figure 25. Climbing performance of knockdown and overexpression lines. **A**: MCU knockdown, **B**: MCU overexpression, **C**: *EMRE* manipulation, **D**: *MICU3* manipulation, with the *da*-Gal4 driver. All genotypes were compared to control (*da*/+) with Kruskal-Wallis test with Dunn's post-hoc correction for multiple comparisons. ****p<0.0001. Error bars = 95% confidence interval. Numbers in bars represent biological n for each genotype. Data for panels **A** and **B** generated by R. Tufi.

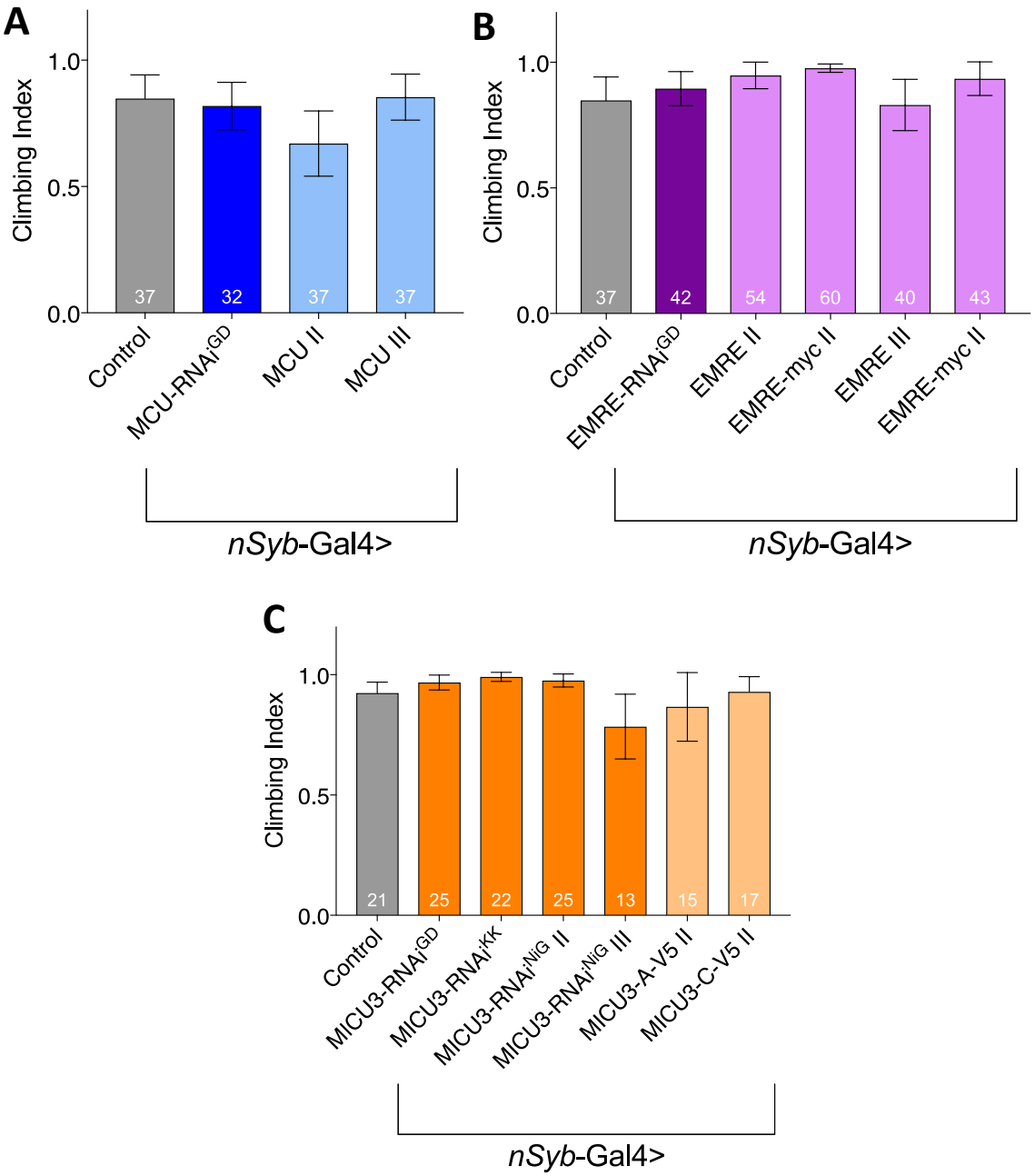

Figure 26. Climbing performance of knockdown and overexpression lines of **A**: *MCU*, **B**: *EMRE*, **C**: *MICU3* lines with the *nSyb*-Gal4 driver. All genotypes were compared to control (*nSyb*/+) with Kruskal-Wallis test with Dunn's post-hoc correction for multiple comparisons. No significant differences were detected ($p>0.05$). Error bars = 95% confidence interval. Numbers in bars represent biological n for each genotype.

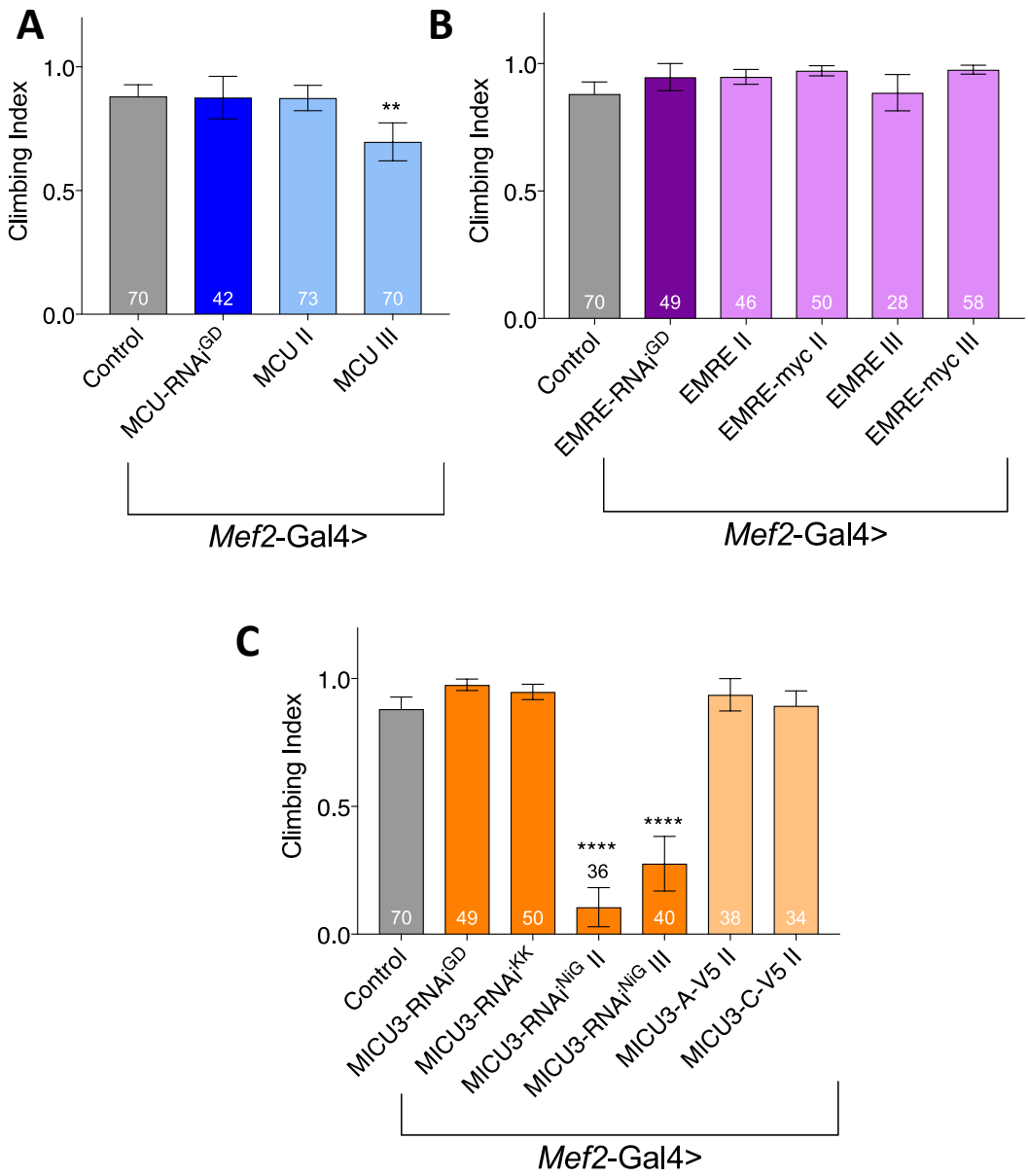

Figure 27. Climbing performance of knockdown and overexpression of **A**: *MCU*, **B**: *EMRE*, **C**: *MICU3* lines with the *Mef2*-Gal4 driver. All genotypes were compared to control (*Mef2*/+) with Kruskal-Wallis test with Dunn's post-hoc correction for multiple comparisons. **p<0.01, ****p<0.0001. Error bars = 95% confidence interval. Numbers in or next to bars represent biological n for each genotype.

Table 10.Summary of viability and climbing ability for uniporter knockdown and overexpression through different gene drivers, coded by cell colour. Green = viable, no climbing phenotype. Orange = viable, with climbing phenotype. Red = lethal.

		da-Gal4	*nSyb*-Gal4	*Mef2*-Gal4
MCU	KD	P{GD446}v9501	P{GD446}v9501	P{GD446}v9501
	OE	UAS-MCU II UAS-MCU III	UAS-MCU II UAS-MCU III	UAS-MCU II UAS-MCU III
EMRE	KD	P{KK109347}VIE-260B		P{KK109347}VIE-260B
		P{GD3797}v45211	P{GD3797}v45211	P{GD3797}v45211
	OE	UAS-EMRE II UAS-EMRE-myc II UAS-EMRE III UAS-EMRE-myc III	UAS-EMRE II UAS-EMRE-myc II UAS-EMRE III UAS-EMRE-myc III	UAS-EMRE II UAS-EMRE-myc II UAS-EMRE III UAS-EMRE-myc III
MICU3	KD	P{GD3076}v6786 P{KK105775} P{NIG.4462R} II	P{GD3076}v6786 P{KK105775} P{NIG.4462R} II P{NIG.4462R} III	P{GD3076}v6786 P{KK105775}
		P{NIG.4462R} III		P{NIG.4462R} II P{NIG.4462R} III
	OE	UAS-MICU3-A-V5 UAS-MICU3-C-V5	UAS-MICU3-A-V5 UAS-MICU3-C-V5	UAS-MICU3-A-V5 UAS-MICU3-C-V5

4.3. *MCU* mutants are less resistant to metabolic stress than *EMRE*

MCU^{1} and *EMRE*^{1} eclose at Mendelian ratios with normal locomotion

The viability of animals lacking mitochondrial calcium uptake has been a source of contention in recent years. Mutants for *MCU* and *EMRE* target different uniporter subunits to achieve the same functional outcome, allowing for greater confidence that any shared phenotypes are ascribed to uniporter activity. Neither mutant showed any evidence of gross developmental lethality (blackened larvae or pupae), and homozygous mutants lacking balancer chromosome markers were observed. Fully homozygous stocks were also possible to establish, and were easily maintained/expanded, supporting both this viability and a reasonable degree of fertility.

To differentiate full viability from partial lethality, crosses were established between balanced parents to yield an expected Mendelian distribution of chromosomes in resulting progeny. Balancer chromosomes carry recessive lethal mutations, so the expected homozygous portion would be one third. This was found to be the case for *MCU*^{1} (Figure 28A), and for *EMRE*^{1} (Figure 28C). Given the contribution of genetic background to the lethality observed in some mouse *MCU* knockout lines, it is worth noting that these experiments were performed in lines outcrossed to the standard isogenic *w*^{1118} background. No gross lethality was observed in the original non-outcrossed stocks (no blackened larvae or pupae, homozygous stock maintained without balancer chromosome). This phenotypic concordance between the two mutants, combined with their functional verification, demonstrates that canonical mitochondrial calcium uptake through the uniporter is dispensable for life in *Drosophila*.

Locomotor behaviour (negative geotaxis) provides a measure of organismal vitality. Young (1-3 days post-eclosion) heterozygous or homozygous MCU^{1} achieved close to the maximum possible score of 1, as well as the non-outcrossed MCU^{12ey} allele (data not shown). Aged climbing performance (at 10 and 20 d.p.e.) was additionally assessed by R. Tufi., finding homozygous MCU^{1} to have no discernible climbing phenotype at all ages tested (Figure 28B). $EMRE^{1}$ flies also showed no difference in climbing performance compared to controls at 2, 10, or 20 d.p.e. (Figure 28D).

Flight is a useful complimentary behaviour to score alongside climbing, requiring different neuromuscular pathways, with flight demanding higher energy requirements that may reveal problems in maximal muscle performance or its metabolic underpinnings (Götz, 1987). Neither MCU^{1} nor $EMRE^{1}$ showed a defect in flight performance (data not shown). In summary, both manipulations to abrogate mitochondrial calcium uptake result in viable animals with normal motor performance, implying the maintenance of the neuronal functionality underpinning this behaviour.

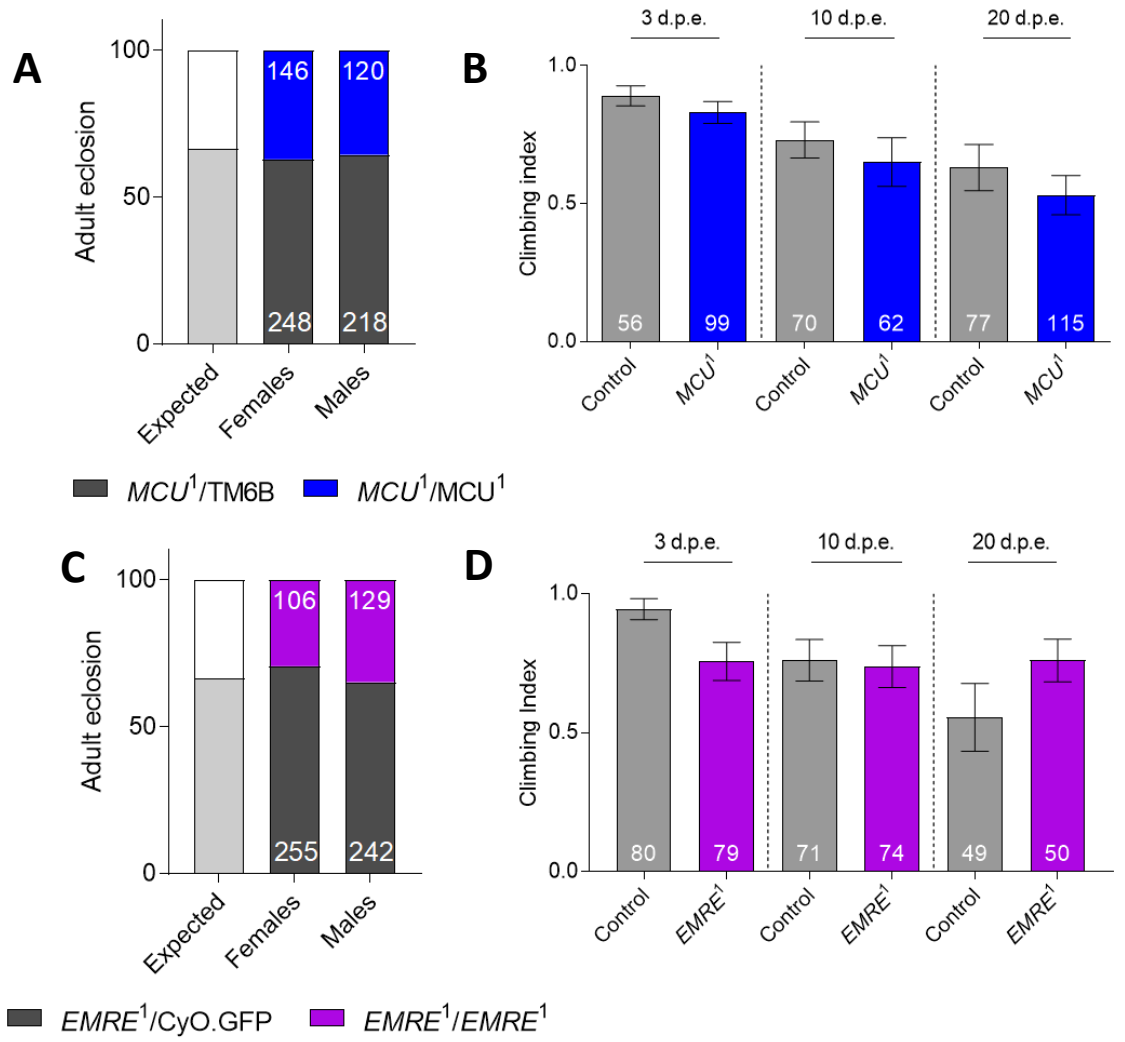

Figure 28. **A** and **C**: Ratio of balanced and homozygous *MCU*[1] (A) or *EMRE*[1] (**C**) adults. An expected Mendelian proportion *(1/3 homozygous)* is given for comparison. Numbers bars give the n for each group. **B** and **D**: Climbing performance of *MCU*[1] (**B)** or *EMRE*[1] (**D**) mutants. Kruskal-Wallis test with Dunn's post-hoc correction for multiple comparisons. Error bars = 95% confidence interval. Numbers in bars represent biological n for each genotype. Data for panels **A** and **B** generated by R. Tufi.

EMRE^{1} flies are short-lived

Previously, *MCU*^{1} flies were observed to have a markedly reduced lifespan (~34% reduction in median survival), despite the lack of gross behavioural abnormalities (Figure 29A). To corroborate this finding, I compared the lifespan of *EMRE*^{1} to *w*^{1118} controls (Figure 29B), finding the mutants to be short-lived (median survival 47 vs. 61, -22%). These two mutants together robustly demonstrate the importance of mitochondrial calcium uptake in longevity. Though highly statistically significant, the *EMRE*^{1} phenotype was of smaller effect size than for *MCU*^{1}, suggesting these mutants are differently tolerated in aging even though their canonical functional effects are equivalent.

MCU^{1} muscle mitochondria morphology is normal throughout aging

The mitochondrial morphology of adult indirect flight muscle was observed by confocal microscopy, utilising mitochondrially targeted GFP ubiquitously expressed via *da*-Gal4 (Figure 30). At 20 days post-eclosion, both control and *MCU*^{1} muscle mitochondria were well aligned and showed no morphological abnormalities. This observation was maintained at an old (40 d.p.e.) age. Interestingly, this approaches the median lifespan outlined above, indicating that *MCU*^{1} mutants do not display muscle mitochondrial disorganisation throughout their shortened lives.

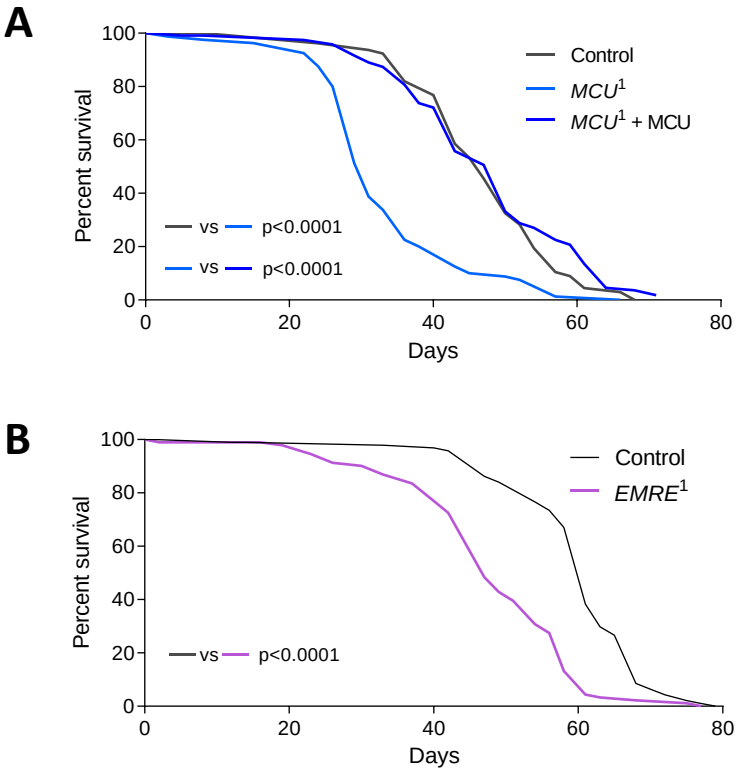

Figure 29. Lifespan of (**A**) control (w^{1118}, n = 80) vs. MCU^1 (n = 80) or (**B**) $EMRE^1$ (n = 94) versus w^{1118} (n = 98) genetic background control. **A**: additionally, transgenic rescue with *da*-Gal4>MCU (n = 120). P value <0.0001 as measured by either Mantel-Cox or Gehan-Breslow-Wilcoxon tests for both experiments. Data for panel **A** generated by R. Tufi.

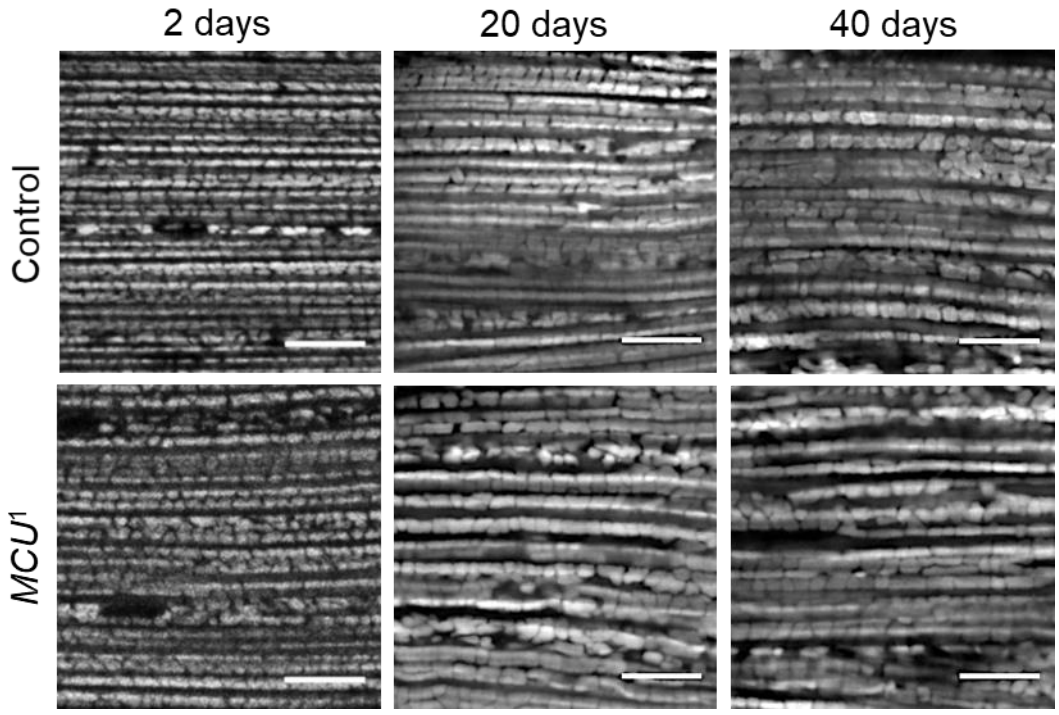

Figure 30. Representative micrographs of control and MCU^1 flies ubiquitously expressing mitochondrially targeted GFP (da>mito.GFP), at 2, 20, and 40 days post-eclosion. Scale bar = 10 µm.

PDH phosphorylation is unaltered in *MCU*^{1}

The phosphorylation of pyruvate dehydrogenase (PDH) represents a key control point in the TCA cycle. Through the calcium responsive phosphatase PDP1, this metabolic pathway can be linked to organismal energy demand (reviewed in Denton, 2009). It would therefore be interesting to see how the phosphorylation status of PDH changes in the context of *MCU*^{1}. Phospho-specific and phospho-agnostic antibodies targeting PDH were multiplexed in a Western blot, and band signal densities were normalised to total protein using the REVERT stain (Figure 31). The epitope recognised by the PDH antibodies maps to two *Drosophila* genes, both homologous to PDP1, and it is unclear which carries out the canonical function (if not both). Accordingly, two bands were detected, but both showed the same result: the ratio of phosphorylated to total PDH was unchanged in *MCU*^{1} (Figure 32A), but the total PDH level was reduced (Figure 32B). PDH from locusts and blowflies has been shown to be Ca^{2+}-insensitive (McCormack and Denton, 1981), but the sensitivity of *D. melanogaster* PDH is unknown. This could explain the lack of difference in *MCU*^{1}, though another possibility is enough mitochondrial calcium is present through a concomitant reduction in efflux to maintain $[Ca^{2+}]_m$ and keep PDP1 active. In the former case, another mechanism may exist to couple energy supply and demand through the abundance of PDH rather than its phosphorylation state.

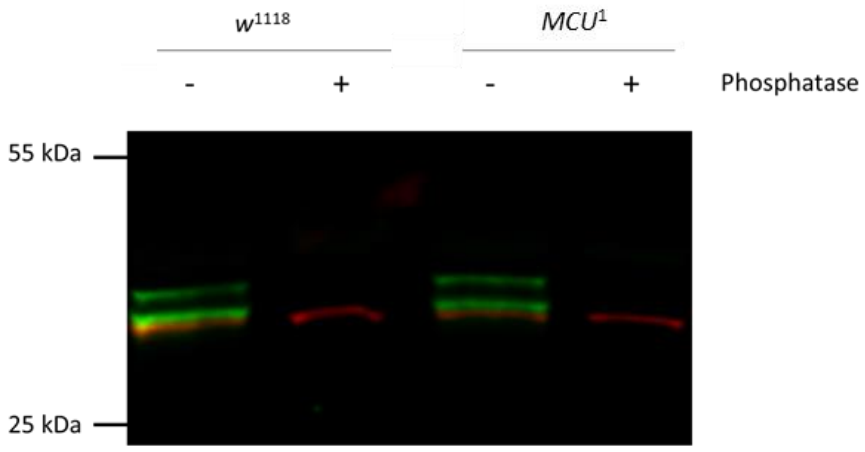

Figure 31. Representative Western blot from *w*^{1118} and *MCU*^{1} whole-fly homogenates, treated with and without alkaline phosphatase. Green: α-pyruvate dehydrogenase phospho-specific (S293), red: α-pyruvate dehydrogenase.

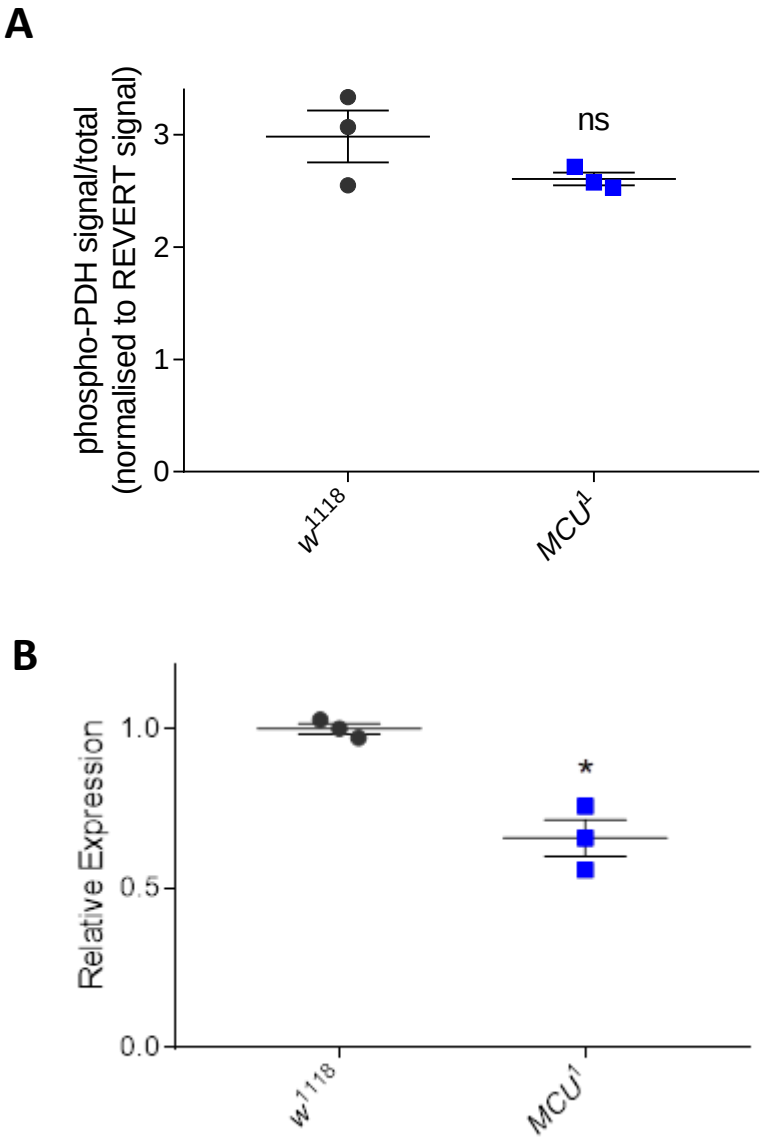

Figure 32. **A**: Ratio of phospho- to total pyruvate dehydrogenase signal and B: relative expression of total pyruvate dehydrogenase for w^{1118} controls and MCU^{1}. Signals were normalised to total protein through REVERT staining (Li-Cor). ns: p = 0.2398, *p = 0.0206 by two-tailed unpaired t-test with Welch's correction for unequal SD. Error bars represent SEM.

EMRE^{1} flies display less metabolic defect than *MCU*^{1}

Canonically, mitochondrial calcium is crucial to couple energy supply and demand through regulation of the TCA cycle. However, direct effects on the respiratory chain, for example through calcium-sensitive dephosphorylation of cytochrome *c* oxidase subunits (Bender and Kadenbach, 2000), remains possible. Previous work identified a respiratory phenotype using Oroboros oxygraphy in mitochondria isolated from whole *MCU*^{1} adults (Figure 33A). I performed this assay with whole *EMRE*^{1} adult mitochondria, and surprisingly, did not observe a difference compared to controls for either Complex I or II-linked respiration (Figure 33B). It is interesting that these mutants have similar behavioural phenotypes despite this dramatic difference in bioenergetic capacity. However, these respiratory measurements take place under substrate excess, and *MCU*^{1} mutants may respire sufficiently to meet physiological demands. The differences between these two mutants may instead be related to handling of external stressors, metabolic or otherwise. I have already shown *EMRE*^{1} to have a shortened lifespan less severe than *MCU*^{1}. Additionally, R. Tufi observed that *MCU*^{1} flies displayed a markedly short lifespan when exposed to either full starvation or sucrose-only feeding (Figure 34A-B). Here, I show that *EMRE*^{1} are less susceptible to this stress (Figure 34C-D). The reasons for this discrepancy between functionally similar mutants are unclear and may indicate a divergence between compensatory mechanisms. Instead, structural features and protein-protein interactors may underlie the difference, as the uniporter is presumably otherwise intact in the *EMRE*^{1} mutants and necessarily disrupted in *MCU*^{1}. Future work could probe these metabolic phenotypes in greater detail to yield candidate pathways to examine in these mutant contexts.

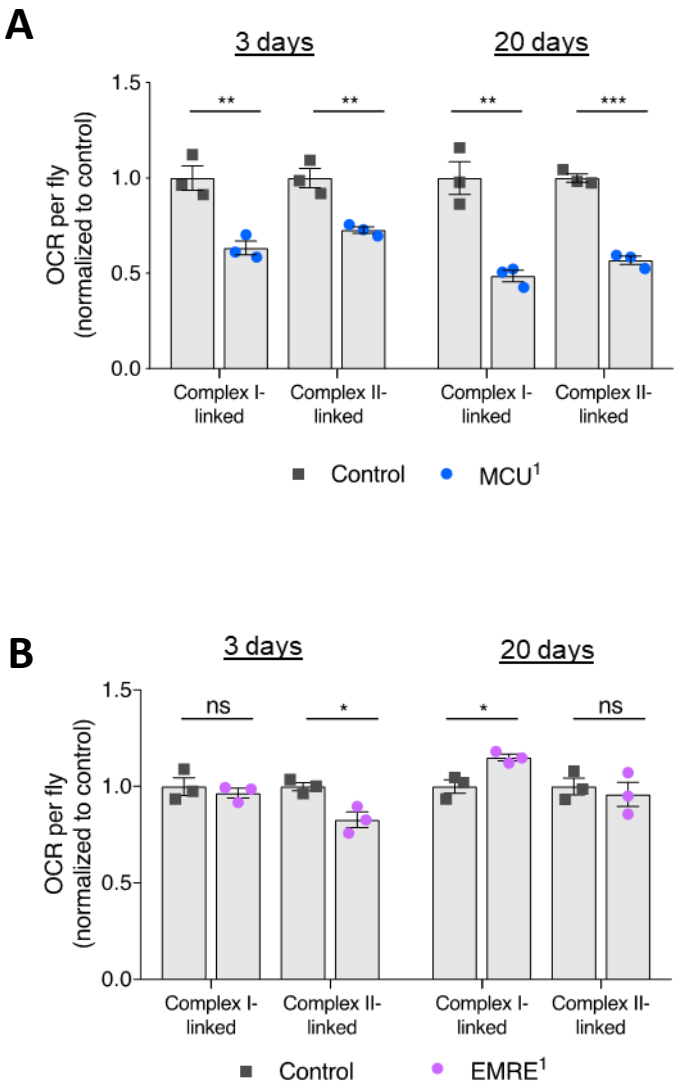

Figure 33. Oxygen consumption rate of control and **A**: *MCU*[1] or **B**: *EMRE*[1] flies at 3 and 20 days post-eclosion, normalised to protein concentration. Complex I-linked respiration was measured in the presence of 10 mM glutamate, 2 mM malate, and 2.5 mM ADP. The addition of 1.5 µM rotenone and 10 mM succinate was used. Error bars = SEM, ns = p>0.05 from unpaired t tests with Welch's correction for unequal standard deviation. Data points indicate individual runs each containing 5 whole flies. Data for panel **A** generated by R. Tufi.

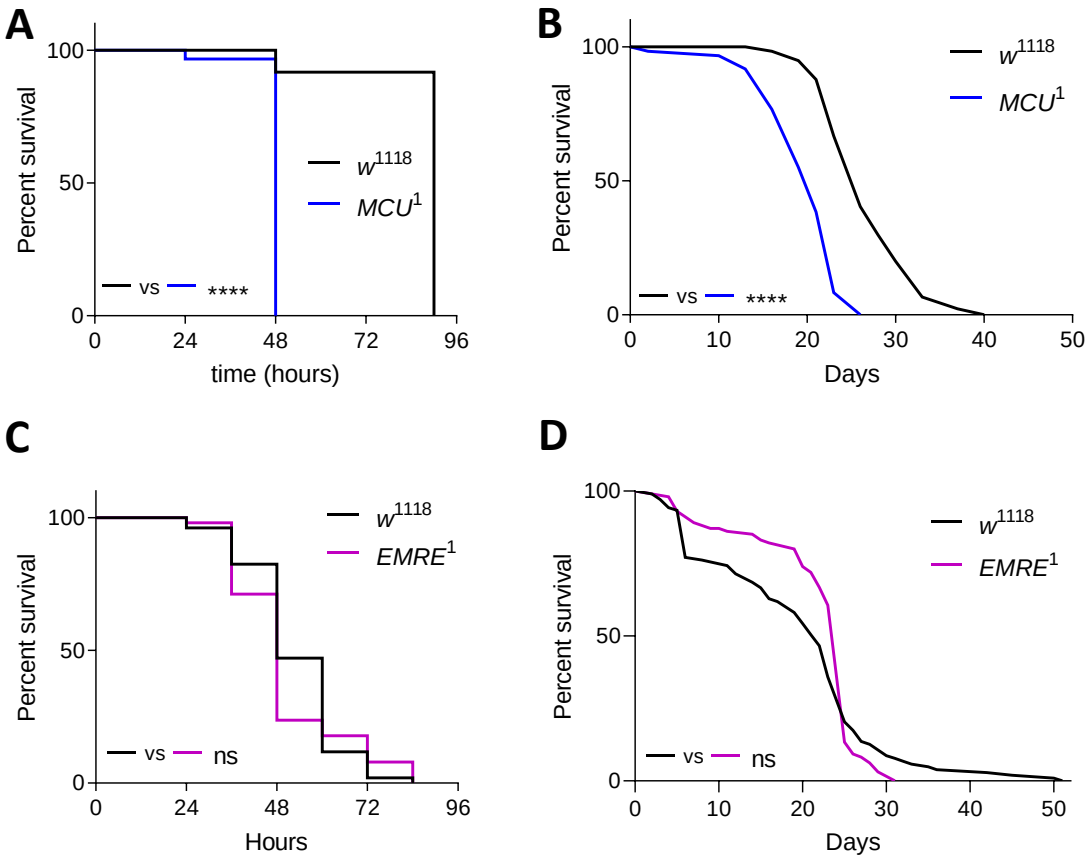

Figure 34. Starvation lifespan of *MCU*[1] and *EMRE*[1] with control (*w*[1118]). **A**: Full starvation of control (n = 60) and *MCU*[1] (n = 60). **B**: Sucrose starvation of control (n = 60) and *MCU*[1] (n = 60). **C**: Full starvation of control (n = 52) and *EMRE*[1] (n = 52). **D**: Sucrose starvation of control (n = 105) and *EMRE*[1] (n = 101). ****p<0.0001 by Mantel-Cox model. Data for panels **A** and **B** generated by R. Tufi.

4.4. *MICU3* loss is globally tolerated with tissue-specific deficits

MICU3^{27} flies eclose in Mendelian proportions

The role of MICU3 has been recently explored in cell lines (Patron *et al.*, 2018), but has not yet been characterised *in vivo*. Stocks of *MICU3*^{27} do not display any obvious signs of lethality, such as necrotic larvae/pupae. Crosses between fully balanced parents yield a Mendelian fraction of homozygous progeny as shown in Figure 35 (females: 37.7% homozygous, males: 35.6%, χ^2-test compared to Mendelian proportion p=0.7401) confirming that *MICU3* loss-of-function is fully compatible with development. The numerous rearrangements present in balancer chromosomes confer slightly reduced organismal fitness, and healthy mutant populations tend to become homozygous over time Interestingly, stocks of *MICU3*^{27} retain the balancer chromosome, suggesting some reduced fitness post-eclosion in the homozygous mutants.

Sterility

Following on the tendency of *MICU3*^{27} stocks to retain balancer chromosomes, the sterility of MICU3 manipulations was examined (Figure 36). MICU3-overexpressing males were similarly fertile to wild-type flies, but no larvae were observed in crosses from either male or female *MICU3*^{27} homozygotes, indicating complete sterility in these mutants. To confirm the specificity of this defect to *MICU3*, transgenic rescue was attempted, through ubiquitous expression of MICU3-A. Some fertile crosses were observed in the rescue condition, though this was not significantly different from *MICU3*^{27} after correcting for multiple comparisons. Some degree of fertility could still be considered biologically significant in a qualitative sense given the severity of the original phenotype, however. It is worth noting that the UAS lines originate from the pUAST.attB plasmid, which expresses poorly in the germline. Further studies could circumvent this by re-cloning with the modified pUASp, optimised for expression in the (female) germline (Rørth, 1998). Such a strong phenotype in the germline for the canonically CNS-restricted *MICU3* is perhaps surprising, but RNA-seq data show the *Drosophila* transcript present in testes at similar levels to the head, with some expression also in ovaries (Brown *et al.*, 2014).

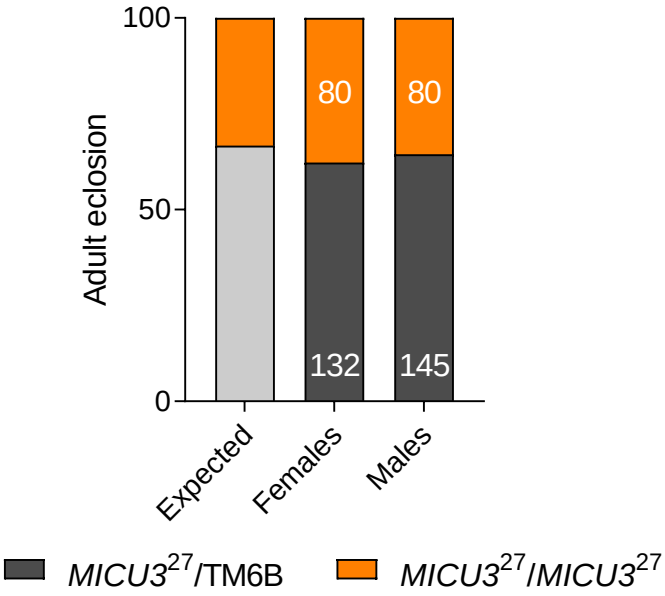

Figure 35. Ratio of balanced and homozygous *MICU3*^{27} adults. An expected Mendelian proportion *(1/3 homozygous)* is given for comparison. Numbers bars give the n for each group.

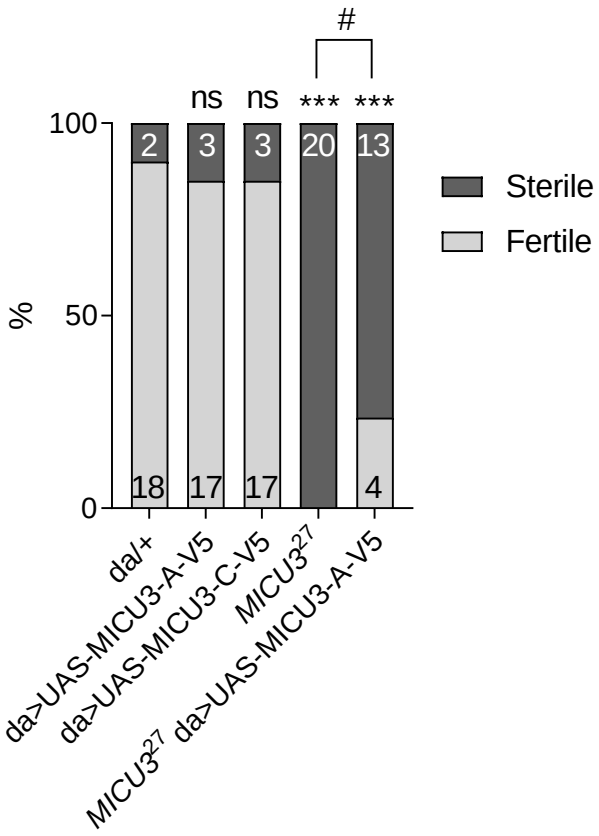

Figure 36. Percentage fertile/sterile crosses arising from males of each genotype. Numbers in bars represent n for each group. Pairwise Fisher exact test ***p<0.001 after multiple comparison correction via the Two-stage linear step-up procedure of Benjamini, Krieger and Yekutieli, with Q set to 5%(Benjamini, Krieger and Yekutieli, 2006). # denotes a comparison significant at p = 0.0360 initially, but 0.0504 post-correction.

MICU3^{27} displays a moderate climbing deficit

Given that *MICU3*^{27} mutants are viable but sterile, they may additionally display behavioural phenotypes, and accordingly the locomotor ability of these mutants was assessed (Figure 37A). Heterozygous *MICU3*^{27} did not show a climbing defect vs. controls, but homozygous flies had a robust deficit that reached a high statistical significance threshold ($p<0.0001$). The phenotype could be completely rescued transgenically using *armadillo*-driven expression (moderate, ubiquitous) of either MICU3-A or MICU3-C (Figure 37B). This indicates the climbing phenotype is specific to *MICU3*^{27}, rather than some unintended target.

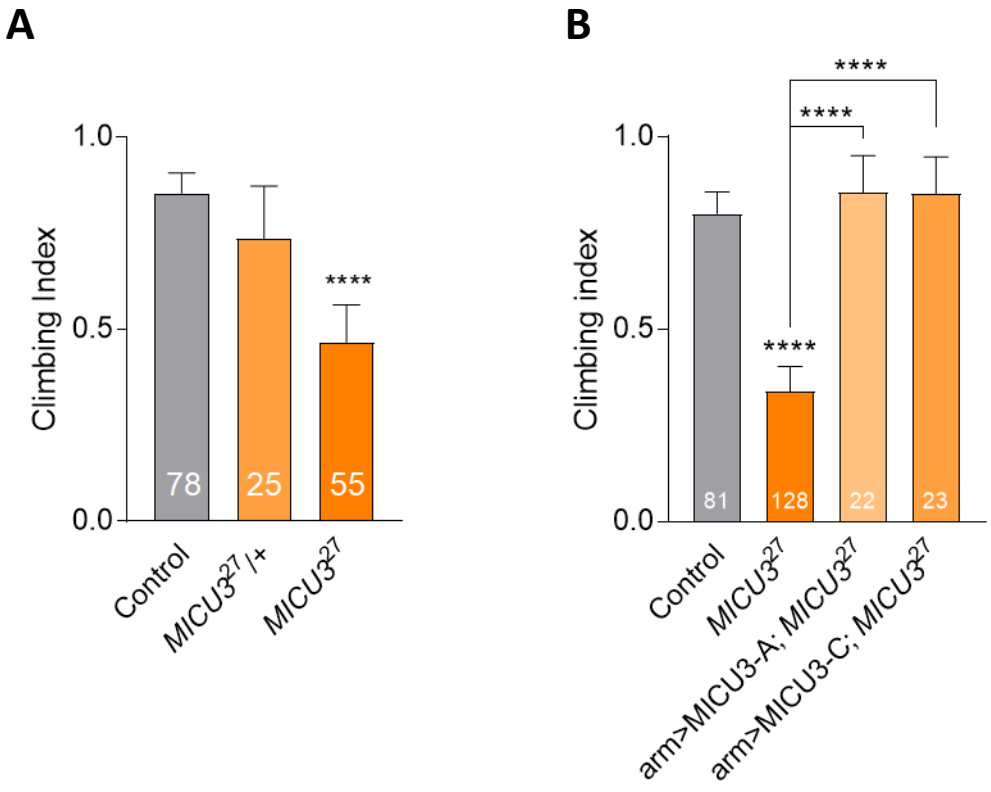

Figure 37. **A**: Climbing ability of *MICU3*^{27} mutants (control: *da*-Gal4/+), **B**: with transgenic rescue (control: *arm*-Gal4/+). ****p<0.0001 by Kruskal-Wallis test with Dunn's post-hoc correction for multiple comparisons. Error bars = 95% confidence interval. Numbers in bars represent biological n for each genotype. Unless specified statistical comparisons are made with the control. Data for panel **B** generated by R. Tufi.

MICU3^{27} is associated with a slightly reduced lifespan

To evaluate whether the reduced fitness of young *MICU3*^{27} flies affects vitality over time, their lifespan was measured (Figure 38). Versus their *w*^{1118} genetic background controls, *MICU3*^{27} show a statistically significant reduction in lifespan, with a small effect size (median lifespan 55 vs. 59 days, 9% reduction). This suggests that, although loss of *MICU3* leads to some quite severe phenotypes, these do not overtly compromise fundamental biological processes, giving otherwise affected flies almost wild-type longevity. This can be related to the proposed role of MICU3 in tuning mitochondrial calcium uptake through its essential partner MICU1. Loss of MICU3 would result in suboptimal tissue-specific shaping of calcium currents leading to specific organismal dysfunction, but without the gross global dysregulation seen in MICU1 mutants.

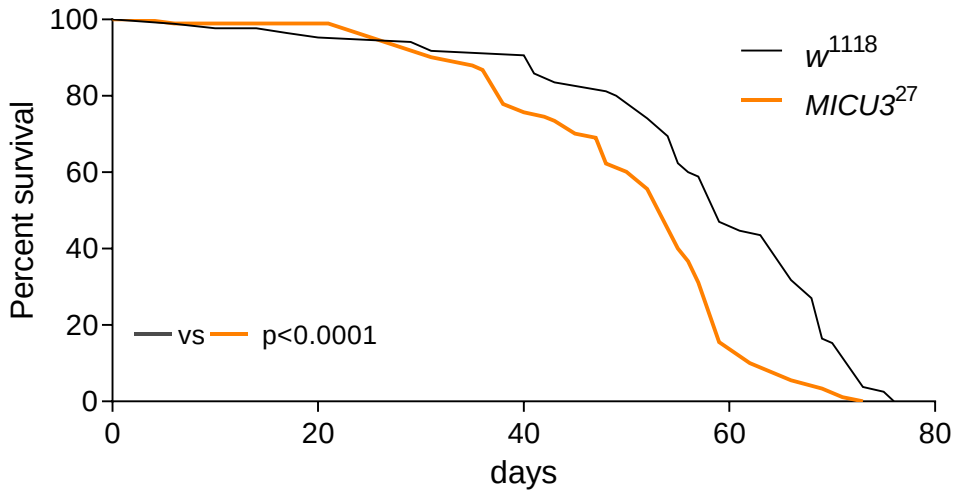

Figure 38. Survival curves of *w*^{1118} (n=86) and *MICU3*^{27} (n=98). P<0.0001 for both Mantel-Cox and Gehan-Breslow-Wilcoxon tests.

MICU3^{27} has reduced ATP levels despite normal oxygen consumption

The locomotor and sterility phenotypes of *MICU3*^{27} can be related to dysfunction of specific tissues were *MICU3* is known to be expressed. By contrast, the more global lifespan and eclosion phenotypes were minimally affected, if at all; the tissue-specific effects of *MICU3* loss appear to be compensated by other tissues to minimise overall phenotypes in the fly. So, to investigate the metabolic consequences of the *MICU3*^{27} mutant, Oroboros respirometry was performed on young and old fly heads (Figure 39A). No significant difference was found at either age, for either Complex I or II-linked respiration. In contrast, a significant reduction in ATP was measured by chemiluminescence in young fly heads (Figure 39B). This was comparable to the *Pink1*^{B9}-associated ATP deficit (Vos *et al.*, 2012). The difference between these two outcomes can be explained by the saturating substrate concentrations present in the respirometry assay leading to maximal respiratory chain activity, compared with direct measurements of ATP concentration. A change in cellular energy demand could lead to reduced physiological ATP without compromising the efficiency of the respiratory chain.

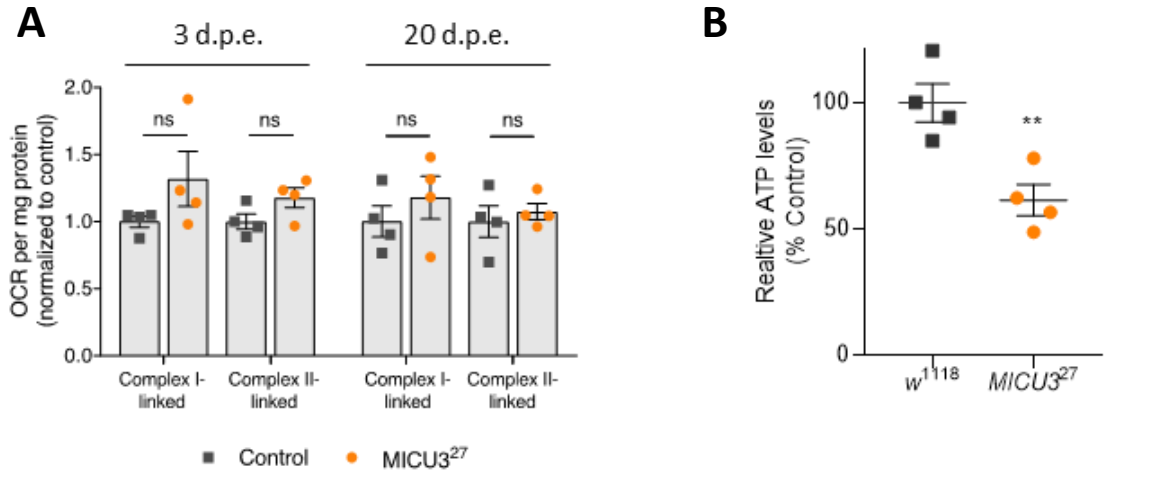

Figure 39. **A**: Oxygen consumption rate of control and *MICU3*^{27} fly heads at 3 and 20 days post-eclosion, normalised to protein concentration. Complex I-linked respiration was measured in the presence of 10 mM glutamate, 2 mM malate, and 2.5 mM ADP. The addition of 1.5 µM rotenone and 10 mM succinate was used. Error bars = SEM, ns = p>0.05 from unpaired t tests with Welch's correction for unequal standard deviation. Data points indicate individual runs each containing 5 fly heads. **B**: ATP levels of control (*w*^{1118}) and *MICU3*^{27} fly heads, normalised to control mean. Error bars = SEM, **p<0.01 from unpaired t test. Data points represent biological n (homogenates from 10 fly heads).

4.5. Discussion

Mitochondrial calcium uptake has been considered until recently to be an essential process for life. The publication of the viable *Mcu* knockout mouse therefore sparked significant controversy, with the diverging phenotype based on genetic background forming the basis for debate as whether this is truly an essential gene. The generation of this *MCU*^{1} knockout fly, which was viable in both its initial background and after outcrossing to a well-established isogenic background, lends weight to the lack of mitochondrial calcium uptake being dispensable during development. The *EMRE*^{1} mutant, which also abrogates mitochondrial calcium uptake, is similarly viable, lending further support to this assertion.

Though both *MCU*^{1} and *EMRE*^{1} seem to be well tolerated up to young adulthood, aging reveals a significant deficit in lifespan, indicating a sensitisation to accumulated stressors. The reduced lifespan was much more pronounced for *MCU*^{1} than *EMRE*^{1} despite their functional equivalence in terms of calcium uptake, suggesting the effect arises from the physical presence or absence of the uniporter pore, and its interaction with other pathways. For instance, MICU1 coordinates the inner and outer mitochondrial membranes at sites of mitochondrial calcium uptake (Gottschalk *et al.*, 2019), and other uniporter components may be involved in this bridging mechanism, which impacts on many other organellar processes beyond calcium dynamics. The differences between *MCU*^{1} and *EMRE*^{1} knockouts was expanded with the observation that *MCU*^{1} mutants display a substantial reduction in maximal respiratory chain capacity, whereas *EMRE*^{1} were not statistically distinguishable from controls. Again, this may arise from uniporter protein-protein interactions driving the coordination of other biochemical processes. For example, MCUR1 regulates mitochondrial calcium influx and Complex IV assembly (Paupe *et al.*, 2015; Vais *et al.*, 2015), and the disruption of one may impact the other.

This work demonstrates the first *in vivo* model of *MICU3* loss. Though well tolerated developmentally, homozygous mutants were sterile, most likely reflecting MICU3 expression in gonadal tissue. To explore this further, the morphology of the testis and ovaries could be examined, and apoptotic markers could be employed to see whether mPTP-induced cell death underlies the dysfunction.

Much as for the sterility, other *MICU3* mutant phenotypes can be mapped onto tissues were its expression has been reported. Global organismal function as indicated by lifespan and eclosion were normal, but the neuronally-associated locomotor behaviour was significantly compromised. One of the more surprising effects of *MICU3* loss was seen in the gross metabolic examination of the head – the compartment with the highest expression of the gene. Complex I- or II-linked maximal respiratory activity was unchanged, but a dramatic reduction in tissue ATP was measured. This indicates that *MICU3*^{27} mitochondria have wild-type capacity for oxidative phosphorylation, but this does not translate to actual energy supply. The possible reasons for this are numerous. Cellular ATP demand may simply be reduced, though the magnitude of the reduction seen is larger than might be expected for this, and the behavioural defects seen in the mutants suggest a more pathological situation. Instead, the supply of reducing equivalents may be compromised, limiting ATP production. Similarly, compromised membrane potential would result in inefficient synthesis. This could be evaluated by measurement of the NAD^+/NADH ratio, or TMRE as a proxy for $\Delta\psi_m$. Alternatively, external stressors such as starvation may reveal sensitisation due to reduced energy supply.

The *MCU*^{1} knockout fly corroborates with the previously published *MCU*^{52} (Choi *et al.*, 2017) in an important way; both are viable. In contrast to the P{EPgy2}EY08610 element mobilised here, the authors targeted the P{GSV6}GS11565 element, which sits in the same region. This, along with the *EMRE*^{1} mutant, provide compelling evidence for the dispensability of mitochondrial calcium uptake for life, at least in *Drosophila*. In contrast, however, the starvation sensitisation seen in *MCU*^{1} runs counter to the lack of metabolic phenotypes seen in *MCU*^{52}. It is worth mentioning that the same assays were not used in the two studies; their approaches may instead work in parallel. For example, the lack of starvation-induced autophagy may underlie the shortened lifespan in the absence of food, and perhaps even provide an explanation for the longevity phenotype in general conditions.

This work provides robust *in vivo* evidence for the physiological requirements of key mitochondrial calcium uniporter constituents. Several surprising phenotypes are observed, with implications for future studies probing their mechanistic basis. Additionally, the first *in vivo* characterisation of MICU3 is reported, revealing highly tissue-specific effects, reflecting its proposed role as a specific modulator of calcium dynamics in cell subsets. These data provide a comprehensive genetic investigation of the uniporter, demonstrating the power of these tools. Further work outlined below begins to combine these manipulations with others to interrogate functional interactions or lack thereof. As well as provide valuable information on the wider context of this protein complex, these are also used to probe pathogenic hypotheses in disease models, with early successes being expanded to related contexts.

5. Characterisation of the uniporter gatekeeper *MICU1*

5.1. Background and Aims

Structural studies of the mitochondrial calcium uniporter show that it is most similar to a class of ion channel, rather than a classical exchanger (Baradaran *et al.*, 2018; Fan *et al.*, 2018; Nguyen *et al.*, 2018; Yoo *et al.*, 2018). However, the uniporter current is coupled to release from intracellular stores such as the ER, serving to link metabolic changes to energy supply. Gatekeeping proteins, in this case the MICU family, achieve this by blocking the channel when extramitochondrial calcium is low, promoting uptake when it is high. The loss of MICU gatekeeping can be hypothesised to lead to calcium uptake over a wide range of extramitochondrial concentrations, resulting in mitochondrial calcium overload.

In contrast to other uniporter components, patient mutations for the MICU family have been reported. A patient cohort of seven families was found to harbour loss-of-function mutations in *MICU1* – in either a splice donor or acceptor site (Logan *et al.*, 2014). This led to muscle weakness and learning difficulties, with progressive extrapyramidal defects in two thirds of the affected cohort. Other symptoms suggested a mitochondrial disorder, but patient skeletal muscle homogenates showed normal respiratory chain activity. In this study, patient mitochondria displayed enhanced mitochondrial calcium uptake in response to histamine, with unaltered membrane potential.

In an additional cohort, two cousins presenting with lethargy and muscle aches were found to share a homozygous 2.8 kb deletion covering exon 1 of *MICU1* (Lewis-Smith *et al.*, 2016). Oxygen consumption and extracellular acidification rates were not significantly altered in patient fibroblasts. Surprisingly, the rate of calcium uptake was reduced in these cells, in extramitochondrial conditions where the absence of MICU1 could be presumed to increase calcium entry. The authors suggest that this might be due to increased $[Ca^{2+}]_m$ reducing the drive for calcium across the membrane. Indeed, the reduced phosphorylated fraction of pyruvate dehydrogenase supports a higher matrix calcium concentration. Complicating this interpretation, mitochondrial calcium concentration is several orders of magnitude higher than the bulk cytosol, and the electrochemical drive for mitochondrial calcium uptake is instead driven by the membrane potential. The membrane potential was not measured in this study.

A homozygous frameshift mutation in *MICU2*, leading to a severely truncated protein, was associated with neurodevelopmental delay and spasticity (Shamseldin *et al.*, 2017). As for *MICU1*, higher basal matrix calcium was observed, but here, the rate of Ca^{2+} influx was reduced. Interestingly, the membrane potential was high in *MICU2* patient fibroblasts, which the authors attribute to increased NCLX activity.

To be able to understand the effects of these mutations, it is crucial to generate precise animal models. Two mouse models have been recently reported (Antony *et al.*, 2016; Liu *et al.*, 2016), but display key phenotypic differences, indicating genetic background effects that have similarly frustrated the interpretation of the *Mcu* knockout mouse (see Section 1.3.1). Additional animal models such as in *D. melanogaster*, can provide evidence to resolve this conflict by leveraging its genetic tractability to carefully control for genetic background, and to demonstrate phenotypic specificity through non-complementation of deficiency lines and transgenic rescue. This potential formed the basis for the present work – characterising the fly *MICU1* knockout and determining its interaction with other uniporter components.

5.2. RNAi/Overexpression Line Characterisation

Mouse models of *MICU1* are aligned on the importance of this gene but differ on the exact severity of its loss. So, I sought to understand the physiological requirements of *MICU1* in *D. melanogaster*, to provide orthogonal confirmation. I again initially used an RNAi approach, which facilitates rapid screening of phenotypic effects in different tissues. Using the ubiquitous *da*-Gal4 driver, *MICU1* knockdown via either P{GD4927}v49349 or P{TRiP.HMS02302}attP2 was lethal during the pupal phase – these became necrotic and failed to eclose. This phenotype was fully penetrant, in accordance with one of the mice studies (Antony *et al.*, 2016), and indicated that *MICU1* was an essential fly gene. Complicating the picture, ubiquitous *da*-driven overexpression of either UAS-MICU1-A-3xHA or UAS-MICU1-B-HA led to the same phenotype. This suggests the level of MICU1 is finely controlled to avoid dysregulated calcium uptake. It is perhaps surprising that excessive MICU1, which might be hypothesised to reduce calcium uptake by increasing the proportion of gated uniporters, is not viable as for the MCU knockdown. However, different compensatory mechanisms may be present in these two conditions, potentially accounting for the discrepancy.

Next, I utilised more specific drivers, to dissect the tissue requirements for *MICU1*, and here differences emerged between the MICU1 manipulations. With both the weaker *elav*-Gal4 and stronger *nSyb*-Gal4 neuronal drivers, both RNAi lines and overexpression constructs were viable. With *nSyb*-Gal4, both over expression lines and the P{TRiP.HMS02302}attP2 knockdown showed a climbing defect of similar magnitude (Figure 40A), but this was not observed for P{GD4927}v49349. With the weaker *elav* drive, only the MICU1-A-3xHA overexpression showed a climbing phenotype, suggesting the overexpression of MICU1-A is less tolerated than MICU1-B. With the muscle-restricted Mef2-Gal4, all except P{GD4927}v49349 were viable, but displayed a strong climbing defect (Figure 40B), up to the point of zero locomotion, indicating the importance of mitochondrial calcium handling for proper muscle function. These results are summarised in Table 11, and provide a useful foundation to give context to the characterisation of mutant phenotypes.

Table 11. Summary of viability and climbing ability for *MICU1* knockdown and overexpression through different gene drivers, coded by cell colour. Green = viable, no climbing phenotype. Orange = viable, with climbing phenotype. Red = lethal.

	da-Gal4	*elav*-Gal4	*nSyb*-Gal4	*Mef2*-Gal4
KD	P{GD4927}v49349 P{TRiP.HMS02302}	P{GD4927}v49349 P{TRiP.HMS02302}	P{GD4927}v49349	P{GD4927}v49349
			P{TRiP.HMS02302}	P{TRiP.HMS02302}
OE	UAS-MICU1-A-HA UAS-MICU1-B-HA	UAS-MICU1-A-HA	UAS-MICU1-A-HA UAS-MICU1-B-HA	UAS-MICU1-A-HA UAS-MICU1-B-HA
		UAS-MICU1-B-HA		

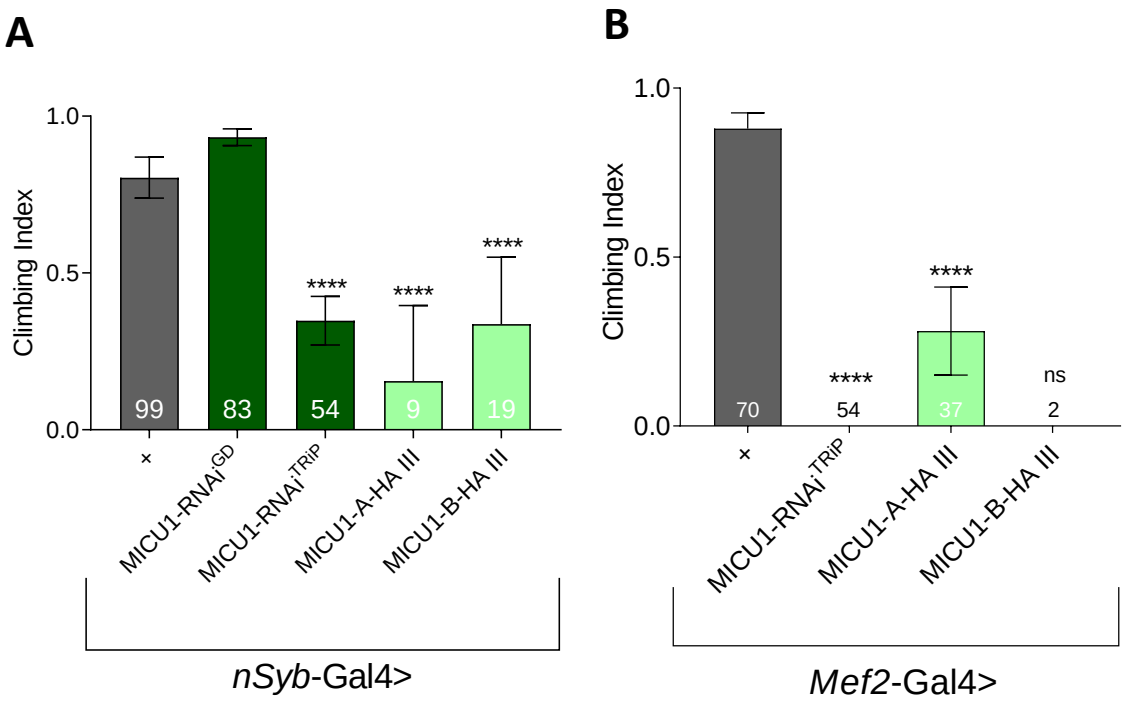

Figure 40. Climbing performance of knockdown and overexpression lines with the **A**: *nSyb*>Gal4, or **B**: *Mef2*-Gal4 driver. All genotypes were compared to control (*Mef2*/+) with Kruskal-Wallis test with Dunn's post-hoc correction for multiple comparisons. ****p<0.0001. Error bars = 95% confidence interval. Numbers in or next to bars represent biological n for each genotype.

5.3. MICU1 loss is developmental lethal with organismal dysfunction

MICU1^{32} is larval lethal with full penetrance

Based on the mouse mutant, we hypothesised that *Drosophila* mutants would similarly be recessive developmental lethal, and the RNAi data suggested a fully penetrant phenotype. The *MICU1*^{32} mutant isolated was initially balanced over the CyO chromosome, which carries the *Duox*^{Cy} dominant mutation that results in curled wings. So, the presence of flies with wild-type wings would indicate viable homozygotes. However, all flies observed displayed curled wings, confirming completely penetrant lethality. The stock was rebalanced over CyO.GFP to provide a marker in all stages of the *Drosophila* life cycle, and beyond the L2/L3 larval instar all surviving animals were GFP positive, demonstrating this as the lethal phase. *MICU1*^{32} homozygous larvae were smaller than controls (Figure 41) and lacked a switch to non-feeding behaviour prior to pupariation, evidenced by them remaining on the food surface. It is unclear whether this is simply due to the lethality occurring during the feeding phase, or foraging prolongation due to insufficient nutritional uptake or other factors. Synchronisation of embryos would allow the length of each developmental stage to be accurately measured.

Figure 41. Comparison of control (*w*^{1118}) and *MICU1*^{32} larvae.

To confirm the specificity of the lethal phenotype to *MICU1*, mutants were first crossed to the Df(2L)Exel8019 deficiency line, which covers the region containing *MICU1*. This combination was also larval lethal, indicating the phenotype arises from somewhere inside this deficiency locus. To provide conclusive evidence, the lethality should be rescued by transgenic re-expression. This was achieved by crossing CyO.GFP balanced *MICU1*^{32} flies that also harboured Gal4 drivers and UAS constructs, allowing for precise control of the re-expressed protein. As discussed above, CyO.GFP features dominant markers in larvae (ubiquitous GFP expression) and adult (red eyes, curled wings) that allow for hetero- and homozygous *MICU1*^{32} animals to be distinguished. This strategy is illustrated in Figure 42.

Overexpression of either MICU1-A or MICU1-B alone under the strong ubiquitous *da*-Gal4 was lethal, and indeed the combination with *MICU1*^{32} did not provide a rescue. *Drosophila* are poikilotherms, and their metabolism is therefore susceptible to external temperature, which allows protein expression to be titrated experimentally. Raising *da*-Gal4 rescue flies at 23°C, a small fraction of rescued flies was observed, lacking balancer chromosome markers and thereby indicating a homozygous mutation. This was verified by PCR as outlined in Section 3.3.3. As a lower temperature, corresponding to lower expression, was needed to obtain viable flies, I reasoned that weaker transgenic expression of MICU1 may improve the proportion of rescue. Using the weaker ubiquitous *arm*-Gal4 driver, an almost Mendelian proportion of progeny was observed with either MICU1-A or MICU1-B, representing complete rescue of developmental lethality. Transgenic rescue was also achieved with *elav*-Gal4, implicating neuronal tissue as key for this lethal phenotype. These results are summarised in Table 12.

Table 12. Viability of *MICU1*^{32} with UAS-MICU1 expressed under the control of the indicated Gal4 driver. Cell colour: red = lethal with complete penetrance, orange = partially viable, green = complete (Mendelian) viability.

Driver	*da*-Gal4	*da*-Gal4 (23 °C)	*arm*-Gal4	*elav*-Gal4
Phenotype	Lethal	Partial	Viable	Partial

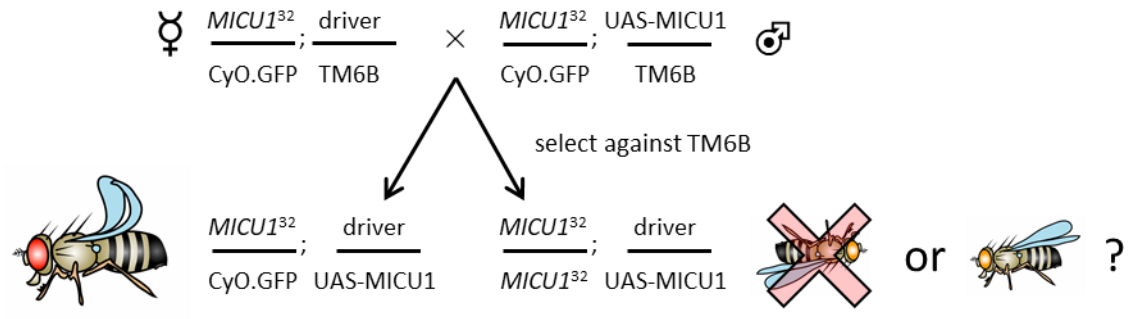

Figure 42. Generalised crossing scheme for transgenic re-expression of MICU1 in a knockout background. Selecting against markers for the Chromosome III balancer TM6B (namely, *Atnp*^{Hu} and *Tb*^{1}) ensures the co-presence of the Gal4 driver and the UAS-MICU1 line. *MICU1*^{32} heterozygotes will necessarily be co-present with the recessive lethal CyO.GFP, and *MICU1*^{32} homozygotes can be detected by their straight (wild-type) wings.

To further demonstrate *MICU1* transgenic rescue, the climbing ability of rescued flies was assessed as a proxy for organismal vitality. *MICU1*^{32} mutants with *arm*-Gal4 re-expression of either MICU1-A or MICU1-B climbed as well as controls (Figure 43), indicating the loss of *MICU1* can be fully rescued in terms of organismal vitality as well as viability.

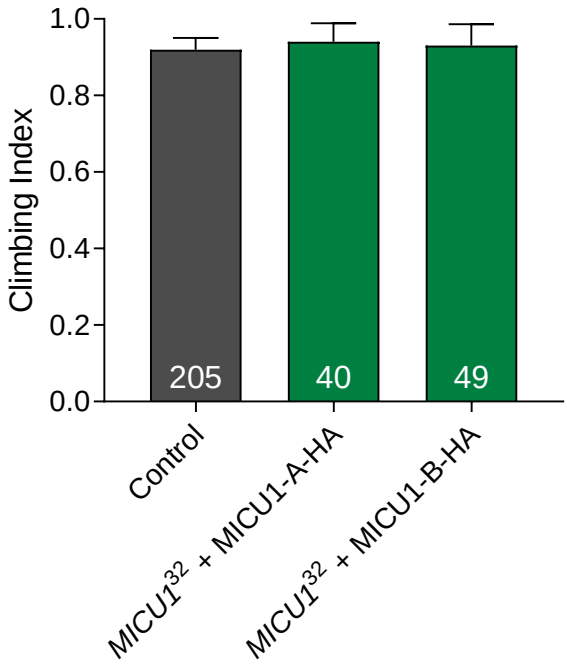

Figure 43. Climbing performance for control (*arm*-Gal4/+) and *arm*-driven rescue of *MICU1*^{32} via transgenic re-expression of either the -A or -B isoform. Error bars = 95% confidence interval. Numbers in bars represent biological n.

Larval locomotion is reduced in *MICU1*^{32}

The size difference between *MICU1*^{32} and wild-type larvae demonstrates that the effects of the mutation are evident before the lethal phase and raises the possibility of other defects at this stage, for example in neuromuscular pathways. To address this, larval locomotion, as measured by the rate of peristalsis, was assessed for *w*^{1118} and *MICU1*^{32} (Figure 44). *MICU1*^{32} were significantly slower than controls (mean 37.8 vs. 27, a 28% reduction), indicating a neuromuscular defect. Both tissues rely heavily on proper calcium handling for their function, so this phenotype can be linked to dysregulated calcium entry.

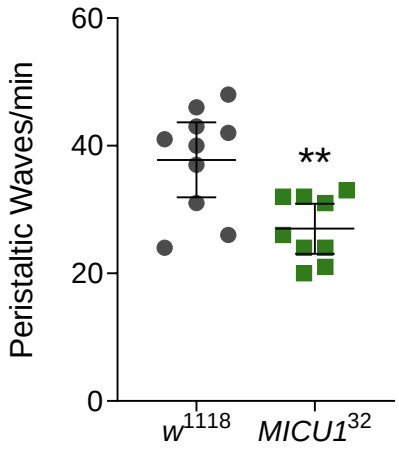

Figure 44. Number of peristaltic waves per minute for control (*w*^{1118}) and *MICU1*^{32} L3 larvae. Error bars represent 95% CI, **p<0.01 by unpaired t test. Data points represent biological n (individual larvae).

Axonal *MICU1*^{32} mitochondria have reduced transport and altered morphology

Having established the behavioural endpoint of a neuromuscular problem, we sought to probe the underlying mechanism for this defect. The efficient transport of mitochondria from the soma to the synapse of such elaborate cells as motoneurons is a significant challenge, and the activity of motor protein adaptors such as Miro is linked to local $[Ca^{2+}]_c$ (reviewed in Niescier, Chang and Min, 2013). So, we hypothesised that altered mitochondrial calcium loading could result in aberrant axonal transport, which may underlie behavioural, or even viability phenotypes.

To this end, V. L. Hewitt. imaged mitochondrial morphology in distal larval motoneurons using the *M12*-Gal4 driver. Representative examples are found in Figure 45. Basic observation of these movies already indicated reduced mitochondrial number, particularly of motile mitochondria, as evidenced from the kymographs included. Manually measuring the mitochondrial length for the first frame of each movie, I found the overall distribution to be quite wide in controls, with overall symmetry around 1.4 µm (Figure 46A). For *MICU1*^{32} the distribution was much narrow and right-skewed, with an average closer to 1.0 µm. Condensing the length distribution to a single metric, I found the average mitochondrial length to be significantly lower in *MICU1*^{32} mutant larvae (Figure 46B). The average number of mitochondria per movie was also reduced in mutant larvae (Figure 46C), which necessitated the length distribution to be expressed as a proportion of total mitochondria. This may reflect reduced transport to this distal region, but other explanations such as reduced biogenesis or enhanced mitophagy are also possible. Categorisation of mitochondrial motility by kymograph analysis uncovered the most dramatic phenotype: the proportion of motile mitochondria was strongly reduced (Figure 46D). In total, *MICU1*^{32} is associated with reduced motoneuron axonal transport and aberrant mitochondrial morphology. Both can impair neuronal signalling and synaptic energy supply. Therefore, insufficient synaptic supply of ‘healthy’ mitochondria may contribute to the locomotor dysfunction observed in Figure 44.

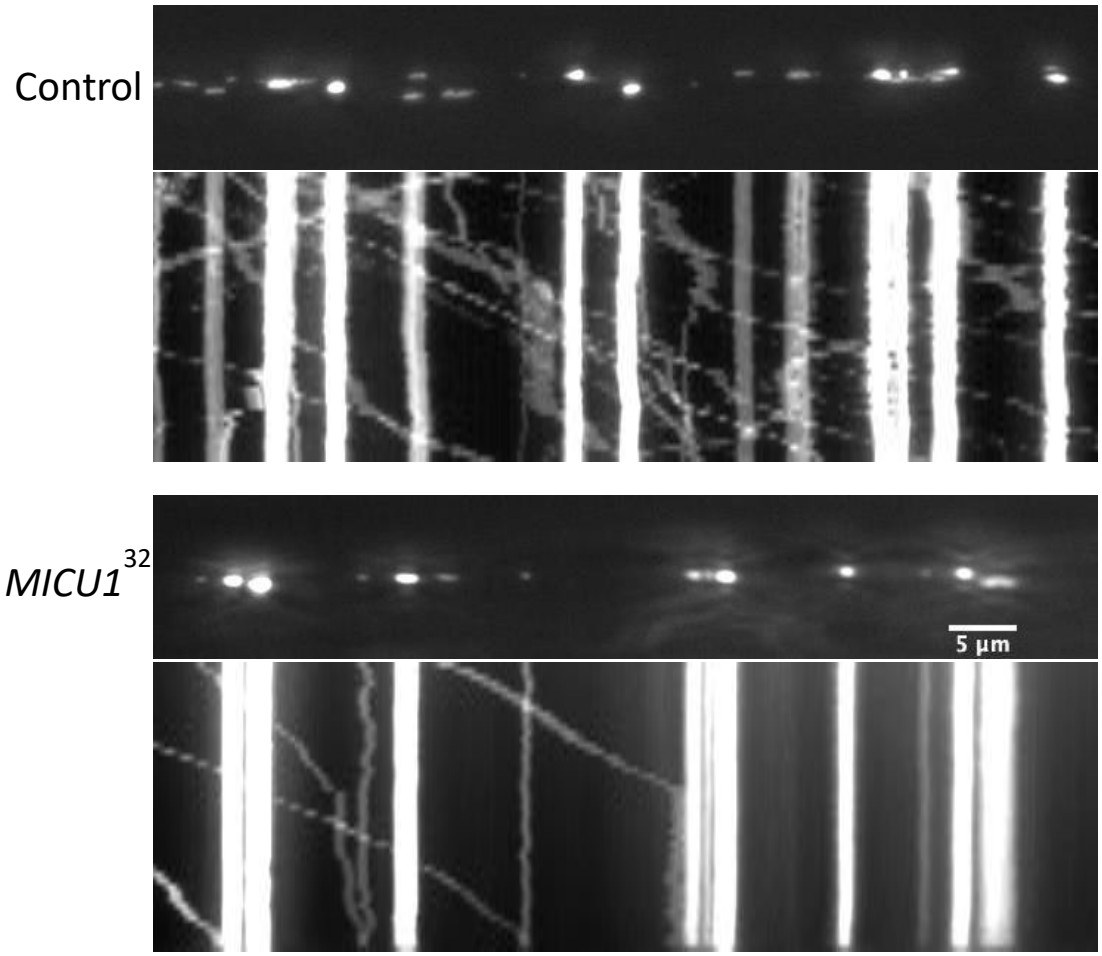

Figure 45. For control (M12>mito.GFP) and *MICU1*[32] larvae, top: representative frame from movie recording mitochondrial motility in motor axons, bottom: resulting kymograph. Scale bar = 5 µm.

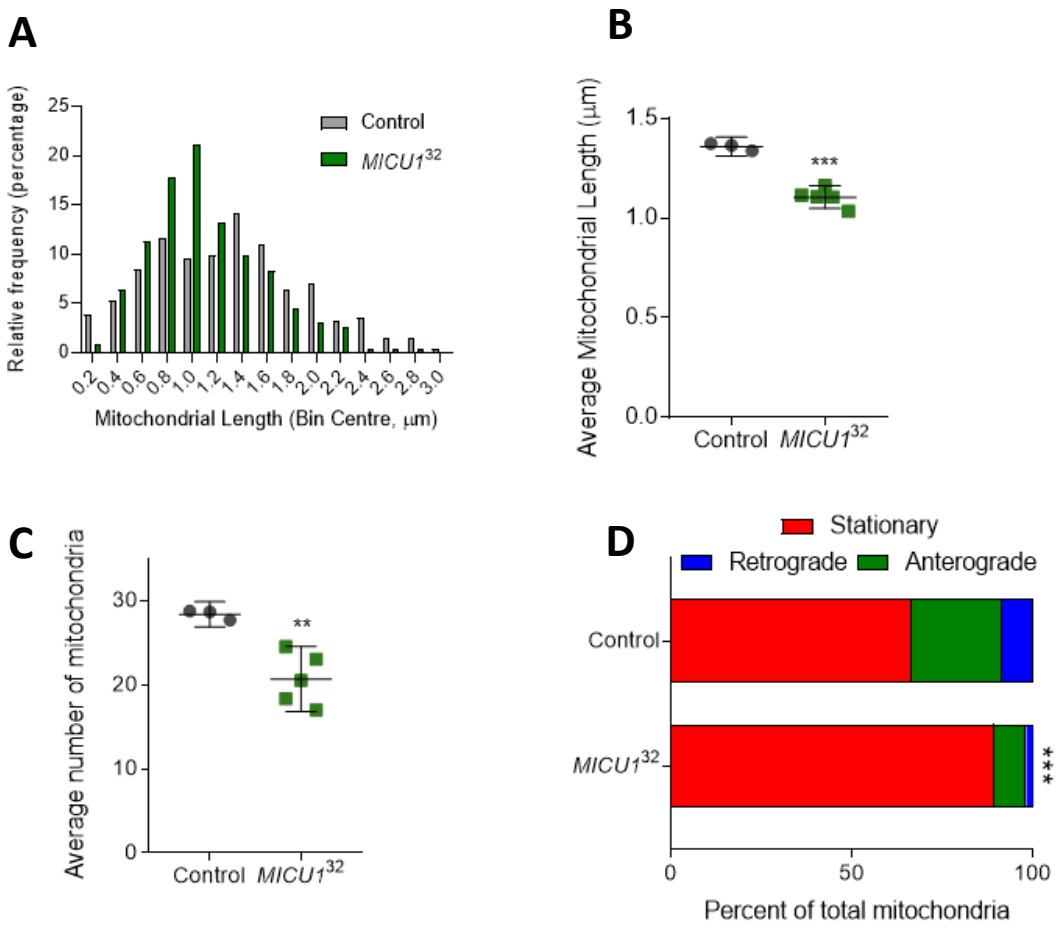

Figure 46. Analysis of control (w^{1118}) and *MICU1*^{32} mutant kymographs. **A**: Histogram of mitochondrial length (grouping: 0.2 µm, values above 3 µm not shown), **B**: Average mitochondrial length per animal (***p=0.0001 by unpaired t test), **C**: Average number of mitochondria per animal (**p=0.0043 by unpaired t test with Welch's correction for unequal SD), **D**: Mitochondrial motility (***p=0.0002 by χ^2 test). Data in **A** and **D** aggregated across all animals, data in **B** and **C** grouped by animal (biological n, control = 3, *MICU1*^{32} = 5). Error bars = 95% confidence interval.

MICU1 loss alters respiratory capacity

Excessive mitochondrial calcium influx can be predicted to result decreased membrane potential that would be compensated for by increased proton pumping activity, with these being diverted to provoke calcium efflux. Prolonged calcium uptake in this fashion may therefore result in futile cycling of protons that could decrease ATP supply. Indeed, when the level of ATP was measured, a significant reduction was observed (Figure 47A). To extend this finding, I sought to determine if a respiratory phenotype was also present, which would lend weight to the futile cycling hypothesis. To test this, control and mutant larval homogenates were assayed with Oroboros oxygraphy (Figure 47B). Surprisingly, though there was no significant difference in Complex I-linked respiration, Complex II-linked respiration was more than two-fold greater in *MICU1* larvae. It bears repeating that this experiment measures maximal respiration under respiratory substrate excess, rather than physiological activity. It may therefore indicate an increase in Complex II expression to compensate for some other respiratory compromise. It is still interesting that the respiratory complex without proton pumping capabilities was the one that showed increased activity. In an alternative explanation, *MICU1*^{32} mitochondria may be partially uncoupled, and indeed increased maximal respiration was observed in MICU1 KD cells (Chakraborty *et al.*, 2017). It was not possible to ascertain the level of mitochondrial coupling in this experimental setup, however, as titration of CCCP did not yield a respiratory rate greater than that for coupled respiration (data not shown).

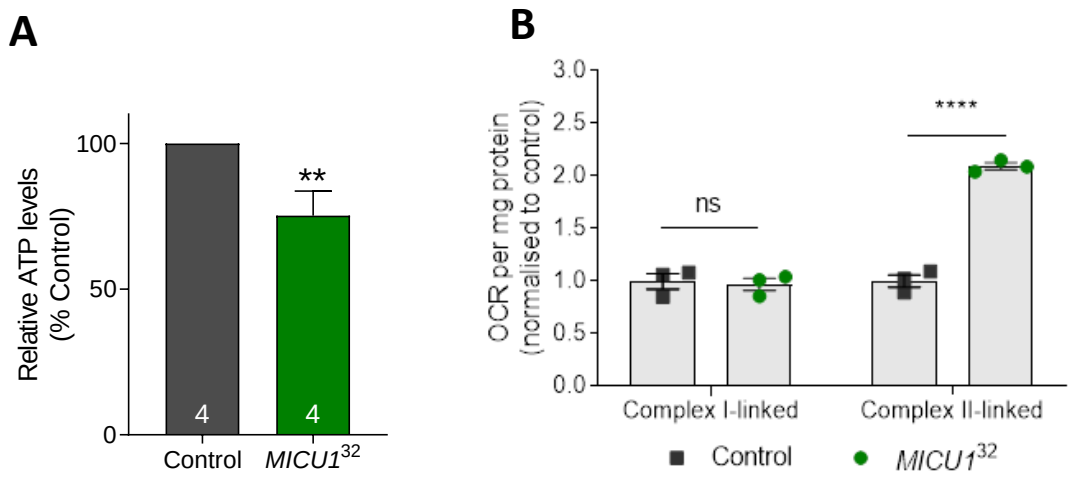

Figure 47. **A**: ATP levels of control (w^{1118}) and *MICU1*^{32} larvae, normalised to control mean. Error bars = SEM, **p<0.01 from unpaired t test. Data points represent biological n (homogenates from 10 larvae). **B**: Oxygen consumption rate of control and *MICU1*^{32} larvae normalised to protein concentration. Complex I-linked respiration was measured in the presence of 10 mM glutamate, 2 mM malate, and 2.5 mM ADP. The addition of 1.5 µM rotenone and 10 mM succinate was used. Error bars = SEM, ns = p>0.05, ****p<0.0001 from unpaired t tests. Data points indicate individual runs each containing 5 larvae. Data for panel **A** generated by R. Tufi.

5.4. Inhibiting cell death does not rescue *MICU1*^{32}

Establishing that *MICU1*^{32}-associated lethality is rescuable by transgenic re-expression of the gene product provides a key validation of the phenotype, making it feasible to probe the underlying mechanism through genetic interaction studies. Calcium overload is a catastrophic situation for mitochondria, but its link to cell death pathways allows for the preservation of neighbouring cells; limiting production of toxic by-products of uncontrolled metabolic signalling such as reactive oxygen species (ROS). However, complete dysregulation of mitochondrial calcium entry as predicted for the *MICU1*^{32} mutants would lead to excessive cell death to the point of organismal failure. Indeed, the pupal transition involves dramatic changes in metabolic requirements (Merkey *et al.*, 2011), requiring high metabolic activity in prior larval stages, and it follows that this would be the point of lethality in these mutants. Inhibiting cell death pathways may rescue this lethality, which would provide clues to the molecular mechanism of the phenotype.

Transgenic expression of the baculovirus P35 prevents many forms of cell death through widespread caspase inhibition (Clem, Fechheimer and Miller, 1991). Unsurprisingly, this potent approach is not well tolerated, with *da*-Gal4 expression of the protein alone conferring developmental lethality. However, when expressed with the weaker *arm*-Gal4 driver, viable flies were observed. Nevertheless, the combination of *MICU1*^{32} and *arm*>BacA\p35 failed to rescue the lethality of the knockout. It remains possible that this broad manipulation of apoptosis is too strong and global to adequately counteract the *MICU1*^{32}-associated changes in calcium dynamics and corresponding cell death. To refine this, the *Drosophila* homolog of the inhibitor of apoptosis family, Diap1, was used. Despite being well tolerated with *da*-Gal4 expression, the combination with *MICU1*^{32} again showed no rescue of the lethality, suggesting this lethality is not associated with Diap1-associated cell death. The Df(3L)H99 deficiency line covers the inhibitor of apoptosis antagonists *grim*, *reaper*, *sickle*, and *head involution defective* (*hid*). Although homozygous lethal like most deficiencies, this aberration in heterozygosity has long been used in the study of cell death. The combination of Df(3L)H99/+ and *MICU1*^{32} did not produce viable adults, further indicating that either the aberrant cell death pathways in *MICU1*^{32} are not Diap1/H99-linked. Cell death may not be the overall driver of the lethal phenotype, though it remains possible that other cell death pathways may be responsible and could be examined in a similar fashion. For example, specifically inhibiting the intrinsic apoptotic pathway through expression of *Buffy*, a *Drosophila* Bcl-2 protein, may prove fruitful.

5.5. *MICU1*^{32} is not rescued by *MCU*^{1} or *EMRE*^{1}

Reasoning that the lethal phenotype of *MICU1*^{32} arises from excessive mitochondrial calcium uptake, I hypothesised that homozygous *MCU* or *EMRE* loss should provide a genetic rescue. Indeed, surviving *Micu1*$^{-/-}$ mice display a reduction in EMRE protein that becomes more marked with age, and *Emre*$^{+/-}$ rescues several phenotypes associated with *Micu1*$^{-/-}$, including the altered birth ratio (Liu *et al.*, 2016). The *MICU1*^{32} and *MCU*^{1} stocks were combined to create *MICU1*^{32}/CyO.GFP;*MCU*^{1}/TM6B, ensuring balancer markers for both chromosomes would be available to score throughout development. Similarly, a recombinant between MICU*1*^{32} and *EMRE*^{1} was generated, yielding the *MICU1*^{32},EMRE^{1}/CyO.GFP stock. Homozygous *MCU*^{1} adults were seen in the relevant stock, but no homozygous *MICU1*^{32} (all expressed GFP). The lethal stage appeared unchanged from the L2/3 transition. Due to the nature of the *EMRE*^{1} combination, both mutants are co-inherited, and all animals past the L2/3 larval transition were GFP positive, demonstrating a lack of rescue with this mutant also. To examine the effect of heterozygous *MCU*^{1} or *EMRE*^{1}, the combination stocks were crossed to stocks of *MCU*^{1} or *EMRE*^{1} respectively. Nevertheless, no rescue of *MICU1*^{32} by these heterozygous mutations was seen.

This simple experiment delivered a highly surprising finding, namely that the lethal phenotype of *MICU1* may be independent of uniporter-mediated calcium influx. This warranted further confirmation. Double homozygous larvae for *MICU1*;*MCU*^{1} and *MICU1*^{32},*EMRE*^{1} were selected based on balancer markers (or rather the absence thereof). PCR analysis as described in Section 3.3.3 confirmed these larvae to be homozygous for *MICU1*^{32}. This proves that the rescue combinations were present in these stocks, but failed to develop, unlike their balanced heterozygous counterparts. These results suggest that *MICU1*-associated lethality arises from a uniporter-independent function of the gene.

5.6. Discussion

MICU1 characterisation through knockdown and overexpression experiments support it as a key developmental gene, with its expression held in a fine balance. This is in concordance with the knockout mutant generated, and contrasts with *MCU* and *EMRE*, which are dispensable. This most likely reflects the importance of channel regulation over the presence of uniporter-mediated influx itself, which makes sense given its role in sensitising cells to apoptosis.

Mutations in MICU family proteins appear to result in heterogenous phenotypes, from a milder muscle impairment in a *MICU1* patient cohort to complete developmental lethality in a mouse knockout model. Even within the same species, the two *MICU1* patient populations identified diverge from each other phenotypically despite sharing the same functional consequence in terms of *MICU1* gene loss. This strongly suggests genetic modifiers, resembling the discrepancies between *Mcu* mouse models. By contrast, the loss of fly *MICU1* results in a strong locomotor deficit even at the larval stage, which may be underpinned by a reduction in motoneuron axonal transport. Less mitochondrial flux down the axon can explain the observation of fewer mitochondria in a specific region, but not the changes in morphology also seen. The mitochondrial fission factor Drp1 is inactive in its phosphorylated form, and this phosphate is removed by the calcium-sensitive calcineurin (Cribbs and Strack, 2007), providing a link between altered calcium dynamics and mitochondrial morphology. Dephosphorylated Drp1 caused by increased calcium flux would hyperfragment mitochondria and sensitise them to apoptosis. Interestingly, mitochondrial shape can influence calcium signalling (Favaro *et al.*, 2019), and this balance may result in a pathological feedback loop in the disrupted *MICU1*^{32} condition.

The respiratory phenotype of *MICU1* larvae is intriguing, indicating a dramatic metabolic alteration in response to this gene loss. Further work will attempt to refine this observation with direct measurements of metabolic indicators (e.g. respiratory chain enzyme activity, ATP levels, NAD^+/NADH ratios), to provide an explanation for this altered respiratory capacity, and possibly also the organismal phenotypes.

The most surprising observation from the present work is that *MICU1*^{32}-associated developmental lethality is not rescuable by loss of either *MCU* or *EMRE*, which would be hypothesised to circumvent any uniporter dysregulation by rendering the channel absent or otherwise inactive. Given the unexpected nature of this finding, it was important to verify that the lethal phenotype seen was attributable to *MICU1* itself, and this was achieved by rescue with transgenic re-expression. Both *MCU*[1] and *EMRE*[1] have been shown to abolish fast mitochondrial calcium uptake (see Section 3.4.3, also Tufi *et al.*, 2019), so in total these results suggest a uniporter-independent function for *MICU1*. Future work will be aimed at identifying this, through genetic modifier screens and identification of binding partners. The structure of *MICU1* suggests a likely role in providing Ca^{2+}-sensing capability, and though more speculative, may also regulate some other machinery for ion flux across the inner mitochondrial membrane. Electrophysiological studies have shown the presence of multiple mitochondrial calcium currents (Bondarenko *et al.*, 2013), and classical experiments aimed at showing the requirement of the uniporter for calcium influx have been performed under specific extramitochondrial conditions. It remains possible that an alternative uptake pathway may be active under conditions not used in classical studies of the uniporter. Instead, this pathway may be active only in response to an unidentified cellular stimulus, though this gating would have to be removed in the electrophysiological protocol. Perhaps more likely, this pathway may be constitutively active, but with kinetics that mask its observation. This scenario been previously suggested (Elustondo *et al.*, 2016), and would serve to maintain basal mitochondrial calcium homeostasis, while the uniporter would provide specific calcium transients for metabolic coupling, for example.

The results from a mouse *Micu1* knockout would seem to argue against a uniporter-independent function, as heterozygous *Emre* loss rescued the lethality seen (Liu *et al.*, 2016). It is worth noting that penetrance for this mouse lethal phenotype was not complete, unlike our model, and may suggest compensatory metabolic changes, or the presence of genetic suppressors in the background used, which may also be introduced by the cross to the *Emre* knockout strain. Additionally, *Emre*$^{-/-}$ mice were completely viable, and so double knockout *Micu1*$^{-/-}$ *Emre*$^{-/-}$ should be similarly rescued. However, no viable *Micu1*$^{-/-}$ *Emre*$^{-/-}$ mice were observed.

An anti-apoptotic strategy seems to be ineffective in rescuing *MICU1*^{32}-mediated lethality, which suggests that it is not the key driver of the lethal phenotype. More necrotic, unregulated forms of cell death may explain the lethality, most likely arising from mPTP opening due to $[Ca^{2+}]_m$ overload. This could be addressed by rescuing *MICU1*^{32} with pharmacological or genetic inhibition of the mPTP, but as will be discussed in Section 6.2, this is not without technical challenges. Alternatively, the lethal phase coincides the high energy demand prior to pupariation, and corresponding metabolic re-wiring. As such, the lethality may be more directly due to a failure in energy supply, perhaps through futile mitochondrial calcium cycling. Plans outlined above to probe the underpinnings of the respiratory phenotype established in this work may also provide crucial evidence here.

Given that *MICU1* appears to have multiple functions, it may only be possible to rescue the lethality with multiple simultaneous interventions. This would presumably include the inhibition of mitochondrial calcium uptake through *MCU*[1] or *EMRE*[1]. Failing this, other gene combinations should be considered. Though *Drosophila* are well suited to screening techniques, these nevertheless become prohibitive when combining manipulations through simple combinatorics. Instead, future work will first ascertain what uniporter-independent functions *MICU1* may have, by identifying its protein interactors, to perform a more targeted approach to rescue this knockout. A complete functional picture of MICU1 is essential not only for understanding its context in the mitochondrial calcium uniporter, but also to open new avenues for treating patients suffering from its deficiency.

6. Uniporter manipulation rescues multiple neurodegenerative models

6.1. Background and Aims

One of the unresolved questions in the study of Parkinson's disease concerns the selective vulnerability of dopaminergic neurons, which display many unique adaptions. Their highly arborized processes and exceptional axon length lead to a strong dependence on mitochondrial transport. Additionally, their slow, broad, pace-making action potentials result in large intracellular calcium flux that is opposed by only a low level of buffering (Foehring *et al.*, 2009). Together, these features suggest a possible role for disrupted mitochondrial calcium in the pathogenesis of PD.

Controversy surrounds the exact aetiology of Alzheimer's disease, but genetic evidence confirms a role for the improper processing of the amyloid precursor protein to generate Aβ. Components of the amyloid model have been associated with mitochondrial dysfunction, and specifically altered mitochondrial calcium dynamics leading to overload and cell death (see Section 1.4.2). Thus, the components of the mitochondrial calcium uptake machinery represent a promising candidate for evaluation as a therapeutic target in AD. Links between these two processes may also inform our understanding over the underlying aetiology and risk factors for Alzheimer's, opening new avenues of research.

This chapter aims to evaluate the potential for mitochondrial calcium uniporter modulation to rescue *Drosophila* neurodegenerative models, focusing on *Pink1* and *parkin* models of Parkinson's disease, as well as an amyloid toxicity model of AD. This information will be of strategic use in pursuing the uniporter as a pharmacological target for neurodegeneration and may also provide insight into the pathobiology of these devastating conditions, which would then open new research lines to identify further therapeutic leads.

6.2. Uniporter manipulation is beneficial in *PINK1*/*parkin* disease models

MCU reduction is beneficial for Pink1/parkin locomotion/flight defects

In contrast to mouse models of PD, *Drosophila Pink1* and *parkin* mutants display several overt phenotypes, including a strong locomotor defect, apoptotic muscle degeneration including abnormal mitochondrial morphology, neuron loss, and reduced lifespan (Greene *et al.*, 2003; Park *et al.*, 2006). The muscle tissue underlying the locomotor phenotype is heavily reliant on appropriate calcium signalling. This makes it a useful candidate to test the ability of the MCU^{1} mutant to rescue *Pink1*/*parkin* loss-of-function. After crossing the disease mutations with MCU^{1}, the locomotor ability was assessed (Figure 48). Loss of *MCU*, either hetero- or homozygous, ameliorated $Pink1^{B9}$-associated climbing dysfunction (Figure 48A). The flight ability was also rescued, though to a more modest degree (Figure 48B). I repeated these key results, with a similar outcome (data not shown). For *parkin* mutants, which have a strong motor impairment compared to *Pink1*, the rescue was less comprehensive. Heterozygous MCU^{1} partially rescued the $park^{25}$-associated climbing defect, but no difference was observed with homozygous MCU^{1} (Figure 48C), and vice versa for the flight assay (Figure 48D). Taken together, these results show that reducing *MCU* improves locomotor performance in the context of *Pink1* loss, and partially for the *parkin* model. This foundational result motivated the rest of this section; evaluating the benefit of *MCU* reduction in a range of PD model phenotypes.

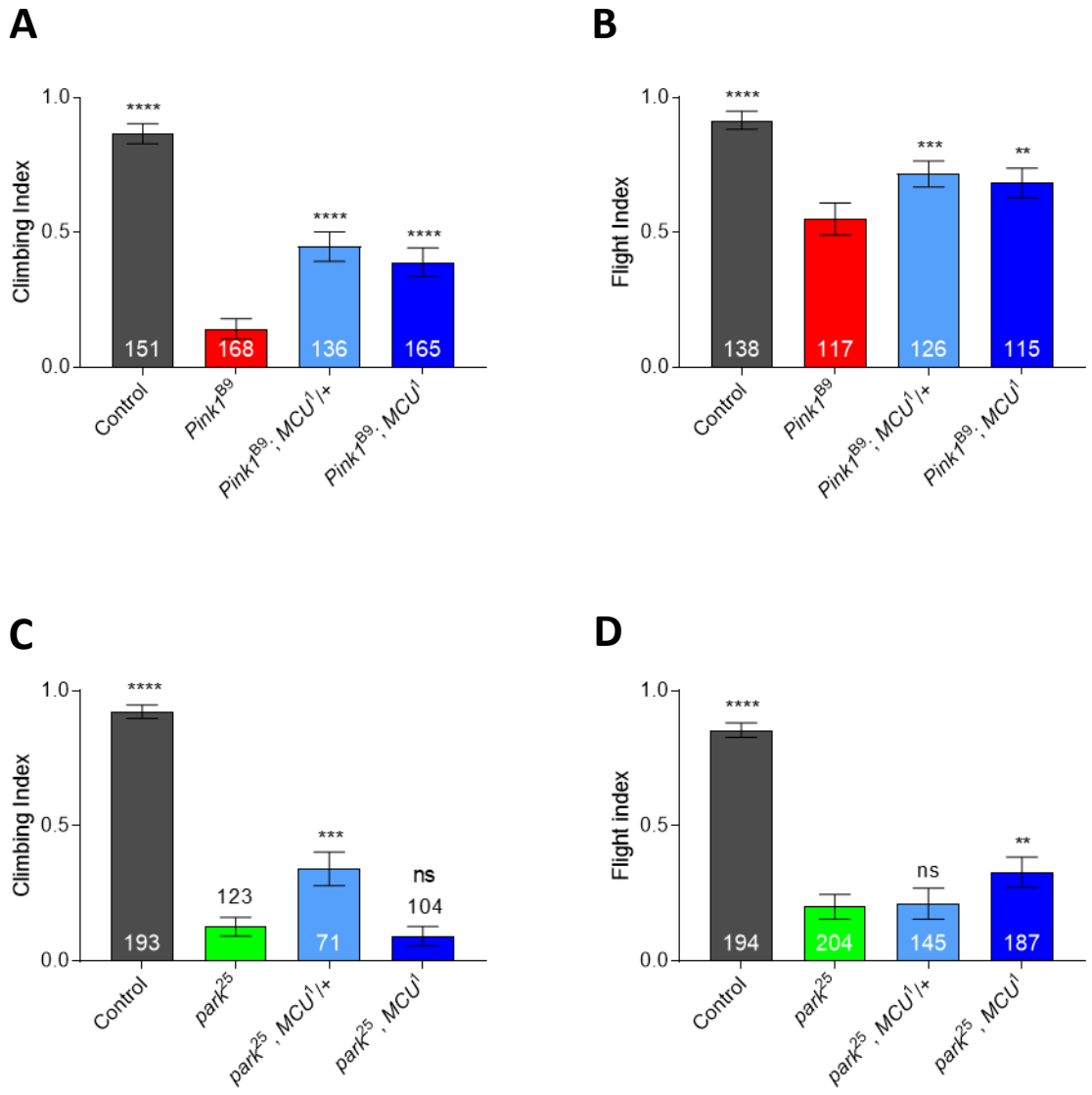

Figure 48. Behavioural performance of PD model flies alone and with *MCU* knockout. **A**: *Pink1*^{B9} and *MCU*^{1} climbing, **B**: flight, **C**: *park*^{25} and *MCU*^{1} climbing, **D**: flight. Error bars = 95% confidence interval. Numbers in/next to bars represent biological n. **p<0.01, ***p<0.001, ****p<0.0001 by Kruskal-Wallis test with Dunn's post-hoc multiple comparison correction. Data for panels A and B generated by R. Tufi.

MCU^{1}/+ ameliorates *Pink1*-, but not parkin-associated muscle mitochondrial disorganisation

The *MCU*^{1} and *Pink1*^{B9} mutants were combined with *da*-Gal4 and UAS-mito.GFP, allowing for visualisation of mitochondrial morphology in various tissues, including the indirect flight muscle. Hemithoraces from young (1-3 days post-eclosion) adults were dissected and mounted as described in Section 2.5. Representative example micrographs are shown in Figure 49A-F. Control thoraces had well organised mitochondria of roughly uniform size and shape, as did both hetero- and homozygous *MCU*^{1}. However, *Pink1*^{B9} flies showed massive accumulation of mito.GFP signal, indicating the presence of swollen/aggregated mitochondria. Additionally, mitochondrial organisation was disrupted, with several gaps present in mitochondrial rows. In most thoraces for the *Pink1*^{B9} *MCU*^{1}/+ rescue condition fewer smaller swellings were present, and mitochondrial organisation was improved. This was not seen in the *Pink1*^{B9} *MCU*^{1} homozygous rescue attempt.

Images were blindly scored as having none, a mild, or severe phenotype (Figure 49G). Unsurprisingly, *Pink1*^{B9} thoraces were easily distinguished from controls – the comparison reaching a robust level of statistical significance. Heterozygous *MCU*^{1} shifted this proportion (p=0.0158). Another attempt with a larger biological n may also improve statistical power to verify this result. Building on the behavioural rescue of *Pink1* by *MCU* reduction, this experiment indicates an interaction at the cellular level, and strengthens the association between the two manipulations beyond indirect behavioural changes compensating for each other.

For *parkin*, stocks were established to combine homozygous *park*^{25} with heterozygous *MCU*^{1} in the presence of da>mito.GFP, and representative images are given in Figure 50A-D. Again, *park*^{25} thoraces displayed mitochondrial disorganisation and swelling, but *MCU*^{1}/+ did not appear to modify this phenotype. Indeed, when classified by blinded observers (Figure 50E), no difference was observed between the *park*^{25} mutants and the rescue condition ($p = 0.6802$ by Fisher's exact test). Due to the distinct lack of rescue by heterozygous *MCU*^{1}, and the homozygous rescue effects previously described being weaker or not present, homozygous rescue of this *park*^{25}-associated muscle disruption was not attempted. The discrepancy of these data compared to *Pink1* suggests a divergence between the two disease models in terms of the significance of altered mitochondrial calcium dynamics to their pathogenesis.

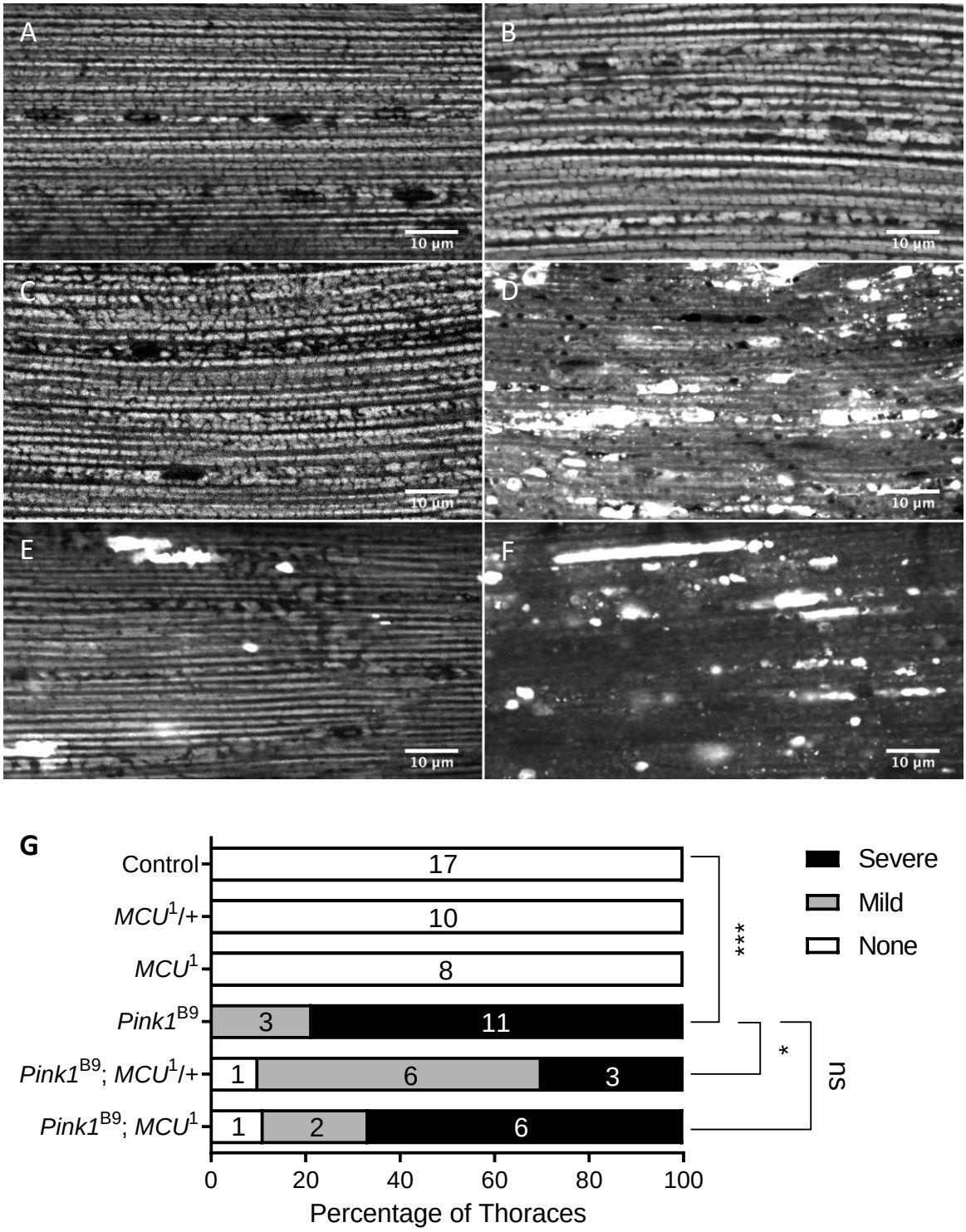

Figure 49. Heterozygous *MCU*[1] rescues *Pink1*[B9]-associated muscle mitochondrial morphology phenotypes. Representative micrographs of *Drosophila* indirect flight muscle (IFM) expressing mitochondrially targeted GFP. **A**: control (da>mito.GFP only). In addition to mito.GFP expression, **B**: *MCU*[1]/+, **C**: *MCU*[1], **D**: *Pink1*[B9], **E**: *Pink1*[B9];*MCU*[1]/+, **F**: *Pink1*[B9];*MCU*[1]. Scale bar:10 µm. **G**: Quantification – images were scored by the disorganisation of mitochondria, and the presence of large signal accumulations. ***p=0.0002 via χ^2 test after multiple comparison correction via the two-stage linear step-up procedure of Benjamini, Krieger and Yekutieli, with Q set to 5%(Benjamini, Krieger and Yekutieli, 2006). * p=0.0158 after correction. ns: p = 0.0673 after correction. Numbers in bars represent biological n for each group.

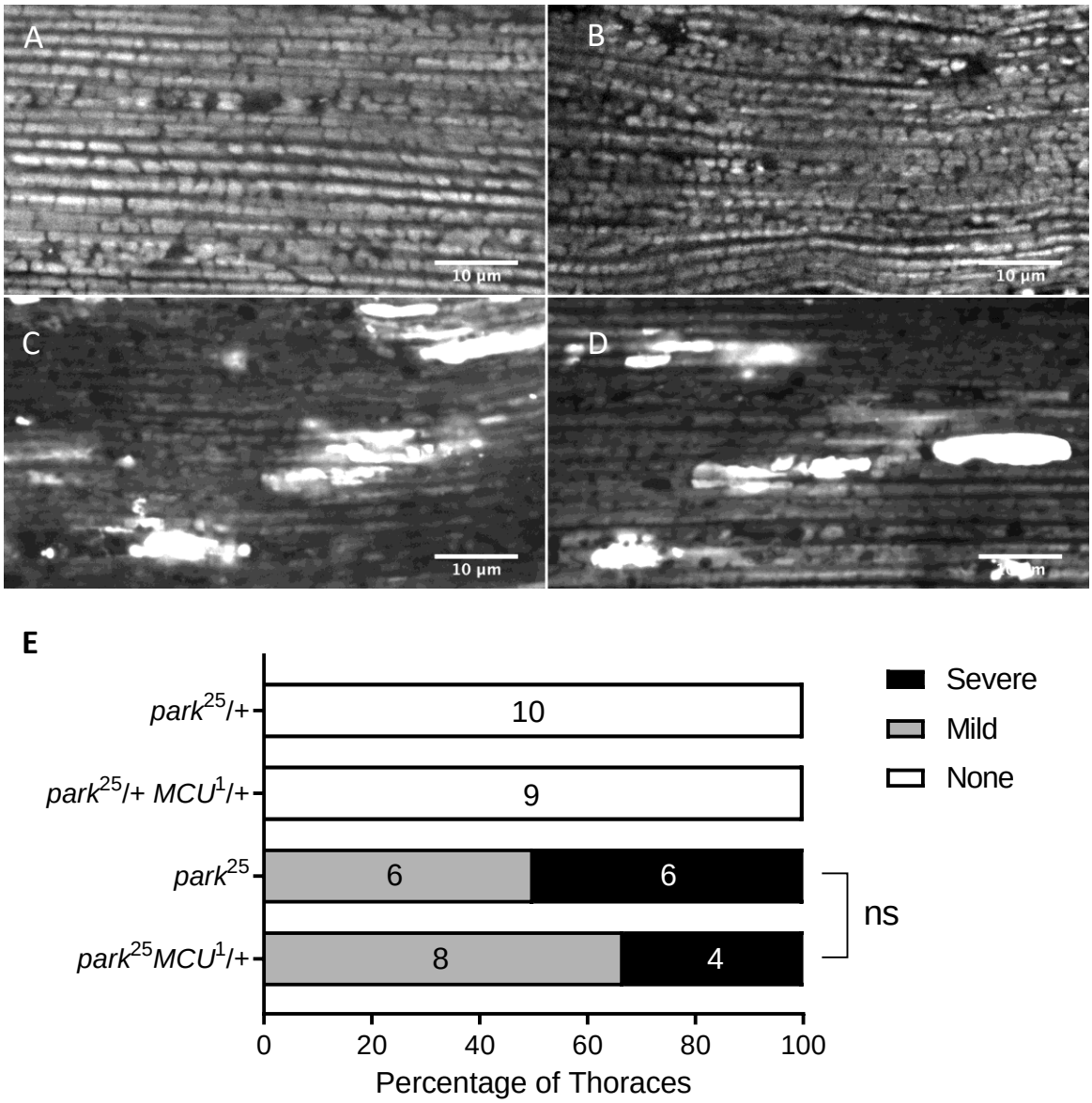

Figure 50. Heterozygous *MCU*[1] does not rescue *park*[25]-associated muscle mitochondrial morphology phenotypes. Representative micrographs of *Drosophila* indirect flight muscle (IFM) expressing mitochondrially targeted GFP. In addition to da>mito.GFP expression, **A**: *park*[25]/+ **B**: *park*[25]/+ *MCU*[1]/+, **C**: *park*[25], **D**: *park*[25] *MCU*[1]/+. Scale bar:10 µm. E: Quantification – images were scored by the disorganisation of mitochondria, and the presence of large signal accumulations. ns: p = 0.6802 by Fisher's exact test. Numbers in bars represent biological n for each group.

MCU[1] rescues *Pink1*-associated lifespan reduction, but not for *parkin*

The short lifespan of *Drosophila* relative to mammalian model organisms makes them well suited to studies of longevity. Also, *Pink1* and *parkin* fly knockouts display reduced lifespan without the need for additional stressors, in contrast to mouse models. Having established that manipulation of mitochondrial calcium uptake could rescue organismal dysfunction in these disease models, we sought to evaluate whether these effects were also borne out in the downstream lethality. First, R. Tufi observed the lifespan of *Pink1*[B9] males alone or in combination with hetero- or homozygous *MCU*[1] (Figure 51A). *Pink1* knockouts lived significantly shorter than *w*[1118] controls (median survival 52 vs 62 days, 16% reduction). Heterozygous *MCU* loss completely rescued this phenotype (median survival 63 days), while homozygous *MCU*[1] showed a statistically significant partial rescue (median survival 57 days). I then extended this observation to the *parkin* context (Figure 51B). Female flies display markedly more variance in lifespan due to mating status than males (Service, 1989). Therefore, males are typically used for this assay. This precluded the use of *Pink1*[B9] heterozygotes, as the gene is found on the X chromosome, but heterozygous *park*[25] (chromosome III) were able to be used as controls. Homozygous *park*[25] showed a much more severe lifespan reduction than *Pink1*[B9] (11-day median survival vs control 71 days, 85% reduction). Here, both heterozygous (12.5-day median survival) and homozygous (19-day median survival) *MCU*[1] did not significantly rescue the phenotype. The discrepancy between *Pink1* and *parkin* in this assay mirrors the results from mitochondrial morphology. Additionally, *parkin*-associated locomotor deficits were rescued to a lesser degree than *Pink1*-associated. Together, these data suggest *MCU* reduction exerts its effect through one of the mechanistic differences between *Pink1* and *parkin* knockouts. The rest of this section accordingly focuses on the interaction between *MCU* and *Pink1*.

A

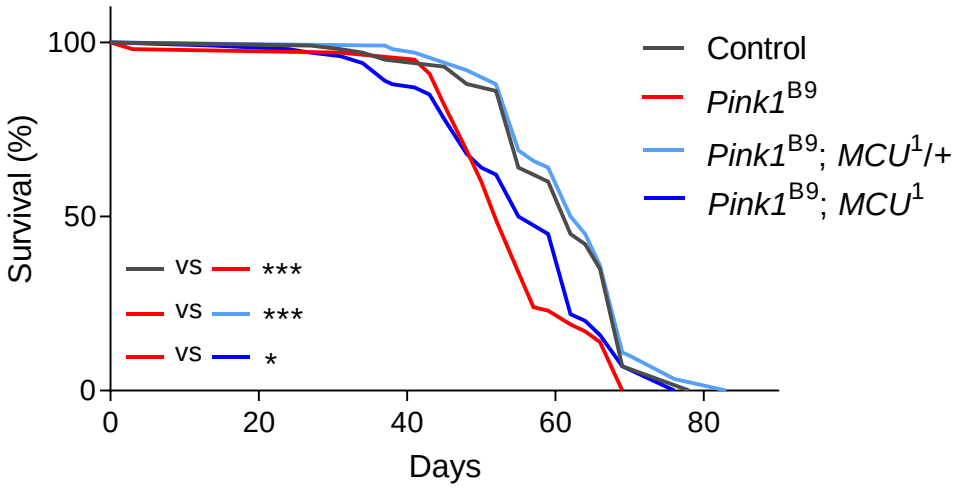

B

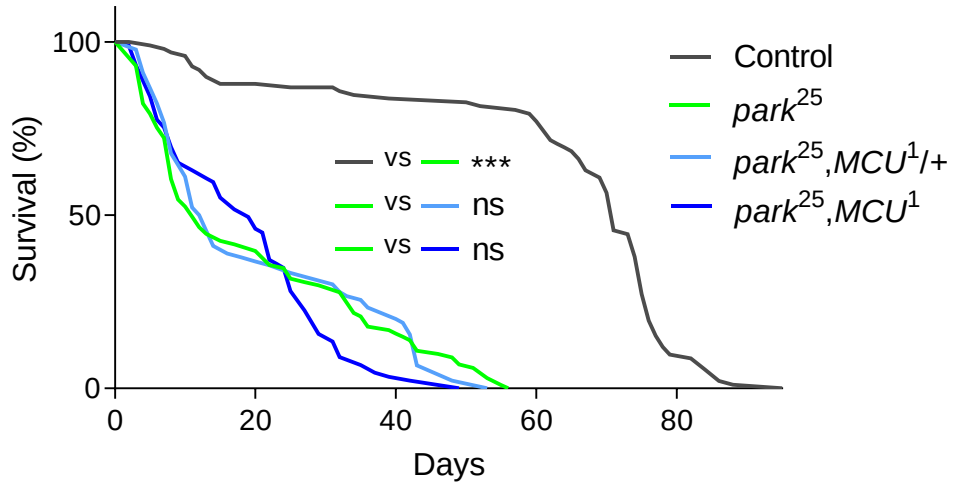

Figure 51. Survival curves of *MCU*[1] interacting with **A**: *Pink1*[B9] (control = w[1118]) or **B**: *park*[25] (control = *park*[25]/+). n≥89 for all genotypes. ***p<0.001, *p<0.05 for both Mantel-Cox test after multiple comparison correction via the Two-stage linear step-up procedure of Benjamini, Krieger and Yekutieli, with Q set to 5%(Benjamini, Krieger and Yekutieli, 2006). Data for panel **A** generated by R. Tufi.

MCU^{1}/+ rescues *Pink1*-induced dopaminergic mitochondrial swelling

To measure the extent of *Pink1*^{B9}-induced DA neuron loss, R. Tufi employed an anti-TH immunofluorescence paradigm in whole adult *Drosophila* brains. One such TH-positive DA neuron cluster is PPL1, which among other functions integrates circadian information and coordinates corresponding changes in locomotor activity (Liu *et al.*, 2012). Therefore, dysfunction in this cluster may be a neural correlate for the reduced locomotor performance seen at an early age in the *Pink1*^{B9} model. Counting the number of TH-positive PPL1 neurons at 40 d.p.e., significantly fewer were seen in the *Pink1* mutants (Figure 52), with the addition of heterozygous *MCU*^{1} completely rescuing the phenotype.

Pink1 loss has also previously been shown to cause mitochondrial swelling in dopaminergic neurons (Yang *et al.*, 2008), before the onset of widespread neuron loss. I combined the highly specific TH-Gal4 driver with UAS-mito.GFP to drive expression in a subset of PPL1 neurons. This was also done in the presence of the *Pink1*^{B9} disease model, or *Pink1*^{B9} with heterozygous *MCU*^{1}. Representative micrographs of these soma are shown in Figure 53A-C. Enlarged mitochondria were observed in all three genotypes, though they were more frequent and larger in the *Pink1*^{B9} disease model.

To quantify mitochondrial size, images were analysed with Fiji (Schindelin *et al.*, 2012; Rueden *et al.*, 2017) by thresholding and measuring mitochondria via the 'Analyze Particles' function, with a minimum size of 0.1 μm^2 to exclude single pixel signal speckles. The distribution of mitochondrial size unsurprisingly displayed a positive skew (Figure 53D), though this was less in the case of *Pink1*^{B9}, indicating a shift to larger mitochondria. Despite this overall shift in skew, *Pink1*^{B9} mitochondrial size had a much longer 'tail' to the distribution, to the point where it could not be clearly shown in a histogram. Instead, individual mitochondrial size is given on a $\log_{10}$ scale in Figure 53E. In general, *Pink1*^{B9} mitochondria were larger than controls ($q<0.0001$), and heterozygous *MCU*^{1} showed significant rescue ($q=0.0454$). However, this analysis is limited by the distributional asymmetry; what is biologically important is likely to be the presence of extra-large, aberrant mitochondria.

I established a threshold of 1 µm^2 as a cut-off for pathological swelling (Yang *et al.*, 2008), and filtered the data accordingly (Figure 53F). Significantly more swollen mitochondria were observed in the *Pink1* mutants (a 1.9-fold increase, q=0.0147). Heterozygous *MCU*^{1} completely rescued this phenotype, bringing the mean number of swellings slightly below controls (q=0.0147). This demonstrates that *MCU* reduction can ameliorate the dopaminergic mitochondrial disorganisation associated with *Pink1* loss-of-function which may underlie the behavioural rescue of locomotor deficits.

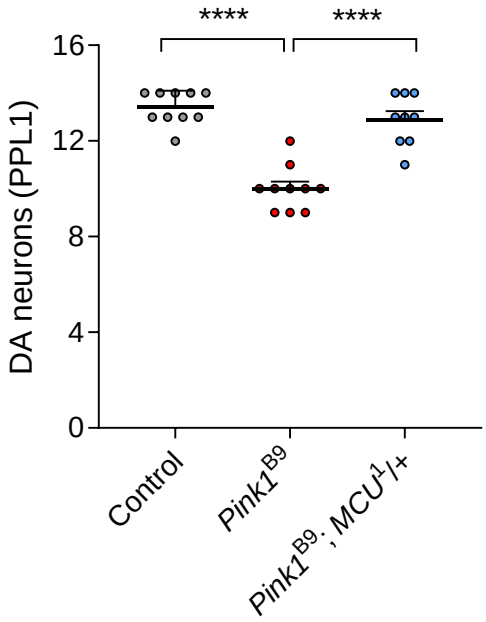

Figure 52. Dopaminergic neurons present in the PPL1 cluster of 40 d.p.e. *Drosophila* brain. ****p<0.0001 by one-way ANOVA with Dunnett's multiple comparison correction. Error bars represent SEM. Data generated by R. Tufi.

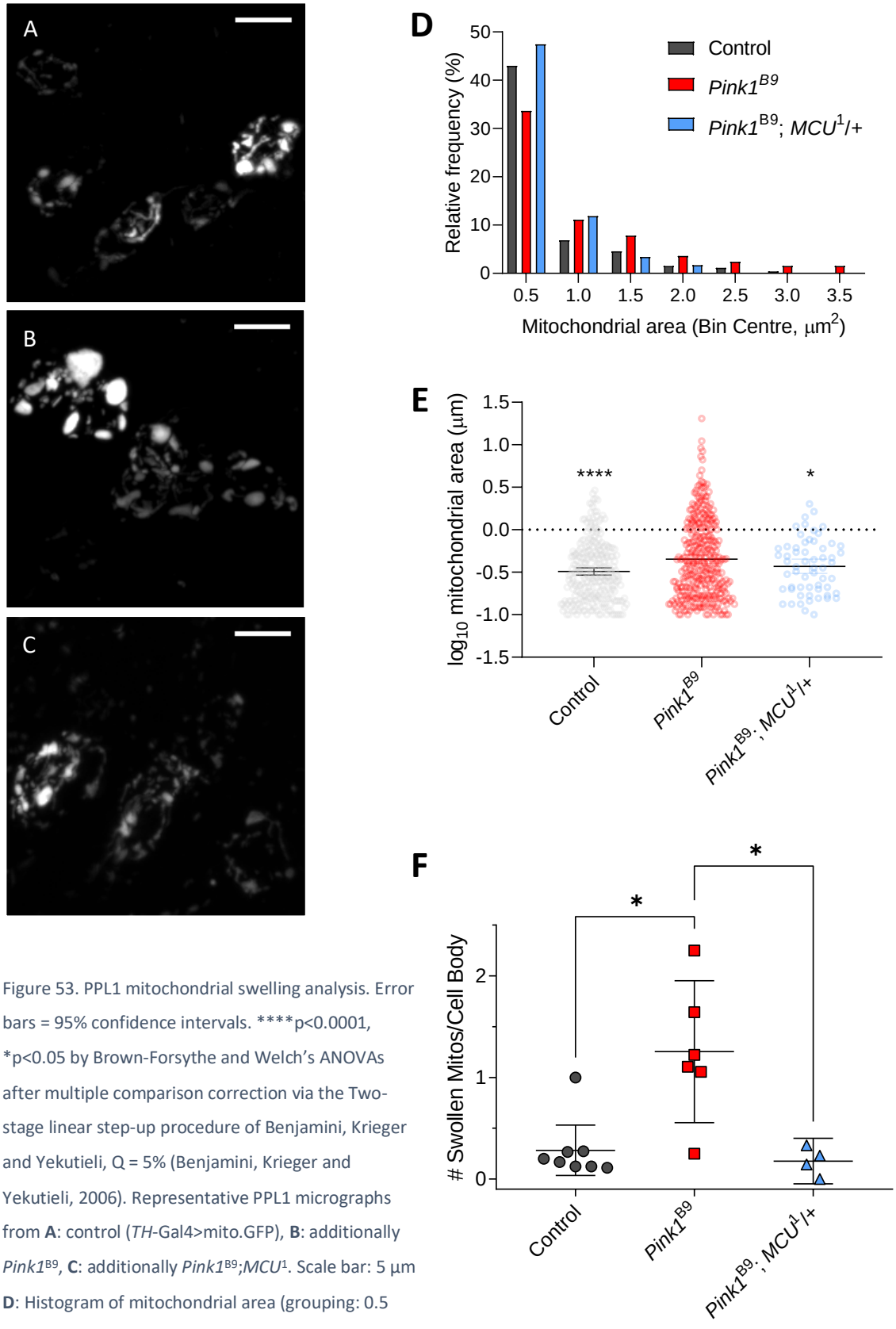

Figure 53. PPL1 mitochondrial swelling analysis. Error bars = 95% confidence intervals. ****p<0.0001, *p<0.05 by Brown-Forsythe and Welch's ANOVAs after multiple comparison correction via the Two-stage linear step-up procedure of Benjamini, Krieger and Yekutieli, Q = 5% (Benjamini, Krieger and Yekutieli, 2006). Representative PPL1 micrographs from **A**: control (*TH*-Gal4>mito.GFP), **B**: additionally *Pink1*^{B9}, **C**: additionally *Pink1*^{B9};*MCU*^{1}. Scale bar: 5 µm **D**: Histogram of mitochondrial area (grouping: 0.5 µm^2, values > 3.5 µm^2 omitted). **E**: $\log_{10}$ mitochondrial area. Data points = individual mitochondria. Dashed line = 1 µm^2 cut-off for swelling **F**: Mitochondrial swellings >1 µm^2/cell body. Data points = hemibrains.

MCU^{1}/+ partially rescues *Pink1*-associated male sterility

The *Pink1*^{B9} *Drosophila* model features a high penetrance male sterility phenotype, related to defects in spermatid individualisation, where interconnected spermatids formed by incomplete cytokinesis are separated so that each is enclosed in its own plasma membrane (Clark *et al.*, 2006; Steinhauer, 2015). To determine if attenuated mitochondrial calcium uptake can rescue *Pink1*^{B9}-induced sterility, single adult males of the appropriate genotypes were separately crossed to virgin females, and the presence of larvae was scored (Figure 54). Though controls were almost entirely fertile, *Pink1* males were completely sterile ($p < 0.0001$). Heterozygous *MCU* loss partially rescued this to 12% fertility ($p = 0.028$ after multiple comparison correction). Though of modest effect size, there is an additional qualitive distinction between some and no fertility that suggests biological significance. Therefore, these data show that reduction of *MCU* is beneficial for male fertility in the *Pink1* loss-of-function model.

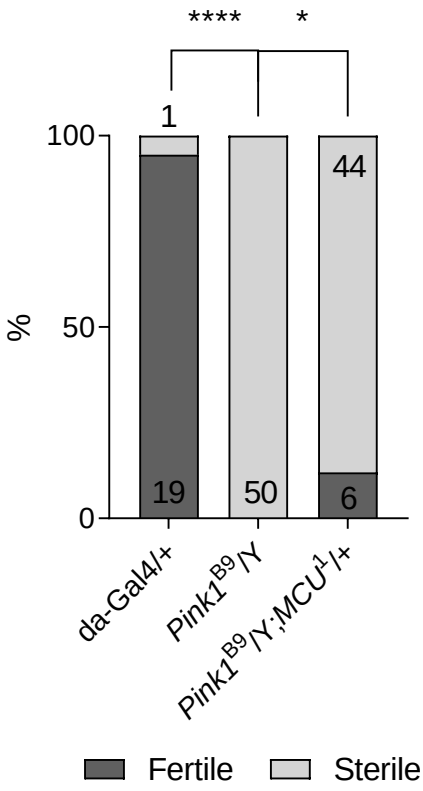

Figure 54. Percentage fertile/sterile crosses arising from males of each genotype. Numbers in/next to bars represent n for each group. Pairwise Fisher exact test ****p<0.0001, *p<0.05 after multiple comparison correction via the Two-stage linear step-up procedure of Benjamini, Krieger and Yekutieli, with Q set to 5%(Benjamini, Krieger and Yekutieli, 2006).

Cyclosporin A does not improve the *Pink1*-associated climbing phenotype

The underlying mechanistic hypothesis for the rescue of *Pink1* by *MCU* is that the loss of *Pink1* causes mitochondrial calcium overload which sensitises cells to the mitochondrial permeability transition, upon which they become permeable to species < 1.5 kDa, leading to mitochondrial swelling and cell death (Gandhi *et al.*, 2009). Though the molecular nature of the mPTP is currently under fierce debate, it is well established to be inhibited by cyclosporin A (CsA), which I hypothesised would have similar beneficial effects as *MCU* reduction. First, I tested a range of concentrations in a pilot study, adding it to the food so that flies were dosed from the larval stage, to determine drug tolerance in terms of viability. Developmental lethality was observed at higher (50 and 100 µM) doses but was well tolerated at 10 µM CsA (summarised in Table 13). This dose was selected to evaluate the rescue of *Pink1* loss. Pan-neuronal knockdown (via *nSyb*-Gal4) of *Pink1* was employed to give a hypomorphic context rather than overt knockout. This resulted in a mild climbing phenotype, with a much stronger deficit in the $Pink1^{B9}$ mutant, but neither of these were improved by the addition of 10 µM CsA (Figure 55A). Similarly, reduced flight ability in either the *Pink1* mutant or pan-neuronal knockdown was not rescued by 10 µM CsA (Figure 55B). These data do not support the involvement of the mPTP in *Pink1*-associated locomotor impairment, though these data are limited, and some groups have suggested that the *Drosophila* permeability transition pore is insensitive to CsA (von Stockum *et al.*, 2011, 2015).

Table 13.Viability to eclosion for 0-100 µM cyclosporin A (CsA). Drug administered in standard fly food from embryonic stage.

Cyclosporin A dose (µM)	Lethality
0	-
10	-
50	+
100	+++

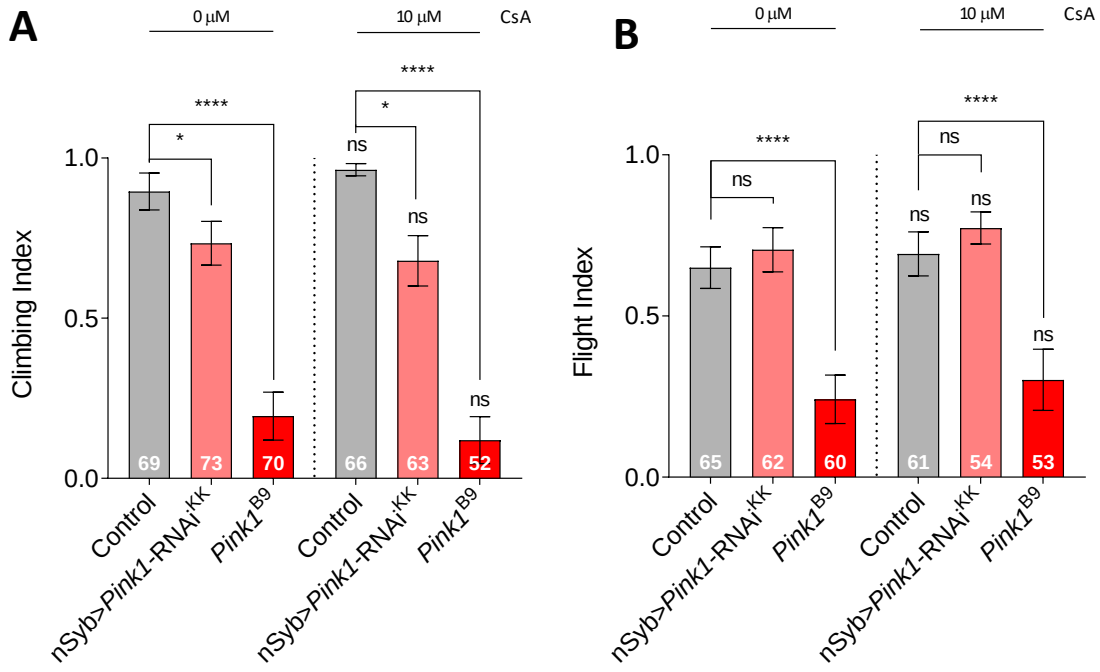

Figure 55. Evaluation of **A**: climbing performance or **B**: flight, for *Pink1* knockdown/knockout with cyclosporin A treatment. All error bars represent 95% confidence intervals. ****p<0.0001, *p<0.05 for Kruskal-Wallis test with Dunn's post-hoc correction for multiple comparisons. Numbers in bars represent biological n for each group.

Pink1 interaction with other uniporter components

The data outlined above show that *MCU* reduction has a strong interaction with *Pink1* loss-of-function, rescuing several phenotypes. Having created knockouts for other uniporter components, combining them with *Pink1* could provide additional insight into the interaction point of the uniporter in the pathogenic mechanism. First, I crossed the *EMRE*^{1} knockout to *Pink1*^{B9}. As this mutant results in the same functional outcome in terms of mitochondrial calcium uptake as *MCU*^{1}, it would be predicted to rescue similarly. Surprisingly, heterozygous *EMRE*^{1} did not improve *Pink1*-associated climbing impairment (Figure 56A). This difference between *MCU* and *EMRE* may reflect uniporter-independent actions on *Pink1* pathobiology.

Based on the mitochondrial calcium overload hypothesis, *MICU1* reduction would be predicted to exacerbate *Pink1* phenotypes. However, when R. Tufi evaluated both climbing (Figure 56B) or longevity (Figure 56C), a strong rescue was instead observed. *MICU1*^{32}/+ alone displayed a long lifespan (Figure 56C), though the control was unusually short-lived in this case, and displayed climbing ability as wild-type (data not shown). This intriguing result points towards the uniporter-independent role of *MICU1* that was proposed in Section 5.5, perhaps relating to the recently proposed role in stabilising cristae junctions to prevent cytochrome *c* release (Gottschalk *et al.*, 2019). Instead, this result may be due to a paradoxical inhibition of mitochondrial calcium uptake due to *MICU1* reduction, arising from changes in mitochondrial organisation, for example. Indeed, *MICU1* loss has been demonstrated to result in altered mitochondrial dynamics (Section 5.3), though this was in the case of homozygous larvae, and heterozygous adult tissue would also need to be evaluated.

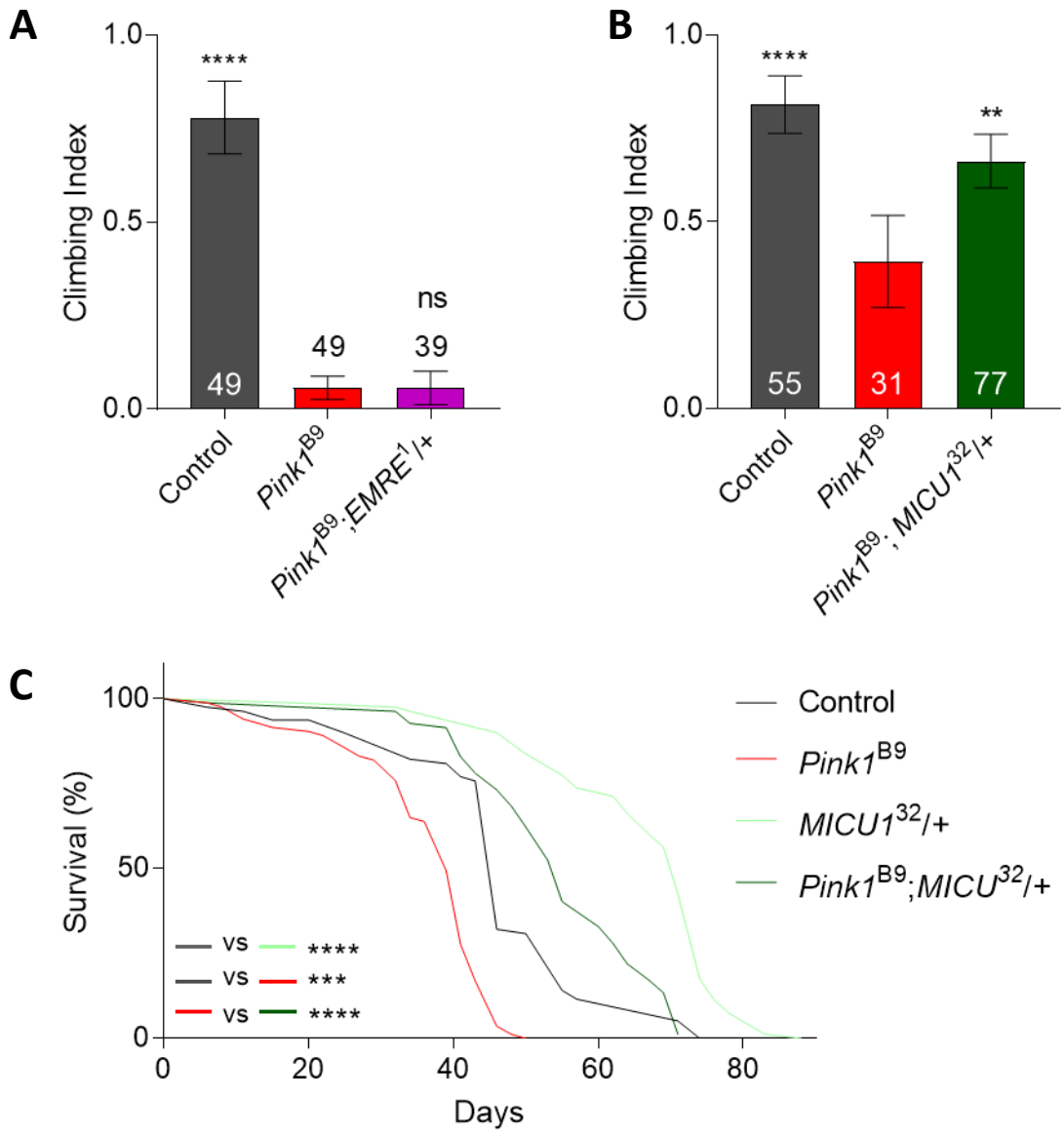

Figure 56. *Pink1* interaction with non-*MCU* uniporter components. All error bars represent 95% confidence intervals. Numbers in/next to bars represent biological n. ****p<0.0001, **p<0.01, ns = p>0.05 **A**: locomotor performance of *Pink1*^{B9} flies and interaction with heterozygous *EMRE*^{1} B: locomotor phenotype (control = da/+) and **C**: lifespan phenotype (control = *w*^{1118}) of *Pink1*^{B9} and interaction with heterozygous *MICU1*^{32}. Climbing statistics by Kruskal-Wallis test after Dunn's correction for multiple comparisons, lifespan statistics by Mantel-Cox model. Data for panels **B** and **C** generated by R. Tufi.

6.3. *MCU*^{1} rescues Alzheimer's disease phenotypes

MCU^{1} rescues Aβ-associated locomotor deficits

The role of calcium dysregulation in the pathogenesis of Alzheimer's disease is being increasingly recognised. For example, oligomeric amyloid beta (Aβ) altered intracellular calcium signalling in a hippocampal cell culture model, and notably, increased the expression of MCU (Calvo-Rodriguez *et al.*, 2019). This disease model is therefore a strong candidate for rescue through uniporter targeting. *Drosophila* with transgenic pan-neuronal expression of $A\beta_{42}$ do not display a marked climbing deficit, but those expressing the mutant $A\beta_{42}^{arc}$ polypeptide, which is more prone to protofibril formation (Nilsberth *et al.*, 2001), have strong locomotor impairment that quickly worsens with age (Long *et al.*, 2014). Expressing $A\beta_{42}^{arc}$ via the *elav*-Gal4 driver, I replicated this phenotype. At two days post-eclosion, $A\beta_{42}^{arc}$ flies displayed a moderate climbing defect (Figure 57A), and by ten days post-eclosion, this had exacerbated almost to the point of total immobility (Figure 57B). Rescue of this phenotype was achieved at both timepoints with heterozygous *MCU*^{1}, and with homozygous mutants at the ten-day timepoint. These results indicate that reducing *MCU* ameliorates organismal dysfunction arising from toxic amyloid species. I further challenged the rescue by bringing the expression of $A\beta_{42}^{arc}$ under the stronger *nSyb*-Gal4 driver. Surprisingly, this did not result in a climbing phenotype at early age (Figure 57C). Though both typically reported as pan-neuronal drivers, granular differences in spatiotemporal expression between *elav* and *nSyb* can lead to altered expression profiles in specific neuron classes, and this may underlie the difference seen. Nevertheless, by ten days post-eclosion a robust climbing defect was observed with *nSyb*>$A\beta_{42}^{arc}$, which was well rescued by heterozygous *MCU* loss (Figure 57D). This provides further evidence for a beneficial effect of reduced mitochondrial calcium uptake in this amyloid aggregation model, motivating additional investigation.

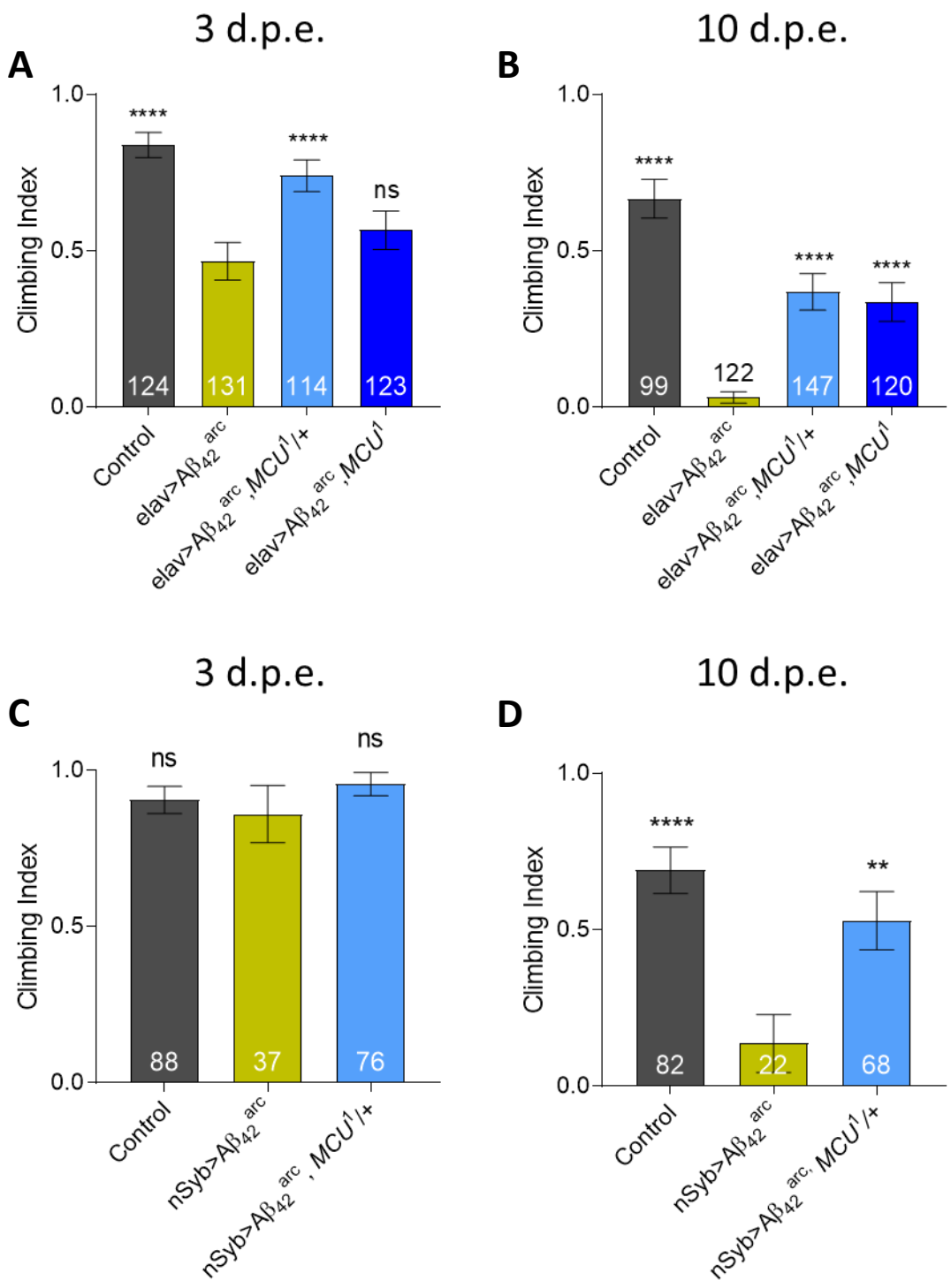

Figure 57. Behavioural performance of $A\beta_{42}^{arc}$ model flies alone and with *MCU* knockout. **A**: Climbing at three days post-eclosion with *elav*-Gal4 driver, **B**: 10 days. **C** and **D** as above, with *nSyb*-Gal4 driver. Error bars = 95% confidence interval. Numbers in/next to bars represent biological n. ****p<0.0001, **p<0.01 by Kruskal-Wallis test with Dunn's post-hoc multiple comparison correction. Comparisons made against nSyb>$A\beta_{42}^{arc}$.

MCU^{1} rescues Aβ-associated shortened lifespan

In addition to locomotor impairment, neuronal amyloid beta expression is associated with a drastic reduction in lifespan (Long *et al.*, 2014; Jonson *et al.*, 2015). To replicate this, I expressed of mutant $A\beta_{42}^{arc}$ with the pan-neuronal *nSyb*-Gal4 driver (Figure 58), resulting in an extremely strong lifespan reduction (median survival 18 days). This was significantly rescued through heterozygous *MCU*^{1} (median survival 28 days, 55% increase). These data, in combination with the climbing results, show that uniporter manipulation can be beneficial in the context of a severe Alzheimer's disease model. The degree of rescue makes this a promising target for further evaluation of therapeutic potential.

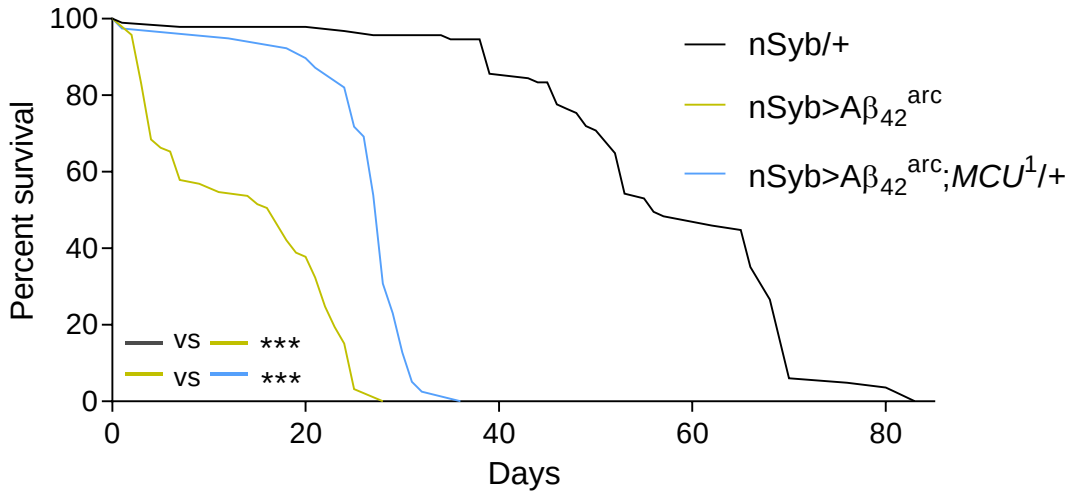

Figure 58. Survival curves of *MCU*^{1} interacting with $A\beta_{42}^{arc}$ (control = w^{1118}). n≥39 for all genotypes. ***p<0.001 for Mantel-Cox test after multiple comparison correction via the Two-stage linear step-up procedure of Benjamini, Krieger and Yekutieli, with Q set to 5% (Benjamini, Krieger and Yekutieli, 2006).

6.4. Discussion

In this chapter, I demonstrate the therapeutic potential of the mitochondrial calcium uniporter in neurodegenerative disease. The most well characterised interaction so far is rescue of *Pink1* knockout models by heterozygous *MCU* knockout. This extended to climbing, flight, sterility, and lifespan. Homozygous MCU^{1} was more variable, improving locomotor performance but only yielding a slight improvement in lifespan, and no discernible effect on muscle mitochondria. Homozygous MCU^{1} is not without its own phenotypes, but MCU^{1} alone show wild-type muscle mitochondrial organisation, suggesting that a lack of rescue of the *Pink1* phenotype in this case was insufficient modification of the pathological process, rather than some unintentional consequence of manipulating *MCU*. Additionally, $Pink1^{B9}$; MCU^{1} were longer lived than MCU^{1} alone (compare with Section 4.3), though these data are from different experiments and would benefit from a side-by-side test, given the sensitivity of lifespan to environmental factors. Nevertheless, the partial inhibition seen in heterozygous MCU^{1} suggests a therapeutic window that may provide benefit in a neurodegenerative context without longevity phenotypes, reinforcing it as a promising target for further evaluation.

In contrast to *Pink1*, the *parkin* knockout model did not benefit to the same extent from *MCU* reduction. Although locomotor performance was improved to some extent, no benefit was observed in muscle mitochondrial morphology, or in longevity. A possible explanation here is that *parkin*-associated phenotypes are often stronger than for *Pink1* and may simply be too severe to be improved in this fashion. However, other genetic interactors of *parkin*, such as *Fbxo7*, can rescue $park^{25}$-associated locomotor deficits and muscle degeneration (Burchell *et al.*, 2013). Instead, the variance between *MCU* and *Pink1*/*parkin* may simply reflect their divergent molecular pathways. Indeed, in addition to its canonical role as the activator kinase of *parkin*, *Pink1* has also been shown to affect Complex 1 activity through NdufA10 (Morais *et al.*, 2009, 2014). Further work confirming the association between the uniporter and mitophagy-independent *Pink1* functions would help discern their contribution to familial PD.

In both brain and muscle tissues, I have demonstrated that heterozygous *MCU*^{1} strongly ameliorates *Pink1*^{B9}-induced alterations to mitochondrial morphology. Tissue degeneration is often preceded by a period of dysfunction. In addition to this rescue in mitochondrial morphology, we have confirmed that the following neuron loss is also prevented by *MCU*^{1}/+. It would be interesting to see if the improvement in muscle mitochondrial morphology similarly extends to a protection from later gross muscle degeneration, which could be evaluated by toluidine blue staining or TEM. It is worth noting heterozygous or indeed homozygous *MCU*^{1} alone showed no alterations in muscle mitochondrial morphology. This implies that the effect of *MCU* reduction on mitochondrial morphology occurs specifically in the context of *Pink1* knockout, acting upstream in the pathological pathway. *Pink1* genetically interacts with fission/fusion factors (Deng *et al.*, 2008), mitochondrial shape influences mitochondrial calcium uptake (Favaro *et al.*, 2019), and alterations in calcium dynamics affect the activity of Drp1, for example (Cribbs and Strack, 2007). This association raises the prospect that *MCU* reduction may exert beneficial effects due to changes in the fission/fusion balance, perhaps compensating for a reduction in mitophagy.

It was surprising not to observe a rescue of *Pink1* mutants by administration of cyclosporin A, though there are myriad complexities with pharmacological treatments, such as dosage timing and route of administration, which could be further explored to provide a more definite negative evidence. Additionally, genetic ablation of cyclophilin D could be an orthogonal approach, though the true homologue would need to be discerned from two candidates (Figure 59). If these experiments fail to show rescue, it would imply that *Pink1*-associated mitochondrial calcium overload is detrimental via another mechanism than mPTP-induced apoptosis.

Search Term	Human GeneID	HGNCID	Human Symbol	Species 2	Fly GeneID	Fly Species Gene ID	Fly Symbol	DIOPT Score	Weighted Score	Rank	Best Score	Best Score Reverse
PPIF	10105	9259	PPIF	Fly	39573	FBgn0036415	CG7768	11	10.96	high	Yes	Yes
PPIF	10105	9259	PPIF	Fly	32595	FBgn0004432	Cyp1	11	10.96	high	Yes	Yes

Figure 59. DIOPT (DRSC Integrative Ortholog Prediction Tool) output searching for fly homologues of human cyclophilin D (PPIF). https://www.flyrnai.org/cgi-bin/DRSC_orthologs.pl (date accessed: 2019/7/26).

More surprisingly, heterozygous *EMRE*^{1}, which would be predicted to have similar effects to heterozygous *MCU*^{1}, failed to show any rescue of *Pink1*^{B9}-induced motor impairment. The different uniporter components are presumably expressed at different initial levels, and EMRE protein is tightly controlled through degradation to limit the prozone effect (Tsai *et al.*, 2017). Therefore, simple heterozygous knockout may result in different effects on uniporter function, with *EMRE* being insufficient, though the literature on EMRE turnover, albeit from non-*Drosophila* models, would suggest the opposite pattern. Additionally, heterozygous *MICU1* knockout, where any reduction of the protein could be predicted to *increase* mitochondrial calcium uptake, rescued both locomotor and lifespan phenotypes. These data suggest the interaction of the uniporter with *Pink1* being simply due to calcium uptake is an insufficient explanation. Alternative uniporter functions are yet to be reported, as it has been relatively recently molecularly identified, though work outlined in Section 5.5 is likely to make the characterisation of such roles a priority.

As well as PD models, I have begun to show a strong protective effect of *MCU* reduction in the context of oligomeric amyloid beta production. The association between Aβ and mitochondria, and more specifically mitochondrial calcium, has been increasingly investigated in recent years (see Section 1.4.2). Specifically, cell models have shown oligomeric Aβ increases ER-mitochondrial calcium flux (Calvo-Rodriguez *et al.*, 2019), and pharmacological inhibition of the uniporter reduces Aβ-associated apoptosis (Xie *et al.*, 2017). Now, this work demonstrates *in vivo* genetic rescue, positioning mitochondrial calcium dynamics as a common process in neurodegeneration. Further work will examine additional Aβ-associated phenotypes to strengthen this hypothesis and probe the role of the uniporter in other neurodegenerative diseases. Comparing pathogenic environments where uniporter targeting is effective versus not can be expected to highlight common pathways between these diseases, which can then be explored for additional therapeutic intervention strategies.

7. Discussion

7.1. Summary of Findings

The initial aim of this thesis, to generate a suite of genetic tools for manipulating the mitochondrial calcium uniporter in *Drosophila*, has been successful. Combining my work with the efforts of R. Tufi in targeting *MCU*, we report knockdown, transgenic expression, and knockout lines for every reported uniporter component conserved in *D. melanogaster*. As well as providing the basis for the rest of this work, the generated lines will provide a useful toolkit for researchers wishing to study the function of this protein complex in a powerful invertebrate model. Additional practical insight in the use of gene editing to construct knockout models will assist further endeavours.

Genetic mouse models of the uniporter have emerged in recent years (Pan *et al.*, 2013; Luongo *et al.*, 2015; Liu *et al.*, 2016), but controversy has emerged regarding the viability of *Mcu* knockouts. Using an orthogonal approach, we report that *Drosophila* lacking *MCU* are completely viable, with no discernible motor impairments. Using the new *EMRE* knockout, I here extend the same observations to this mutant. Both have been confirmed to lack classical fast mitochondrial calcium uptake, so our results provide evidence that uniporter-mediated calcium uptake is dispensable for life. This is in line with evidence from yeast mitochondria, which do not uptake calcium (Carafoli and Lehninger, 1971), and our results extend this to a multicellular *in vivo* system.

Despite the *MCU* knockout being well tolerated at an organismal level in basal conditions, longevity was compromised in the homozygous mutant, indicating a susceptibility to age-related stressors. This phenotype was markedly less severe in the *EMRE* knockout, and so differences between the consequences of these two mutants may provide an explanation for the *MCU* lifespan deficit. Different metabolic adaptations to what could be considered a dramatic alteration in organellar signalling may occur in these knockouts, and this is borne out in the maximal respiratory capacity, where *EMRE* knockouts showed much less reduction than for *MCU*.

The mouse knockout for *Micu1* has been shown to display developmental lethality (Liu *et al.*, 2016), which is recapitulated in the *MICU1*^{32} knockout fly described here. Similarly, both models display gross motor impairment, though a distinction should be drawn between the study of adult escaper animals in the case of the mouse, and a juvenile larval stage in the fly, where the lethal phenotype is fully penetrant. The difference in lethal penetrance could simply be explained by altered susceptibility to mitochondrial calcium overload between organisms. However, genetic ablation of mitochondrial calcium uptake through *MCU* or *EMRE* loss failed to rescue *MICU1*^{32}-mediated lethality, indicating this phenotype is due at least in part to some secondary function.

Calcium uptake experiments have supported our *Drosophila MCU* and *EMRE* knockouts as being true functional nulls, in extramitochondrial conditions where canonical fast calcium uptake would be expected. However, several mitochondrial calcium currents have been proposed, based on electrophysiological recordings (Sparagna *et al.*, 1995; Michels *et al.*, 2009; Bondarenko *et al.*, 2013). The presence of additional modes of mitochondrial calcium uptake cannot be excluded in our mutants, which may explain their vitality. If these were to be regulated by an alternative function of *MICU1*, the inability for uniporter inhibition to rescue *MICU1*-mediated lethality would also be explained. However, no alternative uptake role can be directly ascribed to *MICU1* at this stage, and the molecular identity of any alternative mitochondrial calcium uptake pathways is highly controversial.

This work presents the first *in vivo* model of *MICU3* loss, finding its absence to be broadly compatible with life. However, knockout flies display impairments that can be linked to tissues where MICU3 is highly expressed. One could predict *MICU3* is an essential gene for these tissues, with its absence leading to tissue-restricted phenotypes resembling *MICU1* knockout, but current uniporter models place MICU3 as a modulator of MICU1 rather than a gatekeeper itself (Patron *et al.*, 2018), and we have supported this view by demonstrating the inability of MICU3 to complement for MICU1 (Tufi *et al.*, 2019).

Disrupted calcium dynamics are a common molecular feature of neurodegenerative disorders (Section 1.4), implicating the transport machinery of this key ion as potential targets for therapeutic intervention. To this end, I demonstrate the ability of *MCU* reduction to ameliorate a suite of phenotypes associated with *Pink1* and *parkin*, which are associated with familial forms of Parkinson's disease. The rescue was much more robust in the case of *Pink1* than for *parkin*, suggesting that uniporter interacts with other aspects of *Pink1* function than mitophagy. Given the link between mitochondrial calcium and oxidative phosphorylation, this suggests the participation of the known interaction between *Pink1* and Complex I (Morais *et al.*, 2009). Additionally, the role of mitochondrial calcium overload in *Pink1*-mediated cell death has been recently established (Gandhi *et al.*, 2009; Kostic *et al.*, 2015), through inhibition of calcium influx through NCLX. Thus, the straightforward explanation is that *MCU* reduction balances this by limiting calcium influx. However, this would need to be distinguished from other closely aligned features of *Pink1* deficiency, such as enhanced ER-mitochondrial contacts (K.-S. Lee *et al.*, 2018).

As well as models of Parkinson's disease, the longevity and vitality of a toxic amyloid-beta model of AD was strongly improved by the reduction of *MCU*. Dysregulated mitochondrial calcium entry has been associated with the presence of oligomeric Aβ (see Section 1.4.2), and specifically through *MCU* upregulation (Calvo-Rodriguez *et al.*, 2019). Reduced NCLX-efflux has also been reported (Jadiya *et al.*, 2019), which represents a shared mechanism with the *Pink1* PD model. These initial findings will need to be built upon, but they already demonstrate the potential for the mitochondrial calcium uniporter to yield beneficial drug candidates for an array of otherwise intractable neurodegenerative diseases. Additionally, comparisons between different conditions in terms of their response to uniporter inhibition may reveal commonalities in their aetiology and progression, allowing for greater pathobiological understanding that can be exploited in the creation of novel lead compounds.

7.2. Study Limitations

The generation of genetic mutants is a complicated process with multiple competing methods, each with their own advantages and drawbacks. For example, this work uses the powerful CRISPR/Cas9 system to induce targeted double stranded breaks that serve as a signal for DNA repair, errors in which can create mutations of interest. However, this emerging technology has not been definitively studied, and the potential remains for unexpected effects. Off-target effects may confound mutant characterisation, and have been reported for the CRISPR-Cas9 system (Fu *et al.*, 2013). These can be minimised through protein engineering of the nuclease (Kleinstiver *et al.*, 2016) or through optimised gRNA design (Cho *et al.*, 2014). An unmodified *Streptococcus pyogenes* Cas9 was used in this study, but gRNAs were selected to avoid any predicted off-target effects. Where this was not possible, guides were selected with off-target sites on different chromosomes to the intended locus, to allow any mutations to be easily bred out. Unexpected off-target mutagenesis on the target chromosome cannot be ruled out, but CRISPR mutant lines were outcrossed for several generations (through direct detection of the deletion event, rather than by screening an indirect phenotype), making their presence in the final line unlikely.

CRISPR-mediated knockout lines were created in this study through frameshift mutations creating a premature stop codon that severely truncated any resulting protein, as well as nonsense-mediated decay of the mRNA transcript. This nonsense-mediated decay was shown in a recent paper to trigger adaptive upregulation of related transcripts, compensating for the mutation (El-Brolosy *et al.*, 2019). However, the *EMRE*[1] mutant was confirmed as a functional null mutant, and though there was no canonical function for *MICU3* to measure, transgenic rescue of the knockout phenotype was achieved. No related transcripts for these genes have been reported, except for potentially *MICU1* (that is, *MICU3*), which has already been demonstrated not to be functionally interchangeable (Tufi *et al.*, 2019). Therefore, any confounding effect of this phenomenon is likely to be limited in this case.

A significant roadblock in *Drosophila* research is the availability of high-quality commercial antibodies. Our group has been able to achieve reactivity to fly MCU protein with a custom antibody. Expanding this to other uniporter components would allow for the dissection of their co-expression, but given the resources involved this might be better served in another model system. At the very least, *Drosophila*-reactive anti-MCU would allow for the level of the pore to be assessed in different uniporter manipulations.

The use of genetic mutants, whilst considered the most robust way of studying gene function, are not without their own complexities, which can complicate interpretation. This is especially true for emerging systems with conflicting pre-existing reports, such as the uniporter. In this work, *MCU* and *EMRE* knockouts displayed several unexpected phenotypes, not least their complete viability given the controversy of the mouse knockout strain effect. It is difficult to exclude some genetic compensation for these mutants; it would perhaps even be expected that a chronic lack of mitochondrial calcium uptake from the gamete stage would necessarily require adaption. Thus, observed phenotypes in these mutants could instead represent some overcompensation to an otherwise invisible deficit. This is difficult to dissect genetically, but RNAi knockdown can be restricted to adulthood, and conditional knockout of these genes may also reveal such confounds.

Though the knockout of *MICU3* resulted in several interesting phenotypes, there are no extant *in vivo* models with which to compare. However, these features do map to tissues where MICU3 is enriched according to large-scale RNAseq data in *Drosophila*, and similar datasets in other organisms. Additionally, it was not possible to obtain functional verification of a null allele, and transgenic rescue was partial in the case of sterility. Nevertheless, genetic background is unlikely to have an impact on such phenotypes; flies were outcrossed to w^{1118} which does not display such deficits.

The *MICU1*^{32} mutant breakpoints extend past the target gene region, deleting three long non-coding RNAs, as well as several kilobases of intergenic region. Therefore, despite the mutant being confirmed as an RNA null for *MICU1*, it is not possible to rule out the contribution of the loss of these lncRNAs to *MICU1*^{32}-associated phenotypes. However, in the arguably most important case of the developmental lethality, rescue through transgenic re-expression verifies this as a feature of *MICU1* deletion.

The observation that *MICU1*-associated lethality is not rescuable by *MCU* or *EMRE* loss represents a significant challenge to its canonical role as a uniporter gatekeeper preventing pathological mitochondrial calcium influx. Though specificity of the phenotype was demonstrated through transgenic re-expression of MICU1, it is worth noting that no other manipulation so far has rescued the phenotype. This may indicate multiple essential functions of the gene, perhaps requiring any rescue to be combined with *MCU* or *EMRE* knockout.

Though the use of *D. melanogaster* presents many advantages for the fundamental study of physiological pathways, given their general conservation, there are disadvantages in their use for translational studies; there is no perfect model for human biology. *Drosophila* are more evolutionarily distant from humans than rodents, which may limit applicability of these findings. However, a reasonable fraction of human disease genes are conserved in the fly (Rubin *et al.*, 2000), allowing for the study of the molecular basis of disease. Of relevance to neurodegenerative research, one notable absence in these invertebrate animal models is the adaptive immune system, with implications for neuroinflammatory contributions to neurodegeneration (reviewed for PD in Mosley *et al.*, 2012). However, recent work in the Parkinson's disease field has instead put the innate immune system to the fore (Sliter *et al.*, 2018), which *Drosophila* are well positioned to study. Indeed, the adaptive and innate immune systems display regulatory cross-talk (Shanker *et al.*, 2017) and *Drosophila* may represent an opportunity to dissect such confounds.

Though they act together in the canonical mitochondrial quality pathway, divergent roles for PINK1 and Parkin have begun to be elucidated. In this study, poor rescue of the *parkin* knockout neurodegenerative model was achieved via *MCU* reduction compared to *Pink1*. This could raise concerns about the generalisation of these findings to the human condition, as only a small fraction of PD patients will have mutant *PINK1*. However, the sporadic condition is not necessarily more dependent on altered *PRKN* function; indeed, the aetiology of the sporadic condition is unknown. The treatment of neurodegeneration is more generally hampered by stratification of patients beyond classical disease diagnoses, and treatments are less likely to achieve broad therapeutic benefit. Further work could attempt to demonstrate PD patient grouping based on the presence of mitochondrial calcium overload, which would provide a candidate sample for therapeutic intervention through uniporter inhibition.

The therapeutic benefits of uniporter inhibition in the treatment of neurodegeneration would have to be balanced against any side-effects. In the present work, the most concerning observation for this consideration is the reduced lifespan seen in the *MCU*^{1} homozygous knockout. This was greatly attenuated in the homozygous *EMRE* knockout, suggesting that ablation of mitochondrial calcium uptake *per se* does not lead to strong longevity defects; however, some effect remained. It would be crucial to determine the cause of this phenotype, as it may be possible to bypass through additional treatments or refinement of the approach. Encouragingly, heterozygous *MCU* knockout rescued the neurodegenerative model, and did not cause an overt phenotype alone. This suggests a therapeutic window for pharmacological inhibition of the uniporter, which would need to be evaluated in preclinical toxicological studies.

The contribution of the uniporter to amyloid-associated toxicity has begun to be characterised in this work. However, the interaction with tau-based models has yet to be evaluated. There is significant contention regarding the primary molecular driver of Alzheimer's disease, and expanding this study to tau or mixed models could circumvent this argument if uniporter inhibition was beneficial in all cases. This may suggest a non-specific benefit to neuronal health rather than a true interaction with a disease pathway, though this is countered by the poor rescue of *parkin* mutants.

7.3. Future Directions

The generation of *Drosophila* lines knocking out or expressing each conserved uniporter component represents the completion of a basic genetic toolkit for the study of this protein complex. However, more refined strategies are possible. For example, constructs to express mutant forms, such as MCU with inactivating mutations in the DIME loop, can be used to distinguish mutant phenotypes resulting from canonical calcium uptake activity from others that would be also affected by absence of the protein. These could be expressed in a knockout background or knocked-in using homology-directed repair promoted by the activity of CRISPR-Cas9, to express via endogenous transcriptional promotors and so on. Similarly, mutant MICU1 protein lacking key residues for uniporter coordination could be expressed to see if these rescue the knockout lethality. If they do, this would suggest that the essential function of MICU1 is indeed uniporter independent.

I have observed that *MCU*^{1} reduces the overall protein level of pyruvate dehydrogenase, rather than leading to altered phosphorylation status as in other organisms. This may provide some mechanistic basis for genetic compensation of this mutant, and could be studied through transgenic expression of PDH, which may exacerbate *MCU*^{1} phenotypes. It would also be interesting to see if *EMRE*^{1} mutants do not show such difference at this key control point, given their divergent metabolic phenotypes.

The decreased longevity of *MCU*^{1} suggests a susceptibility to age-related stresses, but flies did not show defects in muscle mitochondrial morphology or locomotor performance when aged. Future work could examine other aging phenotypes such as intestinal epithelial integrity, biomarkers such as lipid peroxidation and protein carbonylation, and sleep loss (Robertson and Keene, 2013; He and Jasper, 2014) to see if these are accelerated in the *MCU* knockout. These may provide clues to a mechanistic explanation for the reduction in lifespan.

Loss of *MCU* and *EMRE* resulted in divergent metabolic phenotypes as measured by high-resolution respirometry and starvation tolerance. This could be complemented by the measurement of other key metabolic processes and indicators such as glycolysis, fatty acid oxidation, and NAD^+/NADH ratios. A metabolomics approach would allow this to be greatly expanded to a suite of metabolites. Mapping out divergent metabolic responses to these mutant conditions will allow for specific compensatory pathways to be identified. These will be of interest in minimising unintended side-effects in therapeutic uniporter inhibition.

The *MICU3* knockout described in this study displayed neuromuscular and reproductive phenotypes, which could be examined in further detail to uncover whether the underlying cause was simple mitochondrial calcium overload-induced cell death, or dysfunction brought about by altered calcium signalling. Muscle degeneration could be evaluated through toluidine blue staining, and antibodies directed at apoptotic markers could be employed in immunofluorescence experiments in dissected testes. Further imaging studies could uncover specific defects, for example in spermatid individualisation.

Of the *MICU1*-associated phenotypes, the most surprising was the substantial increase in Complex II-linked respiration. More granular data on respiratory capacity, through BN-PAGE of the respiratory chain as well as assaying enzymatic activity, would isolate alterations in specific respiratory complexes. The level of mitochondrial coupling may provide an alternative explanation and could be investigated with high-resolution respirometry. Though it was not possible to evaluate mitochondrial uncoupling through the addition of carbonyl cyanide m-chlorophenyl hydrazone (CCCP), direct measurements of the ADP/O flux ratio could be a feasible alternative (Gnaiger, 2001).

The genetic interactions outlined in the present work suggest an alternative non-uniporter role for *MICU1*, that is essential for *Drosophila* development. A logical next step is to ascertain the identity of this role at a functional and molecular level. Immunoprecipitation of tagged MICU1 would allow for mass spectrometry to identify binding partners, suggesting novel functions for the protein that could then be investigated using the genetic tractability of the fly. Orthogonal studies, perhaps in human cell culture, would provide greater confidence to any shared hits.

As well as uncovering interesting features of uniporter function, this work has highlighted its potential for the treatment of neurodegenerative diseases. However, current results are limited to the invertebrate model *Drosophila*. Replicating these findings in other organisms would allow for greater confidence in their applicability to humans. For example, crossing the mouse *Mcu* mutant (Pan *et al.*, 2013) to a amyloid model mouse (such as the PS2APP double transgenic line (Richards *et al.*, 2003)) would present an opportunity to extend our observations and provide strong preclinical evidence of therapeutic benefit. In the case of Parkinson's disease, rodent models suffer from poor correlation with human phenotypes without additional stressors such as mtDNA mutation (Pickrell *et al.*, 2015). A *Prkn*$^{-/-}$;*mutator* or *Pink1*$^{-/-}$;*mutator* mouse could be used as a model to evaluate the benefit of uniporter inhibition, but the potential interaction of mitochondrial calcium dynamics and mtDNA maintenance would have to be evaluated.

The rescue of both *Pink1* loss and Aβ expression through uniporter manipulation indicates common features for these neurodegenerative conditions. However, it remains unclear what other similar pathologies could be rescued through the same intervention. Tau-only models of neurodegeneration exist in *Drosophila*, can be used to assess the benefit of targeting the uniporter in frontotemporal dementia and other tauopathies. Further disease phenotypes to be evaluated could include disrupted axonal transport, or circadian defects.

The genetic basis of conditions such as Huntington's disease are trinucleotide repeat expansions, rather than loss-of-function mutations often seen in other familial forms of neurodegeneration. Additionally, the resulting polyamine tracts present biophysical characteristics that distinguish them from other proteinaceous aggregations. Therefore, they can be considered more distant 'relations' in the family of neurodegenerative conditions. Nevertheless, calcium dysregulation and mitochondrial dysfunction are both key features of Huntington's disease. For example, mutant huntingtin binds to calcium-binding proteins such as calmodulin (Bao *et al.*, 1996). Mutant huntingtin has also been shown to bind to inositol-(1,4,5)-triphosphate receptors, enhancing their substrate sensitivity (Tang *et al.*, 2003). Reciprocally, IP3R inhibition through genetic or pharmacological means was demonstrated to reduce mutant huntingtin aggregation (Bauer *et al.*, 2011). As the IP3R-mediated efflux of calcium from the ER and mitochondrial calcium uptake are necessarily linked through their organellar contact sites, it can be hypothesised that mutant huntingtin-mediated excessive mitochondrial calcium uptake through increased ER-mitochondrial transfer may play a role in the aetiology of Huntington's disease, and that uniporter inhibition may be of therapeutic interest. *Drosophila* have been widely used for preclinical studies of Huntington's disease, and combining a model with uniporter mutants may give insight into this potential strategy.

7.4. Conclusions

This thesis reports the completion of a comprehensive genetic toolkit for manipulating the *Drosophila melanogaster* mitochondrial calcium uniporter, to understand its contribution to *in vivo* physiology and neurodegenerative disease processes, whilst providing useful information for the design of future mutagenesis efforts. Leveraging these tools, I characterise all known conserved *Drosophila* uniporter components. As expected, *MCU* and *EMRE* display similar physiological requirements, though the knockout viability for either gene contributes to the ongoing debate around the dispensability, or ability to adequately compensate for, canonical mitochondrial calcium uptake. Some differences between these two mutants were also observed, for phenotypes reflecting cellular metabolism, and this dichotomy may provide an avenue to understand what compensatory pathways, if any, are present. The uniporter gatekeeper *MICU1* is found to be kept in physiological balance, with either loss or surplus being detrimental for development. The lethality is preceded by dramatic metabolic and mitochondrial trafficking phenotypes that may provide an explanation for the ultimate outcome. Certain cell death pathways do not seem to be associated with *MICU1*-mediated lethality, but more importantly, the lack of rescue with either *MCU* or *EMRE* knockout indicates a uniporter-independent role for this key gene. Additionally, the first *in vivo* characterisation of *MICU3* is reported, finding its loss to cause tissue-specific defects, though its overabundance is broadly tolerated. Genetic interaction studies demonstrate that MICU3 is functionally independent of MICU1, reinforcing its role as a modulator of uniporter gatekeeping. Finally, the importance of controlled mitochondrial calcium dynamics for neuronal health is underscored by the reduction of influx through *MCU* reduction being beneficial in two neurodegenerative models that are associated with matrix overload. As well as further establishing this process as a research avenue to understand the biology of neurodegeneration, these results provide a strong foundation for further evaluation of the mitochondrial calcium uniporter as a therapeutic target for the treatment of these otherwise intractable diseases.

8. References

Altmann, R. (1890) *Die Elementarorganismen und ihre Beziehungen zuden Zellen*.

Alzheimer, A. *et al.* (1995) 'An English translation of Alzheimer's 1907 paper, "Uber eine eigenartige Erkankung der Hirnrinde".', *Clinical anatomy (New York, N.Y.)*, 8(6), pp. 429–31. doi: 10.1002/ca.980080612.

Anandatheerthavarada, H. K. *et al.* (2003) 'Mitochondrial targeting and a novel transmembrane arrest of Alzheimer's amyloid precursor protein impairs mitochondrial function in neuronal cells.', *The Journal of cell biology*, 161(1), pp. 41–54. doi: 10.1083/jcb.200207030.

Angelova, P. R. *et al.* (2018) 'Pharmacological Sequestration of Mitochondrial Calcium Uptake Protects Neurons Against Glutamate Excitotoxicity'. Molecular Neurobiology.

Antony, A. N. *et al.* (2016) 'MICU1 regulation of mitochondrial Ca(2+) uptake dictates survival and tissue regeneration.', *Nature communications*, 7, p. 10955. doi: 10.1038/ncomms10955.

Aradska, J. *et al.* (2015) 'Gel-free mass spectrometry analysis of Drosophila melanogaster heads.', *Proteomics*, 15(19), pp. 3356–60. doi: 10.1002/pmic.201500092.

Arduino, D. M. *et al.* (2017) 'Systematic Identification of MCU Modulators by Orthogonal Interspecies Chemical Screening.', *Molecular cell*, 67(4), pp. 711-723.e7. doi: 10.1016/j.molcel.2017.07.019.

Atakpa, P. *et al.* (2018) 'IP3 Receptors Preferentially Associate with ER-Lysosome Contact Sites and Selectively Deliver Ca2+ to Lysosomes.', *Cell reports*. ElsevierCompany., 25(11), pp. 3180-3193.e7. doi: 10.1016/j.celrep.2018.11.064.

Austin, S. *et al.* (2017) 'LETM1-Mediated K+ and Na+ Homeostasis Regulates Mitochondrial Ca2+ Efflux', *Frontiers in Physiology*, 8(November), pp. 1–12. doi: 10.3389/fphys.2017.00839.

Baldwin, K. R. *et al.* (2016) 'Axonal transport defects are a common phenotype in Drosophila models of ALS.', *Human molecular genetics*, 25(12), pp. 2378–2392. doi: 10.1093/hmg/ddw105.

Bao, J. *et al.* (1996) 'Expansion of polyglutamine repeat in huntingtin leads to abnormal protein interactions involving calmodulin.', *Proceedings of the National Academy of Sciences of the United States of America*, 93(10), pp. 5037–42. doi: 10.1073/pnas.93.10.5037.

Bao, Q. *et al.* (2007) 'Calcium blocks formation of apoptosome by preventing nucleotide exchange in Apaf-1.', *Molecular cell*, 25(2), pp. 181–92. doi: 10.1016/j.molcel.2006.12.013.

Baradaran, R. *et al.* (2018) 'Cryo-EM structures of fungal and metazoan mitochondrial calcium uniporters', *Nature*. Springer US. doi: 10.1038/s41586-018-0331-8.

Barrangou, R. *et al.* (2007) 'CRISPR provides acquired resistance against viruses in prokaryotes.', *Science (New York, N.Y.)*, 315(5819), pp. 1709–12. doi: 10.1126/science.1138140.

Bauer, P. O. *et al.* (2011) 'Genetic ablation and chemical inhibition of IP3R1 reduce mutant huntingtin aggregation.', *Biochemical and biophysical research communications*. Elsevier Inc., 416(1–2), pp. 13–7. doi: 10.1016/j.bbrc.2011.10.096.

Baughman, J. M. *et al.* (2011) 'Integrative genomics identifies MCU as an essential component of the mitochondrial calcium uniporter.', *Nature*. Nature Publishing Group, 476(7360), pp. 341–5. doi: 10.1038/nature10234.

Bellen, H. J. *et al.* (2011) 'The Drosophila gene disruption project: Progress using transposons with distinctive site specificities', *Genetics*, 188(3), pp. 731–743. doi: 10.1534/genetics.111.126995.

Bender, E. and Kadenbach, B. (2000) 'The allosteric ATP-inhibition of cytochrome c oxidase activity is reversibly switched on by cAMP-dependent phosphorylation.', *FEBS letters*, 466(1), pp. 130–4. doi: 10.1016/s0014-5793(99)01773-1.

Benjamini, Y., Krieger, A. M. and Yekutieli, D. (2006) 'Adaptive linear step-up procedures that control the false discovery rate', *Biometrika*, 93(3), pp. 491–507. doi: 10.1093/biomet/93.3.491.

Bezprozvanny, I., Watras, J. and Ehrlich, B. E. (1991) 'Bell-shaped calcium-response curves of Ins(1,4,5)P3- and calcium-gated channels from endoplasmic reticulum of cerebellum.', *Nature*, 351(6329), pp. 751–4. doi: 10.1038/351751a0.

Bick, A. G., Calvo, S. E. and Mootha, V. K. (2012) 'Evolutionary diversity of the mitochondrial calcium uniporter.', *Science (New York, N.Y.)*, 336(6083), p. 886. doi: 10.1126/science.1214977.

Biogen/Eisai (2019) 'Biogen and Eisai to Discontinue Phase 3 ENGAGE and EMERGE Trials of aducanumab in Alzheimer's Disease'. Available at: http://investors.biogen.com/news-releases/news-release-details/biogen-and-eisai-discontinue-phase-3-engage-and-emerge-trials (Accessed: 14 August 2019).

Birks, J. (2006) 'Cholinesterase inhibitors for Alzheimer's disease.', *The Cochrane database of systematic reviews*, 2012(1), p. CD005593. doi: 10.1002/14651858.CD005593.

Birks, J. S., Chong, L. Y. and Grimley Evans, J. (2015) 'Rivastigmine for Alzheimer's disease.', *The Cochrane database of systematic reviews*, 9(4), p. CD001191. doi: 10.1002/14651858.CD001191.pub4.

Birks, J. S. and Harvey, R. J. (2018) 'Donepezil for dementia due to Alzheimer's disease.', *The Cochrane database of systematic reviews*, 6(3), p. CD001190. doi: 10.1002/14651858.CD001190.pub3.

Bischof, J. *et al.* (2013) 'A versatile platform for creating a comprehensive UAS-ORFeome

library in Drosophila.', *Development (Cambridge, England)*, 140(11), pp. 2434–42. doi: 10.1242/dev.088757.

Bondarenko, A. I. *et al.* (2013) 'Characterization of distinct single-channel properties of Ca^{2+} inward currents in mitochondria.', *Pflügers Archiv : European journal of physiology*, 465(7), pp. 997–1010. doi: 10.1007/s00424-013-1224-1.

Bondarenko, A. I. *et al.* (2014) 'Mitochondrial Ca(2+) uniporter (MCU)-dependent and MCU-independent Ca(2+) channels coexist in the inner mitochondrial membrane.', *Pflügers Archiv : European journal of physiology*, 466(7), pp. 1411–20. doi: 10.1007/s00424-013-1383-0.

Bondarenko, A. I. *et al.* (2015) 'UCP2 modulates single-channel properties of a MCU-dependent Ca(2+) inward current in mitochondria.', *Pflugers Archiv : European journal of physiology*, 467(12), pp. 2509–18. doi: 10.1007/s00424-015-1727-z.

Boyman, L. *et al.* (2013) 'NCLX: the mitochondrial sodium calcium exchanger.', *Journal of molecular and cellular cardiology*. Elsevier Ltd, 59, pp. 205–13. doi: 10.1016/j.yjmcc.2013.03.012.

Brand, A. H. and Perrimon, N. (1993) 'Targeted gene expression as a means of altering cell fates and generating dominant phenotypes.', *Development (Cambridge, England)*, 118(2), pp. 401–15. Available at: http://www.ncbi.nlm.nih.gov/pubmed/8223268.

de Brito, O. M. and Scorrano, L. (2008) 'Mitofusin 2 tethers endoplasmic reticulum to mitochondria.', *Nature*, 456(7222), pp. 605–610. doi: 10.1038/nature07534.

Brookes, P. S. *et al.* (2008) 'UCPs--unlikely calcium porters.', *Nature cell biology*, 10(11), pp. 1235–7; author reply 1237-40. doi: 10.1038/ncb1108-1235.

Brookmeyer, R. *et al.* (2007) 'Forecasting the global burden of Alzheimer's disease.', *Alzheimer's & dementia : the journal of the Alzheimer's Association*, 3(3), pp. 186–91. doi: 10.1016/j.jalz.2007.04.381.

Brown, J. B. *et al.* (2014) 'Diversity and dynamics of the Drosophila transcriptome.', *Nature*, 512(7515), pp. 393–9. doi: 10.1038/nature12962.

Burchell, V. S. *et al.* (2013) 'The Parkinson's disease-linked proteins Fbxo7 and Parkin interact to mediate mitophagy.', *Nature neuroscience*, 16(9), pp. 1257–65. doi: 10.1038/nn.3489.

Calcoen, D., Elias, L. and Yu, X. (2015) 'What does it take to produce a breakthrough drug?', *Nature reviews. Drug discovery*. Nature Publishing Group, 14(3), pp. 161–2. doi: 10.1038/nrd4570.

Calvo-Rodriguez, M. *et al.* (2019) 'Amyloid β Oligomers Increase ER-Mitochondria Ca2+ Cross Talk in Young Hippocampal Neurons and Exacerbate Aging-Induced Intracellular Ca2+ Remodeling.', *Frontiers in cellular neuroscience*, 13(February), p. 22. doi: 10.3389/fncel.2019.00022.

Camello, C. *et al.* (2002) 'Calcium leak from intracellular stores--the enigma of calcium signalling.', *Cell calcium*, 32(5–6), pp. 355–61. doi: 10.1016/s0143416002001926.

Cao, C. *et al.* (2017) 'Ion and inhibitor binding of the double-ring ion selectivity filter of the mitochondrial calcium uniporter.', *Proceedings of the National Academy of Sciences of the United States of America*, p. 201620316. doi: 10.1073/pnas.1620316114.

Carafoli, E. (1967) 'In vivo effect of uncoupling agents on the incorporation of calcium and strontium into mitochondria and other subcellular fractions of rat liver.', *The Journal of general physiology*, 50(7), pp. 1849–64. doi: 10.1085/jgp.50.7.1849.

Carafoli, E. (2003) 'Historical review: mitochondria and calcium: ups and downs of an unusual relationship.', *Trends in biochemical sciences*, 28(4), pp. 175–81. doi: 10.1016/S0968-0004(03)00053-7.

Carafoli, E. and Lehninger, A. L. (1971) 'A survey of the interaction of calcium ions with mitochondria from different tissues and species.', *The Biochemical journal*, 122(5), pp. 681–90. doi: 10.1042/bj1220681.

Cárdenas, C. *et al.* (2010) 'Essential regulation of cell bioenergetics by constitutive InsP3 receptor Ca2+ transfer to mitochondria.', *Cell*, 142(2), pp. 270–83. doi: 10.1016/j.cell.2010.06.007.

Casley, C. S. *et al.* (2002) 'Beta-amyloid inhibits integrated mitochondrial respiration and key enzyme activities.', *Journal of neurochemistry*, 80(1), pp. 91–100. doi: 10.1046/j.0022-3042.2001.00681.x.

Chakrabarti, R. *et al.* (2017) 'INF2-mediated actin polymerization at the ER stimulates mitochondrial calcium uptake, inner membrane constriction, and division.', *The Journal of cell biology*, pp. 1–18. doi: 10.1083/jcb.201709111.

Chakraborty, P. K. *et al.* (2017) 'MICU1 drives glycolysis and chemoresistance in ovarian cancer.', *Nature communications*. Nature Publishing Group, 8(May), p. 14634. doi: 10.1038/ncomms14634.

Chang, Y. *et al.* (2014) 'Structural basis for a pH-sensitive calcium leak across membranes.', *Science (New York, N.Y.)*, 344(6188), pp. 1131–5. doi: 10.1126/science.1252043.

Chaudhuri, D. *et al.* (2016) 'Mitochondrial calcium uniporter regulator 1 (MCUR1) regulates the calcium threshold for the mitochondrial permeability transition.', *Proceedings of the National Academy of Sciences of the United States of America*, 1, p. 201602264. doi: 10.1073/pnas.1602264113.

Cho, B. *et al.* (2017) 'Constriction of the mitochondrial inner compartment is a priming event for mitochondrial division.', *Nature communications*. Nature Publishing Group, 8(1), p. 15754. doi: 10.1038/ncomms15754.

Cho, J.-H. and Johnson, G. V. W. (2003) 'Glycogen synthase kinase 3beta phosphorylates tau at both primed and unprimed sites. Differential impact on microtubule binding.', *The Journal of biological chemistry*, 278(1), pp. 187–93. doi: 10.1074/jbc.M206236200.

Cho, S. W. *et al.* (2014) 'Analysis of off-target effects of CRISPR/Cas-derived RNA-guided

endonucleases and nickases.', *Genome research*, 24(1), pp. 132–41. doi: 10.1101/gr.162339.113.

Choi, S. *et al.* (2017) 'Mitochondrial calcium uniporter in Drosophila transfers calcium between the endoplasmic reticulum and mitochondria in oxidative stress-induced cell death.', *The Journal of biological chemistry*, p. jbc.M116.765578. doi: 10.1074/jbc.M116.765578.

Choi, W.-S. *et al.* (2008) 'Mitochondrial complex I inhibition is not required for dopaminergic neuron death induced by rotenone, MPP+, or paraquat.', *Proceedings of the National Academy of Sciences of the United States of America*, 105(39), pp. 15136–41. doi: 10.1073/pnas.0807581105.

Clark, I. E. *et al.* (2006) 'Drosophila pink1 is required for mitochondrial function and interacts genetically with parkin.', *Nature*, 441(7097), pp. 1162–6. doi: 10.1038/nature04779.

Clem, R. J., Fechheimer, M. and Miller, L. K. (1991) 'Prevention of apoptosis by a baculovirus gene during infection of insect cells.', *Science (New York, N.Y.)*, 254(5036), pp. 1388–90. doi: 10.1126/science.1962198.

Van Coppenolle, F. *et al.* (2004) 'Ribosome-translocon complex mediates calcium leakage from endoplasmic reticulum stores.', *Journal of cell science*, 117(Pt 18), pp. 4135–42. doi: 10.1242/jcs.01274.

Cribbs, J. T. and Strack, S. (2007) 'Reversible phosphorylation of Drp1 by cyclic AMP-dependent protein kinase and calcineurin regulates mitochondrial fission and cell death.', *EMBO reports*, 8(10), pp. 939–44. doi: 10.1038/sj.embor.7401062.

Criollo, A. *et al.* (2007) 'Regulation of autophagy by the inositol trisphosphate receptor.', *Cell death and differentiation*, 14(5), pp. 1029–39. doi: 10.1038/sj.cdd.4402099.

Crouch, P. J. *et al.* (2005) 'Copper-dependent inhibition of human cytochrome c oxidase by a dimeric conformer of amyloid-beta1-42.', *The Journal of neuroscience : the official journal of the Society for Neuroscience*, 25(3), pp. 672–9. doi: 10.1523/JNEUROSCI.4276-04.2005.

Crowther, D. C. *et al.* (2005a) 'Intraneuronal Abeta, non-amyloid aggregates and neurodegeneration in a Drosophila model of Alzheimer's disease.', *Neuroscience*, 132(1), pp. 123–35. doi: 10.1016/j.neuroscience.2004.12.025.

Crowther, D. C. *et al.* (2005b) 'Intraneuronal Abeta, non-amyloid aggregates and neurodegeneration in a Drosophila model of Alzheimer's disease.', *Neuroscience*, 132(1), pp. 123–35. doi: 10.1016/j.neuroscience.2004.12.025.

Csordás, G. *et al.* (2010) 'Imaging interorganelle contacts and local calcium dynamics at the ER-mitochondrial interface.', *Molecular cell*, 39(1), pp. 121–32. doi: 10.1016/j.molcel.2010.06.029.

Csordás, G. *et al.* (2013) 'MICU1 controls both the threshold and cooperative activation of the mitochondrial Ca^{2+} uniporter.', *Cell metabolism*, 17(6), pp. 976–87. doi: 10.1016/j.cmet.2013.04.020.

David, G. and Barrett, E. F. (2003) 'Mitochondrial Ca2+ uptake prevents desynchronization of quantal release and minimizes depletion during repetitive stimulation of mouse motor nerve terminals.', *The Journal of physiology*, 548(Pt 2), pp. 425–38. doi: 10.1113/jphysiol.2002.035196.

Davis, G. C. *et al.* (1979) 'Chronic Parkinsonism secondary to intravenous injection of meperidine analogues.', *Psychiatry research*, 1(3), pp. 249–54. doi: 10.1016/0165-1781(79)90006-4.

Deas, E. *et al.* (2011) 'PINK1 cleavage at position A103 by the mitochondrial protease PARL', *Human Molecular Genetics*, 20(5), pp. 867–879. doi: 10.1093/hmg/ddq526.

DeLuca, H. F. and Engstrom, G. W. (1961) 'Calcium uptake by rat kidney mitochondria.', *Proceedings of the National Academy of Sciences of the United States of America*, 47, pp. 1744–50. doi: 10.1073/pnas.47.11.1744.

Deng, H. *et al.* (2008) 'The Parkinson's disease genes pink1 and parkin promote mitochondrial fission and/or inhibit fusion in Drosophila.', *Proceedings of the National Academy of Sciences of the United States of America*, 105(38), pp. 14503–8. doi: 10.1073/pnas.0803998105.

Denton, R. M. (2009) 'Regulation of mitochondrial dehydrogenases by calcium ions.', *Biochimica et biophysica acta*. Elsevier B.V., 1787(11), pp. 1309–16. doi: 10.1016/j.bbabio.2009.01.005.

Denton, R. M., Richards, D. a and Chin, J. G. (1978) 'Calcium ions and the regulation of NAD+-linked isocitrate dehydrogenase from the mitochondria of rat heart and other tissues.', *The Biochemical journal*, 176(3), pp. 899–906. doi: 10.1042/bj1760899.

van Deursen, J. *et al.* (1993) 'Skeletal muscles of mice deficient in muscle creatine kinase lack burst activity.', *Cell*, 74(4), pp. 621–31. doi: 10.1016/0092-8674(93)90510-W.

Devi, L. *et al.* (2006) 'Accumulation of amyloid precursor protein in the mitochondrial import channels of human Alzheimer's disease brain is associated with mitochondrial dysfunction.', *The Journal of neuroscience : the official journal of the Society for Neuroscience*, 26(35), pp. 9057–68. doi: 10.1523/JNEUROSCI.1469-06.2006.

Dickinson, G. D., Swaminathan, D. and Parker, I. (2012) 'The probability of triggering calcium puffs is linearly related to the number of inositol trisphosphate receptors in a cluster.', *Biophysical journal*. Biophysical Society, 102(8), pp. 1826–36. doi: 10.1016/j.bpj.2012.03.029.

Doench, J. G. *et al.* (2014) 'Rational design of highly active sgRNAs for CRISPR-Cas9-mediated gene inactivation.', *Nature biotechnology*. Nature Publishing Group, 32(12), pp. 1262–7. doi: 10.1038/nbt.3026.

Drago, I. and Davis, R. L. (2016) 'Inhibiting the Mitochondrial Calcium Uniporter during Development Impairs Memory in Adult Drosophila.', *Cell reports*. The Authors, pp. 1–14. doi: 10.1016/j.celrep.2016.08.017.

Durcan, T. M. *et al.* (2014) 'USP8 regulates mitophagy by removing K6-linked ubiquitin

conjugates from parkin.', *The EMBO journal*, 33(21), pp. 2473–91. doi: 10.15252/embj.201489729.

Edelstein, A. D. *et al.* (2015) 'Advanced methods of microscope control using μManager software.', *Journal of biological methods*, 1(2), pp. 1–18. doi: 10.14440/jbm.2014.36.

Egan, M. F. *et al.* (2018) 'Randomized Trial of Verubecestat for Mild-to-Moderate Alzheimer's Disease.', *The New England journal of medicine*, 378(18), pp. 1691–1703. doi: 10.1056/NEJMoa1706441.

El-Brolosy, M. A. *et al.* (2019) 'Genetic compensation triggered by mutant mRNA degradation.', *Nature*, 568(7751), pp. 193–197. doi: 10.1038/s41586-019-1064-z.

Elustondo, P. A. *et al.* (2016) 'Mitochondrial Ca 2 + uptake pathways', *Journal of Bioenergetics and Biomembranes*. Journal of Bioenergetics and Biomembranes. doi: 10.1007/s10863-016-9676-6.

Emaus, R. K., Grunwald, R. and Lemasters, J. J. (1986) 'Rhodamine 123 as a probe of transmembrane potential in isolated rat-liver mitochondria: spectral and metabolic properties.', *Biochimica et biophysica acta*, 850(3), pp. 436–48. doi: 10.1016/0005-2728(86)90112-x.

Endele, S. *et al.* (1999) 'LETM1, a novel gene encoding a putative EF-hand Ca(2+)-binding protein, flanks the Wolf-Hirschhorn syndrome (WHS) critical region and is deleted in most WHS patients.', *Genomics*, 60(2), pp. 218–25. doi: 10.1006/geno.1999.5881.

Engelhardt, E. (2017) 'Lafora and Trétiakoff: the naming of the inclusion bodies discovered by Lewy.', *Arquivos de neuro-psiquiatria*, 75(10), pp. 751–753. doi: 10.1590/0004-282X20170116.

Ernster, L. and Schatz, G. (1981) 'Mitochondria: a historical review.', *The Journal of cell biology*, 91(3 Pt 2), pp. 227s-255s. doi: 10.1083/jcb.91.3.227s.

Fan, C. *et al.* (2018) 'X-ray and cryo-EM structures of the mitochondrial calcium uniporter', *Nature*. Springer US. doi: 10.1038/s41586-018-0330-9.

Favaro, G. *et al.* (2019) 'DRP1-mediated mitochondrial shape controls calcium homeostasis and muscle mass.', *Nature communications*. Springer US, 10(1), p. 2576. doi: 10.1038/s41467-019-10226-9.

Fearnley, J. M. and Lees, A. J. (1991) 'Ageing and Parkinson's disease: substantia nigra regional selectivity.', *Brain : a journal of neurology*, 114 (Pt 5(5), pp. 2283–301. doi: 10.1093/brain/114.5.2283.

Feske, S. *et al.* (2006) 'A mutation in Orai1 causes immune deficiency by abrogating CRAC channel function.', *Nature*, 441(7090), pp. 179–85. doi: 10.1038/nature04702.

Fieni, F. *et al.* (2012) 'Activity of the mitochondrial calcium uniporter varies greatly between tissues.', *Nature communications*. Nature Publishing Group, 3, p. 1317. doi: 10.1038/ncomms2325.

Filadi, R. *et al.* (2015) 'Mitofusin 2 ablation increases endoplasmic reticulum-mitochondria coupling.', *Proceedings of the National Academy of Sciences of the United States of America*, 112(17), pp. E2174-81. doi: 10.1073/pnas.1504880112.

Finelli, A. *et al.* (2004) 'A model for studying Alzheimer's Abeta42-induced toxicity in Drosophila melanogaster.', *Molecular and cellular neurosciences*, 26(3), pp. 365–75. doi: 10.1016/j.mcn.2004.03.001.

Finkel, T. *et al.* (2015) 'The ins and outs of mitochondrial calcium.', *Circulation research*, 116(11), pp. 1810–9. doi: 10.1161/CIRCRESAHA.116.305484.

Foehring, R. C. *et al.* (2009) 'Endogenous calcium buffering capacity of substantia nigral dopamine neurons.', *Journal of neurophysiology*, 102(4), pp. 2326–33. doi: 10.1152/jn.00038.2009.

Fu, Y. *et al.* (2013) 'High-frequency off-target mutagenesis induced by CRISPR-Cas nucleases in human cells.', *Nature biotechnology*, 31(9), pp. 822–6. doi: 10.1038/nbt.2623.

Gandhi, S. *et al.* (2009) 'PINK1-associated Parkinson's disease is caused by neuronal vulnerability to calcium-induced cell death.', *Molecular cell*, 33(5), pp. 627–38. doi: 10.1016/j.molcel.2009.02.013.

Garry, D. J. *et al.* (1998) 'Mice without myoglobin.', *Nature*, 395(6705), pp. 905–8. doi: 10.1038/27681.

Gherardi, G. *et al.* (2018) 'Loss of mitochondrial calcium uniporter rewires skeletal muscle metabolism and substrate preference.', *Cell death and differentiation*. Springer US. doi: 10.1038/s41418-018-0191-7.

Gibb, W. R. and Lees, A. J. (1988) 'The relevance of the Lewy body to the pathogenesis of idiopathic Parkinson's disease.', *Journal of neurology, neurosurgery, and psychiatry*, 51(6), pp. 745–52. doi: 10.1136/jnnp.51.6.745.

Gibson, G. E. *et al.* (1988) 'Reduced activities of thiamine-dependent enzymes in the brains and peripheral tissues of patients with Alzheimer's disease.', *Archives of neurology*, 45(8), pp. 836–40. doi: 10.1001/archneur.1988.00520320022009.

Glater, E. E. *et al.* (2006) 'Axonal transport of mitochondria requires milton to recruit kinesin heavy chain and is light chain independent.', *The Journal of cell biology*, 173(4), pp. 545–57. doi: 10.1083/jcb.200601067.

Glenner, George G and Wong, C. W. (1984) 'Alzheimer's disease: initial report of the purification and characterization of a novel cerebrovascular amyloid protein.', *Biochemical and biophysical research communications*, 120(3), pp. 885–90. doi: 10.1016/s0006-291x(84)80190-4.

Glenner, G G and Wong, C. W. (1984) 'Alzheimer's disease and Down's syndrome: sharing of a unique cerebrovascular amyloid fibril protein.', *Biochemical and biophysical research communications*, 122(3), pp. 1131–5. doi: 10.1016/0006-291x(84)91209-9.

Gnaiger, E. (2001) 'Bioenergetics at low oxygen: dependence of respiration and phosphorylation on oxygen and adenosine diphosphate supply.', *Respiration physiology*, 128(3), pp. 277–97. doi: 10.1016/S0034-5687(01)00307-3.

Goedert, M. *et al.* (1988) 'Cloning and sequencing of the cDNA encoding a core protein of the paired helical filament of Alzheimer disease: identification as the microtubule-associated protein tau.', *Proceedings of the National Academy of Sciences of the United States of America*, 85(11), pp. 4051–5. doi: 10.1073/pnas.85.11.4051.

Goedert, M. *et al.* (1989) 'Multiple isoforms of human microtubule-associated protein tau: sequences and localization in neurofibrillary tangles of Alzheimer's disease.', *Neuron*, 3(4), pp. 519–26. doi: 10.1016/0896-6273(89)90210-9.

Goldgaber, D. *et al.* (1987) 'Characterization and chromosomal localization of a cDNA encoding brain amyloid of Alzheimer's disease.', *Science (New York, N.Y.)*, 235(4791), pp. 877–80. doi: 10.1126/science.3810169.

Goodman, Y. and Mattson, M. P. (1994) 'Secreted forms of beta-amyloid precursor protein protect hippocampal neurons against amyloid beta-peptide-induced oxidative injury.', *Experimental neurology*, 128(1), pp. 1–12. doi: 10.1006/exnr.1994.1107.

Gottschalk, B. *et al.* (2019) 'MICU1 controls cristae junction and spatially anchors mitochondrial Ca2+ uniporter complex.', *Nature communications*, 10(1), p. 3732. doi: 10.1038/s41467-019-11692-x.

Götz, K. G. (1987) 'Course-Control, Metabolism and Wing Interference During Ultralong Tethered Flight in Drosophila Melanogaster', *Journal of Experimental Biology*, 128(1), pp. 35–46.

Gratz, S. J. *et al.* (2014) 'Highly specific and efficient CRISPR/Cas9-catalyzed homology-directed repair in Drosophila.', *Genetics*, 196(4), pp. 961–71. doi: 10.1534/genetics.113.160713.

Gray, M. W. (1999) 'Mitochondrial Evolution', *Science*, 283(5407), pp. 1476–1481. doi: 10.1126/science.283.5407.1476.

Greene, A. W. *et al.* (2012) 'Mitochondrial processing peptidase regulates PINK1 processing, import and Parkin recruitment.', *EMBO reports*. Nature Publishing Group, 13(4), pp. 378–85. doi: 10.1038/embor.2012.14.

Greene, J. C. *et al.* (2003) 'Mitochondrial pathology and apoptotic muscle degeneration in Drosophila parkin mutants.', *Proceedings of the National Academy of Sciences of the United States of America*, 100(7), pp. 4078–83. doi: 10.1073/pnas.0737556100.

Greeve, I. *et al.* (2004) 'Age-dependent neurodegeneration and Alzheimer-amyloid plaque formation in transgenic Drosophila.', *The Journal of neuroscience : the official journal of the Society for Neuroscience*, 24(16), pp. 3899–906. doi: 10.1523/JNEUROSCI.0283-04.2004.

Gross, A. and Katz, S. G. (2017) 'Non-apoptotic functions of BCL-2 family proteins.', *Cell death*

and differentiation. Nature Publishing Group, 24(8), pp. 1348–1358. doi: 10.1038/cdd.2017.22.

Groth, A. C. *et al.* (2004) 'Construction of transgenic Drosophila by using the site-specific integrase from phage phiC31.', *Genetics*, 166(4), pp. 1775–82. Available at: http://www.ncbi.nlm.nih.gov/pubmed/15126397.

Grumati, P. and Dikic, I. (2018) 'Ubiquitin signaling and autophagy.', *The Journal of biological chemistry*, 293(15), pp. 5404–5413. doi: 10.1074/jbc.TM117.000117.

Guo, X. *et al.* (2005) 'The GTPase dMiro is required for axonal transport of mitochondria to Drosophila synapses.', *Neuron*, 47(3), pp. 379–93. doi: 10.1016/j.neuron.2005.06.027.

Hamilton, J. *et al.* (2018) 'Deletion of mitochondrial calcium uniporter incompletely inhibits calcium uptake and induction of the permeability transition pore in brain mitochondria', *Journal of Biological Chemistry*, 293(40), pp. 15652–15663. doi: 10.1074/jbc.RA118.002926.

Hanger, D. P. *et al.* (1992) 'Glycogen synthase kinase-3 induces Alzheimer's disease-like phosphorylation of tau: generation of paired helical filament epitopes and neuronal localisation of the kinase.', *Neuroscience letters*, 147(1), pp. 58–62. doi: 10.1016/0304-3940(92)90774-2.

Hansson, C. A. *et al.* (2004) 'Nicastrin, presenilin, APH-1, and PEN-2 form active gamma-secretase complexes in mitochondria.', *The Journal of biological chemistry*, 279(49), pp. 51654–60. doi: 10.1074/jbc.M404500200.

Hansson Petersen, C. A. *et al.* (2008) 'The amyloid beta-peptide is imported into mitochondria via the TOM import machinery and localized to mitochondrial cristae.', *Proceedings of the National Academy of Sciences of the United States of America*, 105(35), pp. 13145–50. doi: 10.1073/pnas.0806192105.

Haworth, R. A. and Hunter, D. R. (1979) 'The Ca2+-induced membrane transition in mitochondria. II. Nature of the Ca2+ trigger site.', *Archives of biochemistry and biophysics*, 195(2), pp. 460–7. doi: 10.1016/0003-9861(79)90372-2.

He, Y. and Jasper, H. (2014) 'Studying aging in Drosophila.', *Methods (San Diego, Calif.)*, 68(1), pp. 129–33. doi: 10.1016/j.ymeth.2014.04.008.

Helle, S. C. J. *et al.* (2013) 'Organization and function of membrane contact sites.', *Biochimica et biophysica acta*. Elsevier B.V., 1833(11), pp. 2526–41. doi: 10.1016/j.bbamcr.2013.01.028.

Hirabayashi, Y. *et al.* (2017) 'ER-mitochondria tethering by PDZD8 regulates Ca(2+) dynamics in mammalian neurons.', *Science (New York, N.Y.)*, 358(6363), pp. 623–630. doi: 10.1126/science.aan6009.

Hochstrasser, M. (1996) 'Ubiquitin-dependent protein degradation.', *Annual review of genetics*, 30(93), pp. 405–39. doi: 10.1146/annurev.genet.30.1.405.

Hogeboom, G. H., Claude, A. and Hotch-Kiss, R. D. (1946) 'The distribution of cytochrome oxidase and succinoxidase in the cytoplasm of the mammalian liver cell.', *The Journal of*

biological chemistry, 165(2), pp. 615–29. Available at: http://www.ncbi.nlm.nih.gov/pubmed/20276128.

Holmström, K. M. *et al.* (2015) 'Assessment of cardiac function in mice lacking the mitochondrial calcium uniporter.', *Journal of molecular and cellular cardiology*. Elsevier B.V., 85, pp. 178–82. doi: 10.1016/j.yjmcc.2015.05.022.

Honig, L. S. *et al.* (2018) 'Trial of Solanezumab for Mild Dementia Due to Alzheimer's Disease.', *The New England journal of medicine*, 378(4), pp. 321–330. doi: 10.1056/NEJMoa1705971.

Horvath, P. and Barrangou, R. (2010) 'CRISPR/Cas, the Immune System of Bacteria and Archaea', *Science*, 327(5962), pp. 167–170. doi: 10.1126/science.1179555.

Hoskins, R. A. *et al.* (2015) 'The Release 6 reference sequence of the Drosophila melanogaster genome.', *Genome research*, 25(3), pp. 445–58. doi: 10.1101/gr.185579.114.

Høyer-Hansen, M. *et al.* (2007) 'Control of macroautophagy by calcium, calmodulin-dependent kinase kinase-beta, and Bcl-2.', *Molecular cell*, 25(2), pp. 193–205. doi: 10.1016/j.molcel.2006.12.009.

Huang, G. and Docampo, R. (2018) 'The Mitochondrial Ca2+ Uniporter Complex (MCUC) of Trypanosoma brucei Is a Hetero-oligomer That Contains Novel Subunits Essential for Ca2+ Uptake.', *mBio*, 9(5), pp. 1–16. doi: 10.1128/mBio.01700-18.

Hunter, D. R. and Haworth, R. A. (1979) 'The Ca2+-induced membrane transition in mitochondria. I. The protective mechanisms.', *Archives of biochemistry and biophysics*, 195(2), pp. 453–9. doi: 10.1016/0003-9861(79)90371-0.

Hunter, D. R., Haworth, R. A. and Southard, J. H. (1976) 'Relationship between configuration, function, and permeability in calcium-treated mitochondria.', *The Journal of biological chemistry*, 251(16), pp. 5069–77. Available at: http://www.ncbi.nlm.nih.gov/pubmed/134035.

Iijima, K. *et al.* (2008) 'Abeta42 mutants with different aggregation profiles induce distinct pathologies in Drosophila.', *PloS one*, 3(2), p. e1703. doi: 10.1371/journal.pone.0001703.

Jackson, G. R. *et al.* (2002) 'Human wild-type tau interacts with wingless pathway components and produces neurofibrillary pathology in Drosophila.', *Neuron*, 34(4), pp. 509–19. doi: 10.1016/s0896-6273(02)00706-7.

Jadiya, P. *et al.* (2019) 'Impaired mitochondrial calcium efflux contributes to disease progression in models of Alzheimer's disease.', *Nature communications*, 10(1), p. 3885. doi: 10.1038/s41467-019-11813-6.

Janssen, J. M. *et al.* (2019) 'The Chromatin Structure of CRISPR-Cas9 Target DNA Controls the Balance between Mutagenic and Homology-Directed Gene-Editing Events.', *Molecular therapy. Nucleic acids*. Elsevier Ltd., 16(June), pp. 141–154. doi: 10.1016/j.omtn.2019.02.009.

Jasin, M. and Rothstein, R. (2013) 'Repair of strand breaks by homologous recombination.', *Cold Spring Harbor perspectives in biology*, 5(11), p. a012740. doi:

10.1101/cshperspect.a012740.

Jiang, D., Zhao, L. and Clapham, D. E. (2009) 'Genome-wide RNAi screen identifies Letm1 as a mitochondrial Ca2+/H+ antiporter.', *Science (New York, N.Y.)*, 326(5949), pp. 144–7. doi: 10.1126/science.1175145.

Jo, D.-G. *et al.* (2004) 'Calcium binding of ARC mediates regulation of caspase 8 and cell death.', *Molecular and cellular biology*, 24(22), pp. 9763–70. doi: 10.1128/MCB.24.22.9763-9770.2004.

Jonson, M. *et al.* (2015) 'Systematic Aβ analysis in drosophila reveals high toxicity for the 1-42, 3-42 and 11-42 peptides, and emphasizes N-and C-terminal residues', *PLoS ONE*, 10(7), pp. 1–24. doi: 10.1371/journal.pone.0133272.

Jouaville, L. S. *et al.* (1995) 'Synchronization of calcium waves by mitochondrial substrates in Xenopus laevis oocytes.', *Nature*, 377(6548), pp. 438–41. doi: 10.1038/377438a0.

Kamer, K. J. *et al.* (2018) 'MICU1 imparts the mitochondrial uniporter with the ability to discriminate between Ca2+ and Mn2+.', *Proceedings of the National Academy of Sciences of the United States of America*, 115(34), pp. E7960–E7969. doi: 10.1073/pnas.1807811115.

Kamer, K. J. *et al.* (2019) 'Crystal structure of MICU2 and comparison with MICU1 reveal insights into the uniporter gating mechanism.', *Proceedings of the National Academy of Sciences of the United States of America*, p. 201817759. doi: 10.1073/pnas.1817759116.

Kamer, K. J., Grabarek, Z. and Mootha, V. K. (2017) 'High-affinity cooperative Ca(2+) binding by MICU1-MICU2 serves as an on-off switch for the uniporter.', *EMBO reports*, p. e201643748. doi: 10.15252/embr.201643748.

Kamer, K. J. and Mootha, V. K. (2014) 'MICU1 and MICU2 play nonredundant roles in the regulation of the mitochondrial calcium uniporter.', *EMBO reports*, 15(3), pp. 299–307. doi: 10.1002/embr.201337946.

Kamer, K. J. and Mootha, V. K. (2015) 'The molecular era of the mitochondrial calcium uniporter.', *Nature reviews. Molecular cell biology*. Nature Publishing Group, 16(9), pp. 545–53. doi: 10.1038/nrm4039.

Kane, L. A. *et al.* (2014) 'PINK1 phosphorylates ubiquitin to activate Parkin E3 ubiquitin ligase activity.', *The Journal of cell biology*, 205(2), pp. 143–53. doi: 10.1083/jcb.201402104.

Kang, J. *et al.* (1987) 'The precursor of Alzheimer's disease amyloid A4 protein resembles a cell-surface receptor.', *Nature*, 325(6106), pp. 733–6. doi: 10.1038/325733a0.

Kennedy, E. P. and Lehninger, A. L. (1949) 'Oxidation of fatty acids and tricarboxylic acid cycle intermediates by isolated rat liver mitochondria.', *The Journal of biological chemistry*, 179(2), pp. 957–72. Available at: http://www.ncbi.nlm.nih.gov/pubmed/18150026.

Kirichok, Y., Krapivinsky, G. and Clapham, D. E. (2004) 'The mitochondrial calcium uniporter is a highly selective ion channel.', *Nature*, 427(6972), pp. 360–4. doi: 10.1038/nature02246.

Kirisako, T. *et al.* (2006) 'A ubiquitin ligase complex assembles linear polyubiquitin chains.', *The EMBO journal*, 25(20), pp. 4877–87. doi: 10.1038/sj.emboj.7601360.

Kischkel, F. C. *et al.* (1995) 'Cytotoxicity-dependent APO-1 (Fas/CD95)-associated proteins form a death-inducing signaling complex (DISC) with the receptor.', *The EMBO journal*, 14(22), pp. 5579–88. doi: 10.1002/j.1460-2075.1995.tb00245.x.

Kitada, T. *et al.* (1998) 'Mutations in the parkin gene cause autosomal recessive juvenile parkinsonism.', *Nature*, 392(6676), pp. 605–8. doi: 10.1038/33416.

Kitada, T. *et al.* (2007) 'Impaired dopamine release and synaptic plasticity in the striatum of PINK1-deficient mice.', *Proceedings of the National Academy of Sciences of the United States of America*, 104(27), pp. 11441–6. doi: 10.1073/pnas.0702717104.

Kleinstiver, B. P. *et al.* (2016) 'High-fidelity CRISPR-Cas9 nucleases with no detectable genome-wide off-target effects.', *Nature*. Nature Publishing Group. doi: 10.1038/nature16526.

Kon, N. *et al.* (2017) 'DS16570511 is a small-molecule inhibitor of the mitochondrial calcium uniporter.', *Cell death discovery*. Nature Publishing Group, 3(May), p. 17045. doi: 10.1038/cddiscovery.2017.45.

Kondapalli, C. *et al.* (2012) 'PINK1 is activated by mitochondrial membrane potential depolarization and stimulates Parkin E3 ligase activity by phosphorylating Serine 65', *Open Biology*, 2(5), pp. 120080–120080. doi: 10.1098/rsob.120080.

König, T. *et al.* (2016) 'The m-AAA Protease Associated with Neurodegeneration Limits MCU Activity in Mitochondria.', *Molecular cell*, pp. 1–15. doi: 10.1016/j.molcel.2016.08.020.

Kornmann, B. *et al.* (2009) 'An ER-mitochondria tethering complex revealed by a synthetic biology screen.', *Science (New York, N.Y.)*, 325(5939), pp. 477–81. doi: 10.1126/science.1175088.

Kostic, M. *et al.* (2015) 'PKA Phosphorylation of NCLX Reverses Mitochondrial Calcium Overload and Depolarization, Promoting Survival of PINK1-Deficient Dopaminergic Neurons.', *Cell reports*. The Authors, 13(2), pp. 376–86. doi: 10.1016/j.celrep.2015.08.079.

Kovács-Bogdán, E. *et al.* (2014) 'Reconstitution of the mitochondrial calcium uniporter in yeast.', *Proceedings of the National Academy of Sciences of the United States of America*, 111(24), pp. 8985–90. doi: 10.1073/pnas.1400514111.

Koval, O. M. *et al.* (2019) 'Loss of MCU prevents mitochondrial fusion in G1-S phase and blocks cell cycle progression and proliferation.', *Science signaling*, 12(579), pp. 1–14. doi: 10.1126/scisignal.aav1439.

Koyano, F. *et al.* (2014) 'Ubiquitin is phosphorylated by PINK1 to activate parkin.', *Nature*. Nature Publishing Group, 510(7503), pp. 162–6. doi: 10.1038/nature13392.

Kwong, J. Q. *et al.* (2015) 'The Mitochondrial Calcium Uniporter Selectively Matches Metabolic Output to Acute Contractile Stress in the Heart.', *Cell reports*. The Authors, 12(1),

pp. 15–22. doi: 10.1016/j.celrep.2015.06.002.

Kwong, J. Q. *et al.* (2018) 'The mitochondrial calcium uniporter underlies metabolic fuel preference in skeletal muscle.', *JCI insight*, 3(22). doi: 10.1172/jci.insight.121689.

Lambert, J. P. *et al.* (2019) 'MCUB Regulates the Molecular Composition of the Mitochondrial Calcium Uniporter Channel to Limit Mitochondrial Calcium Overload During Stress.', *Circulation*, 140(21), pp. 1720–1733. doi: 10.1161/CIRCULATIONAHA.118.037968.

Lamkanfi, M. and Kanneganti, T.-D. (2010) 'Caspase-7: a protease involved in apoptosis and inflammation.', *The international journal of biochemistry & cell biology*, 42(1), pp. 21–4. doi: 10.1016/j.biocel.2009.09.013.

Langston, J. *et al.* (1983) 'Chronic Parkinsonism in humans due to a product of meperidine-analog synthesis', *Science*, 219(4587), pp. 979–980. doi: 10.1126/science.6823561.

Lanner, J. T. *et al.* (2010) 'Ryanodine receptors: structure, expression, molecular details, and function in calcium release.', *Cold Spring Harbor perspectives in biology*, 2(11), p. a003996. doi: 10.1101/cshperspect.a003996.

de Lau, L. M. L. and Breteler, M. M. B. (2006) 'Epidemiology of Parkinson's disease.', *The Lancet. Neurology*, 5(6), pp. 525–35. doi: 10.1016/S1474-4422(06)70471-9.

Lee, J. J. *et al.* (2018) 'Basal mitophagy is widespread in Drosophila but minimally affected by loss of Pink1 or parkin.', *The Journal of cell biology*, 217(5), pp. 1613–1622. doi: 10.1083/jcb.201801044.

Lee, K.-S. *et al.* (2018) 'Altered ER-mitochondria contact impacts mitochondria calcium homeostasis and contributes to neurodegeneration in vivo in disease models.', *Proceedings of the National Academy of Sciences of the United States of America*, p. 201721136. doi: 10.1073/pnas.1721136115.

Lehninger, A. L. (1949) 'Esterification of inorganic phosphate coupled to electron transport between dihydrodiphosphopyridine nucleotide and oxygen.', *The Journal of biological chemistry*, 178(2), pp. 611–44. Available at: http://www.ncbi.nlm.nih.gov/pubmed/18116985.

Levy-Lahad, E., Wijsman, E. M., *et al.* (1995) 'A familial Alzheimer's disease locus on chromosome 1.', *Science (New York, N.Y.)*, 269(5226), pp. 970–3. doi: 10.1126/science.7638621.

Levy-Lahad, E., Wasco, W., *et al.* (1995) 'Candidate gene for the chromosome 1 familial Alzheimer's disease locus.', *Science (New York, N.Y.)*, 269(5226), pp. 973–7. doi: 10.1126/science.7638622.

Lewis-Smith, D. *et al.* (2016) 'Homozygous deletion in MICU1 presenting with fatigue and lethargy in childhood', *Neurology: Genetics*, 2(2), pp. e59–e59. doi: 10.1212/NXG.0000000000000059.

Li, P. *et al.* (1997) 'Cytochrome c and dATP-dependent formation of Apaf-1/caspase-9

complex initiates an apoptotic protease cascade.', *Cell*, 91(4), pp. 479–89. doi: 10.1016/s0092-8674(00)80434-1.

Liao, Y. *et al.* (2015) 'Mitochondrial calcium uniporter protein MCU is involved in oxidative stress-induced cell death.', *Protein & cell*. Higher Education Press, 6(6), pp. 434–42. doi: 10.1007/s13238-015-0144-6.

Liou, J. *et al.* (2005) 'STIM is a Ca2+ sensor essential for Ca2+-store-depletion-triggered Ca2+ influx.', *Current biology : CB*, 15(13), pp. 1235–41. doi: 10.1016/j.cub.2005.05.055.

Liu, J. C. *et al.* (2016) 'MICU1 Serves as a Molecular Gatekeeper to Prevent In Vivo Mitochondrial Calcium Overload.', *Cell reports*, 16(6), pp. 1561–73. doi: 10.1016/j.celrep.2016.07.011.

Liu, Q. *et al.* (2012) 'Two dopaminergic neurons signal to the dorsal fan-shaped body to promote wakefulness in Drosophila.', *Current biology : CB*. Elsevier Ltd, 22(22), pp. 2114–23. doi: 10.1016/j.cub.2012.09.008.

Liu, Z. *et al.* (2008) 'A Drosophila model for LRRK2-linked parkinsonism.', *Proceedings of the National Academy of Sciences of the United States of America*, 105(7), pp. 2693–8. doi: 10.1073/pnas.0708452105.

Logan, C. V *et al.* (2014) 'Loss-of-function mutations in MICU1 cause a brain and muscle disorder linked to primary alterations in mitochondrial calcium signaling.', *Nature genetics*. Nature Publishing Group, 46(2), pp. 188–93. doi: 10.1038/ng.2851.

Lomax, R. B. *et al.* (2002) 'Basal and physiological Ca(2+) leak from the endoplasmic reticulum of pancreatic acinar cells. Second messenger-activated channels and translocons.', *The Journal of biological chemistry*, 277(29), pp. 26479–85. doi: 10.1074/jbc.M201845200.

Long, D. M. *et al.* (2014) 'Relationships between the circadian system and Alzheimer's disease-like symptoms in Drosophila.', *PloS one*, 9(8), p. e106068. doi: 10.1371/journal.pone.0106068.

Luongo, T. S. *et al.* (2015) 'The Mitochondrial Calcium Uniporter Matches Energetic Supply with Cardiac Workload during Stress and Modulates Permeability Transition.', *Cell reports*. The Authors, 12(1), pp. 23–34. doi: 10.1016/j.celrep.2015.06.017.

Macaskill, A. F. *et al.* (2009) 'Miro1 is a calcium sensor for glutamate receptor-dependent localization of mitochondria at synapses.', *Neuron*. Elsevier Ltd, 61(4), pp. 541–55. doi: 10.1016/j.neuron.2009.01.030.

MacEwen, M. J. S. *et al.* (2019) 'Molecular basis of EMRE-dependence of the human mitochondrial calcium uniporter'. doi: 10.1101/637918.

Madreiter-Sokolowski, C. T. *et al.* (2016) 'PRMT1-mediated methylation of MICU1 determines the UCP2/3 dependency of mitochondrial Ca(2+) uptake in immortalized cells.', *Nature communications*. Nature Publishing Group, 7, p. 12897. doi: 10.1038/ncomms12897.

Mahaney, B. L., Meek, K. and Lees-Miller, S. P. (2009) 'Repair of ionizing radiation-induced

DNA double-strand breaks by non-homologous end-joining.', *The Biochemical journal*, 417(3), pp. 639–50. doi: 10.1042/BJ20080413.

Mak, D. O., McBride, S. and Foskett, J. K. (1998) 'Inositol 1,4,5-trisphosphate [correction of tris-phosphate] activation of inositol trisphosphate [correction of tris-phosphate] receptor Ca2+ channel by ligand tuning of Ca2+ inhibition.', *Proceedings of the National Academy of Sciences of the United States of America*, 95(26), pp. 15821–5. doi: 10.1073/pnas.95.26.15821.

Makarova, K. S. and Koonin, E. V (2015) 'Annotation and Classification of CRISPR-Cas Systems.', *Methods in molecular biology (Clifton, N.J.)*, 1311, pp. 47–75. doi: 10.1007/978-1-4939-2687-9_4.

Mallilankaraman, K., Cárdenas, C., *et al.* (2012) 'MCUR1 is an essential component of mitochondrial Ca2+ uptake that regulates cellular metabolism.', *Nature cell biology*. Nature Publishing Group, 14(12), pp. 1336–43. doi: 10.1038/ncb2622.

Mallilankaraman, K., Doonan, P., *et al.* (2012) 'MICU1 is an essential gatekeeper for MCU-mediated mitochondrial Ca(2+) uptake that regulates cell survival.', *Cell*, 151(3), pp. 630–44. doi: 10.1016/j.cell.2012.10.011.

Mammucari, C. *et al.* (2015) 'The mitochondrial calcium uniporter controls skeletal muscle trophism in vivo.', *Cell reports*. The Authors, 10(8), pp. 1269–79. doi: 10.1016/j.celrep.2015.01.056.

Marsden, C. D. and Parkes, J. D. (1977) 'Success and problems of long-term levodopa therapy in Parkinson's disease.', *Lancet (London, England)*, 1(8007), pp. 345–9. doi: 10.1016/s0140-6736(77)91146-1.

Matsumine, H. *et al.* (1997) 'Localization of a gene for an autosomal recessive form of juvenile Parkinsonism to chromosome 6q25.2-27.', *American journal of human genetics*, 60(3), pp. 588–96. Available at: http://www.ncbi.nlm.nih.gov/pubmed/9042918.

Mattson, M. P. *et al.* (1993) 'Evidence for excitoprotective and intraneuronal calcium-regulating roles for secreted forms of the beta-amyloid precursor protein.', *Neuron*, 10(2), pp. 243–54. doi: 10.1016/0896-6273(93)90315-I.

McClintock, B. (1950) 'The origin and behavior of mutable loci in maize.', *Proceedings of the National Academy of Sciences of the United States of America*, 36(6), pp. 344–55. doi: 10.1073/pnas.36.6.344.

McCormack, J. G. and Denton, R. M. (1979) 'The effects of calcium ions and adenine nucleotides on the activity of pig heart 2-oxoglutarate dehydrogenase complex.', *The Biochemical journal*, 180(3), pp. 533–44. doi: 10.1042/bj1800533.

McCormack, J. G. and Denton, R. M. (1981) 'A comparative study of the regulation by Ca2 + of the activities of the 2-oxoglutarate dehydrogenase complex and NAD + -iso-citrate dehydrogenase from a variety of sources', *Biochemical Journal*, 196, pp. 619–624.

McKhann, G. *et al.* (1984) 'Clinical diagnosis of Alzheimer's disease: report of the NINCDS-ADRDA Work Group under the auspices of Department of Health and Human Services Task Force on Alzheimer's Disease.', *Neurology*, 34(7), pp. 939–44. doi: 10.1212/wnl.34.7.939.

McShane, R. *et al.* (2019) 'Memantine for dementia.', *The Cochrane database of systematic reviews*, 3(2), p. CD003154. doi: 10.1002/14651858.CD003154.pub6.

Medler, K. and Gleason, E. L. (2002) 'Mitochondrial Ca(2+) buffering regulates synaptic transmission between retinal amacrine cells.', *Journal of neurophysiology*, 87(3), pp. 1426–39. doi: 10.1152/jn.00627.2001.

Merkey, A. B. *et al.* (2011) 'Energetics of metamorphosis in Drosophila melanogaster.', *Journal of insect physiology*. Elsevier Ltd, 57(10), pp. 1437–45. doi: 10.1016/j.jinsphys.2011.07.013.

Meulener, M. *et al.* (2005) 'Drosophila DJ-1 mutants are selectively sensitive to environmental toxins associated with Parkinson's disease', *Current Biology*, 15(17), pp. 1572–1577. doi: 10.1016/j.cub.2005.07.064.

Michels, G. *et al.* (2009) 'Regulation of the human cardiac mitochondrial Ca2+ uptake by 2 different voltage-gated Ca2+ channels.', *Circulation*, 119(18), pp. 2435–43. doi: 10.1161/CIRCULATIONAHA.108.835389.

Mitchell, P. (1961) 'Coupling of phosphorylation to electron and hydrogen transfer by a chemi-osmotic type of mechanism.', *Nature*, 191(4784), pp. 144–8. doi: 10.1038/191144a0.

Mojica, F. J. M. *et al.* (2005) 'Intervening sequences of regularly spaced prokaryotic repeats derive from foreign genetic elements.', *Journal of molecular evolution*, 60(2), pp. 174–82. doi: 10.1007/s00239-004-0046-3.

Morais, V. A. *et al.* (2009) 'Parkinson's disease mutations in PINK1 result in decreased Complex I activity and deficient synaptic function.', *EMBO molecular medicine*, 1(2), pp. 99–111. doi: 10.1002/emmm.200900006.

Morais, V. A. *et al.* (2014) 'PINK1 loss-of-function mutations affect mitochondrial complex I activity via NdufA10 ubiquinone uncoupling.', *Science (New York, N.Y.)*, 344(6180), pp. 203–7. doi: 10.1126/science.1249161.

Mosley, R. L. *et al.* (2012) 'Inflammation and adaptive immunity in Parkinson's disease.', *Cold Spring Harbor perspectives in medicine*, 2(1), p. a009381. doi: 10.1101/cshperspect.a009381.

Motloch, L. J. *et al.* (2016) 'By Regulating Mitochondrial Ca2+-Uptake UCP2 Modulates Intracellular Ca2.', *PloS one*, 11(2), p. e0148359. doi: 10.1371/journal.pone.0148359.

Mullan, M. *et al.* (1992) 'A locus for familial early-onset Alzheimer's disease on the long arm of chromosome 14, proximal to the alpha 1-antichymotrypsin gene.', *Nature genetics*, 2(4), pp. 340–2. doi: 10.1038/ng1292-340.

Mullin, S. and Schapira, A. (2013) 'α-Synuclein and mitochondrial dysfunction in Parkinson's disease.', *Molecular neurobiology*, 47(2), pp. 587–97. doi: 10.1007/s12035-013-8394-x.

Murphy, E. *et al.* (2014) 'Unresolved questions from the analysis of mice lacking MCU expression.', *Biochemical and biophysical research communications*. Elsevier Inc., 449(4), pp. 384–5. doi: 10.1016/j.bbrc.2014.04.144.

Naon, D. *et al.* (2016) 'Critical reappraisal confirms that Mitofusin 2 is an endoplasmic reticulum-mitochondria tether.', *Proceedings of the National Academy of Sciences of the United States of America*, pp. 1–6. doi: 10.1073/pnas.1606786113.

Nass, M. M. and Nass, S. (1963) 'Intramitochondrial Fibers with DNA Characteristics. I. Fixation and Electron Staining Reactions.', *The Journal of cell biology*, 19, pp. 593–611. doi: 10.1083/jcb.19.3.593.

Nguyen, N. X. *et al.* (2018) 'Cryo-EM structure of a fungal mitochondrial calcium uniporter.', *Nature*. Springer US, 559(7715), pp. 570–574. doi: 10.1038/s41586-018-0333-6.

Niccoli, T. *et al.* (2016) 'Increased Glucose Transport into Neurons Rescues Aβ Toxicity in Drosophila.', *Current biology : CB*, 26(17), pp. 2291–300. doi: 10.1016/j.cub.2016.07.017.

Niescier, R. F., Chang, K. T. and Min, K.-T. (2013) 'Miro, MCU, and calcium: bridging our understanding of mitochondrial movement in axons.', *Frontiers in cellular neuroscience*, 7(September), p. 148. doi: 10.3389/fncel.2013.00148.

Nilsberth, C. *et al.* (2001) 'The "Arctic" APP mutation (E693G) causes Alzheimer's disease by enhanced Aβ protofibril formation', *Nature neuroscience*, 4(9), pp. 887–893. doi: 10.1038/nn0901-887.

Nowikovsky, K. *et al.* (2004) 'The LETM1/YOL027 gene family encodes a factor of the mitochondrial K+ homeostasis with a potential role in the Wolf-Hirschhorn syndrome.', *The Journal of biological chemistry*, 279(29), pp. 30307–15. doi: 10.1074/jbc.M403607200.

Nowikovsky, K. and Bernardi, P. (2014) 'LETM1 in mitochondrial cation transport.', *Frontiers in physiology*, 5(2), p. 83. doi: 10.3389/fphys.2014.00083.

Olson, M. I. and Shaw, C. M. (1969) 'Presenile dementia and Alzheimer's disease in mongolism.', *Brain : a journal of neurology*, 92(1), pp. 147–56. doi: 10.1093/brain/92.1.147.

Oslowski, C. M. and Urano, F. (2011) 'Measuring ER stress and the unfolded protein response using mammalian tissue culture system.', *Methods in enzymology*, 490(508), pp. 71–92. doi: 10.1016/B978-0-12-385114-7.00004-0.

Oxenoid, K. *et al.* (2016) 'Architecture of the mitochondrial calcium uniporter.', *Nature*. Nature Publishing Group, pp. 1–17. doi: 10.1038/nature17656.

Paillard, M. *et al.* (2018) 'MICU1 Interacts with the D-Ring of the MCU Pore to Control Its Ca2+ Flux and Sensitivity to Ru360.', *Molecular cell*, 72(4), pp. 778-785.e3. doi: 10.1016/j.molcel.2018.09.008.

Palty, R. *et al.* (2010) 'NCLX is an essential component of mitochondrial Na+/Ca2+ exchange.', *Proceedings of the National Academy of Sciences of the United States of America*, 107(1), pp. 436–41. doi: 10.1073/pnas.0908099107.

Pan, X. *et al.* (2013) 'The physiological role of mitochondrial calcium revealed by mice lacking the mitochondrial calcium uniporter.', *Nature cell biology*. Nature Publishing Group, 15(12), pp. 1464–72. doi: 10.1038/ncb2868.

Park, J. *et al.* (2006) 'Mitochondrial dysfunction in Drosophila PINK1 mutants is complemented by parkin.', *Nature*, 441(7097), pp. 1157–61. doi: 10.1038/nature04788.

Parker, W. D., Filley, C. M. and Parks, J. K. (1990) 'Cytochrome oxidase deficiency in Alzheimer's disease.', *Neurology*, 40(8), pp. 1302–3. doi: 10.1212/wnl.40.8.1302.

Parkinson, J. (2002) 'An essay on the shaking palsy. 1817.', *The Journal of neuropsychiatry and clinical neurosciences*, 14(2), pp. 223–36; discussion 222. doi: 10.1176/jnp.14.2.223.

Patron, M. *et al.* (2014) 'MICU1 and MICU2 finely tune the mitochondrial Ca2+ uniporter by exerting opposite effects on MCU activity.', *Molecular cell*, 53(5), pp. 726–37. doi: 10.1016/j.molcel.2014.01.013.

Patron, M. *et al.* (2018) 'MICU3 is a tissue-specific enhancer of mitochondrial calcium uptake.', *Cell death and differentiation*. Springer US. doi: 10.1038/s41418-018-0113-8.

Paupe, V. *et al.* (2015) 'CCDC90A (MCUR1) is a cytochrome c oxidase assembly factor and not a regulator of the mitochondrial calcium uniporter.', *Cell metabolism*. Elsevier Inc., 21(1), pp. 109–16. doi: 10.1016/j.cmet.2014.12.004.

Payne, R. *et al.* (2017) 'MICU2 Restricts Spatial Crosstalk between InsP 3 R and MCU Channels by Regulating Threshold and Gain of MICU1-Mediated Inhibition and Activation of MCU', *Cell Reports*. ElsevierCompany., 21(11), pp. 3141–3154. doi: 10.1016/j.celrep.2017.11.064.

Perez, F. A. and Palmiter, R. D. (2005) 'Parkin-deficient mice are not a robust model of parkinsonism.', *Proceedings of the National Academy of Sciences of the United States of America*, 102(6), pp. 2174–9. doi: 10.1073/pnas.0409598102.

Perocchi, F. *et al.* (2010) 'MICU1 encodes a mitochondrial EF hand protein required for Ca(2+) uptake.', *Nature*. Nature Publishing Group, 467(7313), pp. 291–6. doi: 10.1038/nature09358.

Petrungaro, C. *et al.* (2015) 'The Ca(2+)-Dependent Release of the Mia40-Induced MICU1-MICU2 Dimer from MCU Regulates Mitochondrial Ca(2+) Uptake.', *Cell metabolism*, pp. 1–13. doi: 10.1016/j.cmet.2015.08.019.

Phillips, C. B., Tsai, C.-W. and Tsai, M.-F. (2019) 'The conserved aspartate ring of MCU mediates MICU1 binding and regulation in the mitochondrial calcium uniporter complex.', *eLife*, 8, pp. 1–16. doi: 10.7554/eLife.41112.

Phillips, M. J. and Voeltz, G. K. (2016) 'Structure and function of ER membrane contact sites with other organelles.', *Nature reviews. Molecular cell biology*. Nature Publishing Group, 17(2), pp. 69–82. doi: 10.1038/nrm.2015.8.

Pickrell, A. M. *et al.* (2015) 'Endogenous Parkin Preserves Dopaminergic Substantia Nigral Neurons following Mitochondrial DNA Mutagenic Stress.', *Neuron*. Elsevier Inc., 87(2), pp. 371–81. doi: 10.1016/j.neuron.2015.06.034.

Plovanich, M. *et al.* (2013) 'MICU2, a paralog of MICU1, resides within the mitochondrial uniporter complex to regulate calcium handling.', *PloS one*, 8(2), p. e55785. doi: 10.1371/journal.pone.0055785.

Pogson, J. H. *et al.* (2014) 'The complex I subunit NDUFA10 selectively rescues Drosophila pink1 mutants through a mechanism independent of mitophagy.', *PLoS genetics*, 10(11), p. e1004815. doi: 10.1371/journal.pgen.1004815.

Polymeropoulos, M. H. *et al.* (1997) 'Mutation in the alpha-synuclein gene identified in families with Parkinson's disease.', *Science (New York, N.Y.)*, 276(5321), pp. 2045–7. doi: 10.1126/science.276.5321.2045.

Poole, A. C. *et al.* (2008) 'The PINK1/Parkin pathway regulates mitochondrial morphology.', *Proceedings of the National Academy of Sciences of the United States of America*, 105(5), pp. 1638–43. doi: 10.1073/pnas.0709336105.

Port, F. *et al.* (2014) 'Optimized CRISPR/Cas tools for efficient germline and somatic genome engineering in Drosophila.', *Proceedings of the National Academy of Sciences of the United States of America*, 111(29), pp. E2967-76. doi: 10.1073/pnas.1405500111.

Prudent, J. *et al.* (2013) 'Bcl-wav and the mitochondrial calcium uniporter drive gastrula morphogenesis in zebrafish.', *Nature communications*. Nature Publishing Group, 4, p. 2330. doi: 10.1038/ncomms3330.

Prudent, J. *et al.* (2015) 'MAPL SUMOylation of Drp1 Stabilizes an ER/Mitochondrial Platform Required for Cell Death.', *Molecular cell*. Elsevier Ltd, 59(6), pp. 941–55. doi: 10.1016/j.molcel.2015.08.001.

Prudent, J. *et al.* (2016) 'Mitochondrial Ca(2+) uptake controls actin cytoskeleton dynamics during cell migration.', *Scientific reports*. Nature Publishing Group, 6(May), p. 36570. doi: 10.1038/srep36570.

Qiu, J. *et al.* (2013) 'Mitochondrial calcium uniporter Mcu controls excitotoxicity and is transcriptionally repressed by neuroprotective nuclear calcium signals.', *Nature communications*. Nature Publishing Group, 4(3), p. 2034. doi: 10.1038/ncomms3034.

Raffaello, A. *et al.* (2013) 'The mitochondrial calcium uniporter is a multimer that can include a dominant-negative pore-forming subunit', *EMBO Journal*, 32(17), pp. 2362–2376. doi: 10.1038/emboj.2013.157.

Ramsay, R. R. *et al.* (1987) 'The inhibition site of MPP+, the neurotoxic bioactivation product of 1-methyl-4-phenyl-1,2,3,6-tetrahydropyridine is near the Q-binding site of NADH dehydrogenase.', *Archives of biochemistry and biophysics*, 259(2), pp. 645–9. doi: 10.1016/0003-9861(87)90531-5.

Ramsay, R. R., Salach, J. I. and Singer, T. P. (1986) 'Uptake of the neurotoxin 1-methyl-4-phenylpyridine (MPP+) by mitochondria and its relation to the inhibition of the mitochondrial oxidation of NAD+-linked substrates by MPP+.', *Biochemical and biophysical research communications*, 134(2), pp. 743–8. doi: 10.1016/s0006-291x(86)80483-1.

Rasmussen, T. P. *et al.* (2015) 'Inhibition of MCU forces extramitochondrial adaptations governing physiological and pathological stress responses in heart.', *Proceedings of the National Academy of Sciences of the United States of America*, 112(29), pp. 9129–34. doi: 10.1073/pnas.1504705112.

Ray, A., Speese, S. D. and Logan, M. A. (2017) 'Glial Draper Rescues Aβ Toxicity in a Drosophila Model of Alzheimer's Disease.', *The Journal of neuroscience : the official journal of the Society for Neuroscience*, 37(49), pp. 11881–11893. doi: 10.1523/JNEUROSCI.0862-17.2017.

Richards, J. G. *et al.* (2003) 'PS2APP transgenic mice, coexpressing hPS2mut and hAPPswe, show age-related cognitive deficits associated with discrete brain amyloid deposition and inflammation.', *The Journal of neuroscience : the official journal of the Society for Neuroscience*, 23(26), pp. 8989–9003. Available at: http://www.ncbi.nlm.nih.gov/pubmed/14523101.

Rizzuto, R. *et al.* (1992) 'Rapid changes of mitochondrial Ca2+ revealed by specifically targeted recombinant aequorin.', *Nature*, 358(6384), pp. 325–7. doi: 10.1038/358325a0.

Rizzuto, R. *et al.* (1993) 'Microdomains with high Ca2+ close to IP3-sensitive channels that are sensed by neighboring mitochondria.', *Science (New York, N.Y.)*, 262(5134), pp. 744–7. doi: 10.1126/science.8235595.

Rizzuto, R. *et al.* (1998) 'Close contacts with the endoplasmic reticulum as determinants of mitochondrial Ca2+ responses.', *Science (New York, N.Y.)*, 280(5370), pp. 1763–6. doi: 10.1126/science.280.5370.1763.

Rizzuto, R. *et al.* (2009) 'Ca(2+) transfer from the ER to mitochondria: when, how and why.', *Biochimica et biophysica acta*. Elsevier B.V., 1787(11), pp. 1342–51. doi: 10.1016/j.bbabio.2009.03.015.

Robakis, N. K. *et al.* (1987) 'Molecular cloning and characterization of a cDNA encoding the cerebrovascular and the neuritic plaque amyloid peptides.', *Proceedings of the National Academy of Sciences of the United States of America*, 84(12), pp. 4190–4. doi: 10.1073/pnas.84.12.4190.

Robertson, M. and Keene, A. C. (2013) 'Molecular mechanisms of age-related sleep loss in the fruit fly - a mini-review.', *Gerontology*, 59(4), pp. 334–9. doi: 10.1159/000348576.

Roche (2019) *Roche to discontinue Phase III CREAD 1 and 2 clinical studies of crenezumab in early Alzheimer's disease (AD) - other company programmes in AD continue*. Available at: https://www.roche.com/media/releases/med-cor-2019-01-30.htm (Accessed: 14 August 2019).

Ronchi, J. A. *et al.* (2013) 'A spontaneous mutation in the nicotinamide nucleotide transhydrogenase gene of C57BL/6J mice results in mitochondrial redox abnormalities.', *Free radical biology & medicine*. Elsevier, 63, pp. 446–56. doi: 10.1016/j.freeradbiomed.2013.05.049.

Roos, J. *et al.* (2005) 'STIM1, an essential and conserved component of store-operated Ca2+

channel function.', *The Journal of cell biology*, 169(3), pp. 435–45. doi: 10.1083/jcb.200502019.

Rørth, P. (1998) 'Gal4 in the Drosophila female germline.', *Mechanisms of development*, 78(1–2), pp. 113–8. Available at: http://www.ncbi.nlm.nih.gov/pubmed/9858703.

Rossi, C. S. and Lehninger, A. L. (1963) 'STOICHIOMETRIC RELATIONSHIPS BETWEEN ACCUMULATION OF IONS BY MITOCHONDRIA AND THE ENERGY-COUPLING SITES IN THE RESPIRATORY CHAIN.', *Biochemische Zeitschrift*, 338, pp. 698–713. Available at: http://www.ncbi.nlm.nih.gov/pubmed/14087335.

Rubin, G. M. *et al.* (2000) 'Comparative genomics of the eukaryotes.', *Science (New York, N.Y.)*, 287(5461), pp. 2204–15. doi: 10.1126/science.287.5461.2204.

Rubin, G. M., Kidwell, M. G. and Bingham, P. M. (1982) 'The molecular basis of P-M hybrid dysgenesis: the nature of induced mutations.', *Cell*, 29(3), pp. 987–94. doi: 10.1016/0092-8674(82)90462-7.

Rueden, C. T. *et al.* (2017) 'ImageJ2: ImageJ for the next generation of scientific image data', *BMC Bioinformatics*. BMC Bioinformatics, 18(1), p. 529. doi: 10.1186/s12859-017-1934-z.

Samanta, K., Douglas, S. and Parekh, A. B. (2014) 'Mitochondrial calcium uniporter MCU supports cytoplasmic Ca2+ oscillations, store-operated Ca2+ entry and Ca2+-dependent gene expression in response to receptor stimulation.', *PloS one*, 9(7), p. e101188. doi: 10.1371/journal.pone.0101188.

Samanta, K., Mirams, G. R. and Parekh, A. B. (2018) 'Sequential forward and reverse transport of the Na+ Ca2+ exchanger generates Ca2+ oscillations within mitochondria', *Nature Communications*. Springer US, 9(1), p. 156. doi: 10.1038/s41467-017-02638-2.

Sancak, Y. *et al.* (2013) 'EMRE is an essential component of the mitochondrial calcium uniporter complex.', *Science (New York, N.Y.)*, 342(6164), pp. 1379–82. doi: 10.1126/science.1242993.

Sanz-Blasco, S. *et al.* (2008) 'Mitochondrial Ca2+ overload underlies Abeta oligomers neurotoxicity providing an unexpected mechanism of neuroprotection by NSAIDs.', *PloS one*, 3(7), p. e2718. doi: 10.1371/journal.pone.0002718.

Saotome, M. *et al.* (2008) 'Bidirectional Ca2+-dependent control of mitochondrial dynamics by the Miro GTPase.', *Proceedings of the National Academy of Sciences of the United States of America*, 105(52), pp. 20728–33. doi: 10.1073/pnas.0808953105.

Sarkar, S. *et al.* (2005) 'Lithium induces autophagy by inhibiting inositol monophosphatase.', *The Journal of cell biology*, 170(7), pp. 1101–11. doi: 10.1083/jcb.200504035.

Schindelin, J. *et al.* (2012) 'Fiji: an open-source platform for biological-image analysis', *Nature Methods*, 9(7), pp. 676–682. doi: 10.1038/nmeth.2019.

Schmittgen, T. D. and Livak, K. J. (2008) 'Analyzing real-time PCR data by the comparative C(T) method.', *Nature protocols*, 3(6), pp. 1101–8. doi: 10.1038/nprot.2008.73.

Schwarzer, C. *et al.* (2002) 'Voltage-dependent anion-selective channel (VDAC) interacts with the dynein light chain Tctex1 and the heat-shock protein PBP74.', *The international journal of biochemistry & cell biology*, 34(9), pp. 1059–70. doi: 10.1016/S1357-2725(02)00026-2.

Service, P. M. (1989) 'The effect of mating status on lifespan, egg laying, and starvation resistance in Drosophila melanogaster in relation to selection on longevity', *Journal of Insect Physiology*, 35(5), pp. 447–452. doi: 10.1016/0022-1910(89)90120-0.

Shamseldin, H. E. *et al.* (2017) 'A null mutation in MICU2 causes abnormal mitochondrial calcium homeostasis and a severe neurodevelopmental disorder.', *Brain : a journal of neurology*, 140(11), pp. 2806–2813. doi: 10.1093/brain/awx237.

Shanker, A. *et al.* (2017) 'Innate-Adaptive Immune Crosstalk 2016.', *Journal of immunology research*, 2017, p. 3503207. doi: 10.1155/2017/3503207.

Shaw, T. J. and Martin, P. (2009) 'Wound repair at a glance.', *Journal of cell science*, 122(Pt 18), pp. 3209–13. doi: 10.1242/jcs.031187.

Shiba-Fukushima, K. *et al.* (2014) 'Lysine 63-linked polyubiquitination is dispensable for Parkin-mediated mitophagy.', *The Journal of biological chemistry*, 289(48), pp. 33131–6. doi: 10.1074/jbc.C114.580944.

Slater, E. C. (1953) 'Mechanism of phosphorylation in the respiratory chain.', *Nature*, 172(4387), pp. 975–8. doi: 10.1038/172975a0.

Slater, E. C. and Cleland, K. W. (1953) 'The effect of calcium on the respiratory and phosphorylative activities of heart-muscle sarcosomes.', *The Biochemical journal*, 55(4), pp. 566–90. doi: 10.1042/bj0550566.

Slee, E. A. *et al.* (1999) 'Ordering the cytochrome c-initiated caspase cascade: hierarchical activation of caspases-2, -3, -6, -7, -8, and -10 in a caspase-9-dependent manner.', *The Journal of cell biology*, 144(2), pp. 281–92. doi: 10.1083/jcb.144.2.281.

Sliter, D. A. *et al.* (2018) 'Parkin and PINK1 mitigate STING-induced inflammation.', *Nature*. Springer US, 561(7722), pp. 258–262. doi: 10.1038/s41586-018-0448-9.

Smith, I. F. *et al.* (2009) 'Ca(2+) puffs originate from preestablished stable clusters of inositol trisphosphate receptors.', *Science signaling*, 2(98), p. ra77. doi: 10.1126/scisignal.2000466.

Soman, S. *et al.* (2017) 'Inhibition of the mitochondrial calcium uniporter rescues dopaminergic neurons in pink1-/- zebrafish.', *The European journal of neuroscience*, 45(4), pp. 528–535. doi: 10.1111/ejn.13473.

Soman, S. K. *et al.* (2019) 'Restriction of mitochondrial calcium overload by mcu inactivation renders neuroprotective effect in Zebrafish models of Parkinson's disease.', *Biology open*. doi: 10.1242/bio.044347.

Somlyo, A. P., Bond, M. and Somlyo, A. V. (1985) 'Calcium content of mitochondria and endoplasmic reticulum in liver frozen rapidly in vivo.', *Nature*, 314(6012), pp. 622–5. doi: 10.1038/314622a0.

Sorbi, S., Bird, E. D. and Blass, J. P. (1983) 'Decreased pyruvate dehydrogenase complex activity in Huntington and Alzheimer brain.', *Annals of neurology*, 13(1), pp. 72–8. doi: 10.1002/ana.410130116.

Sparagna, G. C. *et al.* (1995) 'Mitochondrial calcium uptake from physiological-type pulses of calcium. A description of the rapid uptake mode.', *The Journal of biological chemistry*, 270(46), pp. 27510–5. doi: 10.1074/jbc.270.46.27510.

Spillantini, M. G. *et al.* (1997) 'Alpha-synuclein in Lewy bodies.', *Nature*, 388(6645), pp. 839–40. doi: 10.1038/42166.

Spradling, A. C. and Rubin, G. M. (1982) 'Transposition of cloned P elements into Drosophila germ line chromosomes.', *Science (New York, N.Y.)*, 218(4570), pp. 341–7. doi: 10.1126/science.6289435.

De Stefani, D. *et al.* (2011) 'A forty-kilodalton protein of the inner membrane is the mitochondrial calcium uniporter.', *Nature*, 476(7360), pp. 336–40. doi: 10.1038/nature10230.

Steinhauer, J. (2015) 'Separating from the pack: Molecular mechanisms of Drosophila spermatid individualization.', *Spermatogenesis*, 5(2), p. e1041345. doi: 10.1080/21565562.2015.1041345.

Stennicke, H. R. *et al.* (1998) 'Pro-caspase-3 is a major physiologic target of caspase-8.', *The Journal of biological chemistry*, 273(42), pp. 27084–90. doi: 10.1074/jbc.273.42.27084.

von Stockum, S. *et al.* (2011) 'Properties of Ca(2+) transport in mitochondria of Drosophila melanogaster.', *The Journal of biological chemistry*, 286(48), pp. 41163–70. doi: 10.1074/jbc.M111.268375.

von Stockum, S. *et al.* (2015) 'F-ATPase of Drosophila melanogaster forms 53-picosiemen (53-pS) channels responsible for mitochondrial Ca2+-induced Ca2+ release.', *The Journal of biological chemistry*, 290(8), pp. 4537–44. doi: 10.1074/jbc.C114.629766.

Stoica, R. *et al.* (2014) 'ER-mitochondria associations are regulated by the VAPB-PTPIP51 interaction and are disrupted by ALS/FTD-associated TDP-43.', *Nature communications*, 5, p. 3996. doi: 10.1038/ncomms4996.

Stowers, R. S. *et al.* (2002) 'Axonal transport of mitochondria to synapses depends on milton, a novel Drosophila protein.', *Neuron*, 36(6), pp. 1063–77. doi: 10.1016/s0896-6273(02)01094-2.

Syder, N. *et al.* (2018) 'Mitochondrial Ca2+ Uptake is Tightly Regulated by the C-Terminal End of EMRE', *Journal of Molecular and Cellular Cardiology*. Elsevier Ltd, 124, p. 122. doi: 10.1016/j.yjmcc.2018.07.115.

Szabadkai, G. *et al.* (2006) 'Chaperone-mediated coupling of endoplasmic reticulum and mitochondrial Ca2+ channels.', *The Journal of cell biology*, 175(6), pp. 901–11. doi: 10.1083/jcb.200608073.

Taguchi, N. *et al.* (2007) 'Mitotic phosphorylation of dynamin-related GTPase Drp1

participates in mitochondrial fission.', *The Journal of biological chemistry*, 282(15), pp. 11521–9. doi: 10.1074/jbc.M607279200.

Tait, S. W. G. and Green, D. R. (2010) 'Mitochondria and cell death: outer membrane permeabilization and beyond.', *Nature reviews. Molecular cell biology*. Nature Publishing Group, 11(9), pp. 621–32. doi: 10.1038/nrm2952.

Tang, S. *et al.* (2015) 'Mitochondrial Ca^{2+} uniporter is critical for store-operated Ca^{2+} entry-dependent breast cancer cell migration.', *Biochemical and biophysical research communications*. Elsevier Ltd, 458(1), pp. 186–93. doi: 10.1016/j.bbrc.2015.01.092.

Tang, T.-S. *et al.* (2003) 'Huntingtin and huntingtin-associated protein 1 influence neuronal calcium signaling mediated by inositol-(1,4,5) triphosphate receptor type 1.', *Neuron*, 39(2), pp. 227–39. doi: 10.1038/nchembio.304.

Tang, Y. and Wu, Y. (2019a) 'Decreased ATP production during mitochondrial calcium uniporter inhibition enhances autophagy and mitophagy to provide cardioprotection in cardiac failure.', *International journal of cardiology*. Elsevier B.V., 282(123), p. 67. doi: 10.1016/j.ijcard.2018.11.130.

Tang, Y. and Wu, Y. (2019b) 'Decreased ATP production during mitochondrial calcium uniporter inhibition enhances autophagy and mitophagy to provide cardioprotection in cardiac failure.', *International journal of cardiology*. Elsevier B.V., 282(123), p. 67. doi: 10.1016/j.ijcard.2018.11.130.

Tanzi, R. E. *et al.* (1987) 'Amyloid beta protein gene: cDNA, mRNA distribution, and genetic linkage near the Alzheimer locus.', *Science (New York, N.Y.)*, 235(4791), pp. 880–4. doi: 10.1126/science.2949367.

Thanvi, B., Lo, N. and Robinson, T. (2007) 'Levodopa-induced dyskinesia in Parkinson's disease: clinical features, pathogenesis, prevention and treatment.', *Postgraduate medical journal*, 83(980), pp. 384–8. doi: 10.1136/pgmj.2006.054759.

Thorpe, H. M. and Smith, M. C. (1998) 'In vitro site-specific integration of bacteriophage DNA catalyzed by a recombinase of the resolvase/invertase family.', *Proceedings of the National Academy of Sciences of the United States of America*, 95(10), pp. 5505–10. doi: 10.1073/pnas.95.10.5505.

Tinel, H. *et al.* (1999) 'Active mitochondria surrounding the pancreatic acinar granule region prevent spreading of inositol trisphosphate-evoked local cytosolic Ca(2+) signals.', *The EMBO journal*, 18(18), pp. 4999–5008. doi: 10.1093/emboj/18.18.4999.

Tiraboschi, P. *et al.* (2004) 'The importance of neuritic plaques and tangles to the development and evolution of AD.', *Neurology*, 62(11), pp. 1984–9. doi: 10.1212/01.wnl.0000129697.01779.0a.

Tomar, D. *et al.* (2016) 'MCUR1 Is a Scaffold Factor for the MCU Complex Function and Promotes Mitochondrial Bioenergetics.', *Cell reports*, 15(8), pp. 1673–85. doi: 10.1016/j.celrep.2016.04.050.

Toye, A. A. *et al.* (2005) 'A genetic and physiological study of impaired glucose homeostasis control in C57BL/6J mice.', *Diabetologia*, 48(4), pp. 675–86. doi: 10.1007/s00125-005-1680-z.

Tran, P. O. *et al.* (1999) 'A wound-induced [Ca2+]i increase and its transcriptional activation of immediate early genes is important in the regulation of motility.', *Experimental cell research*, 246(2), pp. 319–26. doi: 10.1006/excr.1998.4239.

Trenker, M. *et al.* (2007) 'Uncoupling proteins 2 and 3 are fundamental for mitochondrial Ca2+ uniport.', *Nature cell biology*, 9(4), pp. 445–452. doi: 10.1038/ncb1556.

Tsai, C.-W. *et al.* (2017) 'Proteolytic control of the mitochondrial calcium uniporter complex.', *Proceedings of the National Academy of Sciences of the United States of America*, p. 201702938. doi: 10.1073/pnas.1702938114.

Tsai, M.-F. *et al.* (2014) 'Functional reconstitution of the mitochondrial Ca2+/H+ antiporter Letm1.', *The Journal of general physiology*, 143(1), pp. 67–73. doi: 10.1085/jgp.201311096.

Tsai, M.-F. *et al.* (2016) 'Dual functions of a small regulatory subunit in the mitochondrial calcium uniporter complex.', *eLife*, 5, p. e15545. doi: 10.7554/eLife.15545.

Tufi, R. *et al.* (2019) 'Comprehensive Genetic Characterization of Mitochondrial Ca2+ Uniporter Components Reveals Their Different Physiological Requirements In Vivo.', *Cell reports*. ElsevierCompany., 27(5), pp. 1541-1550.e5. doi: 10.1016/j.celrep.2019.04.033.

Vafai, S. B. and Mootha, V. K. (2012) 'Mitochondrial disorders as windows into an ancient organelle.', *Nature*, 491(7424), pp. 374–83. doi: 10.1038/nature11707.

Vais, H. *et al.* (2015) 'MCUR1, CCDC90A, Is a Regulator of the Mitochondrial Calcium Uniporter.', *Cell metabolism*, 22(4), pp. 533–5. doi: 10.1016/j.cmet.2015.09.015.

Vais, H. *et al.* (2016) 'EMRE Is a Matrix Ca(2+) Sensor that Governs Gatekeeping of the Mitochondrial Ca(2+) Uniporter.', *Cell reports*. The Authors, pp. 1–8. doi: 10.1016/j.celrep.2015.12.054.

Valente, E. M. *et al.* (2001) 'Localization of a novel locus for autosomal recessive early-onset parkinsonism, PARK6, on human chromosome 1p35-p36.', *American journal of human genetics*, 68(4), pp. 895–900. doi: 10.1086/319522.

Valente, E. M. *et al.* (2004) 'Hereditary early-onset Parkinson's disease caused by mutations in PINK1.', *Science (New York, N.Y.)*, 304(5674), pp. 1158–60. doi: 10.1126/science.1096284.

Vandecaetsbeek, I. *et al.* (2011) 'The Ca2+ pumps of the endoplasmic reticulum and Golgi apparatus.', *Cold Spring Harbor perspectives in biology*, 3(5). doi: 10.1101/cshperspect.a004184.

Vasington, F. D. *et al.* (1972) 'The effect of ruthenium red on Ca 2+ transport and respiration in rat liver mitochondria.', *Biochimica et biophysica acta*, 256(1), pp. 43–54. doi: 10.1016/0005-2728(72)90161-2.

Vasington, F. D. and Murphy, J. V (1962) 'Ca ion uptake by rat kidney mitochondria and its dependence on respiration and phosphorylation.', *The Journal of biological chemistry*, 237(8), pp. 2670–7. Available at: http://www.ncbi.nlm.nih.gov/pubmed/13925019.

Vecellio Reane, D. *et al.* (2016) 'A MICU1 Splice Variant Confers High Sensitivity to the Mitochondrial Ca(2+) Uptake Machinery of Skeletal Muscle.', *Molecular cell*, pp. 1–14. doi: 10.1016/j.molcel.2016.10.001.

Vig, M. *et al.* (2006) 'CRACM1 is a plasma membrane protein essential for store-operated Ca2+ entry.', *Science (New York, N.Y.)*, 312(5777), pp. 1220–3. doi: 10.1126/science.1127883.

Vincow, E. S. *et al.* (2013) 'The PINK1-Parkin pathway promotes both mitophagy and selective respiratory chain turnover in vivo.', *Proceedings of the National Academy of Sciences of the United States of America*, 110(16), pp. 6400–5. doi: 10.1073/pnas.1221132110.

Vos, M. *et al.* (2012) 'Vitamin K2 is a mitochondrial electron carrier that rescues pink1 deficiency.', *Science (New York, N.Y.)*, 336(6086), pp. 1306–10. doi: 10.1126/science.1218632.

Walkinshaw, E. *et al.* (2015) 'Identification of genes that promote or inhibit olfactory memory formation in Drosophila.', *Genetics*, 199(4), pp. 1173–82. doi: 10.1534/genetics.114.173575.

Wang, X. and Schwarz, T. L. (2009) 'The mechanism of Ca2+ -dependent regulation of kinesin-mediated mitochondrial motility.', *Cell*. Elsevier Inc., 136(1), pp. 163–74. doi: 10.1016/j.cell.2008.11.046.

Wang, Y. *et al.* (2019) 'Structural Mechanism of EMRE-Dependent Gating of the Human Mitochondrial Calcium Uniporter.', *Cell*. Elsevier Inc., 177(5), pp. 1252-1261.e13. doi: 10.1016/j.cell.2019.03.050.

Weingarten, M. D. *et al.* (1975) 'A protein factor essential for microtubule assembly.', *Proceedings of the National Academy of Sciences of the United States of America*, 72(5), pp. 1858–62. doi: 10.1073/pnas.72.5.1858.

Wettmarshausen, J. *et al.* (2018) 'MICU1 Confers Protection from MCU-Dependent Manganese Toxicity', *Cell Reports*, pp. 1425–1435. doi: 10.1016/j.celrep.2018.10.037.

Wideman, J. G. *et al.* (2018) 'PDZD8 is not the "functional ortholog" of Mmm1, it is a paralog.', *F1000Research*, 7(May), p. 1088. doi: 10.12688/f1000research.15523.1.

Williams, D. W., Tyrer, M. and Shepherd, D. (2000) 'Tau and tau reporters disrupt central projections of sensory neurons inDrosophila', *The Journal of Comparative Neurology*, 428(4), pp. 630–640. doi: 10.1002/1096-9861(20001225)428:4<630::AID-CNE4>3.0.CO;2-X.

Wimo, A. *et al.* (2010) 'The economic impact of dementia in Europe in 2008-cost estimates from the Eurocode project.', *International journal of geriatric psychiatry*, 26(8), pp. 825–32. doi: 10.1002/gps.2610.

Wittmann, C. W. *et al.* (2001) 'Tauopathy in Drosophila: neurodegeneration without neurofibrillary tangles.', *Science (New York, N.Y.)*, 293(5530), pp. 711–4. doi: 10.1126/science.1062382.

Woods, J. J. *et al.* (2019) 'A Selective and Cell-Permeable Mitochondrial Calcium Uniporter (MCU) Inhibitor Preserves Mitochondrial Bioenergetics after Hypoxia/Reoxygenation Injury'. doi: 10.1021/acscentsci.8b00773.

Wu, J. S. and Luo, L. (2006) 'A protocol for dissecting Drosophila melanogaster brains for live imaging or immunostaining.', *Nature protocols*, 1(4), pp. 2110–2115. doi: 10.1038/nprot.2006.336.

Wu, S.-C. *et al.* (2017) 'Intestinal microbial dysbiosis aggravates the progression of Alzheimer's disease in Drosophila.', *Nature communications*. Springer US, 8(1), p. 24. doi: 10.1038/s41467-017-00040-6.

Wu, W. *et al.* (2019) 'The crystal structure of MICU2 provides insight into Ca2+ binding and MICU1-MICU2 heterodimer formation.', *EMBO reports*, 20(9), p. e47488. doi: 10.15252/embr.201847488.

Wu, Y. *et al.* (2015) 'The mitochondrial uniporter controls fight or flight heart rate increases.', *Nature communications*. Nature Publishing Group, 6(May 2014), p. 6081. doi: 10.1038/ncomms7081.

Xie, N. *et al.* (2017) 'Inhibition of the mitochondrial calcium uniporter inhibits Aβ-induced apoptosis by reducing reactive oxygen species-mediated endoplasmic reticulum stress in cultured microglia', *Brain Research*. Elsevier B.V., 1676, pp. 100–106. doi: 10.1016/j.brainres.2017.08.035.

Xing, Y. *et al.* (2019) 'Dimerization of MICU Proteins Controls Ca2+ Influx through the Mitochondrial Ca2+ Uniporter.', *Cell reports*. ElsevierCompany., 26(5), pp. 1203-1212.e4. doi: 10.1016/j.celrep.2019.01.022.

Xu, S. and Chisholm, A. D. (2014) 'C. elegans epidermal wounding induces a mitochondrial ROS burst that promotes wound repair.', *Developmental cell*. Elsevier Inc., 31(1), pp. 48–60. doi: 10.1016/j.devcel.2014.08.002.

Yamamoto, S. *et al.* (2014) 'A drosophila genetic resource of mutants to study mechanisms underlying human genetic diseases.', *Cell*. Elsevier Inc., 159(1), pp. 200–214. doi: 10.1016/j.cell.2014.09.002.

Yamamoto, T. *et al.* (2016) 'Analysis of the structure and function of EMRE in a yeast expression system.', *Biochimica et biophysica acta*. Elsevier B.V. doi: 10.1016/j.bbabio.2016.03.019.

Yamamoto, T. *et al.* (2019) 'Functional analysis of coiled-coil domains of MCU in mitochondrial calcium uptake.', *Biochimica et biophysica acta. Bioenergetics*. Elsevier, (August), p. 148061. doi: 10.1016/j.bbabio.2019.148061.

Yang, Y. *et al.* (2008) 'Pink1 regulates mitochondrial dynamics through interaction with the fission/fusion machinery.', *Proceedings of the National Academy of Sciences of the United States of America*, 105(19), pp. 7070–5. doi: 10.1073/pnas.0711845105.

Ying, W. L. *et al.* (1991) 'Inhibition of mitochondrial calcium ion transport by an oxo-bridged dinuclear ruthenium ammine complex.', *Biochemistry*, 30(20), pp. 4949–52. doi: 10.1021/bi00234a016.

Yoo, J. *et al.* (2018) 'Cryo-EM structure of a mitochondrial calcium uniporter.', *Science (New York, N.Y.)*, 4056(June), pp. 1–11. doi: 10.1126/science.aar4056.

Yu, Z. *et al.* (2018) 'Mitochondrial calcium uniporter inhibition provides cardioprotection in pressure overload-induced heart failure through autophagy enhancement.', *International journal of cardiology*. Elsevier B.V., 271, pp. 161–168. doi: 10.1016/j.ijcard.2018.05.054.

Zhang, S. L. *et al.* (2006) 'Genome-wide RNAi screen of Ca(2+) influx identifies genes that regulate Ca(2+) release-activated Ca(2+) channel activity.', *Proceedings of the National Academy of Sciences of the United States of America*, 103(24), pp. 9357–62. doi: 10.1073/pnas.0603161103.

Zhao, H. *et al.* (2019) 'AMPK-mediated activation of MCU stimulates mitochondrial Ca2+ entry to promote mitotic progression.', *Nature cell biology*. Springer US, 21(4), pp. 476–486. doi: 10.1038/s41556-019-0296-3.

Zhao, X.-L. *et al.* (2010) 'Expression of beta-amyloid induced age-dependent presynaptic and axonal changes in Drosophila.', *The Journal of neuroscience : the official journal of the Society for Neuroscience*, 30(4), pp. 1512–22. doi: 10.1523/JNEUROSCI.3699-09.2010.